

User-adaptive autonomous robotic walker driven by artificial intelligence for ataxic rehabilitation

João Pedro Mendes Lopes

UMinho | 2025

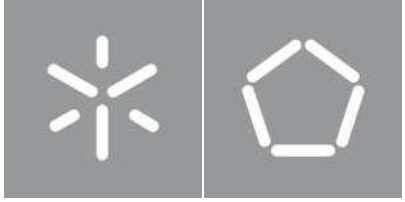


Universidade do Minho
Escola de Engenharia

João Pedro Mendes Lopes

User-adaptive autonomous robotic walker driven by artificial intelligence for ataxic rehabilitation

setembro de 2025



University of Minho
School of Engineering

João Pedro Mendes Lopes

User-adaptive autonomous robotic walker driven by artificial intelligence for ataxic rehabilitation

PhD Thesis
PhD in Biomedical Engineering

Thesis supervised by
Cristina Manuela Peixoto dos Santos
João José Fernandes Cardoso de Araújo Cerqueira
Joana Sofia Campos Figueiredo

september 2025

Direitos de Autor e Condições de Utilização deste Trabalho por Terceiros

Este é um trabalho académico que pode ser utilizado por terceiros desde que respeitadas as regras e boas práticas internacionalmente aceites, no que concerne aos direitos de autor e direitos conexos. Assim, o presente trabalho pode ser utilizado nos termos previstos na licença abaixo indicada. Caso o utilizador necessite de permissão para poder fazer um uso do trabalho em condições não previstas no licenciamento indicado, deverá contactar o autor, através do RepositóriUM da Universidade do Minho.

Licença concedida aos utilizadores deste trabalho



CC BY-NC-ND

https://creativecommons.org/licenses/by-nc-nd/4.0/

Acknowledgements

Após uma longa etapa de altos e baixos, termina aqui o meu percurso académico na Universidade do Minho. Em primeiro lugar, gostaria de endereçar o meu maior agradecimento à minha família, aos meus pais, irmão, e à minha companheira Catarina, por me terem apoiado sempre ao longo destes quatro anos e por me terem motivado sempre nos momentos mais complicados. À Catarina, agradeço por ser a minha companheira de vida, a minha confidente, o meu pilar, e por sempre se manter ao meu lado, mesmo nos momentos de maior fraqueza que esta jornada trouxe. Ajudaste-me sempre a manter o foco, a manter a calma, e a usufruir mais desta passagem na Terra. Agradeço, também, aos seus pais por todo o apoio, principalmente na etapa final deste percurso. De seguida, endereço o meu agradecimento aos meus orientadores, Professora Cristina Santos, Doutora Joana Figueiredo e Professor João Cerqueira, especialmente à Professora Cristina Santos por me ter proporcionado a oportunidade de integrar este projeto desafiador, com elevado impacto social, e de desenvolver esta tese de doutoramento. Agradeço aos três pelo apoio e conhecimento transmitido. Agradeço também à equipa do BiRDLab, por manterem sempre um ambiente divertido e de cooperação, e em especial aos amigos do Porta Aberta, que foram muito importantes em tornar esta jornada mais divertida e que também me aconselharam muito no desenrolar deste projeto. Além disso, um agradecimento a todos os membros que trabalharam comigo na equipa WALKit e que contribuíram para o sucesso deste projeto. Agradeço também à equipa clínica do Hospital de Braga, Orthos XXI e 2CA-Braga, por terem possibilitado a implementação do estudo clínico, e um agradecimento especial a todos os participantes envolvidos no estudo.

FINANCIAL SUPPORT: This work has been supported by the *Fundação para a Ciência e Tecnologia* (FCT) with the Reference Scholarship under Grant 2020.05708.BD, and under the national support to R&D units grant, through the reference project UIDB/04436/2020 and UIDP/04436/2020, and with support of computing facilities provided by "Search-ON2: Revitalization of HPC infrastructure of UMinho" (NORTE-07-0162-FEDER-000086), co-funded by the North Portugal Regional Operational Programme (ON.2 – O Novo Norte), under the National Strategic Reference Framework (NSRF), through the European Regional Development Fund (ERDF).

Statement of Integrity

I hereby declare having conducted this academic work with integrity.

I confirm that I have not used plagiarism or any form of undue use of information or falsification of results along the process leading to its elaboration.

I further declare that I have fully acknowledged the Code of Ethical Conduct of the University of Minho.

University of Minho, Braga, september 2025

João Pedro Mendes Lopes

Resumo

A ataxia cerebelar é uma condição neurológica caracterizada por descoordenação dos membros inferiores, variabilidade da marcha e instabilidade postural, que resulta em perda de equilíbrio e redução da mobilidade. Atualmente, a reabilitação física intensiva é o principal tratamento da ataxia, envolvendo equipas multidisciplinares e exigindo um enorme esforço e dedicação por parte dos terapeutas. Assim, torna-se necessário encontrar meios complementares que promovam a recuperação da capacidade motora e reduzam o ónus da terapia manual, atenuando os impactos socioeconómicos. A terapia assistida por robô tem vindo a desempenhar um papel fundamental na terapia física, não só por se revelar eficaz, mas também porque permite o alívio na carga dos terapeutas, oferecendo uma abordagem colaborativa. Esta tese de doutoramento apresenta a próxima geração do ASBGo Smart Walker, um andarilho robótico desenvolvido para o treino da marcha atáxica. Esta tese visa otimizar o dispositivo, agora designado por WALKit, dotando-o de funcionalidades inovadoras que maximizam o envolvimento do utilizador na terapia.

Esta tese está estruturada em cinco partes. Primeiro, optimizou-se o *software* do dispositivo, tornando-o mais intuitivo e funcional, considerando requisitos técnicos e clínicos. Segundo, realizou-se um estudo profundo sobre a descodificação do movimento do utilizador de forma indireta e intuitiva com base em *deep learning*. O modelo revelou ser preciso, mas, ocasionalmente, desvia o foco do utilizador. Em terceiro lugar, foram introduzidas duas estratégias de controlo: uma abordagem *Human-in-the-loop* que presta assistência de acordo com as intenções de movimento do utilizador e uma estratégia *Assist-as-Needed* que supervisiona os comandos do utilizador, assistindo, de forma inteligente, em caso de necessidade. Quarto, foi desenvolvida uma estratégia integrada de *biofeedback* audiovisual e um jogo sério baseado em realidade virtual não imersiva, que visam maximizar a participação ativa do utilizador e tornar a terapia com o WALKit mais envolvente e diversificada. Por fim, foi realizado um estudo clínico de intervenção para determinar a eficácia do WALKit na reabilitação da ataxia. Os resultados globais indicam que o WALKit promove uma melhoria na velocidade e qualidade da marcha, e no controlo do equilíbrio.

Palavras-chave Ataxia cerebelar, Colaboração Humano-Robô, Descodificação do movimento, Inteligência Artificial, Interação Humano-Robô, Treino Assistido por Robô

Abstract

Cerebellar ataxia is a neurological condition characterized by incoordination of the lower limbs, gait variability, and postural instability, leading to loss of balance and reduced mobility. Currently, intensive physical rehabilitation the mainstay of ataxia treatment, which involves multidisciplinary teams and requires a huge effort and commitment from therapists. Thus, it becomes necessary to find complementary means of rehabilitation that promote motor skills recovery and reduce the heavy burden of manual therapy, mitigating the social-economic impacts. Robot-Assisted Gait Training (RAGT) is playing a pivotal role not only in enhancing the rehabilitation effectiveness, but also alleviating the therapists' burden by offering a collaborative and supportive approach. This Ph.D. thesis presents the next generation of ASBGo Smart Walker, a user-friendly robotic walker for ataxic gait training. This research aims to optimize this device, currently named WALKit, by providing it with innovative functionalities that maximize user interaction and involvement in therapy.

This thesis is divided into five parts. Firstly, the device's software was redesigned and optimized, turning it more intuitive and functional, considering technical and clinical requirements. Secondly, an in-depth study was conducted on novel ways of indirectly and intuitively decode the user's motion based on deep learning. The model revealed accurate, but occasionally diverts the focus away from the user. Thirdly, two assistive control strategies were introduced: a Human-in-the-loop approach that provides assistance according to the user's motion intentions and an Assist-as-Needed strategy that supervises the user's commands and intelligently assists or overrides the user in the case of need. Fourth, an integrated audiovisual biofeedback strategy and an exergame based on non-immersive virtual reality were developed, maximizing user active participation and turning therapy with WALKit more engaging, diverse, and problem-oriented. Lastly, a clinical intervention protocol was conducted to determine the effectiveness of WALKit in ataxic rehabilitation. In short, the main findings indicate that WALKit promotes an overall improvement in gait speed, gait quality, and balance control.

Keywords Artificial Intelligence, Cerebellar Ataxia, Human-Robot Interaction, Human-Robot Collaboration, Motion Decoding, Robot-Assisted Gait Training

Contents

List of Figures xi

List of Tables xvii

I Introduction 1

1 Introduction 2

1.1 Motivation . . . 2
1.2 Problem statement . . . 5
1.3 Goal and Objectives . . . 8
1.4 Research Questions . . . 11
1.5 Contributions to Knowledge . . . 11
1.6 Manuscript Outline . . . 14

II Literature Review 15

2 Literature Review 16

2.1 Introduction . . . 16
2.2 An overview to smart walkers . . . 16
2.3 Motion Intention Perception . . . 20
2.3.1 Methodology . . . 21
2.3.2 Results . . . 22
2.3.3 Discussion . . . 30
2.4 Assistive Control Strategies . . . 33
2.4.1 Shared control . . . 33
2.5 Human-Robot Interaction strategies . . . 36

2.5.1 Methodology . . . 37
2.5.2 Results . . . 37
2.5.3 Discussion . . . 47
2.6 General Conclusion . . . 48

III WALKit Smart Walker 50

3 WALKit Smart Walker: an overview 51
3.1 Introduction . . . 51
3.2 Prototype overview . . . 51
3.3 System Architecture . . . 52
3.4 Optimized Graphic User Interface . . . 53
3.4.1 Stakeholder Requirements . . . 54
3.4.2 Interface development . . . 55
3.4.3 Experimental validation . . . 57
3.4.4 Results and Discussion . . . 58
3.5 Clinical Support and Feedback Tool . . . 59
3.5.1 Stakeholder requirements . . . 60
3.5.2 Application development . . . 60
3.5.3 Experimental validation . . . 61
3.5.4 Results and Discussion . . . 63
3.6 General conclusion . . . 64

IV Motion Intention Perception 65

4 Motion Intention Perception 66
4.1 Introduction . . . 66
4.2 Proposed Strategy . . . 67
4.3 Methodology . . . 68
4.3.1 Dataset Acquisition . . . 68
4.3.2 Experimental Protocol . . . 69
4.3.3 Dataset labeling . . . 70
4.3.4 Dataset Preparation . . . 70

4.3.5 Model's Input Preparation . . . 70
4.4 Deep Learning Approaches . . . 71
4.5 Ablation study . . . 73
4.6 Training Pipeline . . . 74
4.6.1 Dataset split . . . 74
4.6.2 Training Details . . . 75
4.7 Model evaluation . . . 76
4.7.1 Classification Metrics . . . 76
4.7.2 Quantitative focus evaluation . . . 77
4.7.3 Trial simulations and Post-processing . . . 77
4.8 Results and Discussion . . . 78
4.8.1 Multi-class classification . . . 78
4.8.2 Multi-class segmentation-classification . . . 89
4.8.3 Trial Simulations . . . 90
4.8.4 Ablation Study . . . 94
4.9 General conclusion . . . 99

V Assistive Control Strategies 100

5 Assistive Control Strategies 101

5.1 Introduction . . . 101
5.2 Human-in-the-loop Control of a Smart Walker through DL-based Human Motion Decoding 101
5.2.1 Proposed strategy . . . 101
5.2.2 Methodology . . . 103
5.2.3 Results and Discussion . . . 106
5.3 Deep Reinforcement Learning based Shared Control Strategy for Robotic Walkers . . . 112
5.3.1 Proposed strategy . . . 113
5.3.2 User Intention Detector . . . 114
5.3.3 Autonomous Driving System . . . 115
5.3.4 RL-based control strategy . . . 116
5.3.5 Experimental Protocol . . . 119
5.3.6 Results and Discussion . . . 120

5.4 General Conclusion 125

VI Human-Robot Interaction Strategies 127

6 Human-Robot Interaction strategies for balance and posture rehabilitation 128

6.1 Introduction 128

6.2 Audiovisual Biofeedback Strategy 128

6.2.1 Proposal 129

6.2.2 Methodology 130

6.2.3 Validation Protocol 135

6.2.4 Results and Discussion 138

6.3 Non-immersive Virtual Reality based Exergame 149

6.3.1 Proposal 150

6.3.2 Methodology 150

6.3.3 Validation Protocol 154

6.3.4 Results and Discussion 155

6.4 General conclusions 156

VII Robot-Assisted Gait Training in Ataxia 158

7 Introducing WALKit Smart Walker in Ataxia Rehabilitation 159

7.1 Introduction 159

7.2 Ataxia treatment: current status 159

7.3 Intervention Study 160

7.3.1 Participants 161

7.3.2 Clinical Protocol 163

7.3.3 Participant Instrumentation 166

7.3.4 Rehabilitation outcomes 167

7.3.5 Usability and functionality 169

7.3.6 Data Processing and Analysis 169

7.4 Results 170

7.4.1 Training Phase 1 171

7.4.2 Training Phase 2 180

7.4.3 Usability and functionality . . . 188
7.5 Discussion . . . 190
7.5.1 Motor rehabilitation . . . 191
7.5.2 Usability and acceptability . . . 195
7.6 General Conclusion . . . 195

VIII General Overview **197**

8 Main Conclusions **198**
8.1 Research Questions . . . 201
8.2 Future Perspectives . . . 206

Bibliography **207**

A Appendix A **227**
A.1 System Usability Questionnaire . . . 227
A.2 Scale for the Assessment and Rating of Ataxia . . . 227
A.3 Berg Balance Scale . . . 230

B Appendix B **235**
B.1 Multi-class classification approach . . . 235
B.2 Multi-class segmentation-classification approach . . . 236
B.3 Ablation study . . . 238

C Appendix C **239**
C.1 Training Phase 1 . . . 239
C.2 Training Phase 2 . . . 240

List of Figures

1 Worldwide prevalence of cerebellar ataxia according to study [6]. 3

2 Flow diagram for the literature review of MI along with SRW. 22

3 Flow diagram for the literature review of biofeedback systems and games. 38

4 WALKit SRW developed at University of Minho with partnership with ORTHOS XXI, Tecnicunha, and 2CA-Braga, that was used in this doctoral thesis. 52

5 WALKit software architecture. It is divided into high- and low-level, which constantly communicate in a bidirectional manner via UART. 53

6 GUI of ASBGo prototype, the predecessor of WALKit. 54

7 New GUI developed as part of the redesign of the device's software: **(a)** login system, **(b)** home menu, **(c)** session configuration menu, and **(d)** real time session menu. . . . 55

8 Snapshots of the database's menu of new GUI embedded in WALKit: **(a)** home menu, **(b)** search for patient, **(c)** add new patient, **(d)** add clinical score, **(e)** archive menu, and **(f)** session's information. 57

9 Video demonstration of the new GUI of WALKit SRW. 59

10 Screenshots of the developed clinical feedback tool for both health professionals and final users of WALKit Smart Walker. Note that data presented on these screenshots are fictitious and merely illustrative. 62

11 Video demonstration of the new clinical support and feedback tool of WALKit SRW. . . . 64

12 Overall pipeline followed for human motion decoding using RGB videos. GT stands for Ground-Truth. 68

13 Illustration of two TR circuits used for data collection. 69

14 Four inputs that were studied in this work: **(a)** uncropped *DIF*, **(b)** cropped *DIF*, **(c)** uncropped *ADD*, and **(d)** cropped *ADD*. 71

15 Illustration of the adapted VGG16 implemented in this work. 71

16 Illustration of the attention blocks investigated in this thesis: **(a)** CHATT mechanism, **(b)** SE layer, and **(c)** SPATT mechanism. 72
17 Adapted U-Net neural network for multi-class classification used in this work along with the segmentation-classification network. 73
18 Example of input images considering: **(a)** STOP class with different background, **(b)** WALK class with different background, **(c)** STOP class without background, and **(d)** WALK class with background. 74
19 Confusion matrices for the ResNet-50 model with CHATT mechanism, over the four types of input and considering the test set. 82
20 Grad-CAM visualization, temporally ordered, for each one of the transitions in the slow trial (trial A). The green and blue labels correspond to the first prediction and GT label, respectively, of the action that is beginning (P = predicted class). 83
21 Grad-CAM visualization, temporally ordered, for each one of the transitions in the fast trial (trial B). The green and blue labels correspond to the first prediction and GT label, respectively, of the action that is beginning (P = predicted class). The orange ones correspond to the perturbations in the model's predictions that do not correspond to the post-processed predicted class. 84
22 Confusion matrices for the ResNet-50 model with both: **(a)** SE and **(b)** SPATT mechanisms considering the test split. 86
23 Examples of Grad-CAM for MI decoding considering ResNet-50 with the additional SE layer, considering: **(a)** STOP, **(b)** TL, **(c)** TR, and **(d)** WALK classes. Below it can be observed the segmented region of the heatmap with a threshold of 0.5. 88
24 Examples of Grad-CAM for MI decoding considering ResNet-50 with the additional SPATT mechanism, considering: **(a)** STOP, **(b)** TL, **(c)** TR, and **(d)** WALK classes. Below it can be observed the segmented region of the heatmap with a threshold of 0.5. 88
25 Plot of the GT (solid blue line), predicted (dotted green line) and post-processed predicted labels (solid red line) for **(a)** trial A - 0.5 m/s, **(b)** trial of participant 11, 0.7 m/s, **(c)** trial of participant 11, 1.0 m/s, **(d)** trial of participant 15, 0.5 m/s, **(e)** trial of participant 15, 0.7 m/s, and **(f)** trial B - 1.0 m/s. Class: 0 stands for STOP, 1 stands for WALK, 2 stands for TR and 3 stands for TL. 91

26 Grad-CAM of trial A - participant 11 walking with the SRW at 0.5 m/s - considering the ResNet50 with the SE layer. GT, marked in green, represents the true label. An indication is given of how long it took the model to correctly decode MI. 93
27 Confusion matrices of ResNet-50 considering validation and test sets with background removed (a and b), and validation and test sets with background changed (c and d). . . 96
28 Confusion matrices for the dual-task classification approach considering: **(a)** validation set, and **(b)** test set. 98
29 Examples of Grad-CAM for the two-class early recognition of MI: **(a)** and **(b)** STOP, **(c)** and **(d)** WALK. Below it can be observed the segmented region of the heatmap with a threshold of 0.5. 98

30 Overview of the proposed HIL control strategy. 102
31 Representative trials of the experimental validation of the proposed HIL control strategy considering: **(a)** 0.3 m/s and **(b)** 0.7 m/s. GT and UL stand for Ground Truth and Upper Limit, respectively. 107
32 Instantaneous Accuracy (IA) of the two representative trials considering the lowest and fastest gait speeds, namely: **(a)** 0.3 m/s and **(b)** 0.7 m/s. 107
33 Zoom of transition WALK $\rightarrow$ STOP considering the representative trial of: **(a)** 0.3 m/s and **(b)** 0.7 m/s. GT and UL stand for Ground Truth and Upper Limit, respectively. . . . 109
34 Representative trials of the proposed HIL control strategy with the adaptability module activated, considering an initial walking speed of 0.3 m/s. GT, UL, AFLL, AFUL stand for Ground Truth, Upper Limit, Adaptability Factor Lower Limit, and Adaptability Factor Upper Limit, respectively. 110
35 Representative trials of the proposed HIL control strategy with the adaptability and safety modules activated, considering an initial walking speed of 0.3 m/s. GT, UL, AFLL, AFUL, WThr stand for Ground Truth, Upper Limit, Adaptability Factor Lower Limit, Adaptability Factor Upper Limit, and Warning Threshold, respectively. 111
36 Overview of the implemented RL-based shared control strategy. 113
37 A representation of the deep neural network used as policy function. The number of entries (inputs/outputs) in this figure is not representative of the actual number present in the network. 118

38 Representative trials of the path taken by the HRS with the ADS (red trajectory) in comparison to the planned paths (green trajectory) considering the five scenarios tested considering the ADS: **(a)** scenario 0, **(b)** scenario 1, **(c)** scenario 2, **(d)** scenario 3, and **(e)** scenario 4. 121
39 Representative trials of the path taken by the HRS with the proposed shared control strategy (trajectory with heatmap) in comparison with the planned path by the global planner (green trajectory) in the five scenarios tested: **(a)** scenario 0, **(b)** scenario 1, **(c)** scenario 2, **(d)** scenario 3, and **(e)** scenario 4. 122
40 Operating frequency box plot of the proposed shared control strategy. 125
41 Biofeedback system embeeded in WALKit Smart Walker proposed to control the postural sway of ataxic patients. 129
42 Video demonstration of the novel BS embedded in WALKit SRW. 130
43 Example of the configuration of the biofeedback strategy. 133
44 Snapshots of a user using the BS developed in this doctoral thesis and the corresponding visual biofeedback. 134
45 Ellipses created for audio biofeedback. 134
46 Diagram of the experimental protocol for the technical and usability validation of the BS. 136
47 Representative illustration for the estimated pitch and roll of static trials: **(a)** trial 1, **(b)** trial 2, and **(c)** trial 3. 139
48 Representative illustration for the estimated pitch and roll of stance trials: **(a)** trial 1, **(b)** trial 2, and **(c)** trial 3. 140
49 Representative illustration for the estimated pitch and roll of sit-to-stand trials: **(a)** trial 1, **(b)** trial 2, and **(c)** trial 3. 140
50 Representative illustration for the estimated pitch and roll of walk trials at 0.3 m/s: **(a)** trial 1, **(b)** trial 2, and **(c)** trial 3. 141
51 Heatmap of the Spearman's correlation coefficient considering both sensor fusion algorithms, roll and pitch angles, and the different activities (Wx stands for each walking activity considering each gait speed, QS stands for quiet standing, and SD stands for sitting down and standing up activity). 142

52 Example of users' compensatory response for bipedal stance, considering: **(a)** the participant with the highest activation (AP limit: $\pm 1.2°$, ML limit: $\pm 0.5°$), **(b)** extra bipedal stance (AP limit: $\pm 0.3°$, ML limit: $\pm 0.1°$), **(c)** bipedal stance for the participant with the lowest activation (AP limit: $\pm 1.8°$, ML limit: $\pm 0.7°$), and **(d)** extra bipedal stance (AP limit: $\pm 0.9°$, ML limit: $\pm 0.5°$). 144

53 Example of users' compensatory response considering: **(a)** tandem stance for the participant with the highest activation (AP limit: $\pm 0.7°$, ML limit: $\pm 2.3°$), **(b)** extra tandem stance (AP limit: $\pm 0.6°$, ML limit: $\pm 0.2°$), **(c)** unipedal stance for the participant with the highest activation (AP limit: $\pm 5.3°$, ML limit: $\pm 1.9°$), and **(d)** extra unipedal stance (AP limit: $\pm 0.9°$, ML limit: $\pm 0.4°$). 145

54 Screenshot of the novel SG proposed for WALKit SRW. 151

55 Example of controlling the tilt of the avatar through the user's motion. 152

56 Example of hitting mole event. 153

57 Video demonstration of the novel exergame of WALKit SRW. 153

58 Experimental protocol design of the intervention study. 164

59 Example of participants with CA during the interventions sessions. 166

60 Inertial sensors placement following Xsens guidelines. Note that each sensor was placed in the inner part of the strap to better secure the sensors. 166

61 Ratio of time to complete the 10-MWT and ratio of gait speed, considering post-training with WALKit SRW and treadmill. 174

62 Ratio of time to complete TUG test considering post-training with WALKit SRW and treadmill. 175

63 Symmetry Ratio of temporal gait metrics: stride time, step time, stance and swing times, considering both day 0 and day 16 for RAGT with the robotic walker and for treadmill training. 176

64 Symmetry Ratio of spatial gait metrics: stride and step excursion, considering both day 0 and day 16 for RAGT with the robotic walker and for treadmill training. 178

65 CoM displacement considering AP and ML axes for for P3 (a and b), P5 (c and d), and P6 (e and f); panels a, c and e consider all data, and b, d, f consider the 98% most representative data. 181

66 CoM variation during execution of BBS 7 for P5, considering day 0 and day 16: **(a)** total data, **(b)** 98% most representative data. 183

67 CoM variation during execution of BBS 13 for P5, considering day 0 and day 16: **(a)** total data of Left Foot Front (LFF), **(b)** 98% most representative data of LFF, **(c)** total data of Right Foot Front (RFF), and **(d)** 98% most representative data of RFF. 184

68 Accuracy and loss training curves for VGG16 model: **(a)** DIF, **(b)** ADD, **(c)** DIF cropped, **(d)** ADD cropped. 235

69 Accuracy and loss training curves for ResNet-50 model: **(a)** DIF, **(b)** ADD, **(c)** DIF cropped, **(d)** ADD cropped. 235

70 Accuracy and loss training curves for ResNet-50 with an additional CHATT mechanism: **(a)** DIF, **(b)** ADD, **(c)** DIF cropped, **(d)** ADD cropped. 236

71 Accuracy and loss training curves for ADD cropped input with ResNet-50 and: **(a)** an additional SE layer and **(b)** a SPATT mechanism. 236

72 Dice and loss training curves for segmentation: **(a)** DIF, **(b)** ADD, **(c)** DIF cropped, **(d)** ADD cropped. 236

73 Accuracy and loss training curves for the adapted U-Net model for classification: **(a)** DIF, **(b)** ADD, **(c)** DIF cropped, **(d)** ADD cropped. 237

74 Examples of the best (upper) and worst (lower row) cases of segmented images, along with the respective DIF, ADD, DIF cropped, and ADD cropped inputs. 237

75 Accuracy and loss training curves for the ablation studies: **(a)** erased background, **(b)** different and random hospital background, and **(c)** frames of **(b)** but classes were constrained to STOP and WALK. 238

List of Tables

1 Main smart walkers in literature and their respective target population, sensors, mode(s) of operation and functionalities 17

2 Included studies in the literature review of decoding the user's motion intentions: type of sensors, location, sampling frequency, and intention to decode 23

3 Approach, the AI-based model, the input, the calculated features, the evaluation and normalization method, the participants, metrics, and the main results extracted from the included manuscripts 24

4 Included studies that present and discuss both biofeedback strategies and exergames for ataxia rehabilitation 39

5 SUS scores for the experimental validation of the optimised GUI of WALKit Smart Walker 59

6 SUS scores for the experimental validation of the developed clinical feedback tool 64

7 Number of input frames of the model for each dataset split 75

8 Validation results, in percentage, of the VGG16 and ResNet-50, as well as the training time, in hours 78

9 Percentage of correct classifications for both models (VGG16 and ResNet-50) and for each input regarding the test split 79

10 Quantative evaluation results, in percentage, for validation Grad-CAM, when predicting with the VGG16 and ResNet-50 models 80

11 Validation results, in percentage, of ResNet-50 with a CHATT mechanism, as well as the training time, in hours 80

12 Quantative evaluation results, in percentage, for validation Grad-CAM, when predicting with the ResNet-50 model with the CHATT mechanism 81

13 Percentage of correct classifications for ResNet-50 with the CHATT mechanism and for each input regarding the test split 82

14 Validation results, in percentage, of ResNet-50 with both SE layer and a SPATT mechanism, as well as the training time, in hours 85
15 Test results, in percentage, of ResNet-50 with both the SE layer and the SPATT mechanism 86
16 Quantative evaluation results, in percentage, for validation Grad-CAM, when predicting with the ResNet-50 model with both the SE layer and the SPATT mechanism 87
17 Validation results, in percentage, of the U-Net model, as well as the training time, in hours, for 30 epochs 89
18 Validation results of the adapted U-Net classification model as well as the training time, in hours, for 100 epochs 90
19 Quantitative focus evaluation results, in percentage, of the validation Grad-CAM, when predicting with the adapted U-Net model for classification 90
20 Accuracy value, in percentage, for the tested trials in offline simulations for both ResNet-50 with CHATT and the SE layer with r $= 16$ 92
21 Delays of the final predicted labels in relation to the respective GT labels, considering the specific trials of participants 11 and 15 94
22 Validation results, in percentage, of ResNet-50 with erased background and with a random background 95
23 Test results, in percentage, of ResNet-50 with erased background and with random hospital backgrounds 95
24 Validation and test results, in percentage, and training time, in hours, for dual-class classification model with different backgrounds 97

25 Overall precision and recall for the AI-based model of the proposed HIL control strategy, considering the GT labels and the model's prediction after the post-processing algorithm 106
26 Delay estimated between the GT labels, obtained with a remote control and by visual inspection, and the raw prediction of the model (D_1) and the final label after post-processing (D_2), considering the STOP to WALK and WALK to STOP transitions 108
27 Operation times, in ms, of the proposed HIL control strategy with WALK and STOP classes. The pre-process time corresponds to the time of preparing the input frame . . . 112
28 KTE values (m) registered for the both the ADS and the proposed strategy 120
29 URC, in percentage, registered all over the five scenarios tested with the shared control strategy 124

30 RMSE of both sensor fusion algorithms considering static trials 139
31 RMSE for the different activities that healthy individuals performed and considering both the KF and CF and AP (pitch) and ML (roll) axes 141
32 Difference in ROM of the CoM position between trials with and without biofeedback, the corresponding mean, standard-deviation, and *p*-value, considering the different activities and participants 146
33 Difference in ROM of the CoM position between trials with and without biofeedback, the corresponding mean, standard-deviation, and *p*-value, considering the extra trials 147
34 SUS scores of the proposed biofeedback system 148
35 SUS scores for the proposed postural control and weight transfer game 155

36 General overview of all participants of this intervention study 163
37 Intervention programme of training phase 1 165
38 Intervention programme of training phase 2 165
39 Gait-related spatiotemporal outcomes that were evaluated in this study 168
40 SARA sub-scores of gait, stance, and sitting balance for both RAGT and TAGT. A negative variation represents improvement on day 16 171
41 Total ROM and gain on day 16 obtained for all participants, considering BBS 2, 7, and 13, both day 0 and day 16, and the 98% most representative data 182
42 Forward displacement of right arm considering exercise 8 of BBS 185
43 Torso inclination (pitch) considering exercise 8 of BBS 186
44 Time, in seconds, to complete exercise 9 of BBS 186
45 Descent and ascent time, in seconds, to complete exercise 9 of BBS 187
46 Torso rotation, in degrees, while performing exercise 10 of BBS 187
47 SUS scores for the experimental validation of WALKit SRW with pathological users . . . 189
48 SUS scores for the experimental validation of the proposed BS with pathological users . 189
49 SUS scores for the experimental validation of the proposed non-immersive VR-based exergame with pathological users 190

50 Portuguese version of the SUS [119] 227

51 10-MWT and TUG times, in s, for both RAGT with WALKit and treadmill-assisted training. 239
52 Spatiotemporal parameters obtained for each trial of the 10-MWT considering both interventions (WALKit and treadmill) 240

53 TUG times and BBS scores of both day 0 and day 16 considering RAGT with WALKit and an additional biofeedback strategy 241
54 TUG times and BBS scores of both day 0 and day 16 considering RAGT with WALKit and an additional VR-based exergame 241

Acronyms

10-MWT 10-Meter Walk Test

20-MWT 20-Meter Walk Test

2CA-Braga Clinical Academic Centre of Braga

AAN Assist-As-Needed

ADS Autonomous Driving System

AES Advanced Encryption Standard

AI Artificial Intelligence

AP Anteroposterior

BBS Berg Balance Scale

BiRDLab Biomedical Robotic Devices Laboratory

BoS Base of Support

BS Biofeedback Systems

BWS Body-Weight Support

CA Cerebellar Ataxia

CCU Central Control Unit

CF Complementary Filter

CHATT Channel-Wise Attention

CMEMS Centre for Microelectromechanical Systems

CNN Convolutional Neural Networks

CoG Centre-of-Gravity

CoM Centre-of-Mass

COP Centre-of-Pressure

CoP Centre-of-Pressure

CRUD Create, Read, Update, Delete

DL Deep Learning

DNN Deep Neural Networks

DOF Degree-Of-Freedom

DWA Dynamic Window Approach

EML Equipamento Multifuncional de Auxílio Técnico à Locomoção

FC Fully Connected

FOV Field-of-View

GAP Global Average Pooling

GDPR General Data Protection Regulation

Grad-CAM Gradient-weighted Class Activation Mapping

GT Ground Truth

GUI Graphical User Interface

HAR Human Activity Recognition

HIL Human-in-the-Loop

HMI Human-Machine Interface

HRC Human-Robot Collaboration

HRI Human-Robot Interaction

HRS Human-Robot System

HS Heel Strike

HTA Health Technology Assessment

IA Instantaneous Accuracy

ICARS International Cooperative Ataxia Rating Scale

IDE Integrated Development Environment

ILOCA Idiopathic Late Onset Cerebellar Ataxia

IMU Inertial Measurement Units

IoU Intersection over Union

IRS Infrared Sensors

KF Kalman Filter

KNN K-Nearest Neighbors

KPI Key Perfomance Indicators

KTE Kinematic Estimation Error

LRF Laser Range Finder

LSTM Long Short-Term Memory

MI Motion Intention

ML Mediolateral

MSA Multiple System Atrophy

MSE Mean Square Error

ONNX Open Neural Network Exchange

PCA Pilocytic Astrocytoma

PD Parkinson's Disease

PID Proportional-Integral-Derivative

PPO Proximal Policy Optimization

PRISMA Preferred Reporting Items for Systematic Reviews and Meta-Analyses

QoL Quality of Life

RAGT Robot-Assisted Gait Training

RGB-D Red Green Blue and Depth

RL Reinforcement Learning

RMSE Root Mean Square Error

ROI Region-of-Interest

ROM Range-Of-Motion

ROS Robot Operating System

RTOS Real-Time Operating System

SARA Scale for the Assessment and Rating of Ataxia

SCA Spinocerebellar Ataxia

SCI Spinal Cord Injury

SDLC Software Development Life Cycle

SE Squeeze-and-Excitation

SFA Single-Factor Authentication

SG Serious Games

SGD Stochastic Gradient Descent

SLAM Simultaneous Localization and Mapping

SPATT Spatial Attention

SR Symmetry Ratio

SRW Smart Robotic Walker

SUS System Usability Scale

SVM Support Vector Machine

TAGT Treadmill-Assisted Gait Training

TBI Traumatic Brain Injury

TL Turn Left

TO Toe-off

TR Turn Right

TUG Timed Up and Go

UN United Nations

URC User Relative Control

US Ultrasonic Sensors

VR Virtual Reality

WHO World Health Organization

Chapter I

Introduction

Chapter 1

Introduction

This doctoral thesis presents the main work developed in the last four years related to the project entitled *User-adaptive autonomous robotic walker driven by artificial intelligence for ataxic rehabilitation*, financed by FCT - *Fundação para a Ciência e Tecnologia* - under grant 2020.05708.BD, in the scope of the Doctoral Program in Biomedical Engineering from University of Minho. This work has been developed in the Biomedical Robotic Devices Laboratory (BiRDLab) at the Centre for Microelectromechanical Systems (CMEMS) of University of Minho, Portugal, considering the scientific advice of Professor Doctor Cristina P. Santos, Professor Doctor João Cerqueira, and Doctor Joana Figueiredo, and support of WALKit team members of BiRDLab, and Clinical Academic Centre of Braga (2CA-Braga).

This doctoral thesis followed the R&D project "Equipamento Multifuncional de Auxílio Técnico à Locomoção (EML)" and aimed to optimize a Smart Robotic Walker (SRW) named ASBGo, which is being developed by BiRDLab in partnership with ORTHOS XXI, a leading company of orthopedics in Portugal, Tecnicunha, and 2CA-Braga. This work intended to optimize this device with personalized Assist-As-Needed (AAN) mobility assistance considering the user's needs and Motion Intention (MI) driven by Artificial Intelligence (AI), and novel and interactive Human-Robot Interaction (HRI) strategies to support human-robot symbiosis towards a more effective motor rehabilitation. Furthermore, this work intended to validate the proposed robotic device with end users at Braga Hospital, through clinical evidence and usability, providing a significant advance in the status of Robot-Assisted Gait Training (RAGT).

1.1 Motivation

Gait disorders **significantly affect Quality of Life (QoL)**, affecting the independence and social interactions of individuals. According to the World Health Organization (WHO), nearly 16% of the world's population suffer from some form of disability [1, 2]. Dysfunctional gait, for example, was considered one of the most common disabilities in Europe [3]. These disorders result from a variety of causes, including

neurological conditions such as Cerebellar Ataxia (CA) and Parkinson's disease, orthopedic problems, and other medical conditions such as obesity or tumors [4, 5]. Among these, CA, resulting from dysfunction of the cerebellum due to acquired causes (*e.g.*, cardiovascular disorders or neurodegenerative disorders involving the cerebellar pathways) or inherited, although rare [6], is particularly debilitating. Among other functions, the cerebellum plays an important role in gait and postural control by regulating the movement of the limbs. Thus, damage to the cerebellum leads to gait abnormalities [5].

The prevalence of hereditary ataxia varies around the globe, as shown on Figure 1, and depends on the population's genetics [6]. A systematic review conducted by Ruano *et. al.* [7] reported an average prevalence of 2.7 per 100000 for autosomal dominant hereditary ataxia, being Machado-Joseph disease (Spinocerebellar Ataxia (SCA) type 3) the most prevalent, and an average of 3.3 per 100000 for autosomal recessive ataxia, being Friedreich ataxia the most common. Regardless of its etiology, CA is **profoundly debilitating**, characterized by **incoordination of the lower limbs**, **gait variability**, and **postural instability**, leading to **loss of balance** and **reduced mobility** [8]. Ataxic gait is characterized by an unstable and stumbling walk, with variable foot placement, decreased step length and gait speed, increased step width, and postural sway [5, 9, 10]. The latter is particularly present when standing considering both Anteroposterior (AP) and Mediolateral (ML) axes [11]. In fact, the literature shows that the increased step width is considered a compensatory mechanism of patients to increase the limits of their Base of Support (BoS), and the reduced step length may be related to another compensatory mechanism to reduce the time of single support [12]. These patients additionally report an increased fear of falling, which contributes to a progressive immobilization [13]. Furthermore, when inherited, the gait impairment is progressive, culminating in permanent disability [7]. Consequently, the patients' QoL is **highly impacted**, affecting their daily life activities and **social well-being** [9, 14].

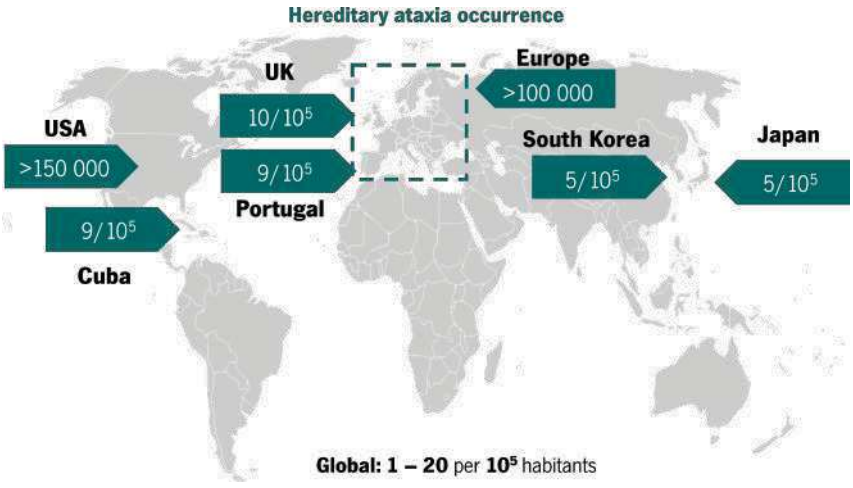


Figure 1: Worldwide prevalence of cerebellar ataxia according to study [6].

Currently, evidence of pharmacological treatment is still limited. There is no approved pharmacological treatment for inherited ataxias [15], while acquired ataxias can generally be improved if the underlying cause is diagnosed and treated. **Intensive physical rehabilitation is, therefore, the mainstay of ataxia treatment**. Indeed, patients require intensive and regular physical intervention to maintain motor function and to control their symptoms [10, 16]. This, in turn, involves multidisciplinary teams and requires **a huge effort and commitment** from therapists [3].

Several studies that analyze the effects of rehabilitation in persons with some type of ataxia have been presented [17, 18]. Milne *et. al.* [17], inclusively, presented a systematic review of rehabilitation for individuals with genetic degenerative ataxia. The authors of the included studies verified that the rehabilitation interventions, that included coordination and balance training, balance exercises with biofeedback and, among others, treadmill training, improved function, mobility, and balance. Tercero-Pérez *et. al.* [18] also concluded that moderate and intensive training in patients with SCA type 7 allowed a significant improvement in the Scale for the Assessment and Rating of Ataxia (SARA) score when compared with a control group, that was subject to no training. This improvement was particularly evident in SARA sub-scores regarding gait and dysmetria, which is the inability to perform accurate and smooth movements.

An effective comprehension of the rehabilitation effects may enable the development of more effective, time-efficient, and user-oriented therapies. According to the literature, the interventions should be **intensive and challenge balance, must be individualized and, above all, should be motivating** [10]. However, given the growing pressure on healthcare services, clinicians simultaneously attend to several patients in a constrained time, thus these requirements are hard to meet. Consequently, new strategies should be proposed to overcome this difficulty, namely to create complementary means of rehabilitation that **i)** promote motor skills learning and training to patients; **ii)** provide repetitive and intensity-adapted rehabilitation scenarios; and last but not least, **iii)** reduce the heavy burden of manual therapy to clinicians. The ultimate goal of these complementary means is to alleviate the pressure on palliative care and health services in general, and hopefully help optimize both resources and costs [3, 14].

Assistive technologies have shown promising results in providing independence and improving the patients' participation in their rehabilitation therapies [1]. RAGT has been growing significantly and playing a pivotal role not only in enhancing the rehabilitation effectiveness by allowing more symmetric gait patterns, reproducible and intensity-adapted training, but also alleviating the therapists' burden by offering a collaborative and supportive approach. Furthermore, robots are equipped with several sensors that constantly analyze and collect data from patients [3], allowing for a more accurate assessment through

objective data that can help refine and personalize therapies.

As with other pathologies [3, 19], RAGT is being introduced in the rehabilitation of patients with ataxia [20–24], and some results have been promising, justifying the development of these devices and encouraging their future integration into health services, which is already happening in some clinics and rehabilitation centers of Portugal with the Lokomat exoskeleton. More specifically, the authors of [20] presented a case study of an adult patient undertaking overground therapy with UAN.GO®exoskeleton. They found an improvement of SARA, Berg Balance Scale (BBS), the distance traveled at 6-Minute Walking Test, and more physiological spatiotemporal parameters. Another study, [21], also concluded that chronic stroke patients with ataxia presented significant improvements in balance and independence, either with RAGT with Lokomat®exoskeleton and Therapy-Assisted Gait Training, with no significant differences between groups (with/without RAGT). Hong *et al.* [22], in their study, also found that RAGT with a wearable exoskeleton allowed an improvement of gross motor and gait functions in pediatric gait disorders, namely cerebral palsy, CA, and chronic traumatic brain injury. Also in the field of pediatric diseases, Yoo *et al.* [23] presented two case reports of children with ataxic cerebral palsy, and the authors emphasized the significance of RAGT, together with conventional therapy, in improving balance and functional walking ability. Lastly, a 15-day protocol with curara®robot revealed a motor improvement of patients with degenerative ataxia [24].

Indeed, several studies have motivated the further development of these devices, which actually have a **major impact on society and on these patients' lives**. Even though the results point to improvements, their study and development must continue. In this way, it directly contributes to the success of the 2030 Agenda for Sustainable Development, presented by the United Nations (UN), namely the third and ninth goals, which aim to **ensure healthy lives and promote well-being for all at all ages** and **foster innovation**, respectively. This doctoral thesis actively pursues this motivation, continuing the development and optimization of a robotic device, the ASBGo Smart Walker, whose main purpose is to improve the QoL of patients with CA.

1.2 Problem statement

In addition to intensive rehabilitation, ataxic patients require assistive devices, including canes and walkers, to enhance residual locomotion and foster independence in daily activities [25]. Conventional walkers, for instance, improve the patient's static and dynamic stability by offering BoS [25, 26]. For ataxic patients, this BoS is important given their poor balance and multi-articular coordination. However, accord-

ing to [26], between 30% and 50% of users stop using their mobility aids. Many difficulties may explain this behavior, but self-prescribed assistive devices, inadequate user training and poor usability that leads to heavy difficulties in using the device, often with high cognitive demands, may be the probable causes. Moreover, conventional walkers, in their configurations, may **i) augment the user's walking energy expenditure** by requiring increased force levels of the upper limbs (standard walker), **ii) increase the risk of falls**, specially for rollators in situations where patients require full Body-Weight Support (BWS), and **iii) compromise the dynamic stability during walking**, namely for the two-wheeled walkers and rollators [25]. Further, assistive devices should be **tailored to each patient** such that the resulting assistance just provides the required aid while still fully engaging the patient in the treatment. Each patient has his own disability level and needs, which further change during the rehabilitation process, so the assistance the device provides should vary accordingly. Therefore, there is a considerable need for advanced rehabilitation devices that not only provide patients with repetitive and effective therapies and personalized and AAN strategies, but also provide stability, confidence, safety, and relieves clinicians from the burden of manual therapy. A solution may be the use of RAGT and, for CA patients, multi-functional SRWs due to their need for BWS in more severe ataxias.

Current SRWs endow several functionalities, mainly based on embedded or wearable sensors. These functionalities include MI decoding [27–32], navigation assistance [27, 28, 33–35], and shared driving mode [30, 36, 37]. Additionally, some include tools able to objectively analyze the user's gait [38–41], primarily based on biomechanical parameters, including both spatial (*e.g.*, stride length, step length, step width) and temporal gait metrics (*e.g.*, stride duration, stance/swing duration, step time, double support time). In general, SRWs show a strong potential for becoming a prominent intervention to tackle the necessity of physical rehabilitation therapies for ataxic patients based on highly intensive and personalized gait training. However, most of the available SRWs **present poor clinical evidence**, and current solutions for personalized assistance strongly rely on **expensive sensors or demand environments specially designed for the application**, which highly compromise a possible deployment to the market for home and hospitals, nursing homes, or rehabilitation centers. This is especially relevant if one aims the SRWs to be included in standard rehabilitation for ataxic people.

Current challenges are manifold. At the perception level, it is necessary to decode MI indirectly from multi-modal built-in sensors to timely trigger the assistance delivered by the SRW. Despite recent advancements, most of the MI decoding tools integrated into SRWs rely on **direct ways of giving the intention** by using force-sensing technology, which are not reliable in the long-term when considering low-cost options [35]. Additionally, strategies that do not consider direct ways of measuring the user's

intention, make use of **expensive sensors**, namely 2D laser technology [32], or wearable ones, namely Inertial Measurement Units (IMU). Although inertial units are a low-cost solution when compared to other technologies (reliable force sensors or lasers), these may cause **discomfort for daily use, considering a high number of sensors**, especially when dealing with persons with reduced mobility. Furthermore, it may increase the time of intervention sessions since it requires specific setups, adding an extra task to physiotherapists, which directly contributes to increase the burden of care. Some SRWs present cameras embedded in the device, but **few explore its information for action recognition and MI decoding**. Thus, it is important to investigate more intuitive and yet technological advanced solutions to early decode MI and use this information to further control SRWs to follow human motion based on active human involvement. Therefore, this doctoral thesis tackles the issue of MI decoding using a reliable, yet low-cost approach by using Red Green Blue and Depth (RGB-D) cameras through Deep Learning (DL) algorithms. This novel HRI strategy would be relevant for later stages of intervention since: **i)** it encourages the user's active participation, **ii)** it increases the user's autonomy and sense of involvement and control of the device, **iii)** it enables the user to fully focus on their gait performance, addressing the training of trunk sway control and the refinement of foot position, possibly contributing to the improvement of dysmetria, and **iv)** it enables the physiotherapist to focus on analyzing, correcting, and improving gait.

At the control level, new algorithms should be explored to achieve targeted and personalized assistance. In fact, as stated previously, SRWs must be able to recognize the user MI and guide the device accordingly in an intuitive manner, towards a Human-in-the-Loop (HIL) approach. However, dealing with pathological users, it is natural that this demands the incorporation and exploration of AAN strategies, namely incorporating an "entity" that supervises the users' behavior and **assist them as and when necessary in dangerous situations**. Additionally, this would also relieve physiotherapists from other secondary tasks, as verifying if the user is correctly steering the device, without colliding with any potential static or dynamic obstacle, and **focusing their full attention into gait accuracy and postural control**.

Another challenge consists of monitoring constantly the end-user through embedded and reliable sensors and use this information to give biofeedback considering novel HRI strategies. Biofeedback Systems (BS) use patient-related parameters acquired with both embedded or wearable sensors, and provide patients with visual, auditory, and/or vibrotactile cues [42]. With this, patients can have immediate feedback of their performance in activities and, consequently, self-correct their behavior. This may potentiate neuroplasticity, *i.e.*, the central nervous system reorganization, contributing to the patients' motor relearning [43]. Recent research suggest that BS are a useful tool to complement RAGT [44], since they provide

intuitive HRI and Human-Robot Collaboration (HRC). Despite that, **biofeedback is still not commonly used in the rehabilitation of ataxic people while using SRWs**. Therefore, it is paramount to develop different BS integrated into just one device to **accelerate the motor recovery of CA patients** and assess its effectiveness in providing intuitive cues that may contribute to more time-efficient gait and posture rehabilitation. Therefore, this doctoral thesis explored multi-modal biofeedback and more advanced technology, namely incorporating Virtual Reality (VR), to increase the system's acceptability and efficacy and enable its use by ataxic patients with variable sensory deficits and disease levels.

Lastly, although RAGT is starting to be applied to CA rehabilitation, more evidence is still needed to emphasize the role of RAGT to investors, innovation agencies, and healthcare systems, so it can become a gold standard in rehabilitation. Additionally, recent studies are mainly related to acquired CA, so **there is still the need to verify if this is also beneficial for individuals with hereditary degenerative CA**, which is strongly characterized by progressive damage of motor skills. This doctoral thesis tackles this issue by involving patients from Braga Hospital considering a proof-of-concept validation protocol of WALKit SRW.

1.3 Goal and Objectives

This doctoral thesis aimed to improve the treatments and facilitate walking of ataxic patients via smart rehabilitation in a multidisciplinary manner. The main goal was to present the next generation of ASBGo Smart Walker, optimizing this prototype with cutting-edge technologies to assist users during gait and posture training. Specifically, this thesis aimed to study AI-based tools for monitoring the user from the SRW multimodal sensor information, and thereby design and implement a HIL control strategy that adapts the linear velocity of the device to the MI in an intuitive, fast but smooth manner. The aim is to provide more natural and seamless assistance, according to the user's intentions, without any additional cognitive or physical effort. In addition, this doctoral thesis also aimed to introduce the AAN concept into the device's control, where the device analyzes the user's commands and the environment and assists when necessary to ensure the safety of ataxic patients. Another goal was to develop monitoring algorithms of posture and balance, which are severely affected in patients with ataxia, and thereby develop novel HRI and HRC strategies. These included a BS that guide patients during their rehabilitation, and the exploration of Serious Games (SG) based on VR that encourage users' participation and improves their motivation. Finally, another objective was to introduce this renewed device into gait, posture and balance training sessions for ataxic patients. The aim was to analyze its rehabilitative effects and to take a step forward in

the use of robotic walkers in the rehabilitation of CA.

To achieve this main goal, several objectives were identified, measured by Key Perfomance Indicators (KPI):

- **OB. 1: To conduct a detailed and critical literature review on robotic walkers and their main functionalities**, including: **i)** decoding MI in robotic walkers and ways to control the device according to this information; **ii)** assistive control strategies implemented in robotic walkers; and **iii)** development, incorporation, and effects of biofeedback strategies and/or serious games in the rehabilitation of ataxic patients. The KPI 1 for this objective is a critical analysis of the current state-of-the-art, that will serve as the basis to tackle the challenges inherent to gait and posture analysis, biofeedback and control. Chapter 2 addresses this objective.

- **OB. 2: To optimize the SRW software, developing an user-friendly Graphical User Interface (GUI) and a new clinical support and feedback tool**, with high usability and functionality, for clinicians to verify the patients evolution throughout therapy. This objective is measured by KPI 2, considering the validation of the renewed software with final users, achieving a minimum System Usability Scale (SUS) [45, 46] of 70 points, according to grading scale of SUS [47]. Chapter 3 addresses this objective.

- **OB. 3: To develop and deploy a MI decoding algorithm** in WALKit SRW, exploring AI-based algorithms, namely DL, to timely recognize the users' intention to walk, turn, and stop. This AI-based algorithm will be the basis for a HIL assistive control strategy. This objective is measured by KPI 3, considering a minimum accuracy, precision, recall, and F1-score of 95% for the best model. Moreover, this objective also aimed to evaluate how the model is early decoding the user's MI, using explainable AI, namely Gradient-weighted Class Activation Mapping (Grad-CAM). Additionally, to quantify if the AI model extracted features within the human body region, a KPI 4 was considered, namely Dice and Intersection over Union (IoU) metrics, that should be at least 50%. Chapter 4 addresses this objective.

- **OB. 4: To implement closed-loop motion control strategies, focusing on AAN and HIL approaches**, to tailor the walker's assistance autonomously considering the patient's MI. This objective aims: **i)** to deploy the best AI model of OB. 3 in WALKit SRW modular architecture, and verify if it timely triggers the walker's assistance according to the user's commands; and **ii)** to deploy an AAN shared control strategy in WALKit SRW that encourages the user engagement in controlling the device, while ensuring his/her safety considering the surrounding environment. This objective

is measured by KPI 5 and 6: **i)** KPI 5 is related to the first assistive control strategy, including: the delay in early recognizing the user's intention, that should be less than 0.64s (average step time while walking with the device at the highest speed), an Instantaneous Accuracy (IA) of at least 95%, following OB. 3, and a minimum operating frequency of 15 Hz so as not to incur aliasing in the gait analysis; **ii)** KPI 6 is related to the second assistive control strategy, including: a Kinematic Estimation Error (KTE) higher in comparison with that observed when the SRW is controlled by the Autonomous Driving System (ADS), a User Relative Control (URC) higher than 70%, and an ideal operation frequency of 10 Hz. Chapter 5 addresses this objective.

- **OB. 5: To devise and deploy novel and intuitive HRI strategies that encourage the user's active participation, increasing motivation and maximizing rehabilitation outcomes**. This objective considers the implementation of monitoring algorithms in WALKit SRW to assess postural control and balance and use this information along with a BS and a SG. The BS aims to indirectly reduce the Centre-of-Mass (CoM) sway, providing improvements in functional balance of ataxic. As for the SG, it aims to explore non-immersive VR for balance training, focusing on weight transfers. This objective is measured by KPI 7 and 8. KPI 7 is related to the proposed BS that should be validated with at least 5 healthy individuals, assessing mainly usability with a minimum SUS of at least 70 points, and functionality with a decrease of the total Range-Of-Motion (ROM) of CoM sway; and validated with, at least, 3 pathological participants, with improvements on static balance measured by an increase of BBS, a decrease of Timed Up and Go (TUG) test, and a decrease of total ROM of CoM sway after RAGT. In addition, it is expected a high usability and acceptability of the BS with SUS scores above 70 points. As for KPI 8, this is related to the proposed SG, that should be validated with at least 5 healthy participants assessing mainly usability with a minimum SUS of at least 70 points; and validated with, at least, 3 pathological participants, showing an improvement on weight-shifting balance considering an increase of BBS and specific sub-scores of weight transfer assessment, and a decrease of TUG. Lastly, it is also expected a high usability and acceptability with SUS scores above 70 points. Chapters 6 and 7 address this objective.

- **OB. 6: To perform a clinical study in hospital environment, validating WALKit SRW considering usability and recovery of motor control in ataxic rehabilitation**, performing benchmark against actual interventions, namely treadmill-assisted gait training. This objective aims to assess the main effects of using RAGT with WALKit SRW in patients diagnosed with CA, considering mainly kinematic measures and gold standard clinical assessment scales, namely SARA,

10-Meter Walk Test (10-MWT), and TUG. This objective is measured by KPI 9, considering: **i)** a decrease of SARA, 10-MWT, and TUG test after RAGT, **ii)** an improved gait speed and a decreased gait asymmetry, and **iii)** a minimum SUS of 70 points, ensuring technology acceptance. Chapter 7 addresses this objective.

1.4 Research Questions

The outlined objectives, namely the literature review (**OB. 1**), the software renewal (**OB. 2**), the MI decoding tool (**OB. 3**), the novel control strategies and HRI strategies (**OB. 4** and **5**, respectively), and the clinical interventions (**OB. 6**), will allow answering to the following research questions (RQ):

- **RQ. 1:** How can the motion intention be decoded in a more intuitive way and be used to foster personalized assistance? This research question is related to **OB. 1**, **OB.3**, and **OB.4**.
- **RQ. 2:** How to encourage the user's active participation in therapy while reducing the workload of the physiotherapist? This research question is related to **OB.4** and **OB.5**.
- **RQ. 3:** How does multimodal biofeedback affect postural sway control of users? This research question is related to **OB.5**.
- **RQ. 4:** How usable and functional is WALKit Smart Walker? This research question is related to **OB.2** and **OB.6**.
- **RQ. 5:** How does RAGT with WALKit Smart Walker affects motor rehabilitation of patients with cerebellar ataxia? This research question is related to **OB.6**.

1.5 Contributions to Knowledge

This doctoral thesis contributes with an optimised prototype of ASBGo Smart Walker, renamed to WALKit Smart Walker, which has culminated in completely renewed software with several new functionalities that were integrated into just one device, namely: **i)** AI-based tools for motion decoding; **ii)** novel, personalized, and intuitive control strategies that increase the device's compliance to the user's intentions; and **iii)** motivating, interactive, and innovative HRI and HRC strategies, contributing to the technological innovation of RAGT. Furthermore, this doctoral thesis investigates and evaluates the motor effects of using

this new prototype in gait, posture, and balance rehabilitation of patients with CA considering a clinical intervention with final users from Braga Hospital. Consequently, this doctoral thesis provides a considerable step forward in clinical research and technological innovation, following the 2030 Agenda for Sustainable Development presented by UN, contributing with:

- A **detailed and critical analysis of recent advances in literature** related to the perception of MI in robotic walkers and the use of this information to control the device (Chapter 2 and OB. 1);
- A **detailed analysis of recent advances in literature** related to the use of BS and SG for the rehabilitation of gait and balance in patients with mobility disorders (Chapter 2 and OB. 1);
- A **redesigned, innovative prototype with advanced technology** specially designed for the rehabilitation of balance disorders, featuring: **i)** a **completely redesigned software with high usability and acceptability** from stakeholders (clinicians); **ii)** a **sophisticated and yet user-friendly Clinical Support and Feedback Tool**, with high scores of usability, that will help clinicians to manage the rehabilitation sessions with WALKit Smart Walker, to implement clinical evaluation protocols, and to assess the user's progression throughout therapy, acting as a complement tool to be used with WALKit SRW (Chapter 3 and OB. 2);
- A **comprehensive research of different AI-based approaches to detect MI** (STOP, WALK, TURN) when using WALKit Smart Walker, in order to determine the best solution for controlling the device, thereby making the robot **compliant to the user** and enabling a step forward in the development of novel personalized control strategies (Chapter 4 and OB. 3);
- **Two assistive control strategies**, namely a **HIL control strategy** based on early human MI decoding that fosters personalized assistance without additional cognitive effort and physical interaction, and an **AAN shared control strategy** that supervises the user's commands and assists or overrides accordingly to increase the user's safety and to allow patients to focus on improving their gait pattern, without having to divert their attention to possible existence of permanent and/or dynamic obstacles (Chapter 5 and OB. 4).
- **Two innovative and intuitive HRI strategies, namely an audiovisual BS and a non-immersive VR-based SG** for ataxic posture and balance rehabilitation integrated into WALKit Smart Walker, making therapy more engaging, diverse, problem-oriented, and motivating (Chapter 6 and OB. 5);

- **A clinical intervention study involving a total of six patients with CA** of Braga Hospital, allowing Health Technology Assessment (HTA) of WALKit SRW by assessing the device's **clinical impact on gait and balance rehabilitation**. This strongly contributes to the investigation on the use of RAGT in motor rehabilitation (Chapter 7 and OB. 6).

Given these contributions, this doctoral thesis has led to the production of the following manuscripts:

Publications in Journals:

- **Lopes, J. M.**, Gonçalves, C., Moccia, S., Berardini, D., Migliorelli, L., & Santos, C. P. (2023). Deep learning-based approaches for human motion decoding in smart walkers for rehabilitation. Expert Systems With Applications, 228, 120288. https://doi.org/10.1016/j.eswa.2023.120288. Gonçalves, C. and Lopes, J. M. share first authorship of the manuscript. [IF = 7.5, Q1]

- Palermo, M., **Lopes, J.M.**, André, J. *et al.* A multi-camera and multimodal dataset for posture and gait analysis. Sci Data 9, 603 (2022). https://doi.org/10.1038/s41597-022-01722-7 [IF = 5.8, Q1]

Manuscripts in submission process:

- **Lopes, J. M.**, Pereira, A. & Santos, C. P. (2025). Deep Reinforcement Learning based shared control strategy for robotic walkers.

- **Lopes, J. M.**, Matias, C., Cruz, C., Pereira, T., Cerqueira, J. & Santos, C. P. (2025). Evaluation of the effects of a biofeedback strategy integrated into a robotic walker in patients with cerebellar ataxia.

- **Lopes, J. M.**, Rodrigues, A., Matias, C., Cruz, C., Pereira, T., Cerqueira, J. & Santos, C. P. (2025). The impact of walker-assisted virtual reality exergame training on balance in patients with cerebellar ataxia.

- **Lopes, J. M.**, Matias, C., Cruz, C., Pereira, T., Cerqueira, J. & Santos, C. P. (2025). Comparing the effects of treadmill and robotic walker-assisted gait training on patients with cerebellar ataxia.

Book chapters:

- **Lopes, J. M.**, André, J., Pereira, A., Palermo, M., Ribeiro, N., Cerqueira, J., & Santos, C. P. (2021). ASBGo: a smart walker for ataxic gait and posture assessment, monitoring, and rehabilitation. In CRC Press eBooks (pp. 51–86). https://doi.org/10.1201/9781003112273-4

- Pereira, A., **Lopes, J. M.**, Afonso, J., Costa, L., Figueiredo, J., & Santos, C. (2021). Implementation and assessment of an autonomous control for human supervision replacement in a robotic walker toward an adaptive shared control. In CRC Press eBooks (pp. 280–283). https://doi.org/10.1201/9781003217152-62.

Conference presentations:

- Pereira, A., **Lopes, J. M.**, Afonso, J., Costa, L., Figueiredo, J., & Santos, C. (2021). Adaptive shared-control of a robotic walker to improve human-robot cooperation in gait biomechanical rehabilitation. Presentation at *Congresso Nacional de Biomecânica*, Porto, Portugal.

During the course of this doctoral thesis, scientific and technical support and training was provided to master's students, contributing to three Master's dissertations in Biomedical Engineering, two Master's dissertations in Informatics Engineering, and two Master's dissertation in Industrial Electronics and Computers Engineering that are still in course. Additionally, technical training was given to five Industrial Electronics and Computer Engineering students from University of Minho, and three Biomedical Engineering students, two from University of Minho and one from University of Porto, who undertook an internship program at BiRDLab.

1.6 Manuscript Outline

This thesis is organized in eight chapters. **Chapter 2** presents a review on the key topics addressed in this doctoral thesis, namely: **i)** smart walkers and their main functionalities; **ii)** methods for decoding MI in smart walkers; **iii)** control strategies in smart walkers; and **iv)** an overview of HRI strategies for postural control, gait, and balance rehabilitation in CA. **Chapter 3** introduces WALKit Smart Walker, presenting its architecture, and the respective optimizations that were addressed in this thesis, including its validation with final users from Braga and Guimarães Hospitals. **Chapter 4** presents the research of MI decoding, presenting the different approaches to early recognize the intention of stop, walk and turn through cameras and AI modeling. **Chapter 5** presents the development and validation of HIL and AAN control strategies, and their proof-of-concept application. **Chapter 6** presents different HRI strategies developed as part of this doctoral thesis, namely a biofeedback strategy for postural sway control, shoulder posture control and serious games for balance training through weight shifting, and their functional validation. **Chapter 7** presents the key findings of the clinical intervention study conducted at Braga Hospital, in collaboration with 2CA-Braga. Lastly, **Chapter 8** presents the overall conclusion and future prospects of this doctoral thesis.

Chapter II

Literature Review

Chapter 2

Literature Review

2.1 Introduction

In the last decades, the high incidence of neurodegenerative and cardiovascular disorders worldwide has led to an increase of gait disabilities. The use of assistive devices for gait rehabilitation and assistance helps to restore the gait pattern, decreases the lower-limbs asymmetry, and provides support. With the introduction of robotic devices, new strategies as user-oriented therapies can be developed, enhancing the users' recovery.

In this chapter, the literature review regarding the objectives proposed in this doctoral thesis will be addressed. In a first phase, current smart walkers of the literature will be presented, discussing their sensors, functionalities, and target population. Subsequently, a more in-depth analysis of current methods of decoding MI in smart walkers and the use of HRI strategies will be addressed, namely the use of BS and SG. Its relevance for the rehabilitation of mobility disorders will be highlighted to sustain its integration into WALKit Smart Walker.

2.2 An overview to smart walkers

Walkers are a very common medical device, usually associated with the elderly due to their need for support, attempting to overcome gait difficulties experienced with advancing age and the gradual loss of balance. Despite their considerable rehabilitation potential for patients with gait and balance disabilities [25, 48], conventional walkers present some limitations that justify the research of novel ways to accomplish a more effective assistance and rehabilitation by following a more user-centered approach. In order to harness the benefits of walkers, but overcome their shortcomings, researchers developed SRWs, an evolution of conventional walkers that gather the concepts of medical robotics, control, and automation, to create fully assistive devices. Table 1 presents some of the most cited SRW of literature, their sensors,

modes of operation, and functionalities.

Table 1: Main smart walkers in literature and their respective target population, sensors, mode(s) of operation and functionalities

Study	Target population	Sensors	Modes of operation	Functionalities
PAMM [49]	Elderly	Sonar, camera, force sensor	User-control, path following	Obstacle avoidance, localization, and health monitoring.
GUIDO [27, 28]	Visually impaired	Laser, sonar, buttons in the handlebar	User-control, autonomous mode	Voice feedback, obstacle avoidance, localization, navigation, decode user's turning intention.
i-Walker [29, 30]	Elderly and motor-impaired	Force sensor, inclinometer	User-control, cooperative mode, adaptive mode	Decode user's intention, navigation, safety mechanism
JARoW [31, 32]	Elderly	Infrared sensor, laser	User-control	Decode user's intention, obstacle detection
Simbiosis [50]	Elderly and motor-impaired	Force sensor, sonar	User-control	Physical support, decode user's intention, gait monitoring.
CAIROW [33]	Parkinson patients	Laser, camera, force sensor	User-control, autonomous mode	Decode user's intention, obstacle detection, graphical user interface, localization, path planning and navigation.
UFES [25, 51]	Elderly and motor-impaired	IMU, laser, force sensor	User-control	Physical support, decode user's intention, visual feedback for path following, obstacle detection, gait monitoring.
N/A [52, 53]	Elderly	Force sensor, IMU[a]	User-control	Decode the user's intention, observation of user status, fall detection, safety mechanisms.

Table 1: (continuation)

Study	Target population	Sensors	Modes of operation	Functionalities
MOBOT [34]	Elderly	Force sensor, laser, cameras, microfone	User-control and autonomous	Decode the user's intention, sit-to-stand, stand-to-sit assistance, voice command, gesture recognition, fall detection, navigation, obstacle avoidance.
ISR-AIWALKER [35]	Motor-impaired	Infrared and RGB-D cameras	User-control, navigation assistance	Decode user's intention, gait monitoring and analysis, gait classification, navigation assistance.
AGoRA [36, 37]	Elderly and motor-impaired	Laser, sonar, force sensor, camera	User-control, supervised and autonomous	Decode user's intention, detect user's presence and support, localization, path planning, and navigation, obstacle detection, gait monitoring.
FriWalk [54]	Elderly	Camera	User-control and Robot-control	Navigation assistance with shared control.

According to Table 1, the most cited SRWs in the literature contain multiple integrated sensors, namely lasers, ultrasonic sensors, force sensors, cameras, infrared sensors, and IMU. These are used to feed their main modes of operation and functionalities to a fully assistive device. All have an assistive purpose, from helping the elderly to helping people with mobility or visual impairments. All of them can be controlled by the end user, and some of them present navigation assistants and shared control architectures. With these embedded sensors, they present several functionalities, including **i)** stability and physical support, **ii)** decoding of the user's MI, **iii)** gait monitoring and analysis, and **iv)** cognitive and navigation assistance.

PAAM [49] is one well-known smart walker in literature [50]. It provides a user control mode and path following functionality. This walker is embedded with sonars for obstacle detection, a roof-facing camera for location, and force sensors to decode the user's MI. As for the GUIDO [27, 28], it is an assistive device to help the visually impaired. It includes a laser for localization and navigation and sonar sensors for obstacle detection. The walker is embedded with force sensors to detect the user's MI. It provides

a shared control architecture that gives the user as much control as possible, with the control system intervening only for safety. The i-Walker [29, 30] also provides force sensors on its handles to detect the user's interaction and MI. It offers three types of controls: **i)** a passive control, which is controlled by the end-user; **ii)** a cooperative control, since it tries to infer the end-user's path and uses this information to decide how to avoid certain obstacles along the way; and **iii)** an adaptive/submissive control, since it monitors the end-user's input and checks if he/she is resisting certain actions, adapting movements accordingly. Therefore, this walker provides analysis, support and navigation assistance [30].

JARoW [31, 32] is another smart walker, that features four omnidirectional wheels designed to assist the elderly. The first prototype [31] is embedded with Infrared Sensors (IRS) to monitor the user's legs (at shin level) and control the walker considering the user's MI. Later, the IRS were replaced by two 2D Laser Range Finder (LRF) sensors. The information gathered by the two LRF is also used to detect obstacles in the area. The Simbiosis walker is another walker to assist the elderly [50]. This walker provides body weight support by incorporating forearm support platforms in its structure. In addition, these forearm support platforms include force sensors to decode the user's MI. Since the force sensors are affected by oscillations due to trunk motion, the authors estimate the gait cadence in real time using Ultrasonic Sensors (US) by placing an emitter on the walker and two receivers on the user's feet. UFES SRW [25, 51] is another assistive device with forearm support platforms on its structure. It also provides force sensors that are used to decode the user's MI. This information is combined with a LRF to estimate the user's leg positions and two wireless IMU, one on the walker and another on the user's pelvis, to obtain the walker and human angular velocity and orientation, respectively.

The walker proposed in Ye *et. al.* [52] and Huang *et. al.* [53] also aims to help the elderly. It provides three omnidirectional wheels that allow users to move in any direction. In addition, it provides force sensors embedded in the handlebars that are used to decode the MI [52]. Later, Huang *et.al.* [53] introduced the use of wearable sensors, namely IMU in both shins, thighs, and waist, for monitoring user status, posture assessment, and fall detection. Also for the elderly population, the MOBOT [34] is another SRW that contains several functionalities, namely sit-to-stand and stand-to-sit assistance, voice command, gesture recognition, fall prevention, obstacle avoidance, and navigation. It also includes a MI decoding algorithm using LRF sensors embedded in the assistive device.

CAIROW SRW [33] is designed to assist patients with Parkinson's disease who are severely affected by gait freezing. It includes a LRF sensor, one at the front of the walker for localization, path following, and navigation, and another at the back that monitors the user's legs and detects their steps to control forward motion. It also includes force sensors (FlexiForce) to more easily and instinctively detect the user's

intention to turn. The walker offers two modes of assistance: **i)** a rehabilitation mode (*i.e., user controlled*) and **ii)** an autonomous mode.

More recent walkers include the ISR-AIWALKER [35], the AGoRA [36, 37], and the FriWalk [54]. The ISR-AIWALKER is a SRW designed to assist people with motor disabilities. It provides several functionalities, from decoding the user's MI to gait analysis using cameras. It also provides navigation assistance. Similar to the AGoRA walker [36, 37], this device also provides cameras, but for person detection. It includes LRF for environment and obstacle sensing and ultrasonic sensors for both user and low obstacle detection. Its functionalities include user MI decoding, autonomous navigation, and gait monitoring with cadence estimation. Finally, the FriWalk [54] is a robotic walker with the ability to assist the elderly with navigation, using visual cues to help the end-user follow a predefined path. In addition, it includes a "user in control" mode and a "robot in control" mode for shared control between the user and the walker that is activated when needed.

Although there has been a lot of development in smart walkers, there are still challenges in terms of continuous patient monitoring and consequent evaluation based on concrete data. Similarly, there is still room for improvement in the perception of MI and the automatic adjustment of the walker to the user's needs and intentions. For example, more research is needed towards shared control by incorporating AAN control strategies. In order to achieve the main goals and objectives outlined for this thesis, it becomes relevant to perform a literature review regarding **i)** the algorithms used to decode the user's MI; **ii)** how to use this information to control the SRW accordingly, approaching AAN and HIL strategies, and **iii)** HRI and HRC strategies applied to gait and balance rehabilitation in CA. The following subsections will present this state-of-the-art review by describing methods, formulating research questions, and presenting and discussing results. Finally, an overall conclusion will be presented.

2.3 Motion Intention Perception

The extraction of the user's MI is relevant for the control of assistive devices to tailor their assistance to the user's intentions. Decoding the MI will allow a practical and intuitive HRI that is automatically tailored to the user's intentions, making the device adaptable to each user's needs and enabling personalized assistance.

This subsection presents an in-depth literature analysis aimed at assessing how the user's MI are decoded during SRW-assisted gait. The search methodology, selection strategy, and data extraction are described. The results are then presented and discussed, highlighting the challenges that this thesis

addresses. Two research questions were formulated for this literature review, as follows **i)** What sensors and features are used to decode the user's MI in smart walkers? and **ii)** What are the typical MI addressed and what methods are used for decoding?

2.3.1 Methodology

Search methodology

An electronic search was conducted on the Scopus database until the end of 2020, searching for articles that decode the end-user MI along with SRW. The literature search followed the guidelines of Preferred Reporting Items for Systematic Reviews and Meta-Analyses (PRISMA). For that purpose, the following combinations were used: ("motion intention" OR "user intention" OR "user intent" OR "motion intent") AND ("robotic walker" OR "smart walker" OR "human companion" OR "rollator"); "user commands" AND ("robotic walker" OR "smart walker" OR "human companion" OR "rollator"); ("user commands" OR "navigation commands" OR "user intent" OR "user intention") AND ("robotic" OR "smart") AND "walker"; ("smart walker" OR "robotic walker") AND "intention"; ("robotic assistant" OR "robotic companion") AND ("human-robot" OR "human-robot interaction" OR "HRI" OR "human-robot interface" OR "human-robot coupled navigation") AND ("walking" OR "walk" OR "gait"); ("motion intention" OR "user intention") AND ("recognition" OR "classification") AND ("walker" OR "rollator"). The search was limited to title, abstract, and keywords. A manual search was also conducted considering the references of the selected articles. Review articles were not included in this literature review.

Selection strategy

Studies were included in the review if they met a list of inclusion criteria, namely: **i)** be an original article; **ii)** be written in Portuguese or English; **iii)** involve the use of smart/robotic walkers; **iv)** use embedded and/or wearable sensors to infer the user's MI; and **v)** results were published since 2010. Articles that, upon review of their abstract, were out of scope or did not fulfill the inclusion criteria, were discarded. The remainder were selected for full-text analysis.

Data extraction

To properly answer the two research questions, each included article was analyzed considering: **i)** sensor system, **ii)** sensor location, **iii)** intention to be decoded, **iv)** approach to decoding the user's intention, **v)** type/number of participants, and **vi)** main results. Additionally, if the included article used

AI algorithms, the input features, normalization method, and evaluation method were also collected.

2.3.2 Results

Figure 2 shows the flow chart of this literature review. The methodology identified 81 original records from the Scopus database. In addition, 3 records identified through other sources were also considered. Out of these, 32 papers were considered as duplicates, leaving 52 papers to be screened. For this purpose, the title and abstract were read. Of the 52 articles, 18 were excluded because they did not meet the inclusion criteria, leaving 34 full-text articles eligible. Of these, 17 articles were excluded: **i)** they were not written in Portuguese or English (n = 1), **ii)** they were out of scope (n = 4); **iii)** they were not implemented in robotic walkers (n = 2); **iv)** articles from the same project presented the same/similar results or more recent articles (n = 7), or **v)** the paper was not accessible (n = 3). Considering this, 17 studies were included for qualitative analysis. Tables 2 and 3 show the included studies and the extracted data.

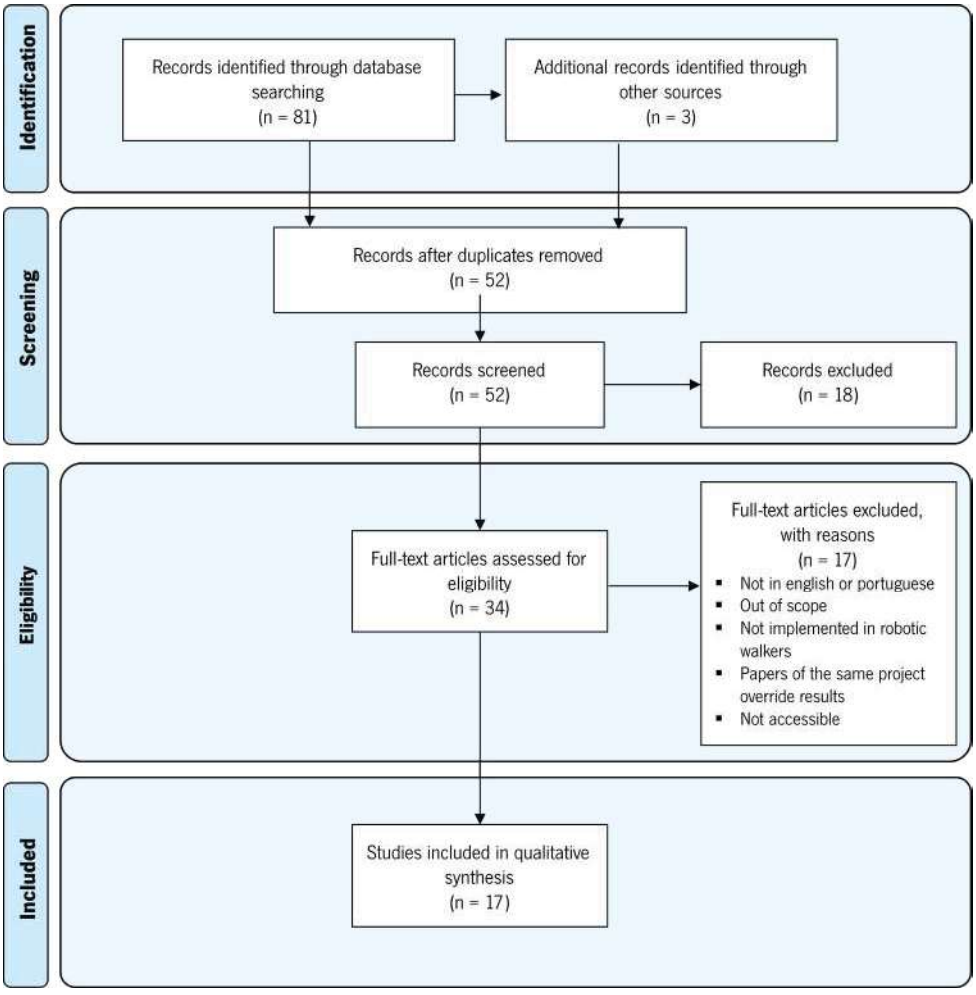


Figure 2: Flow diagram for the literature review of MI along with SRW.

Table 2: Included studies in the literature review of decoding the user's motion intentions: type of sensors, location, sampling frequency, and intention to decode

Study	Sensor			R / P	Intention to decode
	Type	Location	Sampling frequency		
[55]	Force sensors	Walker	N.M.	R	N.M.
[56]	IMU & encoder	Walker	40 Hz	R	MF, TR, TL
[57]	Camera	Walker	60 fps	R	N.M.
[58]	LiDAR & IR thermometer	Walker	N.M.	R	MF, TR, TL
[59]	Multi-channel proximity sensors	Walker	N.M.	P	User's walking intention speed at the next moment
[60]	Hall sensors	Walker (handles)	N.M.	R	MF, MB, TR, TL
[61]	Force & torque sensors	Walker	N.M.	R	MF, MB, TR, TL
[62]	LRF and RGB-D camera	Walker	LRF = 35.7 Hz	P	Human trajectory over a time horizon
[36]	Tri-axial load cells	Handles (Walker)	N.M.	R	N.M.
[63]	IMU and force sensor	On body (IMU) and force sensor on walker	IMU (100 Hz) ; force sensor (50 Hz)	R	MF
[64]	LIDAR & IMU	Walker and IMU on foot	N.M.	R	MF, TR, TL
[35]	Leap motion	Walker	100 Hz	R	MF, TR, TL
[65]	Pressure sensors	Handle (Walker)	N.M.	R	MF and staying
[66]	Hall sensors	Walker	N.M.	R	MF, TR, TL
[67]	Current sensor and encoder	Walker	N.M.	R	Linear velocity
[32]	LRF	Walker	10 Hz	R	MF, TR, TL
[68]	Force sensors	Walker	N.M.	R	MF, TL, TR, STOP

R / P = Recognition / Prediction; N.A. = Not applicable; N.M. = Not mentioned; MF = Moving forward; MB = Moving Backward; TR = Turning Right; TL = Turning Left;

What sensors and features are being used to decode the user's MI in smart walkers?

Analyzing Table 2, 17 included studies decoded the user's MI and used this information to control the smart walker accordingly. Several algorithms, either heuristic rule-based or AI-based, were proposed using different embedded or wearable sensors. Considering the results, most of the included studies used force or pressure sensors (n = 5, [36, 55, 61, 65, 68]) to obtain the user's MI. These, along with hall sensors (n = 2, [60, 66]), are usually considered a direct way to obtain the user's MI [35, 48], since the user directly intervenes by applying force (physical interaction [48]) to indicate where to go. Another study, [67], uses encoders to measure the rotation speeds and a hall sensor to measure the motor currents. This was further used to indirectly estimate the user's force and output the robot's linear velocity using compliant motion control. Although this study did not directly use force sensors, the users must use physical interaction to indicate their intent and modulate the robot's linear velocity accordingly. The remaining studies in this literature review used indirect methods to decode the user's MI, which are obtained by analyzing the human motion [60, 66]. Included studies reported the use of IMU (n = 3, [56, 63, 64]), cameras (n = 3, [35, 57, 62]) and laser technology (n = 4, [32, 58, 62, 64]) or proximity sensors (n = 1, [59]).

Table 3: Approach, the AI-based model, the input, the calculated features, the evaluation and normalization method, the participants, metrics, and the main results extracted from the included manuscripts

Study	Approach	AI method	Input	Features	Evaluation	Normalization method	Participants	Metrics	Results & Conclusions
[55]	User's intentions are converted using a fuzzy logic controller into linear and angular speeds.	N.A.	N.A.	N.A.	N.A.	N.A.	12 (VE) and 4 (RS) (healthy)	N.A.	Results are related to the navigation assistance mode and not directly to the user's intentions. However, the authors reported that all users were able to control the device.
[56]	Method to classify the user's intent based on artificial intelligence	DT, KNN, LSTM	Longitudinal and lateral accelerations and velocity, yaw rate, wheels speed and difference in wheel speed	Mean, variance, min, max of a window	Train/Test split	N.M.	8 (healthy)	Accuracy	Final model presents an accuracy of 92.9%. Final model was a KNN with K = 15.
[57]	Camera's data was used to calculate the human position and orientation relative to the walker and control the walker accordingly with a PID controller and with a sway suppression	N.A.	N.A.	N.A.	N.A.	N.A.	1 (healthy)	Tracking error	Tracking error of human-robot position achieved a maximum of 3 cm and an average of 1 cm; robot was able to respond to the step inputs rapidly with no visible overshoot; sway suppression reduced the robot sway by over 50%
[58]	Track the to provide close-proximity walking safety support and turn according to user's intention, by detecting lower limb the user	K-means clustering + NN	LiDAR: leg's positions; IR thermometer: leg's orientations	Sequence of 8 points (thermal image vector and leg positions)	N.M.	Thermal image is normalized considering maximum and minimum value	1 (N.M.)	Error in °	NN performance not reported. Orientation error of 5.5° The walker can change direction according to the user's expected angle
[59]	Predict the user's walking intention speed to obtain the desired movement speed of the robot	LSTM + FC layer	Distance and speed of both legs	N.A.	Train/Test split	MAX-MIN [-1,1]	N.M.	RMSE	The proposed model produced a RMSE of 0.445 cm/s at constant speed and 0.695 cm/s at varying speed.
[60]	Detect the user's motion intention based on classifying the signals of the hall sensors	SVM with radial kernel	Data from hall sensors	% values of voltage, instantaneous variation	10-fold cross-validation	MAX-MIN	3 (healthy)	Accuracy, Recall, F1-score	Two SVM models. First, 98.9% of accuracy, recall>0.9 and F1-score = 0.99. Second model yield accuracy of 95.2% and recall of 0.96.

Table 3: (continuation)

Study	Approach	AI method	Input	Features	Evaluation	Normalization method	Participants	Metrics	Results & Conclusions
[61]	Detect the user's motion intentions using rule-based algorithm with the force and torque sensors to further control the walker using speed control	N.A.	Sum of force and sum of torque	N.A.	N.A.	N.A.	4 (healthy)	Normalised ISE	Two experiments performed. Average error of 6.45 for experiment 1 (infinite path painted on the ground), and 12.1 for experiment 2 (same pattern but simulating a patient).
[62]	Unified method for continuous monitoring of each user and adaptation of the robotic platform's motion accordingly	2 FC Layer + 2 LSTM	Position and velocity along the x- y-axis and human-related coupling parameters	N.A.	Train/Test split	N.M.	14 (pathological)	MSE loss	MSE training loss was $4e{-}4$ while the testing loss was $2e^{-3}$, meaning that the model accurate future predictions for the human motion intention
[36]	Force and torque applied on the SW are inputs of an admittance controller	N.A	N.A	N.A	N.A	N.A	1 (healthy)	Graphics	The user's commands were in accordance with the ideal path. Walker's trajectory was like the ideal
[63]	IMUs were used on body to detect gait phases. Force sensors were used to measure the interaction. A pendulum model was used to calculate instantaneous walking speed	N.A	N.A	N.A	N.A	N.A	5 (healthy)	RMS of force and graphics	RMS of the pressure difference was 6.7 N, 7.1 N, and 7.7 N at preferred, slower, and faster walking speed. Based on the fusion of IMU and force, the robotic walker was controlled to accompany the user walking
[64]	LIDAR sensor determines the walking direction by detecting the knees. IMUs are used to obtain the angular rate of gait	N.A	N.A	N.A	N.A	N.A	1 (N.M.)	Graphic results	Authors reported that the walker correctly follows the user in a straight path. In the turn movement, the angle of the detected direction is larger than the user's movement
[35]	Two leap motions are positioned below the handles. A fuzzy logic is used to get the user's commands and control the walker using a PID controller	N.A	N.A	N.A	N.A	N.A	5 (healthy)	Graphic results	Participants were able to navigate along the path; considered intuitive and the platform was easily maneuvered. Walker's motion was in sync with the users' intents

Table 3: (continuation)

Study	Approach	AI method	Input	Features	Evaluation	Normalization method	Participants	Metrics	Results & Conclusions
[65]	The applied pressure is converted to voltage. AdaBoost Classifier is then used to detect user's intention	AdaBoost	600 input vectors of output pressure sensor	N.M.	2-fold cross-validation	N.M.	N.M.	Accuracy and error rate	AdaBoost Classifier is set to 20 weak classifiers, but 5 was considered ideal. Best model achieved an accuracy of 98%
[66]	A joystick with springs is used. Three signals measured in volts are used in a fuzzy logic controller. Y-axis is used as a forward motion and Z-axis used for the turning motion	N.A	N.A	N.A	N.A	N.A	11 (healthy)	Graphic results	Proposed control system showed good results. It presented low computational cost and allowed a smooth driving. The walker provided a fast response
[67]	The motion intent of a user is handled by the compliance controller, which outputs the linear velocity. User's force is estimated indirectly	N.A	N.A	N.A	N.A	N.A	1 (healthy)	Graphic results	User successfully walked inside the corridor indicating his motion intention with obstacle detection and avoidance (using an LRF)
[32]	Two LRF were placed on the walker to estimate the legs' position using Kalman filter approach. The feedback motion control outputs the desired velocity	N.A	N.A	N.A	N.A	N.A	1 (N.M.)	Mean and STD	Walker's displacement was according to the user's step length. The proposed feedback control enables the walker to generate smooth turning motion
[68]	The force the user applies is used to control the walker with a force-velocity mode and a force-acceleration mode. Algorithm is based on a set of rules	N.A	N.A	N.A	N.A	N.A	N.M.	Graphic results	Two experiments (force-velocity and force-acceleration control). Experiment 1: users control the SW using $15N$ on each hand. Experiment 2: users control the SW using $10N$ (less force). Force-acceleration allows a more steady and stable speed compared to Force-velocity mode

N.A. = Not applicable; N.M. = Not mentioned; DT = Decision Tree; KNN = K-Nearest Neighbours; LSTM = Long short-term memory; fps = frames per second; FC = Fully Connected; MF = Moving forward MB = Moving Backward; TR = Turning Right; TL = Turning Left; ISE = Integral Square Error; NN = Neural Network; STD = standard-deviation; VE = Virtual Environment; RS = Real Scenario

What are the typical MI addressed and what methods are used for decoding?

Regarding the direct Human-Machine Interface (HMI), this employs the use of force sensing technology. In [68], the authors detect three actions: forward, Turn Right (TR)/Turn Left (TL), and stop, and control the walker accordingly considering two approaches: force-velocity mode or force-acceleration mode. The results showed that both modes could control the walker, but the force-acceleration mode provided a more stable speed compared to the force-velocity mode. In [66], 6 pressure sensors were applied to the handle of the walker to detect forward and stance movements. An AI-based classifier, AdaBoost, was used to detect the user's intentions with an accuracy of 98%. However, the control of the walker was not explicit and results on the performance of the walker were not reported. Another approach using force sensing was presented in [37]. Triaxial load cells were introduced in the AGoRA SRW to measure the force and torque applied to the walker handles and use this information as input to an admittance controller. The proposed method was validated on a healthy participant, but only graphical results were reported. The authors reported that the user's MI and the walker's trajectory matched the ideal path. Another study, [61], introduced force and torque sensors in a pelvic support mechanism of the iReGo SRW. The MI, which consists in the detection of forward movement, backward movement, TR/TL, are performed considering the dynamics of the pelvis. The method is based on a set of rules considering the sum of forces and torques to further control the walker's speed using a proportional-derivative controller. The proposed algorithm has been validated with 4 healthy participants considering two experiments: **i)** the participants had to perform an infinite path painted on the floor, and **ii)** the participants performed the same pattern but simulating a patient's gait pattern. The authors reported that the volunteers were able to follow the intended path, albeit with some error, and that the proposed strategy allowed the individuals to walk naturally with minimal effort. In [55], the authors used a force/torque sensor in the ISR-AIWALKER to decode the user's MI. The force and torque applied to the walker's handles are inputs to a fuzzy logic controller responsible for converting the forces into linear and angular velocities. The proposed algorithm is accompanied by a Kinect sensor at the front of the walker for environment perception. An algorithm based on Reinforcement Learning (RL) shares the control with a navigation assistant. The proposed method has been validated with 12 healthy participants in a virtual environment and 4 healthy participants in a real scenario. The proposed solution based on fuzzy logic control is effective in controlling the SRW. Moreover, the robot assisted navigation approach helped the users in the presence of obstacles and narrow passages.

Direct HMI also includes the use of Hall-effect sensors placed on joysticks [60, 66, 67]. In [60], the authors positioned Hall sensors in each of the walker's handles to decode the forward, backward, and

TR/TL intentions based on AI-based techniques. The authors proposed two Support Vector Machine (SVM) models with radial kernels and evaluated the model using cross-validation. The first SVM model, which used normalized data (in percentages) and instantaneous variation, showed accuracy and recall above 0.9 (accuracy of 98.9%) and an F1 score of 0.99. The second SVM, which was simpler since it used only normalized data, achieved an accuracy of 95.2% and a recall of 0.96. However, no results were reported regarding the control of the walker. In [66], the use of joysticks with springs was considered in an earlier prototype of the ASBGo SRW. The joystick was equipped with Hall-effect sensors that were used as inputs to a fuzzy logic controller to classify the user's intention to move forward and TR/TL. The proposed strategy outputs the desired walker speed considering the user's inputs. The proposed strategy was validated on 11 healthy participants, but only graphical results were considered. The authors reported that the proposed control strategy showed good results, had a low computational cost, and allowed for smooth walking. In addition, they reported no sense of delay as the walker provided a fast response. In [67], Hall-effect sensors were used in combination with encoders to estimate the user's external force. This was used in a compliant motion controller to estimate the linear velocity of the SRW. The angular velocity was calculated by a navigation assistant using LRF. This approach was validated on a healthy user, but few quantitative results were presented (only graphical results). Nevertheless, the authors reported that the user successfully walked with the proposed force-cooperative controller by adjusting the velocity according to the force applied by the user. Although no force-sensing technology was used in this study, users must use physical interaction to adjust the SRW behavior.

The literature also suggests the use of IMU in combination with other sensors to decode the user's intent [56, 63, 64]. In [56], the authors proposed the use of an IMU and the walker's motor encoder to decode the forward, TR/TL movements using decision tree, K-Nearest Neighbors (KNN), and Long Short-Term Memory (LSTM) neural networks. As inputs, the authors used the longitudinal and lateral accelerations and velocities, the yaw rate, the wheel speed, and the wheel speed difference. With these data, they calculated the mean, variance, minimum, and maximum of a 125 ms window. The proposed model, a KNN algorithm with K = 15, achieved an accuracy of 92.9%. However, the proposed algorithm has not yet been tested. In [63], a IMU and a force sensor were used to detect the intention to move forward. The IMU were used on the body, namely in each thigh and shin, and a force sensor was placed on the walker at the level of the armpit. The inertial units were used to detect gait phases, while the force sensors were used to measure the user's interaction with the walker. The proposed strategy was based on decoding the user's MI by estimating the instantaneous walking velocity using a 2D pendulum model. The authors reported that the walker followed the speed set by the user. The interaction force was used

as feedback so that the walker could better adapt to the human gait. Finally, study [64] used a IMU placed on each foot and a LRF sensor pointed at the user's knee to detect the directional angle (heading angle) and evaluate the speed of movement. This was used to control the robot to move in the user's desired walking direction. The authors reported that when straight walking is considered, the walker follows the user's intention. However, when a directional intention is given, the authors reported that the angle of the detected direction is greater than the user's movement.

Other approaches to decode the user's MI rely on the use of laser technology [32, 58, 62, 64]. In [32], two LRF were placed on the walker to estimate the position of the legs using the Kalman filter approach. This information was used to determine the user's intention to move forward, TR/TL, and to control the walker using a Proportional-Integral-Derivative (PID) controller. The authors verified that the walker's displacement was consistent with the user's stride length. In [58], the authors used a LiDAR sensor and an infrared thermometer to track the position and orientation of the legs. The proposed algorithm was based on K-means clustering to discriminate the computed leg positions and a neural network to decode the MI. However, the authors did not report the accuracy of the model. Based on the leg positions and the classified intent, a virtual position is computed in terms of the velocity of the left and right wheels. The authors reported an average error of 5.5°, showing that the walker followed the user with a low error. Another approach was proposed in study [62], which used a LRF together with an RGB-D camera to decode the user's MI by predicting the human trajectory over a time horizon. The authors used a unified method in which the LRF tracked the position and velocity of the user's legs, and the RGB-D camera tracked the upper body to estimate the CoM motion. With this information, the authors propose a deep learning approach with 2 Fully Connected (FC) layers followed by two LSTM units. They trained the network using a train/test split of 80% − 20% and 500 epochs. For training, the authors used the Stochastic Gradient Descent (SGD) optimizer and evaluated the Mean Square Error (MSE) loss. The authors reported a MSE of $4e^{-4}$ for the training split and $2e^{-3}$ for the test split. Another approach was presented in [59], where the authors used multichannel proximity sensors to predict the user's intended speed to achieve the desired motion of the walker. They used a LSTM unit followed by a dense layer. As input, the authors use the distance and speed of both legs measured by the proximity sensors. They found a Root Mean Square Error (RMSE) of 0.445 cm/s and 0.695 cm/s considering constant and varying speed, respectively.

Finally, another approach to decode the user's MI considers the use of cameras [35, 57, 62]. Although [35] used cameras, this approach can be considered a direct HMI. In this study, two leap motion controllers were placed above the handles of the walker to detect the displacement of the handles. A fuzzy logic controller was used to classify the user's MI into forward and TR/TL. The output of the fuzzy logic controller

was the desired speed of the walker, which was then used in a PID controller. The results showed that five participants were able to navigate along a predefined path and found it an intuitive way to control the walker. Furthermore, the walker's motion was synchronized with the user's intentions, with no sense of delay. However, in a recent study, the authors replaced the leap motion with force sensors [55]. In [57], the authors calculated the user's torso position and orientation relative to the walker. This information was used in a hybrid PID controller with sway suppression (given the upper body sway) to control the smart walker accordingly. In evaluating the robot's performance, the authors reported a maximum tracking error of 3 cm and an average of 1 cm. In addition, the user feedback was that the robot was able to follow the user. In terms of sway suppression, the proposed strategy reduced the robot's sway by over 50%.

2.3.3 Discussion

According to the literature analysis, two ways of decoding MI have been identified: **i)** direct mode, which requires physical intervention from the user, and **ii)** indirect mode, in which the walker is responsible for analyzing the end-user's movement and inferring the MI when walking forward, turning right, turning left, and stopping. In terms of direct HMI, this type of HMI requires the use of force-sensing technology (or pressure sensors, or torque sensors). Study [35] consider that **force-sensing technology may degrade over time, presenting low repeatability when low-cost options are considered**. In addition, the **signal is noisy and affected by trunk sway during walking**, requiring the use of real-time filtering techniques [69]. The use of joysticks with Hall-effect sensors has also been considered within the included studies [60, 66], also representing a direct way of decoding the user's MI through physical interaction, requiring the user to use one (or both) hand(s) to control the walker. Additionally, the proposal of [60] **could be demanding from a cognitive perspective** and challenging from a motor coordination perspective. In addition, some authors consider that this approach may not be the most reliable since the sensor signal is noisy [14].

The indirect HMI do not require any physical interaction between the user and the robot. The literature reports the use of IMU [56, 63, 64], cameras [35, 62, 70], and laser technologies [32, 58, 62, 64] or other proximity sensors [59]. Using these approaches, the walkers are embedded with intelligence in such a way that they perceive the user's MI by performing continuous body monitoring. Moreover, this approach can be perceived as a motivational strategy, since users may need to train their gait and postural behavior to control the SRW correctly. However, these strategies also require intelligent controls that constantly evaluate the user's performance and ensure safe driving.

Commonly used sensors have some shortcomings, namely IMU and laser technologies. In the case

of IMU, they can cause **discomfort during prolonged use** and, if used in large numbers, reduce user acceptance. Laser technologies may struggle to cope with walking irregularities and are also a **very expensive technology**. Cameras, on the other hand, have a superior Field-of-View (FOV) that allows them to infer the user's 3D pose and use this information for several functionalities, from continuous monitoring to decoding intentions. Moreover, thanks to DL approaches, it is possible to better handle with occluded limbs due to gait irregularities, while LRF struggle since they typically provide sparse point-based measurements, which makes it difficult to infer the shape or position of occluded limbs. Further research on this topic should be considered to effectively decode the user's MI in an intuitive and safe way.

Regarding the methods to decode the user's MI, several have been presented, but not all studies have presented concrete results of device recognition and/or control. Most of the included articles decode the user's MI using heuristic rule-based algorithms (*e.g.*, fuzzy logic) [35, 55, 61, 66], mathematical models (*e.g.*, pendulum models, admittance controllers) [32, 36, 57, 63, 64, 67, 68] or AI-based algorithms [56, 58, 60, 65]. These studies have decoded the movements of: **i)** forward, TR/TL (n = 7); **ii)** forward, backward, TR/TL (n = 2) and **iii)** forward (n = 2). Another study estimated the MI by estimating the user's instantaneous linear velocity [67], and three others did not mention the motion to be decoded. In [59], the MI was decoded by predicting the user's walking speed, and in [62] by predicting the user's trajectory over a time horizon. The authors then use this information to control the smart walker. As for the heuristic models, they are usually based on rules and associations and are commonly used in direct HMI. However, the reported studies lack validation with pathological individuals who, due to their motor condition, may interact differently with the device (*e.g.*, due to muscular weakness or impaired coordination). In this sense, it is often necessary to adapt the algorithm. In addition, the force and torque sensors in [61] are positioned in a pelvic mechanism and thus rely on the natural sway of the user. Given the impaired balance of CA patients and their constant swaying while walking, this solution would not be the most appropriate. Regarding the mathematical models, the results also show that they are effective in controlling the walker. However, these algorithms are mainly **based on force sensors**, which provide noisy signals that require real-time signal pre-processing. Only studies [32, 57, 64] do not rely on force sensing technology using LRF, IMU or a camera. However, in [32] and [64], the LRF **only allows to observe some points of the lower limb**, in this case the shin, which depends on the anatomy of the user. Furthermore, **the authors did not report the behavior of the algorithm in case of limb occlusion**. In [57], the use of a differential model feed from a camera allowed the SRW control to take into account the position and orientation of the torso. However, this algorithm is **affected by the torso sway**, similar to [61], which may vary considering the user's disability level.

As for AI-based algorithms, they have aroused curiosity in the scientific community and in industry. They are often used in situations where the solution is non-linear and difficult to model. Considering the results of the literature review, these techniques are also used in the field of HRI to decode MI and further control assistive devices. Most of the techniques detect user intent using machine learning classifiers, namely Decision Trees [58], K-Nearest Neighbors [56], SVM [60], AdaBoost [65], but also DL techniques, namely LSTM neural networks [56]. These algorithms have proven to be reliable, with accuracy values above 90%. However, in [56], the recognition is not performed with data acquired from the user, *i.e.*, from the user's interaction with the device. Since the IMU and the encoder are embedded in the device and do not record any user parameters, this work only recognizes the current movement. In [60] and [65], the intention is classified by a direct HMI, achieving accuracy as high as 95%. However, **no results on the control of the walker using this approach have been reported**. In addition, in [65], the authors **did not consider the turning movement**, only the intention to start/stop walking. In [58], an AI based model was also considered. The authors proposed a neural network with two hidden layers of 512 units to classify 6 possible outcomes (it detects the leg movement and classifies which leg is moving and in which direction). The authors reported that the walker is able to change the direction in time according to the user's movement. However, they do not properly explain the dataset, how many participants were used, what metrics were evaluated, and what is the error of the neural network. Finally, in [59] and [62] a LSTM neural network is used for the prediction process. The authors probably chose this deep neural network because of its ability to retain temporal information. In [59], however, only the linear velocity was predicted, which indicates that only forward motion is considered and **no directional intentions are taken into account**. In [62], the MI is given using a neural network, which effectively predicts the human trajectory, but this algorithm requires more than one sensor (an RGB-D camera and a LRF), which **increases the cost of this approach**. Nevertheless, this was the only study that validated their approach with pathological patients and used the collected real data to develop the proposed AI-based models.

This topic has been the subject of much research to obtain an effective algorithm capable of understanding the user's MI and acting accordingly. The use of cameras, for example, can allow the recognition of intentions through DL techniques. The use of Convolutional Neural Networks (CNN) to evaluate the user's movement could be a starting point. These techniques may also be computationally expensive as their complexity increases, but a trade-off between available resources, the system's responsiveness, and the user's own interaction, given the time required to give the intention, must be considered. The difference between successive RGB frames [71] could be a fast way to give a sense of time and motion.

2.4 Assistive Control Strategies

Rehabilitation requires personalized, repetitive, and intensity-adapted training for effective assistance [10]. Robotic walkers are an appropriate tool to achieve these goals while promoting better assistance in navigation and gait monitoring. However, according to [48], these devices should be designed to **continuously shape/modulate their behavior based on the perception of the user's needs, fostering an intuitive and close HRC**. In this way, users will have a relevant role in the control of the device, approaching HIL control strategies that are **important to foster user-adaptive assistance**. However, since the target population is people with walking disabilities, **the robot must constantly monitor the user's actions to ensure that they are safe and meet a specific rehabilitation goal**. In certain circumstances, it may be essential for the robot to assist the user by providing the necessary assistance to achieve a given goal. This can be achieved through shared control strategies, the purpose of which is to create harmony between the human and the device so that the device **only assists when necessary, a type of assistance termed AAN**. However, **effective sharing of control and perception of MI is still a challenge** [72].

Morris *et al.* [73] recognized shared control as an essential component in robotics, noting that the misalignment of goals between humans and robots highlights the importance of prioritizing commands based on context. Several walkers in the literature, namely XR4000 [73], PAAM [49], COOL Aide [74], Care-O-bot II [75], MOBOT [76], UFES [51], AGoRA [37], ISR-AIWALKER [55, 77], and FriWalk [78], have implemented shared control strategies. In general, shared control strategies can typically consist of three modules: **i)** user intention detection, **ii)** the supervisor, and **iii)** the prioritizer. The user intention detection module interprets the user's MI using embedded or wearable sensors, while the supervisor evaluates the user's choices to enhance security. The prioritizer then selects the most appropriate command.

2.4.1 Shared control

In [73], the walker detects the user's intentions by measuring how much force the user applies to the walker using specific force sensors, similar to studies [37, 49, 51, 74, 75], but study [49] adds the use of voice commands for additional input. As a supervisor, the authors of [73] implemented an ADS using LRF data, with three modes that are set when the user starts a navigation task: **i)** passive, where the user moves freely and the robot's primary function is to avoid collisions with obstacles; **ii)** active, where the robot's intended trajectory is used as the desired trajectory, and if the user's estimated trajectory represents a deviation greater than a given reference angle, the robot's motion is slowed and eventually stopped;

and **iii)** forced mode, where the user has no control over the walker. However, while this approach is functional, **it does not give the device intelligence in decision making, nor does it allow for active contextual adaptation of the control**. In addition, **it does not correct the trajectory in active mode**, only slowing or stopping based on alignment with the desired system trajectory. This limitation is also seen in [75], where the authors also used a threshold technique for prioritization. The user's desired linear velocity and direction of motion are compared to the planned path. In case of large differences, the system will hand over control to the user and no longer consider the initial goal. On the other hand, if the deviation is small, the robot follows the planned path or searches for path modifications taking into account the obstacle evaluation.

Spenko *et al.* [49] proposed an admittance-based shared controller authority between computer and human through performance-based adaptation laws, complemented by navigation assistance using ceiling markers for localization - **a method constrained by the environmental setup** [36]. Jiménez *et al.* [51] used an admittance controller with a 9-Degree-Of-Freedom (DOF) inertial unit and 3D force sensors for MI detection and RP-LIDAR for obstacle detection, using orientation error and user torque to modulate the admittance damping, improving the walker's responsiveness to user input. When the orientation error is zero, the damping is minimal, allowing the walker to move with great ease. On the other hand, as the error increases, the damping is increased, making it more difficult for the walker to move, and the linear velocity decreases accordingly. Sierra M. *et al.* [37] strategy for the AGoRA SRW combines user commands, obtained through force sensors, and navigation commands to dynamically grant control, ensuring that user commands align with the calculated window of possible motion ranges before authority is transferred. However, **this strategy does not maximize user autonomy** because control is only guaranteed when the user's intent is within the computed window. Furthermore, this approach only quantifies when the robot should intervene, but does **not quantify how much assistance is needed**.

In study [76], the authors use a drift-diffusion model and propose a mathematical formulation to adapt the parameters of a shared control strategy. This strategy is based on **i)** cognitive support, which helps the user to follow a desired path; **ii)** sensory support, which is used to reduce the risk of collisions with obstacles; and **iii)** physical support, which measures the user's performance and fatigue. These three decision blocks adapt the parameters of an admittance controller in real time. In this study, the user's MI are obtained using force and torque applied to the robot's handles. The proposed strategy adapts the damping parameters of force and torque as well as the robot's contribution to its orientation. Another approach was proposed by Ferrari *et al.* [54], who proposed a novel two-mode operation called "simulated passivity" that shifts control based on the user's proximity to a predefined path and employs a hysteresis

mechanism for smooth transitions, giving the user a sense of control even when the robot is dictating the pace. This conceptually innovative approach emphasizes user perception in shared control dynamics. However, this control sharing strategy is based on a simple heuristic that **does not provide the device with the intelligence** to understand whether to give control to the user or to the device. Furthermore, this strategy does not take advantage of **dynamic and/or permanent obstacles to authority sharing**, as it does not provide an autonomous driving mode.

Garrote *et al.* [55] and Xu *et al.* [79] explored RL for shared control, using Q-learning and Sarsa-learning, respectively, to adapt motion commands based on user input and environmental context. In [55], the authors presented a RL-based approach with a Dynamic Window Approach (DWA). This proposal aimed at learning possible corrections to the motion commands based on the environment context and the user's MI. The user's MI are obtained through 6-DOF force sensors, and a fuzzy logic is used to interpret these commands. The RL algorithm used was the Q-learning, and as state space the authors used the user's MI, the environment model, and the previous state and action. The strategy gives full control to the user until obstacles are detected. In [79], a RL-based strategy to dynamically adjust the user's weight on the control based on his/her performance, the robot's walking state, and the current environment information. As a state space, the authors used the distance to obstacles, the user's velocity commands estimated with a MI estimation algorithm, and the robot's planned velocity, which is defined considering the distance to obstacles through a thresholding technique. The RL algorithm used was the Sarsa-learning algorithm, which is an improved form of Q-learning [79]. However, this strategy does not take into account an ADS that overrides the user's commands in an unsafe context. Moreover, both strategies, which focus on discrete action spaces, **face limitations in complex, continuous environments** such as autonomous navigation, highlighting a gap in the application of RL to more nuanced and dynamically variable scenarios.

A recent strategy has been proposed by [72]. The authors proposed a novel concept of sharing control between user and robot by presenting a bimodal control system governed by a compliance-controlled handle. The system has two modes: **i)** user in control and **ii)** robot in control, and only one can operate the device. In the first mode, the user gives his MI by changing the orientation of the handle and the robot follows the user's commands. In the other mode, the robot tracks and follows a target person in front of the walker, using YOLOv2 [80] for this task. Actually, this strategy allows only one of the modes to work because the authors believe that sometimes there may be a conflict between the robot's commands and the user's commands. However, this type of strategy **should be user-compliant**, *i.e.* it should give the user maximum freedom and only intervene when and if necessary. The robot should be seen as a

supervisor, similar to a physiotherapist who constantly monitors his patient.

Finally, Sierra *et al.* [81] presented a novel shared control strategy for their UFES SRW. This strategy combines virtual forces with user torque obtained from 3D force sensors to provide haptic feedback when users deviate from the desired path. In addition, the haptic feedback is adjusted by modulating a gain that changes the level of user involvement in the control. This virtual torque is added to the user's torque to control the angular velocity of the SRW. The authors found a KTE of 0.13 m for the proposed strategy. In this strategy, the authors intend for the user to follow a predefined path and only allow greater freedom when the gain is set to a low value. However, **there is no real-time adjustment of this value, nor is the device equipped with the intelligence** to perceive whether it should assist the user or not. Therefore, more research should be considered on this topic of shared control, in order to provide devices with the intelligence to understand whether or not they should intervene and assist the user.

2.5 Human-Robot Interaction strategies

Recent evidence considers the use of HRI strategies, namely BS, as promising [42, 43, 82]. In fact, Giggins *et al* [82] states that providing biofeedback to both patients and clinicians can have a therapeutic effect by making users more aware of their actions. In addition, BS promote a more engaging therapy by encouraging the active participation of users in their rehabilitation. This type of HRI strategy is seen as a complement to gait training that directly contributes to the user's self-correction. SG are another HRI strategy used in gait rehabilitation, either as the main intervention tool or as a complement to traditional therapies [83]. This concept was developed in 1970 by Clark Abt [84], who defined SG as a strategy not intended for entertainment, but rather for educational purposes. When used for rehabilitation exercise purposes, they are usually referred to as exergames and operate as VR technologies. In fact, the literature suggests that SG can significantly improve the status of patients, as improvements in the primary rehabilitation outcomes of motor function, balance, and cognitive function have been found [83].

A literature review revealed a **lack of BS and SG used in conjunction with RAGT using smart walkers**. However, research considers their use relevant and an important tool in rehabilitation [3, 85]. In particular, in CA rehabilitation, the use of BS and SG can benefit the patient's postural sway [86], balance and coordination [85, 87]. Therefore, this section presents a literature review on the use of BS and exergames in CA rehabilitation and discusses their applicability in RAGT, aiming at more engaging, motivating, and effective therapies.

2.5.1 Methodology

Search methodology

An electronic search was conducted on the Scopus database, searching for articles that present the development and assessment of both BS and SG, including the use of VR, for ataxia rehabilitation. The literature search followed the guidelines of PRISMA. For that purpose, the following combinations were used: ("balance" AND "ataxia" AND "biofeedback"); ("postural sway" AND "ataxia" AND "biofeedback"); ("posture" AND "ataxia" AND "biofeedback"); ("biofeedback" AND "gait" AND "cerebellar ataxia"); ("games" AND "rehabilitation" AND ("balance" OR "posture") AND "ataxia"); ("virtual reality" AND "rehabilitation" AND ("balance" OR "posture") AND "ataxia"); and ("smart walker" OR "robotic walker") AND ("biofeedback" OR "feedback"). The search was limited to title, abstract, and keywords. A manual search was also conducted considering the references of the selected articles. Review articles were not included in this literature review.

Selection strategy

Studies were included in the review if they met a list of inclusion criteria, namely: **i)** be an original article; **ii)** be written in Portuguese or English; **iii)** present the development and functional validity of the proposed strategy; **iv)** be used to improve gait, balance and/or coordination in ataxia; and **iv)** be published since 2010. Articles that, upon review of their abstract, were out of scope or did not fulfill the inclusion criteria, were discarded. The remainder were selected for full-text analysis.

Data extraction

Each included article was analyzed considering: **i)** sensor system, output, and location; **ii)** approach used in the study; **iii)** participants involved; **iv)** experimental protocol used; **v)** specific metrics used by the authors; and **vi)** main results and conclusion.

2.5.2 Results

Figure 3 shows the flow chart of this literature review. According to the methodology, 60 original records were identified from the Scopus database. In addition, 1 record identified through other sources was also considered. Out of these, 6 papers were considered as duplicates, leaving 55 papers eligible for review. For this purpose, the title and abstract were read. Of the 55 articles, 32 were excluded for not meeting the inclusion criteria, leaving 23 full-text articles eligible. Of these, 6 articles were excluded as: **i)**

they were out of scope or are perspective studies (n = 4); and **ii)** they were not accessible (n = 2). Taking this into account, 18 studies were included in the qualitative analysis. Table 4 presents the results of this literature review.

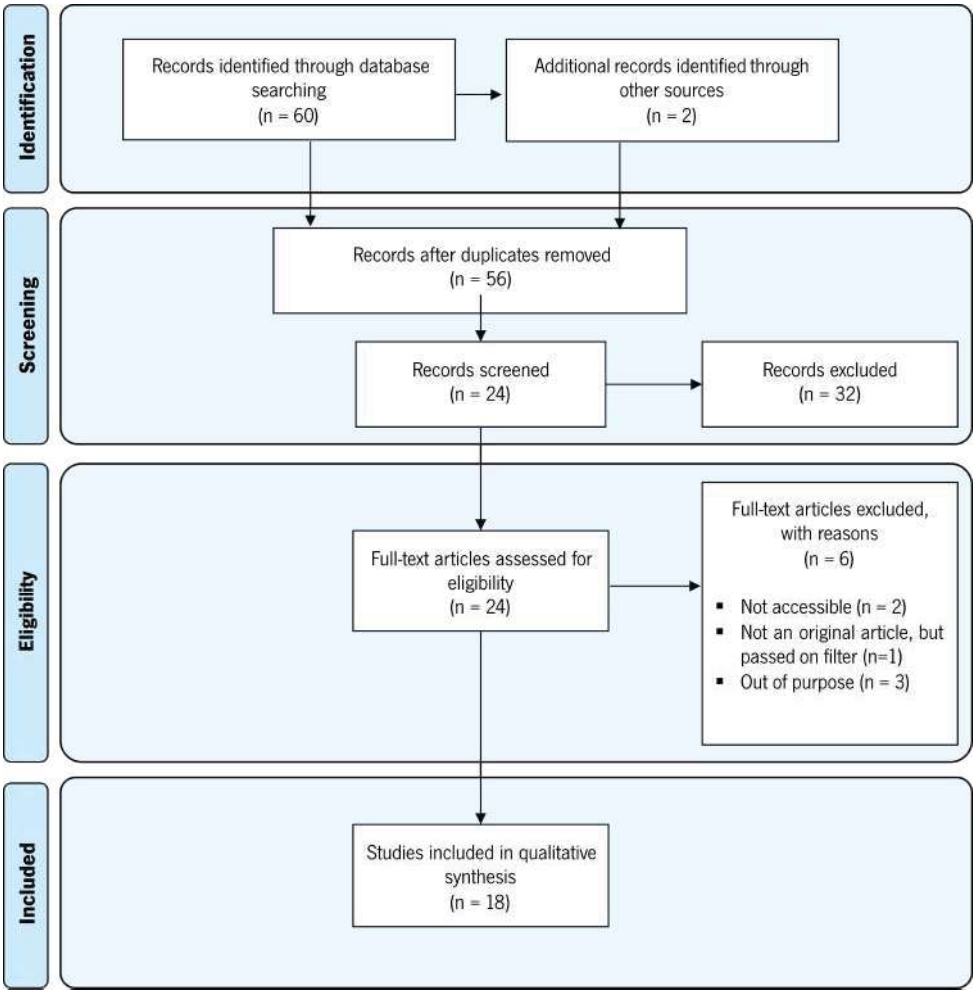


Figure 3: Flow diagram for the literature review of biofeedback systems and games.

Table 4: Included studies that present and discuss both biofeedback strategies and exergames for ataxia rehabilitation

Study	Goal	Approach	System	Actuator	Participants	Protocol	Metrics	Main results
[88]	Study the effect of VR in lower limb ROM	VR Feedback	IMU	Head-Mounted Display	20 patients with ataxia or hemiparesis	3 cycling sessions over 1 week. Each session consisted of 2 sets of 5-min pedaling exercised spaced with a 2-min break	Knee and hip ROM	VR-based training was not better than non-VR-based training
[89]	Assess the effectiveness of VR on balance impairment	Exergames	Nitendo Wii Fit Plus with balance board	Screen	64 children with ataxia	60-min of specially designed physical therapy program for the control group. Experimental group had 30-min of VR training and 30-min of same physical intervention as the control group.	OASI, APSI, MLSI, and PBS	Significant increase in PBS and decrease of OASI, APSI, and MLSI for both groups, but more for the experimental group with VR.
[90]	Verify the impact of CAREN in ataxia rehabilitation	Exergames	CAREN System	Wide screen	8 patients with ataxia	20 sessions (3 to 4 times a week). Each session lasted 45 minutes.	BBS, 6 mWT, TUG, 10-MWT, FES-I, TS, gait analysis	Improvements in BBS, TS, TUG, FES-I found in post-intervention. It improved gait quality, turning it stable, safe, and coordinated.
[91]	Compare telerehabilitation and virtual reality	Exergames	Non-immersive VR system "USE-IT"	Touch Screen	34 patients with ataxia due to multiple sclerosis	8 week protocol, 3 session per week, 1 hour per session	TIS, kinetic function of ICARS, ABILHAND, MMDT, trunk and upper limb kinematics	VR was more effective than telerehabilitation in improving dynamic trunk control and kinetic function
[92]	Describe the effect of home-based exergame for upper body movements control	Exergames	NiuRion kit - P2R	Computer screen	18 young patients with ataxia	Each participant of the experimental group performed the prescribed exercises five days a week for 12 weeks (total of 60 sessions for each exercise). Additionally, they maintained their physical therapy. Control group performed their usual therapeutic regimen.	9HPT, SARA, T25FW	The proposed intervention improved hand dexterity of participants of the intervention group, while those of the control group worsened their performance.
[93]	Investigate the effect of exergame training of postural control	Exergames	Xbox Kinect	Not mentioned but probably screen	19 patients with ataxia	Randomized controlled, assessor blinded, crossover trials. Participants performed a 16 week program, 3 sessions of 1 hour per week	ICARS, TUG, BBS, LoS with static posturography, Mini-BESTest	ICARS and BBS scores improved after exergame training. Some parameters of the LoS test improved significantly. No improvements were registered in the Mini-BESTest regarding the reactive postural control and sensory orientation subscale. Improvement of TUG with additional cognitive task after exergame training.

Table 4: (continuation)

Study	Goal	Approach	System	Actuator	Participants	Protocol	Metrics	Main results
[94]	Detect and monitors feet placement and gives audiovisual feedback when incorrect usage is detected	Audiovisual biofeedback	Camera and 2 US	Walker	N.M.	N.M.	N.M.	It was not validated with healthy or pathological users or it is not reported. Walker detects foot placement and gives biofeedback of walking too far behind the walker, out of center, or crossing feet.
[95]	Case report of patient that performed rehabilitation with VR-based exergame	Exergames	Riablo (foot platform and IMU)	Screen	1 patient patient with Primary Sjogren's Syndrome	20-session rehabilitation program divided into 2 parts: 1) traditional therapy and 2) VR exergame using Riablo. Two 60-minute session every week	BBS and stabilometric tests (BBOE, BBCE). CoP sway, path, and velocity. Gait parameters and gait profile score improved.	VR could be an effective complement to traditional physiotherapy during the rehabilitation cycle
[96]	Case report of a patient with acquired ataxia that performed a protocol with VR	Exergame	mediVR KAGURA	Head-Mounted Display	1 patient with ataxia after right cerebellar and brainstem infarction	VR-guided body balance training for 2 weeks, performing two 20 min sets per day, 5 days a week.	SARA, FBS, Mini-BESTest	All scores improved. VR guided body balance training may be useful for the rehabilitation of patients with cerebellar ataxia
[97]	Evaluation and comparison of postural stability while maintaining balance in people with MS with ataxia and AV	Visual biofeedback	Pressure platform	Screen	45 women (15 with MS, 15 with AV, 15 are control)	Participant stood on the platform barefoot. One-time standard examination was performed with 1) eyes open, 2) eyes closed, and 3) with visual biofeedback.	SAS, VCI, VMCI	Visual feedback allowed a reduction of SAS for MS; for AV, it allowed a reduction but only in comparison with eyes closed condition. Biofeedback was positive for MS patients with a domination of ataxia.
[86]	Effects on postural sway during stance were assessed in audio-biofeedback group vs control group	Audio biofeedback	IMU	Headphones	23 experimental + 17 control patients with ataxia	Participants completed a sequence of quiet stance conditions, each of them lasting 30 seconds.	Extent of trunk sway by the path length of CoG	Audio biofeedback was beneficial to reduce postural sway with eyes closed condition. Patients with strongest postural sway exhibited reduced postural sway also with eyes open. No changes were observed in the control group.
[98]	Assess changes in locomotion and balance in patients (adolescents) affected by ataxia	VR & biofeedback	GRAIL system	Wide screen	11 patients with ataxia	20 sessions of 45-min with GRAIL system and 20 sessions of 45-min of physiotherapy within one month	SARA, GMFM-88, 6 mWT, BBS, 3D gait analysis	Significant decrease of 20% in SARA; BBS improved significantly; 6 mWT improved significantly; GMFM-88 also improved significantly; gait was closer to healthy; coefficient of variation of gait outcomes reduced after therapy.

Table 4: (continuation)

Study	Goal	Approach	System	Actuator	Participants	Protocol	Metrics	Main results
[99]	Test the effects of balance rehabilitation with VR	Exergames	Nitendo Wii (balance board and remotes)	Not mentioned but probably screen	28 patients with SCA	20 sessions of 50-min with VR (2 sessions per week). Different games were used considering ML and AP weight shifting and displacement	DHI, BBS, SF-36	Significant improvements in balance control, dizziness, and overall self-reported quality of life
[100]	Assess the effectiveness of home training with videgames	Exergames	Camera (Xbox Kinect) and balance board (Nitendo)	Not mentioned but probably screen	10 young patients with degenerative ataxia	Training was divided into two consecutive phases of 6 weeks. Phase I was introduced by a one week lab-training and phase II included a two-day session at lab. Then, home-training was performed (3 times a week, 45 min per session).	SARA, GAS, changes in portural stability using the Romberg sitting task	Clinically relevant improvement of SARA scale (2.5 points) ; body sway decreased
[101]	Detect trunk of users and provide visual biofeedback of CoM	Visual biofeedback	Camera	Monitor of the device	N.M.	N.M.	Only graphics results	Graphics show the proposed strategy is functional but lacks of validation with pathological individuals
[102]	Assess the effectiveness of a 2-week intensive tongue electrotactile biofeedback	Haptic biofeedback	IMU	BrainPort (electrotactile stimuli in the dorsum of the tongue)	7 patients with ataxia	2-week intensive training program, twice per day and sessions of 20 minutes with at least 4 hours between them. Total of 20 sessions over the two weeks	95% confidence ellipse of body sway, path and mean velocity of CoP ; MCTSIB	CoP mean velocity decrease in post-training exercise with eyes open; decreased in post-training exercise and in retention assessment considering eyes closed; area of sway decreased in post-training and retention assessment, but only significant for eyes closed
[103]	Assess the effectiveness of coordinative training with videogame	Exergames	Camera (Xbox Kinect)	Screen	10 children with SCA	8-week exergame-base training: 2 weeks of training phase (4 sessions of 1h); 6 weeks of home training	SARA, DGI, ABC	Improvements in SARA mainly due to posture subscore; scores of DGI increased; decreased in step variability and lateral sway
[104]	Assess postural stability and the effect of balance training	Visual biofeedback	Biodex Stability System	Monitor	38 patients (12 performed balance training)	Exercises of bilateral stance weight-shifting exercises. Each session lasted 30 minutes, one per week for 15 weeks.	OASI	Significant improvement in OASI and decrease of hands support

VR: Virtual Reality; IMU: Inertial Measurement Unit; ROM: Range-of-Motion; OASI: Overall Stability Index; APSI: Anteroposterior Stability Index; MLSI: Mediolateral Stability Index; PBS: Pediatric Balance Scale; BBS: Berg Balance Scale; TS: Tinetti scale; 6 mWT: 6 minute Walk Test; TUG: Timed Up and Go; 10-MWT: 10 Meter Walk Test; FES-I: Falls Efficacy Scale International; 9HPT: 9-Hole Peg Test; ICARS: International Cooperative Ataxia Rating Scale; MMDT: Minnesota Manual Dexterity test; SARA: Scale for the Assessment and Rating of Ataxia; T25FW: Timed 25-Foot Walk Test; LoS: Limits of Stability; Mini-BESTest: Mini Balance Evaluation Systems Test; N.M.: Not Mentioned; US: Ultrasonic Sensors; CoP: Center-of-Pressure; BBO/CE - Bipodalic Balance Open/Closed Eyes; GPS: Gait Profile Score; FBS: Functional Balance Scale; SAS: Surface Area of Stabilogram; VCI: Vision Control Index; VMCI: Vision-Motion Control Index; MS - Multiple Sclerosis; AV - Atrial Vertigo; CoG: Center-of-Gravity; GMFM-88: Gross Motor Function Measure; ML: Mediolateral; AP: Anteroposterior; DHI: Dizziness Handicap Inventory; SCA - Spinocerebellar Ataxia; GAS: Goal Attainment Scaling; CoM: Center-of-Mass; DGI: Dynamic Gait Index; ABC: Activity-specific Balance Confidence Scale

Biofeedback Strategies

Giggins *et al.* [82] define different types of BS, namely: **i)** physiological biofeedback, which includes neuromuscular, cardiovascular, and respiratory biofeedback; and **ii)** biomechanical biofeedback, which includes the measurement of movement, postural sway, balance, and forces produced by the body. According to this study, various sensors can be used to provide biofeedback, such as IMU, force plate systems, electrogoniometers, pressure biofeedback units, and camera-based systems. In addition, several forms of feedback can be provided to users, including auditory, visual, and tactile signals.

A review of the literature reports a lack of use of biofeedback in assistive robotic walkers. To date, only three studies, study [101] (teamwork), study [40], and study [94], have been considered that provide biofeedback to their end users while using a robotic walker, as shown in Table 4.

Lim *et al.*, in study [40], present a biofeedback strategy for a robotic walker that provides adaptive sensory cues, namely visual cues projected on the ground, to assist patients with Parkinson's Disease (PD). Two visual cues were provided to the user: **i)** a white colored footprint and **ii)** a white colored transverse line. In addition, the SRW provides a rhythmic audio cue to remind the user to walk according to the visual cue projected on the floor. Seven elderly participants were recruited to evaluate the effect of using the sensory cues. Four of them were patients with the PD (experimental group) and the remaining were elderly people without the need for assistance (control group). Stride length and gait speed were measured in a pre-test and during therapy where visual cues were given. The results suggest that the sensory cues provided a more stable gait and the improvements in stride length were superior for the PD group compared to the control group. Study [101] presents a preliminary approach of biofeedback integrated in ASBGo SRW. In this work, the SRW uses an RGB-D camera to detect the user and compute specific points of interest, including the user's CoM. This information is also used to verify that the user is grasping the walker's handles correctly, giving an audible warning if not; and to provide visual biofeedback of the user's posture, namely the shoulder tilt and the lateral and frontal tilt of the upper body. However, this approach has not been validated with either healthy or pathological users. Finally, study [94] presents algorithms based on computer vision and AI to detect and monitor the user's feet and then use this information to provide audiovisual feedback when incorrect use is detected. The authors use a camera and two ultrasonic sensors: the camera is used to detect feet in order to later keep the user in a specific position on the device and to avoid crossing feet; the ultrasonic sensors are used to detect the user's distance from the device and to correct his/her position based on visual feedback using LEDs. However, the proposed strategy does not appear to have been thoroughly validated, either in healthy people or in the target population, so its effectiveness is unknown.

Auditory and tactile biofeedback have also been used with patients with ataxia in [102] and [86], but not with robotic walkers. In [102], the authors propose a head position-based electrotactile biofeedback approach for balance rehabilitation. The study included seven participants with degenerative CA whose static body sway was assessed using the foot Centre-of-Pressure (COP). The authors found a statistically significant improvement in the mean velocity of the COP under closed eyes after training and at a four-week follow-up. After the follow-up, the mean velocity of COP increased compared to the "post" condition, but it was not statistically significant. Regarding the sway path, electrotactile biofeedback also improved in the closed-eye condition in both post-training and follow-up. Regarding the study [86], a BS with auditory cues was proposed to improve postural sway in patients with degenerative ataxia. The BS consisted of a IMU placed on the torso and a smartphone application that received the information. The audio biofeedback (ABF) was given through headphones. Participants were evaluated in five different conditions, with both eyes open and eyes closed: **i)** *PreABF*, **ii)** *Training I*, **iii)** *Training II*, **iv)** *TestABF*, and **v)** *PostABF*. Balance performance was assessed using the Vicon Motion Capture System (Vicon Motion Systems Ltd, United Kingdom). The intervention group received audio biofeedback in all conditions except **i)** and **v)**. Differences in postural sway were verified for the intervention group in the eyes-closed condition. Postural sway decreased in the *TestABF* phase (in which audio biofeedback was given) compared to the *PreABF* phase (no audio biofeedback was given). Without audio biofeedback (*PostABF*), the intervention group significantly increased postural sway compared to the *TestABF* condition. In the control group, no statistically significant improvements were observed with eyes open or closed.

Other forms of stimuli have also been evaluated, namely the use of visual biofeedback of Centre-of-Pressure (CoP) movements in studies [97] and [104]. In fact, the main goal of Kahl *et al.* [97] was not to present and validate a BS, but rather to compare the postural stability of patients with multiple sclerosis with a predominance of ataxia and atrial vertigo in different conditions, one condition being the application of biofeedback. Participants stood barefoot on a platform and performed a single assessment considering **i)** eyes open, **ii)** eyes closed and **iii)** with biofeedback. The authors verified that the visualization of the CoP path allowed a reduction of the area of the stabilogram, but only in comparison with the eyes closed, considering both conditions. Nevertheless, in patients with multiple sclerosis, biofeedback allowed a reduction of this metric when comparing open and closed eyes. Regarding the study by Januário *et al.* [104], visual biofeedback of CoP was given while performing bilateral stance weight bearing exercises. The authors found that visual biofeedback was beneficial for these patients, allowing for a significant improvement in the overall stability index. In addition, the authors reported that patients also reduced hand support during bilateral stance exercises.

Overall, the results suggest that the use of BS may be useful in rehabilitation sessions for individuals with ataxia. However, this topic has not been extensively studied for this condition, especially when applied to RAGT. Other studies have proposed different BS to improve balance and trunk sway in other conditions that affect gait and balance, namely stroke, multiple sclerosis, cerebral palsy, or even in healthy individuals, exploring vibrotactile cues [105, 106] and visual cues [107–110]. The results are mixed, with some studies reporting improvement and others reporting no significant difference. However, the positive results encourage and justify further development of BS, aiming at a more interactive, engaging, motivating and problem-oriented therapy.

Serious Games

Serious games, or exergames when used for training, have also been presented as a complement to rehabilitation programs for patients diagnosed with ataxic gait, with VR being an emerging field [43, 85]. In fact, the results of this literature review show that most of the studies found (n =11, 61%) used either immersive or non-immersive VR as a way to improve patients' balance and gait quality. However, none of them were presented together with RAGT. As shown in Table 4, different systems were used to provide immersive and non-immersive VR-based training, namely Nitendo Wii (n =3), Xbox Kinect (n =3), CAREN and GRAIL systems (n =2), Riablo system (n =1), NiuRion Kit - P2R (n =1), and mediVR KAGURA or other head-mounted displays (n =2).

Studies [89, 99, 100] have applied non-immersive VR-based interactive exergames of Nitendo Wii, which includes force platforms, for the rehabilitation of patients with ataxia. In [89], the authors introduced commercially available games, namely tennis, baseball, and bowling games, to rehabilitation programs of children with ataxia. The application of these games had different goals: tennis and baseball games were used to increase muscle strength, while bowling game was used to improve balance but also core muscle strength. In fact, this tool also provided patients with visual biofeedback of CoP measured with the force platform, which highlights the relevance of this type of technology, as it can be both ludic and educational. The authors reported a significant increase in the Pediatric Balance Scale and a significant decrease in the overall stability index, anteroposterior stability index, and mediolateral stability index in both the experimental and control groups. In addition, the experimental group trained with the interactive games showed a significant improvement in all metrics compared to the control group. Regarding study [99], 28 patients with SCA underwent an intervention program with VR, where different games (soccer heading, table tipping, tightrope walk, and ski slalom) were used to train AP and ML weight shifting and displacement. The authors reported significant improvements in balance control, dizziness, and overall

QoL after daily sessions with VR-based games. However, the results show a decrease in the BBS scale, although very small (less than 2 points on average). Finally, study [100] presents a controlled trial where the authors implemented a clinical protocol with commercially available games of both Nintendo Wii and Xbox Kinect, which were performed considering two phases of training. These games were specifically designed to train trunk and postural control, namely Penguin Slide, Ski Slalom, Balance Bubble, Table Tilt, Tilt City, Big Top Juggling, Tightrope, Table Tennis, Light Race, and 20000 Leaks. The authors reported a decrease in the SARA scale, mainly due to gait and posture sub-scores, but also in body sway when sitting with eyes closed. In addition, the authors found that the benefits of training may depend on the amount of training performed.

In addition to Schatton *et al.* [100], other studies have also used Microsoft Kinect games [93, 103]. Study [93] presented a randomized controlled crossover study of nineteen patients diagnosed with ataxia who completed a 16-week program of interactive exergames. The exergames included Joy Ride, Adventures River Rush, Adventures Rally Ball, Kinect Sport Skiing, and Adventures 20000 Leaks, each with specific targeted motor gains. The authors reported an increase in International Cooperative Ataxia Rating Scale (ICARS) and BBS, only after the exergame training program. In addition, some parameters of the limit of stability test improved significantly, namely maximum excursion, endpoint excursion, and directional control. In addition, while no significant improvement was observed in the sub-score of postural control and sensory orientation of the mini-BESTest's considering both exergame training or conventional exercise program, the authors found a significant improvement of the TUG scale with additional cognitive tasks after training with exergames. Therefore, the results are quite positive for the application of exergames to reduce the severity of ataxia. Regarding study [103], Ilg *et al.* demonstrated that Microsoft Xbox Kinect video games allowed a significant reduction in ataxia symptoms, including improvements in balance skills, in children with progressive SCA. The authors reported a decrease in SARA after training, mainly in the posture sub-score. In addition, the dynamic gait index increased significantly, indicating an improvement in dynamic balance. Finally, the authors also found an improvement in the Activity-Specific Balance Confidence Scale, a decrease in step variability, and a decrease in lateral sway.

Literature also reports the use of more advanced technology, such as the use of CAREN [90] and GRAIL systems [98], aimed at improving the overall QoL of persons with ataxia. The [90] study aimed to verify the impact of using the CAREN system in the rehabilitation of patients with acquired ataxia, either due to stroke, posterior fossa tumors, or arteriovenous malformations. The CAREN system consists of a split-belt treadmill on a 6-DOF platform with a wide screen for an immersive experience and a camera-based motion capture system to collect relevant gait data from the users. Eight ataxic patients completed a 20-session

protocol, with a frequency of 3 to 4 sessions of 45 min per week, of immersive VR-based exergames in addition to conventional physical therapy. According to the authors, the intervention program was user-specific and tailored to the patients' needs. The authors reported that the VR intervention program resulted in an improvement of **i)** kinematic data, namely a more symmetrical gait in terms of temporal parameters, a slight decrease in step width and an improvement in trunk rotation; **ii)** kinetic data, namely a more symmetrical hip moment and mediolateral ground reaction force; **iii)** electromyography parameters, namely improved muscle activations of the lower limbs; and **iv)** in clinical scales, namely an improvement in BBS, Tinetti Scale, TUG and Falls Efficacy Scale - International. As for the study [98], Peri *et al.* presented an intervention study with the GRAIL system similar to CAREN. Eleven young patients with ataxia underwent a 20-session intervention protocol with the GRAIL system and 20 additional sessions of physiotherapy. In addition to playing VR-based exergames, patients also received visual biofeedback of both kinematic and kinetic gait characteristics, which was relevant for training balance and coordination control. The authors reported a significant improvement in the SARA scale, a significant increase in gross motor function, particularly in the standing and walking subscores, an increase in total distance walked in the 6-minute walk test, and a significant increase in BBS. In addition, the authors reported improved gait quality by demonstrating a decrease in the coefficient of variability of both kinematic and kinetic gait parameters. Thus, these findings support the use of VR-based intervention programs in ataxia. Nevertheless, both studies [90, 98] lack a control group to verify if these improvements are indeed substantial compared to other forms of intervention programs.

In another paper presented by Lo Voi *et al.* [95], the authors describe a case report of a patient with cerebellar atrophy associated with primary Sjögren's syndrome. The authors implemented a 20-session intervention program consisting of VR-based exergames performed with Riablo, a medical device equipped with IMU and force platforms that allows for exercises to be performed with biofeedback, ROM assessment, and functional and balance assessment. The intervention protocol included 20 to 25 minutes of physiotherapy (treadmill, passive stretching and mobilization, and coordinative exercises) and 30 to 35 minutes of interactive exergames with visual biofeedback of the patient's CoP. An increase in CoP path length and speed was observed, which is not so positive. However, significant improvements in BBS and body sway during open-eye bipedal stance were found, and improvements in temporal and kinematic gait parameters were reported. In addition, the authors reported an improvement in the gait profile score.

Romano *et al.* [92] also presented an interactive system, the NiuRion kit, based on IMU and non-immersive VR exergames. In this study, eighteen young patients with ataxia participated in a controlled intervention program designed to assess the effect of home-based training for upper body coordination

rehabilitation. The patients were divided into an experimental and a control group, where the experimental group performed prescribed exercises with the non-immersive VR exergames. Meanwhile, the control group maintained their program of physical intervention. The authors reported a significant improvement in the dominant hand dexterity of those in the intervention group when considering the 9-hole peg test, while those in the control group worsened their performance. A similar result was found for the non-dominant hand, but it was not statistically significant. In addition, the SARA score was maintained for participants in the intervention group, while those in the control group showed a significant increase. Small improvements were found in the timed 25-foot walk, but not significant.

More immersive experiences with head-mounted displays have been explored by Rojo *et al.* [88], Takimoto *et al.*, and [96]. The first study, [88], aims to verify the effect of VR-oriented training on lower limb ROM. Twenty patients with ataxia or hemiparesis performed a one-week protocol of cycling sessions, and the authors verified whether knee and hip ROM increased. The results showed that training with the VR-based exercise program is roughly similar to training with the non-VR-based exercise program. As for the study by Takimoto *et al.* [96], the authors presented a case report examining the effect of an immersive VR-based gaming intervention on seated body balance. The protocol consisted of 3 weeks of conventional physical therapy, followed by a daily 40-minute session of immersive VR-guided head-mounted display balance training for 2 weeks. The goal of the interactive game was to make contact with falling objects in virtual space. The authors reported a decrease of 4 points on the SARA scale and an increase on the functional balance scale, both of which represent improvements.

Finally, Doğan *et al.* [91] compared two therapy approaches, namely telerehabilitation using a mobile application ("Fizyo") and VR-based task-oriented circuit therapy, for the rehabilitation of upper limb, trunk function and functional activity kinematics in patients with multiple sclerosis who showed ataxia symptoms. The VR-based training program was based on the non-immersive system "USE-IT", which presents a touch screen for visualization and different games. The authors reported that both groups showed improvement in ataxia severity, but the VR-based training program was more effective in terms of dynamic balance.

2.5.3 Discussion

Several studies have been reported in the literature evaluating the effectiveness of advanced HRI and HRC strategies in improving the overall QoL of patients with ataxia. These include training programs based on BS [86, 94, 97, 98, 101, 102, 104] and exergames based on VR [88–93, 95, 96, 98–100, 103], the latter being widely explored. However, **few studies in the literature include this type of technology along with robotic walkers**, while there are already studies demonstrating its benefits with exoskeletons

[111].

In fact, only three studies included in this review use BS embedded in robotic walkers, and only one, Lim *et al.* [40], validated their approach with the target population. The remaining studies, overall, showed positive results for the use of biofeedback or exergames in patients with ataxia symptoms, **but not all of them could be easily integrated and used in robotic walkers**, given their **i)** use of force/pressure platforms [89, 95, 99, 100, 104]; **ii)** use of fixed and extremely complex systems that require specific locations and environments and are not often found in hospitals or rehabilitation clinics due to their high cost [90,98], **iii)** use of commercial camera-based exergames that may not be adaptable to robotic walkers [90, 93, 98, 100, 103]; or **iv)** use of head-mounted displays which, based on immersive VR, do not allow the user to perceive the real world and therefore cannot be used for gait training with robotic walkers [88, 96].

Since a robotic walker is an external, non-wearable device, **it would be ideal to use sensors that are embedded in the device itself and do not require a specific, complex setup**. In this way, the use of cameras and IMUs would be ideal, although the use of IMUs in large numbers may be an additional time-consuming task for clinicians and may cause discomfort due to prolonged use. In addition, the integration of these technologies as a feature in robotic walkers would be highly relevant as it would make these devices more attractive to stakeholders and facilitate their use in the target population as it is a more accessible, user-friendly technology and does not require specific environments or complex setups.

2.6 General Conclusion

This chapter presented the current state of the art in the various topics covered in this thesis, from an overview of the main robotic walkers presented in the literature, to the different ways of decoding MI in robotic walkers and how this information can be used to develop novel control strategies, to new, more technologically advanced rehabilitation approaches that motivate patients and encourage their active participation in therapy.

The challenges are many. In terms of motion intent decoding, new indirect ways to detect or recognize MI in a timely manner must be explored in order to achieve an **intuitive solution that is natural to the user and does not increase physical interaction more than necessary**. Then, novel control strategies must be developed that provide **seamless, natural assistance and allow the user to focus on the essential task of gait and balance training**. Thus, intelligent AAN approaches need to be explored that allow the device to assess the user's intentions as well as the environment and use

this information to assist the user in avoiding permanent or dynamic obstacles while he/she focuses on his/her therapy. Furthermore, new **interactive and collaborative** strategies that encourage **active user participation** and increase their **motivation** in therapy, such as BS and SG, should be developed and integrated into these devices using embedded sensors to **maximize technology acceptance**. Finally, **more clinical intervention studies should be conducted** to evaluate the effects of RAGT with robotic walkers on gait and balance rehabilitation of ataxic patients.

Chapter III

WALKit Smart Walker

Chapter 3

WALKit Smart Walker: an overview

3.1 Introduction

One of the main goals of this doctoral thesis was to optimize the ASBGo SRW prototype [14, 112] with new software that addresses the usability concerns of clinicians and endows the device with several new features that favor HRI for the rehabilitation of ataxic gait and balance. This chapter provides a more technical insight into the optimized prototype, the WALKit Smart Walker, presenting its main hardware and software architecture. This thesis followed the objective of the industrial R&D contract project EML (POCI-01-0247-FEDER-033067), which allowed the mechanical development of the novel, more robust and reliable prototype. First, WALKit is presented from a mechanical and hardware perspective. Then, the system architecture is presented, followed by the new and redesigned GUI, including its validation with end users (clinicians) from both Braga and Guimarães hospitals. Finally, an overview of the novel user-friendly clinical support and feedback tool to complement therapy sessions with the robotic device will be presented, as well as its validation with stakeholders regarding technical functionality and usability.

3.2 Prototype overview

WALKit SRW consists of a user-friendly, personalized and user-oriented three-wheeled robotic walker specially designed to provide assistance and gait and balance rehabilitation to ataxic patients. It includes several sensors on its vast mechanical structure, from RGB-D cameras, load cells, LRF, ultrasonic sensors and encoders. The project counts with some prototypes that were developed all over the years. The last prototype, used in this thesis, is illustrated in Figure 4. Each prototype was developed by following a user-centered approach, considering several brainstorms with the team's engineers and clinicians to achieve the most ergonomic and personalized device, maximizing its usability and technology acceptance.



Figure 4: WALKit SRW developed at University of Minho with partnership with ORTHOS XXI, Tecnicunha, and 2CA-Braga, that was used in this doctoral thesis.

The WALKit Smart Walker, as shown in Figure 4, consists of two motorized rear wheels coupled to an encoder. The front wheel is passive and moves in the desired direction. Each motor is controlled independently by a dedicated architecture, allowing it to move forward, turn left, and turn right. The device is controlled by an ergonomic and user-friendly handlebar, specially designed for ataxic incoordination. A remote control is also included to allow the physiotherapist to control the walker when the patient does not have sufficient dexterity. Its mechanical structure also has enlarged dimensions to cope with the variability of the ataxic gait, as well as an ergonomic curved wooden platform to ensure posture and BWS when using the device. Finally, the height of the platform is electrically adjustable, allowing to maximize the use of the device by easily adapting it to the user.

3.3 System Architecture

The software architecture follows a modular and hierarchical architecture, divided into high-level and low-level layers, as shown in Figure 5. This is a common architecture and transversal to other types of assistive devices, such as orthoses and prostheses [113].

The low-level layer is considered to be the execution layer. It runs a Real-Time Operating System (RTOS) on a STM32F4 Discovery. Currently, this dedicated board is used to operate and read the SRW low-level sensors and to control the device in terms of linear velocity, activating/deactivating the motors considering the response of a proportional controller. This controller is responsible for generating an appropriate response taking into account the deviation between the measured and the reference linear velocity. Low level sensors, acquired at 100 Hz, include: **i)** navigation and safety sensors, namely 9

ultrasonic sensors used to detect punctual obstacles that are near the device and expose the user to risks, an infrared sensor located just above the wooden platform and pointing directly at the user, which can be used as a safety mechanism or to adapt the assistance of the walker to the user, and an emergency button that directly cuts the power to the motors, immediately stopping the device; **ii)** monitoring sensors, namely an IMU to be placed on the user at the L3-L5 vertebrae to detect trunk sway and control postural stability, and two load cells that can be used to evaluate the user's posture when using the device; and **iii)** control sensors, namely an IMU embedded on the handlebars to infer the user's MI taking into account the direct interaction of the user; and encoders of each rear wheel, which allow to measure the real linear speed used to close the control loop.

The high-level layer is the device's Central Control Unit (CCU), which is supposed to be the bridge between man and machine. It runs in an Intel NUC computer on a Robot Operating System (ROS) layer. It has three sensors directly connected to this layer, namely two RGB-D cameras and a LRF, acquiring data at 30 *fps* and 10 Hz, respectively. This layer is responsible for implementing all the control algorithms, clinical tools, BS and SG developed during this thesis. It also has a dedicated graphical interface, accessible via a LCD, which allows session configuration, access to patient data and access to HRI strategies in real time.

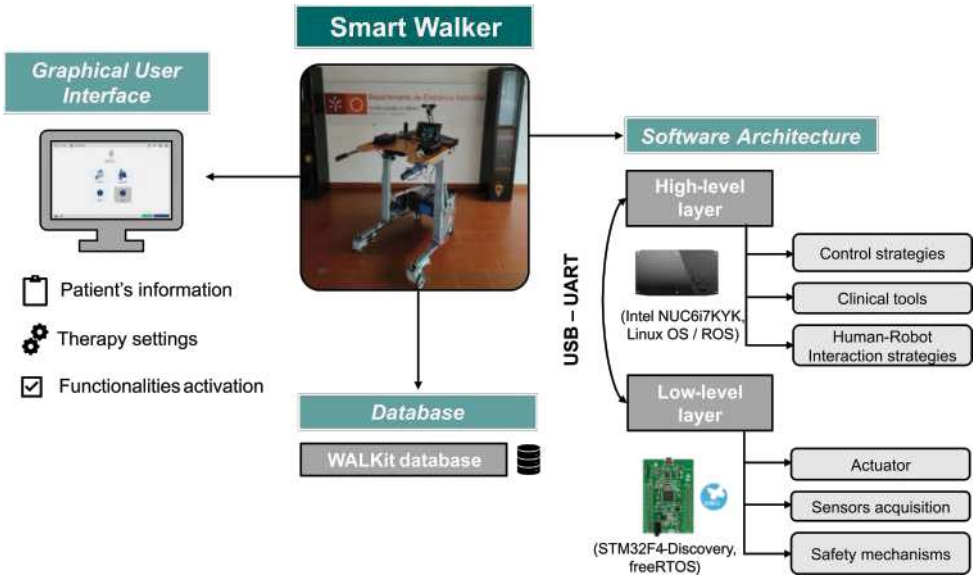


Figure 5: WALKit software architecture. It is divided into high- and low-level, which constantly communicate in a bidirectional manner via UART.

3.4 Optimized Graphic User Interface

A central point of this thesis was to optimize the WALKit Smart Walker to be a **more intuitive and user-friendly device with high usability and functionality** rates. Therefore, there was a significant

need to develop a new GUI that would **meet the technical and clinical needs** of both end users and clinicians who will be using this device on a daily basis. This is a critical step towards **technology acceptance** and overcoming the high dropout rates associated with the use of such devices. In fact, the GUI of the previous prototype proved to be insufficient: it did not meet the basic clinical requirements, it was not user-friendly; and it was not prepared for the evolution of the device, since it became a **major obstacle to the integration of new control and HRI strategies**. As a result, the GUI has been thoroughly redesigned. Figure 6 shows the GUI of the previous prototype.



Figure 6: GUI of ASBGo prototype, the predecessor of WALKit.

The development of the new GUI followed the waterfall model [114,115], which is a sequential process for software development. It is one of the **Software Development Life Cycle (SDLC)** models that aims to describe phases of the software cycle and the order in which they should be executed [114]. This model includes five sequential phases consisting of **i)** requirements analysis, **ii)** design, **iii)** implementation, **iv)** testing, and **v)** maintenance. It is usually applied to user-specific interfaces [115] and where requirements are well defined [114].

3.4.1 Stakeholder Requirements

Before idealizing the new user interface, several brainstorming sessions were held with the clinical team to design a new intuitive and appealing interface. A number of clinical and technical requirements were then identified. Clinically, the application would need to be able to **i)** quickly and easily introduce new patients undergoing therapy with the device, **ii)** intuitively access, modify, archive or delete stored patient data, *i.e.*, perform basic Create, Read, Update, Delete (CRUD) operations, **iii)** introduce clinical

evaluations, and **iv)** display some data about the sessions, such as the chosen velocity and algorithms used, and how many sessions were performed.

From a technical point of view, the new application should make it possible to set up a new rehabilitation session, allowing the user to choose a single control strategy, one or more clinical tools, and one or more HRI strategies. Furthermore, the new GUI should allow the user to modify some control parameters in real time, namely the device speed, and display the selected strategies and clinical tools.

3.4.2 Interface development

Once the clinical and technical requirements were gathered, the application was prototyped and developed. The development of the application was divided into two layers, the backend and the frontend. The frontend was developed in QML, a multi-paradigm application development language that is part of the Qt framework (under the Qt Open Source Model). The backend was developed in C++, which is compatible with ROS. Figure 7 shows screenshots of the newly developed GUI application.

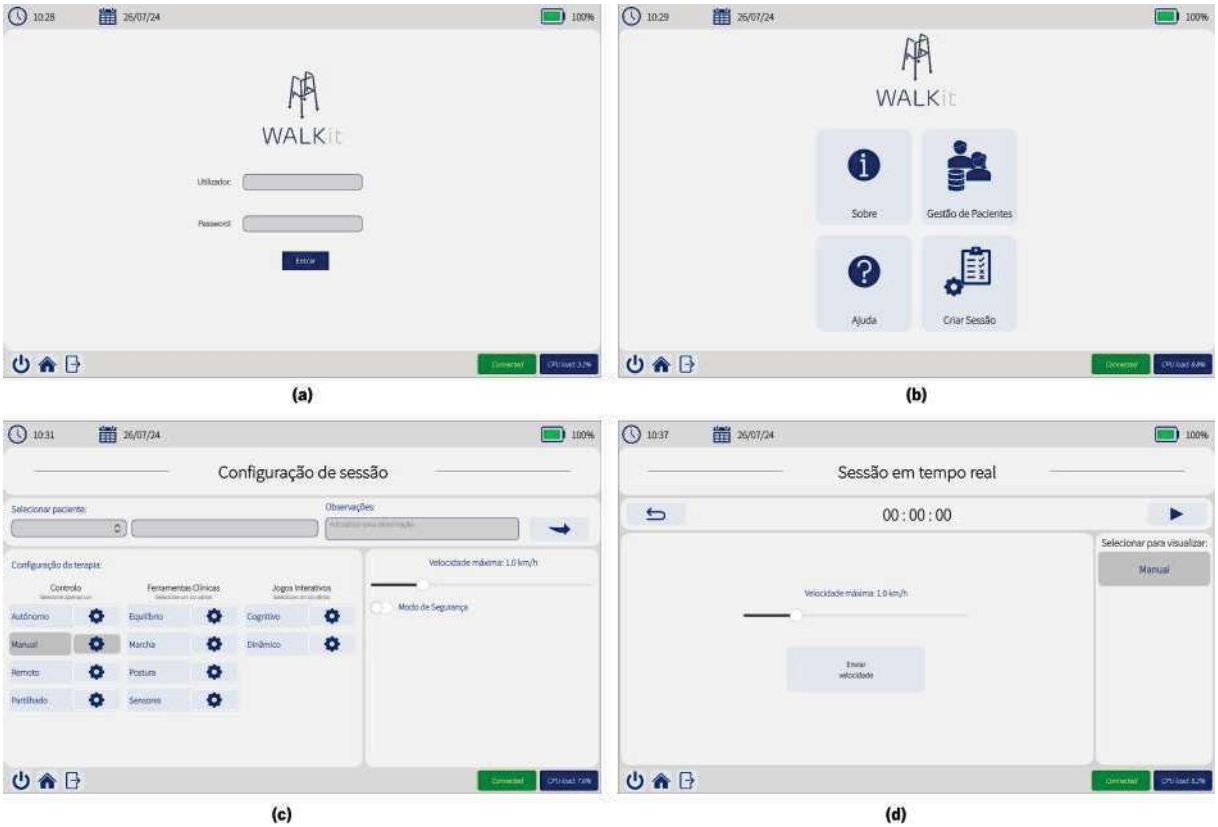


Figure 7: New GUI developed as part of the redesign of the device's software: **(a)** login system, **(b)** home menu, **(c)** session configuration menu, and **(d)** real time session menu.

Since the application handles sensitive data, security mechanisms have been included to ensure data

confidentiality, following General Data Protection Regulation (GDPR) considerations. For this purpose, a login system based on Single-Factor Authentication (SFA) was created, and the password was encrypted with the *Argon2* algorithm (Figure 7a), which is a cryptographic hashing algorithm. Once authenticated, the application displays an attractive menu with four options (Figure 7b), the most important of which are patient management and session creation. To set up the device for a new session, the user must click on 'Create Session'. Once clicked, a new page will open (Figure 7c) where the user should first select a patient who will perform the rehabilitation session and, as a confirmation, the patient's name will appear. If the user prefers, it is also possible to enter the patient's ID instead of searching for the ID in the list of possible patients. This is preferable when the device is used by multiple patients. The user must then select a control strategy, and only one will be accepted, one or more clinical tools, which is optional, and one or more interactive games, which is also optional. In addition, each algorithm has its own parameter configuration, which can be configured by clicking on the gear wheel, which brings up a small window on the right side of figure 7c. In this window it is possible, for example, to adjust the session speed, activate the security mode, activate/deactivate certain sensors or configure HRI strategies. Finally, the user has to click on the arrow that allows to move to the next layout (Figure 7d), but only if a patient ID is selected, otherwise it does not move. This layout allows to visualize the developed HRI strategies, as well as to change the control settings in real time (*e.g.* the linear velocity of the device).

Database Management System

A major challenge in the previous prototype was to store the data collected during a session in an **effective, time-efficient manner without iterating over text files**. The software was therefore optimized by introducing a polyglot persistence database management system [116]. This consisted of a relational database, SQL database, to store relevant but strictly necessary data related to patients and session configuration (*e.g.* type of control, device speed, clinical tools), and a non-relational document-oriented database, $MongoDB$, to store all time series data, namely data obtained by the low-level sensors, which are acquired at 100 Hz. This allowed efficient storage of data up to 200 Hz, with a maximum sample loss of 0.04%, which is considered residual. This loss was obtained by emulating intervention sessions lasting 30 and 60 minutes, using acquisition frequencies of 100 and 200 Hz. In addition, the walker's CCU was set to maximum capacity to check the effectiveness of the solution.

As for the patient's personal information, it is stored in the SQL database after being encrypted with the Advanced Encryption Standard (AES) algorithm, considering the Cipher Block Chaining mode.

The graphical interface has also been optimized to allow basic CRUD operations, following a clinical

requirement. Figure 8 shows screenshots of the GUI where it is possible to search for a patient (Figure 8b), enter a patient (Figure 8c), enter clinical scores for patients (Figure 8d), archive one or more patients (Figure 8e), and review short session configuration information (Figure 8f).

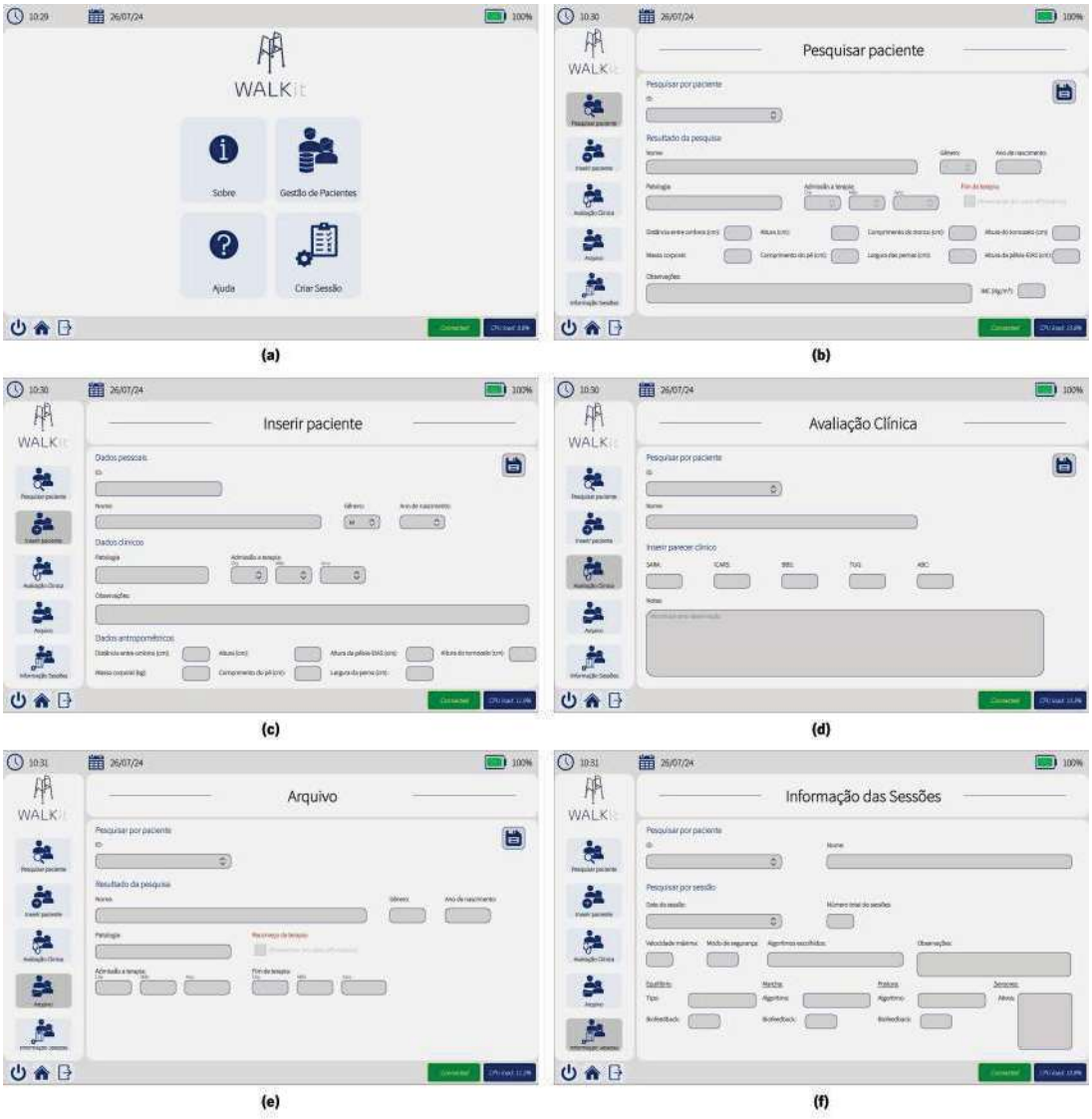


Figure 8: Snapshots of the database's menu of new GUI embedded in WALKit: **(a)** home menu, **(b)** search for patient, **(c)** add new patient, **(d)** add clinical score, **(e)** archive menu, and **(f)** session's information.

3.4.3 Experimental validation

Following the waterfall model, the application was developed based on clinical and technical requirements and validated with end users. Data collection was carried out under the ethical procedures of the Life and Health Sciences Ethics Committee (CEICVS 147/2021), in accordance with the Declaration of Helsinki and the Oviedo Convention.

Participants

Six participants, all female health professionals from Braga Hospital and Guimarães Hospital, were invited to participate in the usability testing of WALKit's optimized GUI. Each participant gave informed consent to participate in the following experimental validation. Of these six participants, two were specialists in Physical Medicine and Rehabilitation (one from Braga Hospital and another from Guimarães Hospital, Portugal), one is a physiotherapist, and the remaining three are residents of the Physical Medicine and Rehabilitation Service of Braga Hospital, Portugal.

Methodology

To maximize user interaction with the new GUI, 10 experimental validation tasks were outlined for users to complete. These tasks included **i)** accessing the application using specific credentials; **ii)** inserting a new patient to hold sessions with the device; **iii)** searching for a patient with a specific ID; **iv)** searching for a patient, reporting their therapy with the device as completed, and saving; **v)** restarting the therapy of an archived patient; **vi)** enter a clinical assessment for a given patient; **vii)** review the information for a given session; **viii)** return to the main menu and configure a new rehabilitation session, selecting a clinical tool; **ix)** customize the clinical tool for the user; and **x)** start the rehabilitation session and reconfigure the clinical tool in real time. Simultaneously with performing the tasks, the participants were asked to give their opinions following the think-aloud protocol [117]. After completing these tasks, participants were asked to answer the SUS [118], a worldwide scale used to evaluate the usability of various products and user interfaces, translated and validated for the Portuguese language [119] (see appendix A.1).

3.4.4 Results and Discussion

Table 5 presents the usability results considering the application of SUS for the new GUI. According to the results, although there is one participant who considered the optimized GUI marginally acceptable with a SUS score of 57.5, all other participants rated the optimized GUI with **usability scores above 90 points**. The results indicate that users generally perceived the new GUI as intuitive and easy to use, with positive ratings across key usability questions (Q2: 1.83, Q3: 4.17, Q4: 1.50, Q8: 1.50). Additionally, users reported that the functionalities were well integrated and free of inconsistencies (Q5: 4.33, Q6: 1.67). Moreover, the analysis of Table 5 reveals that five out of six participants showed strong agreement on Q1 (4.67) and Q10 (1.33), emphasizing the importance of this new GUI and highlighting the system's high learnability for new users. Therefore, an average score of 84.17 ± 13.57 was obtained, which

is considered **acceptable and almost "excellent"** according to the SUS rating scale presented by Bangor *et al.* [47]. Moreover, this score **highlights the intuitiveness** of the GUI, which is extremely relevant for technology acceptance and was also confirmed by most of the participants after completing the SUS questionnaire. In addition, following the think-aloud protocol, the participants gave their opinions and suggestions for modification, all of which were considered and culminated in the final GUI of Figures 7 and 8.

Table 5: SUS scores for the experimental validation of the optimised GUI of WALKit Smart Walker

Question	Participants						Mean	Std
	P1	P2	P3	P4	P5	P6		
Acho que gostaria de utilizar este produto com frequência.	5	5	5	5	3	5	**4.67**	**0.82**
Considerei o produto mais complexo do que o necessário.	2	2	1	2	2	2	**1.83**	**0.41**
Achei o produto fácil de utilizar.	4	5	4	4	3	5	**4.17**	**0.75**
Acho que necessitaria de ajuda de um técnico para conseguir utilizar este produto.	1	1	2	1	2	2	**1.50**	**0.55**
Considerei que as várias funcionalidades deste produto estavam bem integradas.	5	3	5	5	3	5	**4.33**	**1.03**
Achei que este produto tinha muitas inconsistências.	1	1	1	2	3	2	**1.67**	**0.82**
Suponho que a maioria das pessoas aprenderia a utilizar rapidamente este produto.	4	5	5	2	4	5	**4.17**	**1.17**
Considerei o produto muito complicado de utilizar.	1	1	1	2	3	1	**1.50**	**0.84**
Senti-me muito confiante a utilizar este produto.	4	5	4	5	3	4	**4.17**	**0.75**
Tive que aprender muito antes de conseguir lidar com este produto.	1	1	1	1	3	1	**1.33**	**0.82**
	90	**92.5**	**92.5**	**82.5**	**57.5**	**90**		

Figure 9 shows a short video demonstrating the new software of WALKit SRW.

Figure 9: Video demonstration of the new GUI of WALKit SRW.

3.5 Clinical Support and Feedback Tool

The ability to access the information recorded during the use of the robotic device is essential **to promote a more user-centered therapy** focused on the individual's difficulties. This feedback would be of significant clinical value, helping to adapt the rehabilitation strategies and to evaluate the effectiveness of the SRW. Therefore, another goal of this thesis was to develop a **clinical support and feedback tool** to assist clinicians during RAGT with WALKit SRW.

First, the requirements of the key stakeholders, *i.e.* the clinicians and physiotherapists, were identified. Then, a prototype of the final application was designed and optimized according to the interim assessments made by the clinicians. Finally, the final application was developed and thoroughly tested with end users for usability and functionality. This subsection describes the requirements and visualizations of the proposed solution, as well as the usability and functionality results obtained.

3.5.1 Stakeholder requirements

The technical and clinical requirements were analyzed by means of a questionnaire sent to seven health professionals from hospitals in Braga and Guimarães, Portugal.

Regarding the technical requirements, the application should allow: **i)** access to patient data and perform basic CRUD operations; **ii)** manage the sessions that each patient performs, namely access the session configuration; **iii)** identify the patients who are still in therapy and those who have already undergone therapy; and **iv)** access the data collected by the sensors and download the raw and eventually processed data from the device. In terms of clinical requirements, the application must allow **i)** the visualization of the data collected in a single session, raw or processed, in the form of graphs and objective values; **ii)** the visualization of the progress during the different rehabilitation sessions; **iii)** the application of clinical scales (*e.g.*, SARA, TUG, 10-MWT) and their evolution over time; and **iv)** the insertion of the number of falls, which is critical in ataxic patients, and their evolution over time.

Non-functional requirements were also raised regarding intuitiveness of use. An important non-functional requirement was the possibility to use the application on different electronic devices, such as computers, smartphones or tablets.

3.5.2 Application development

A responsive web application, suitable for different interfaces, was developed following the SDLC prototyping model [120]. The frontend of the application is based on *React*, a JavaScript library suitable for developing web user interfaces. The backend is based on *Node.js*, also a JavaScript library. Due to privacy concerns, and similar to the new GUI, the AES algorithm is used for data security. Figure 10 shows screenshots of the web application developed.

Once the web application is launched, users are prompted to enter their credentials. Once logged in, the user can access the home page (Figure 10A), which displays some statistics about the use of the device, such as the number of patients undergoing therapy, the number of sessions already completed, and the number of patients archived. Similarly, on the left side, the user can access a menu that allows

him/her to navigate directly to his/her profile, to the page dedicated to the management of patients and archives, and to the management of users (clinicians and patients). By clicking on the *Gerir Pacientes* sub-menu, a table with the different patients undergoing therapy with the device will appear (Figure 10B). In this subpage it is possible to visualize the profile of the patient and also to archive or delete this patient. Figure 10C illustrates the patient's profile, where it is possible to access both personal and anthropometric data stored in the SQL database. On the same page, it is possible to perform a clinical evaluation and visualize the evolution of specific scales (Figure 10D), which are commonly used to assess the severity of ataxia. It is also possible to visualize the number of falls recorded (Figure 10E).

This application also allows users to access information related to specific sessions, including data collected in real time by the device (Figures 10F-J). Examples of such data are the acceleration and angular velocity of the upper body collected with the IMU positioned at the level of the L3-L5 lumbar vertebrae, the orientation of the upper body, the load distribution on the walker platform, as well as the user's performance in HRI strategies. In addition, it is prepared to receive and display objective spatial and temporal gait monitoring parameters whose algorithms are still in development.

3.5.3 Experimental validation

Following the prototyping model, after the development and further validation of the app prototypes according to the requirements of the stakeholders, the final clinical support and feedback tool was validated with the final users, namely health professionals from the Hospital of Braga. Data collection was carried out under the ethical procedures of the Life and Health Sciences Ethics Committee (CEICVS 147/2021), following the Declaration of Helsinki and the Oviedo Convention.

Participants

Four participants, all female and health professionals from Braga Hospital, were invited to participate in the usability testing of the WALKit web application. Each participant gave informed consent to participate in the following experimental validation. Of these four participants, one is a specialist in Physical Medicine and Rehabilitation, one is a physiotherapist, and the remaining two are residents of the Physical Medicine and Rehabilitation Service of Braga Hospital.

Methodology

To validate the clinical support and feedback tool, a strategy similar to that used to validate the new GUI of the device was adopted. However, due to the unavailability of two healthcare professionals to

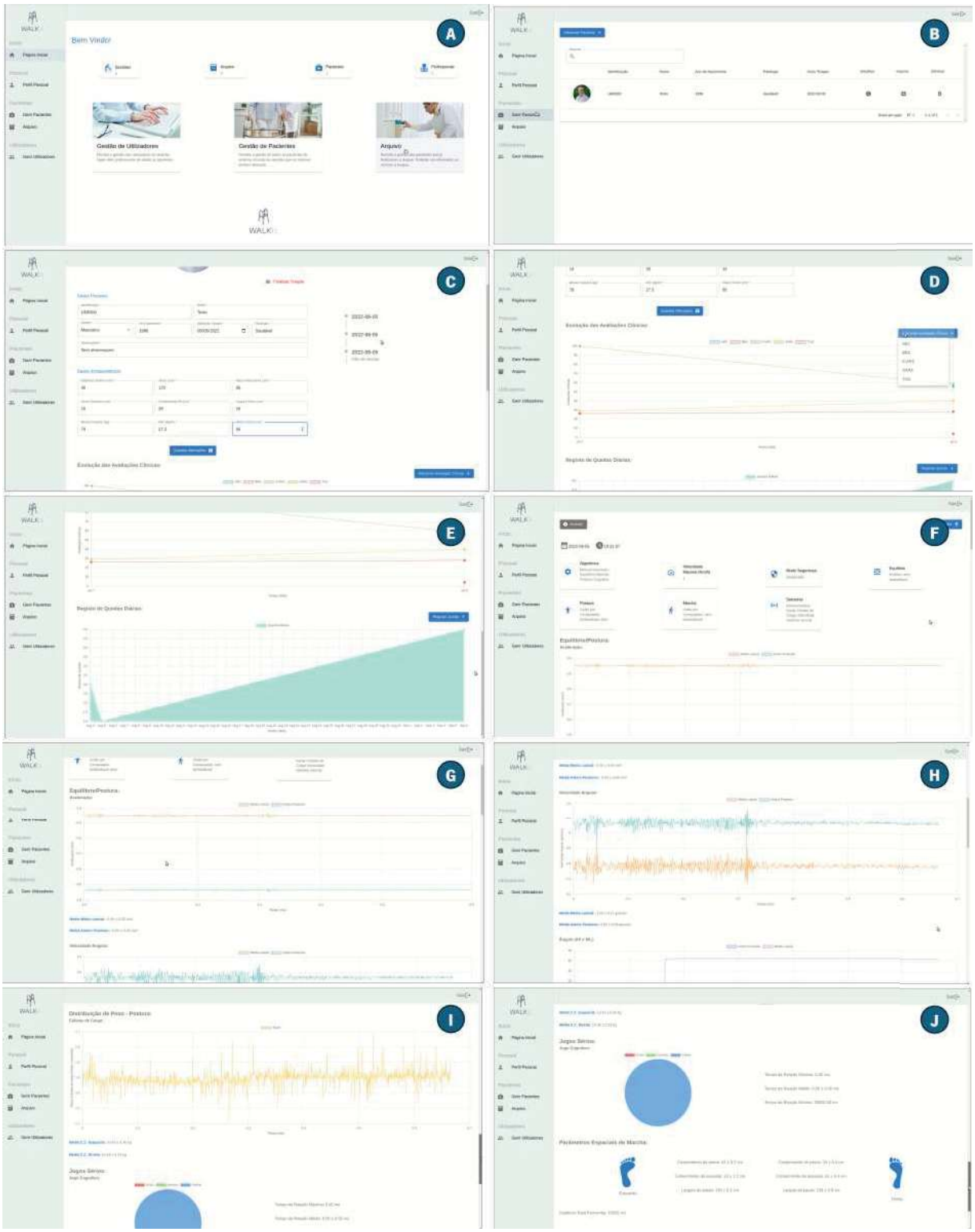


Figure 10: Screenshots of the developed clinical feedback tool for both health professionals and final users of WALKit Smart Walker. Note that data presented on these screenshots are fictitious and merely illustrative.

perform the in-person test, the remote usability testing method [121] was followed. For the remaining two participants, the in-person think-aloud protocol was conducted. To validate the clinical feedback tool, 10 different tasks were designed to ensure maximum user interaction with the application. These tasks included the following activities **i)** accessing the system with specific credentials; **ii)** entering a specific patient into the database with specific personal and clinical data; **iii)** finalizing therapy for a specific patient; **iv)** add a clinical evaluation scale for a specific given patient; **v)** assign a specific number of falls to the previous patient on this specific day; **vi)** for the same patient, review his/her sessions with the device and access his/her temporal evolution; **vii)** for the same patient, check a specific session on a specific day and download the acquired sensor data; **viii)** access the archive and delete a patient with a specific ID; **ix)** add a new user to the database so that he/she can access the website; and **x)** access the personal profile page, change the name, save the changes and log out of the web application. Simultaneously with performing the tasks, the participants were asked to express their opinions according to the think-aloud protocol [117]. After completing these tasks, participants were asked to complete the SUS [118], taking into account the translated and validated scale for the Portuguese language [119] (see appendix A.1).

3.5.4 Results and Discussion

Table 6 shows the usability results considering the developed web application. According to the results, all five participants rated the **clinical support and feedback tool** with **usability scores above 85 points**, ranging from 87.5 to 100 points. The results indicate that users generally perceived the clinical support and feedback tool as intuitive and easy to use, with positive ratings across key usability questions (Q2: 1.25, Q3: 4.75, Q4: 1.00, Q8: 1.00). Additionally, users reported that the functionalities were well integrated and free of inconsistencies (Q5: 4.75, Q6: 1.00). Moreover, the analysis of Table 6 reveals that all participants showed strong agreement on Q1 (5.00) and Q10 (1.00), emphasizing the importance of this software and highlighting the system's high learnability for new users. Therefore, an average score of 95.63 $\pm$ 5.54 was obtained, which is considered between **"excellent" and "best imaginable"** according to the SUS rating scale [47]. Although the sample size was smaller than for the validation of the new GUI, the average usability score was higher and the standard deviation was lower, indicating that the end users unanimously found the application to be **very intuitive and functional**. Figure 11 shows a short video demonstrating the new **clinical support and feedback tool** of WALKit SRW.

Table 6: SUS scores for the experimental validation of the developed clinical feedback tool

Question	Participants				Mean	Std
	P1	P2	P3	P4		
Acho que gostaria de utilizar este produto com frequência.	5	5	5	5	**5.00**	**0.00**
Considerei o produto mais complexo do que o necessário.	1	2	1	1	**1.25**	**0.43**
Achei o produto fácil de utilizar.	5	4	5	5	**4.75**	**0.43**
Acho que necessitaria de ajuda de um técnico para conseguir utilizar este produto.	1	1	1	1	**1.00**	**0.00**
Considerei que as várias funcionalidades deste produto estavam bem integradas.	5	4	5	5	**4.75**	**0.43**
Achei que este produto tinha muitas inconsistências.	1	1	1	1	**1.00**	**0.00**
Suponho que a maioria das pessoas aprenderia a utilizar rapidamente este produto.	5	4	4	4	**4.25**	**0.43**
Considerei o produto muito complicado de utilizar.	1	1	1	1	**1.00**	**0.00**
Senti-me muito confiante a utilizar este produto.	5	4	5	5	**4.75**	**0.43**
Tive que aprender muito antes de conseguir lidar com este produto.	1	1	1	1	**1.00**	**0.00**
	100	**87.5**	**97.5**	**97.5**		

Figure 11: Video demonstration of the new clinical support and feedback tool of WALKit SRW.

3.6 General conclusion

This section presented, in general, the robotic device optimized within the scope of this thesis, in terms of software architecture and its renewal. The development and validation of a redesigned graphical interface for the control of the device, **which meets the requirements of the stakeholders, while being visually appealing, intuitive and functional**, was briefly presented. Furthermore, the development and validation of a new **clinical support and feedback tool** was presented, which allows the management of both patients and rehabilitation sessions, as well as the visualization of objective and specific data of each session, which can help the clinician to **adjust the therapy taking into account directly the patient's interaction with the device**. The results achieved made it possible to reach KPI 2, obtaining usability scores above 70 points, demonstrating the intuitiveness of the device and the redesigned software. This result is very important as it demonstrates the technology's acceptability among clinical stakeholders.

Chapter IV

Motion Intention Perception

Chapter 4

Motion Intention Perception

4.1 Introduction

As discussed in Chapter 2, most of the studies involving robotic walkers decode the intention of movement in a direct way, *i.e.* requiring additional physical interaction. Typically, they resort to force-sensing technologies [55,63,65,68], usually embedded in the device's handles or handlebars or in a pelvic mechanism [61], which are either an **expensive technology** if robustness is prioritized, or **not very accurate** when considering low-cost sensors [35]. Other studies also resort to load cells [36], pressure sensors [65], and Hall-effect sensors [60], having similar shortcomings of force-sensing technology or requiring additional cognitive effort [60]. Indirect ways of decoding MI have also been presented in the literature, namely using IMU [56, 63, 64], LRF [31, 58, 62, 64], proximity sensors [59], and cameras [35, 57, 58, 62]. As for the IMU, it is a very interesting wearable sensor that can be used to tackle several challenges, but for a complete gait analysis and decoding the intention from it, it may be necessary to use several units (*e.g.* [122]), which could cause discomfort during prolonged use. Furthermore, as the robotic walker is a non-wearable device, it would be relevant to consider other sensors that could be embedded in the device, namely cameras or LRF. Cameras appear to be a more advantageous technology as they have a large FOV, can correctly distinguish what is and is not the user, and are widely used in the literature in several research areas. LRF technology, on the other hand, in addition to being extremely expensive compared to a vision-based approach, may not allow for a holistic view of the user, for example, if it is a 2D laser that only sees certain parts of the body. As a result, it can be more difficult to interpret the data when limbs are occluded due to gait irregularities. Current camera-based solutions, although functional, resort to additional, extremely expensive sensors (LRF) [58, 62], use cameras to analyze the user's torso [57, 62], or require upper limb dexterity [35] which may also be affected in patients with CA. Therefore, further research is still needed in this area in order to achieve a solution that allows for real-time MI decoding in a **natural and intuitive way, without additional physical interaction and**

considering the user's gait. Therefore, new AI-based algorithms must be investigated to provide the device with the intellect to decode this intention by analyzing the user's gait in real time. This doctoral thesis was based on the premise that although gait is affected in ataxic patients, the use of a robotic walker promotes a more stable gait, as will be discussed later in Chapter 7 and was also concluded in study [48].

Based on the literature review, this chapter presents an in-depth investigation of several approaches based on AI with RGB images to accurately early detect human MI when using WALKit SRW. This in-depth research involved the collection of a custom dataset and the training and evaluation of various DL-based algorithms using RGB-D videos recorded with the SRW's embedded gait camera, and later using this information to develop a closed-loop HIL control strategy capable of making WALKit SRW **responsive to the user's needs and intentions in a more natural way**. This chapter presents the methodology used in this thesis for the early detection of the human MI, the main results obtained and their critical discussion.

4.2 Proposed Strategy

This chapter investigates several DL-based approaches responsible for classifying walking activities through different inputs obtained from the RGB videos of WALKit's gait camera. In an attempt to avoid more complex neural networks to extract both spatial and temporal features, this thesis proposes to merge this information into one single RGB frame. Furthermore, it proposes the use a DL-based model to automatically extract relevant human features that help decode the user's intention of WALK, STOP, TR, TL, which were considered relevant to enable a seamless control of the robotic device. This model should focus solely on the user's gait, which was hypothesized to encode the most relevant motion information to obtain MI, extracting spatial and temporal dependencies towards an intuitive way of controlling the device. Thus, to efficiently decode walking directions from RGB videos, three requirements were established to evaluate the DL-based models, namely: **i)** accurately detect 4 classes, namely STOP, TR, TL, WALK, while viewing small temporal sequences to increase the efficiency of the algorithm in real time; **ii)** extract human-focused features to avoid background distortions and motion due to camera movement; **iii)** efficiently detect motion intention with a maximum delay of 0.64s, calculated as the average duration of a healthy step while walking at the fastest walking speed assumed by WALKit SRW, which is 1.0 m/s.

4.3 Methodology

This section describes the methodology used in this thesis to detect human motion while walking with WALKit SRW using DL-based models. Given the specificity of the challenge, this work involved a number of tasks, including recording gait data with the SRW, since there are no public datasets that can be used for context. It was therefore necessary to create the dataset needed to train the AI models, and to devise a strategy for decoding the MI by studying different designs of the model's input, *i.e.* different image configurations that will be employed to train the model to decode the different MI. Figure 12 illustrates, in a general sense, the methodology followed in this chapter, from data collection to the development and evaluation of the models for MI detection.

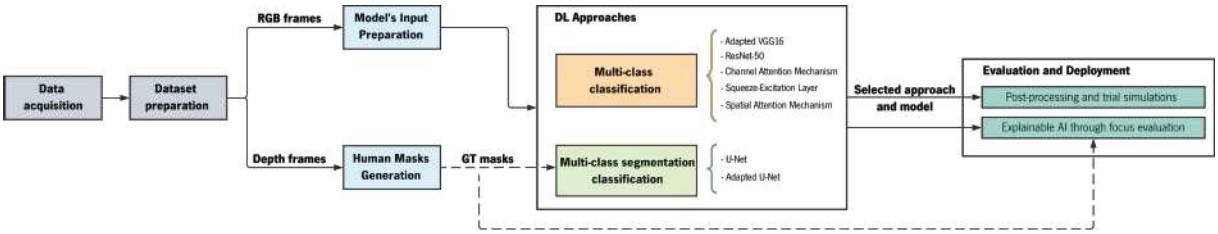


Figure 12: Overall pipeline followed for human motion decoding using RGB videos. GT stands for Ground-Truth.

4.3.1 Dataset Acquisition

This work integrated the acquisition of a custom dataset recorded with the cameras of WALKit SRW, which always maintained a frontal perspective of the user. The data acquisition was carried out under the ethical procedures of the Life and Health Sciences Ethics Committee (CEICVS 147/2021), following the Declaration of Helsinki and the Oviedo Convention. Data were collected at the School of Engineering of the University of Minho, outside a controlled laboratory space.

The dataset consisted of RGB-D frames acquired at 30 *fps* from 15 healthy adults (9M, 6F, mean age 25.27 $\pm$ 2.54 years, body mass 65.15 $\pm$ 9.22 kg, and height 168.47 $\pm$ 7.42 cm). In addition, Xsens MVN Awinda (Xsens Technologies B.V., The Netherlands), a motion capture system composed of 17 wearable IMUs, was used in a full-body configuration to accurately place the Ground Truth (GT) labels of the different actions, taking into account specific gait events, namely Heel Strike (HS) and Toe-off (TO) [123], allowing more accurate labels to mark action transitions. Data synchronization was achieved by sending a digital pulse from the WALKit SRW to the Xsens MVN Awinda. This mobile acquisition setup allowed real-time data acquisition through predefined and realistic scenarios, covering non-ideal lighting

conditions and dynamic backgrounds to maximize data variability. In addition, recordings were made at different times of day (morning and afternoon) and on different days, contributing to a more general and variable dataset with different light conditions. It is also noteworthy that the outfit of the participants was not controlled to account for different types of clothing (different colors, different types of pants, looser or tighter fitting clothing, etc.), which also contributed to the variability of the dataset.

4.3.2 Experimental Protocol

The dataset was recorded using an automatic trajectory mode, considering four circuit sequences consisting of **i)** 10s standing, **ii)** 3m walking, **iii)** 90° turn (right or left, with a wider or narrower radius), **iv)** 3m walking, and **v)** 10s standing. The automatic trajectory mode was developed due to the heavy weight of WALKit SRW, which could cause abnormalities in the user's gait when used in passive mode. Using the automatic trajectory mode allowed WALKit to actively follow given trajectories, acting only as a recorder and generating velocity commands for each wheel according to a desired linear velocity and turning angle and radius. Each participant performed 2 valid trials per circuit, considering three walking speeds: 0.5 m/s, 0.7 m/s, and 1 m/s. These gait speeds were chosen according to the most commonly used speed range of the walker, as well as considering the typical self-selected slow, normal, and fast walking speeds for healthy subjects [124]. Participants were instructed not to simply follow the SRW, but to interact with it along the designed and marked course. This allowed for realistic scenarios while capturing the user's MI as naturally as possible. Some familiarization trials were also performed before the actual recording procedure to encourage the HRI. In total, each subject performed 24 trials (4 circuits $\times$ 3 speeds $\times$ 2 valid trials). Figure 13 illustrates two of the circuits considered in the data collection, including the different radius of curvature.

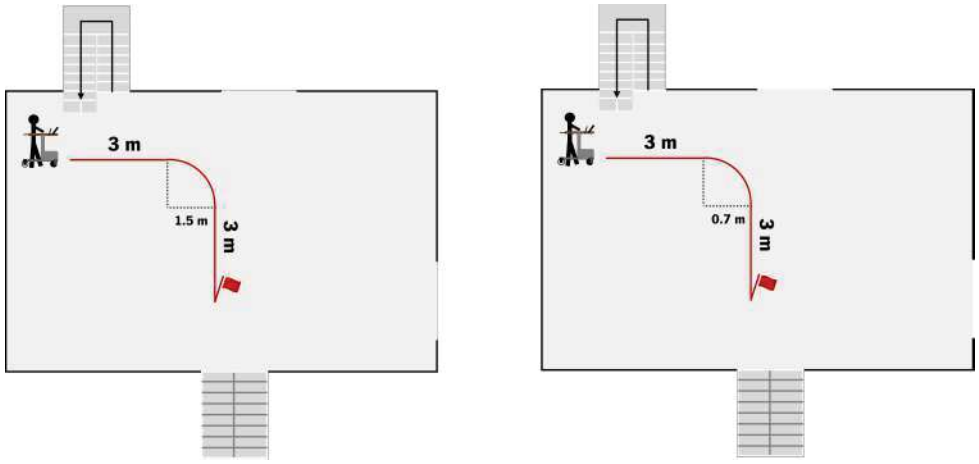


Figure 13: Illustration of two TR circuits used for data collection.

4.3.3 Dataset labeling

Dataset labeling was done in two different ways during data collection: **i)** considering a joystick command inspired by Figueiredo *et al.* [122], which was used by an external person to mark transitions between visible actions by observing distinct foot movements (*JOY* labels), and **ii)** considering the speed commands of the walker's wheels published by the automatic trajectory generator mode (*VEL* labels) and recorded in WALKit's CCU in real time. *JOY* labels denote the user's interaction and intention, while *VEL* labels represent the device's actions.

4.3.4 Dataset Preparation

The dataset was downsampled to 15 Hz to cover more action time with a smaller number of similar samples. This was done because literature shows that the main walking frequency does not exceed 2 Hz for walking speeds above 1 m/s [125], so there is no risk of aliasing. Considering the different number of frames obtained for the turning actions, and aiming to create a balanced dataset, 40 frames were extracted from each RGB video sequence. This extraction was performed avoiding the boundaries or transitions of the action, in order to avoid any possible bias in the labeling procedure. Therefore, the beginning of each class was marked with the most recent of the two labels (*JOY* and *VEL*).

The final dataset contained a total of 720 sequences, each consisting of 40 consecutive frames, for a total of 28800 RGB frames. The sequences were equally divided among the four classes (STOP, TL, TR, and WALK), resulting in 180 sequences of 40 frames per class.

4.3.5 Model's Input Preparation

This thesis proposes different types of input, considering a sliding window approach over successive frames: **i)** the difference between the last and the first RGB frame (*DIF* input) and **ii)** the sum of all RGB frames (*ADD* input), in each window. The window length was empirically defined as 4 (0.27s at 15 *fps*), since it contains visible motion while never containing information from more than 1 different step.

The designed inputs were also cropped according to a predefined Region-of-Interest (ROI) focused on the user's lower limbs. A pre-defined ROI was used instead of bounding box localization nets because the user always assumes a central position in the image. In total, four input forms for human MI recognition and detection were generated and studied in this thesis: cropped and uncropped *DIF* and *ADD* images, as shown in Figure 14.

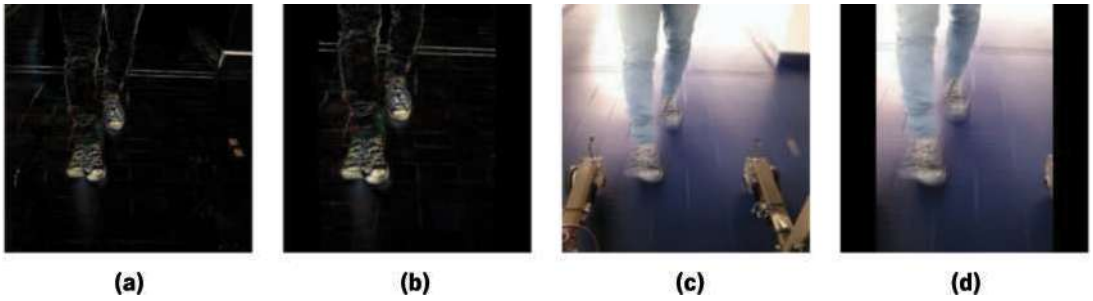


Figure 14: Four inputs that were studied in this work: **(a)** uncropped *DIF*, **(b)** cropped *DIF*, **(c)** uncropped *ADD*, and **(d)** cropped *ADD*.

4.4 Deep Learning Approaches

This thesis investigated two different approaches for the early detection of human MI, namely: **i)** multi-class classification, and **ii)** multi-class segmentation-classification.

Regarding the first approach, it was a single image classification. Following the literature of Human Activity Recognition (HAR), which usually employs CNNs [126, 127], the VGG16 was implemented without its top layers, only with a Global Average Pooling (GAP) followed by a *softmax* classification layer, as shown in Figure 15. Batch normalization layers were also added to improve the optimization and generalization performance. Furthermore, the activation function of the last convolution layer was changed from ReLU to a hyperbolic tangent function (*tanh*). In addition, ResNet-50 was also investigated for this task of early detection of human MI using its traditional configuration presented in [128].

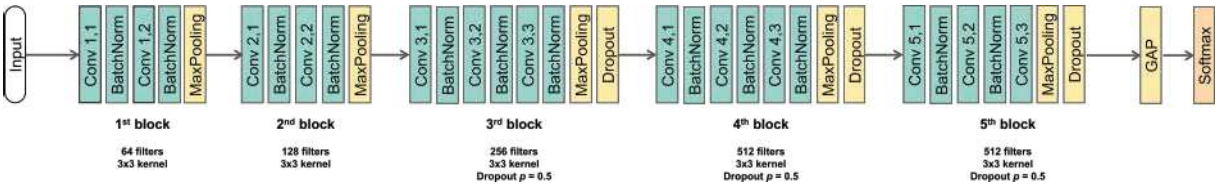


Figure 15: Illustration of the adapted VGG16 implemented in this work.

In an attempt to increase the classification performance and also to maximize the model's focus on the user's lower limbs, as expected, a Channel-Wise Attention (CHATT) mechanism, presented in Figure 16a, was added to the backbone of the best neural network obtained in the previous step, similar to that presented in [127]. In addition, a Squeeze-and-Excitation (SE) layer, presented in Figure 16b, was also investigated, which was responsible for performing feature recalibration to emphasize relevant informative features and suppress less relevant ones [129]. Finally, a Spatial Attention (SPATT) mechanism, as presented in Figure 16c, was also evaluated. The latter was introduced because these networks are

particularly interesting for redirecting the focus of the network to where there is an informative region. Figure 16 illustrates the CHATT mechanism, as well as the SE layer and the SPATT mechanism. For the SE layer, a ratio (r) of 4, 8, and 16 was used for the first FC layer, resulting in dense layers of 512, 256, and 128 neurons, respectively.

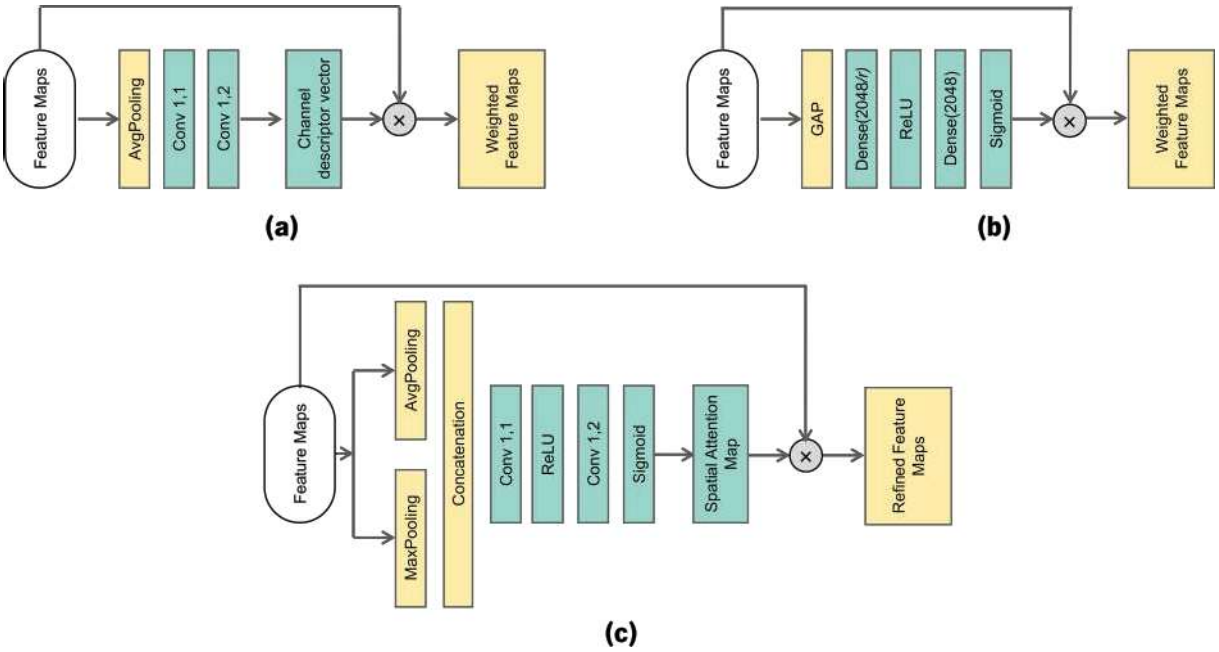


Figure 16: Illustration of the attention blocks investigated in this thesis: **(a)** CHATT mechanism, **(b)** SE layer, and **(c)** SPATT mechanism.

As presented in Berardini et al. [126], transfer learning technique was used for all approaches. The backbone weights of VGG16 and ResNet-50 classification models were initialized to the weights of these same state-of-the-art networks pre-trained on the general object classification benchmark, ImageNet [130], towards accuracy maximization, while using large amounts of computational resources, which trains the models to detect and produce general features.

The second approach consisted of a multi-class segmentation-classification network. In this case, the U-Net neural network [131] was trained to segment the user's legs and feet, in order to obtain the optimized weights to direct the network's focus to this region of the user's body. U-Net was trained with GT human masks obtained with a computer vision algorithm of ours [38] (see Figure 74 of Appendix B.1), using depth frames, which were pre-processed to verify that they were not corrupted by sunlight. In case of corrupted masks, these were duly removed from the dataset. The rationale of this approach was to use only U-Net encoder that was pre-trained to capture the most relevant features of the lower limb region, and to adapt this network to create a novel classification model. Thus, the model consisted of the U-Net encoder followed by two convolutional blocks. A dropout layer (p=0.5) was added, followed by a GAP

and a *softmax* layer to decode the user's MI of STOP, WALK, TR, and TL. The U-Net encoder weights of the classification model were initialized with the ones learned in the previous training of the U-Net model for segmentation, while the remaining layers were initialized with the He normal function. The first 16 layers of this encoder were also frozen during classification training. Figure 17 illustrates the novel neural network proposed in this work.

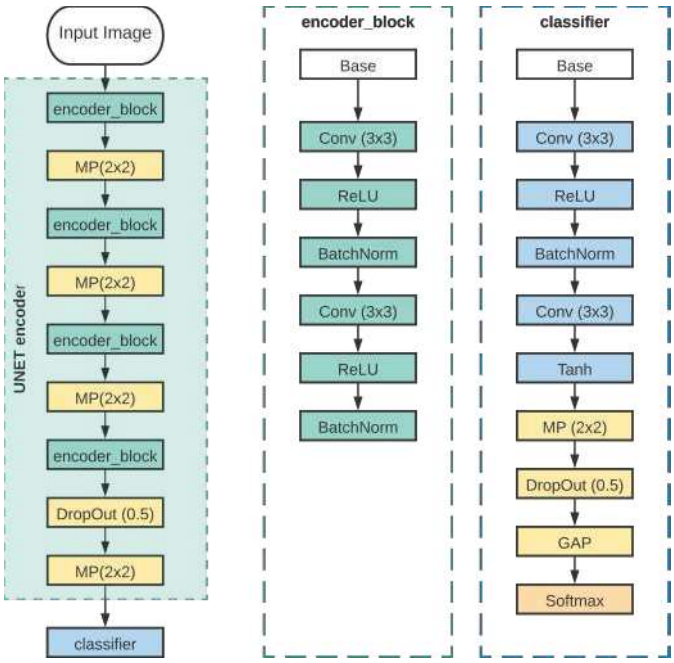


Figure 17: Adapted U-Net neural network for multi-class classification used in this work along with the segmentation-classification network.

4.5 Ablation study

Although the cameras are static on the walker, *i.e.* the FOV of the cameras remains unchanged, the walker is moving, so the background of the image can vary. However, considering that the gait camera has a considerable tilt, the background is mostly ground, as shown in Figure 14c and 14d. Nevertheless, the information provided in the background may provide relevant information to indicate whether the user is standing still, walking, or turning, relevant to classify the current motion, but not the intention. Therefore, the performance of the best neural network was analyzed by removing the background and verifying that the model actually retains the most relevant features in the region of the user's lower limbs.

Three approaches were studied: **i)** the first consists of the real-time segmentation of the user using U-Net, followed by the model for MI decoding. Here, it was decided to make the background green so as not to be confused with the user's clothing; **ii)** the second approach consisted of training the best

neural network with a new dataset obtained by changing the background. In the latter, the background of some images was removed using the user's GT masks obtained with a computer vision algorithm of ours [38]. It was then replaced by static images representing hospital floors (different backgrounds but with uniform colors), with 80% of the training and validation sequences placed with the randomly changed background and 20% with the original background. Regarding the test set, only 50% of the images were replaced with the random background to check if the model is indeed able to generalize correctly; and **iii)** the third approach is similar to the second, but only considers two main classes: STOP and WALK. Figure 18 presents examples of input images used in the three approaches.

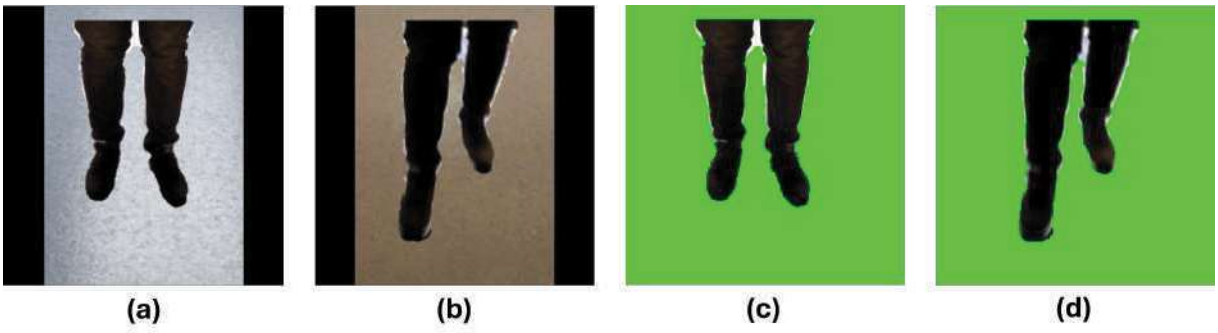


Figure 18: Example of input images considering: **(a)** STOP class with different background, **(b)** WALK class with different background, **(c)** STOP class without background, and **(d)** WALK class with background.

4.6 Training Pipeline

4.6.1 Dataset split

The dataset split followed the 80−20 split configuration, considering the number of participants: 80% was used for training (12 participants) and the remaining 20% was used for testing (3 participants). To control the training process, one participant was left in the validation set, similar to [132]. The use of cross-validation was considered, but due to limited computational resources and the size of the dataset, it was decided to train the model by randomly dividing the participants into training, validation, and testing. Table 7 describes each of these splits.

For the segmentation and quantitative focus evaluation tasks, the dataset used was slightly smaller because some sequences were removed due to mask corruption (the depth image was highly corrupted by sunlight).

Table 7: Number of input frames of the model for each dataset split

Split	Participants	Classification	Segmentation	2-class Classification
Train	[1,15[\{5, 8, 11}	19 536	13 209	7252
Validation	5	1 776	1 295	703
Test	8, 11, 15	5 328	4 736	2368
TOTAL	-	26 640	19 240	10 323

4.6.2 Training Details

CNN configuration

Hyperparameters were extracted from literature dealing with similar tasks and models (study [133] for single image classification and study [131] for segmentation). For classification, parameters were optimized using Mini Batch Gradient Descent with a learning rate of 0.001, a Nesterov momentum of 0.9, and a batch size of 64. The initial learning rate was decreased by 50% to a minimum of $1e^{-4}$ if the training loss did not improve within 4 epochs. The loss function used was the categorical cross entropy. For segmentation, the Adam optimizer was used instead, with a learning rate of $1e^{-4}$ and a batch size of 16. The U-Net convolutional layers were initialized with the He normal weight initialization. Binary cross entropy was used as the loss function. At the end of training, the best model was selected according to the validation accuracy or loss for classification and segmentation, respectively. Regarding the batch size, we performed a manual tuning and used the maximum allowed considering the available computational resources, adjusting the learning rate accordingly.

Dataset preparation

The input images were resized from a resolution of 480×480 pixels to a resolution of 224×224 pixels, preserving the aspect ratio of the images, to match the input size of the pre-trained networks. For the cropped inputs, the original aspect ratio was reduced by the cropping process, so the image was resized as much as possible to the target resolution. The image was then centered and padded to fit the 224×224 dimensions.

Data augmentation was used on the fly to avoid overfitting and the presence of shortcut learning, and to improve the model's focus on the human body despite its global position in the images. Color space transformations were applied by applying random brightness and contrast to simulate different lighting conditions. Spatial transformations were also considered, namely height and width shifts and zooming.

Since directions are an important feature to distinguish between TR, TL and straight walking, rotations were not considered. A random Gaussian blur was also added. Finally, the images were normalized between 0 and 1.

Training Hardware

All models were developed offline using TensorFlow and the Keras DL library in a Python environment. The experiments and DL approaches shown were trained on a computer with the following hardware specifications **GPU**: 1× Nvidia GeForce RTX 3080 Ti/PCIe/SSE2; **CPU**: Intel(R) Core(TM) i9-10940X @3.3GHz (14 core, 28 threads); **RAM**: 65.5 GB.

4.7 Model evaluation

4.7.1 Classification Metrics

The classification was evaluated using common metrics for this task, namely accuracy, precision, recall, and F1-score [126, 133], as follows from equations 4.1 to 4.4. Accuracy gives an overall measure of the model's performance and is straightforward to interpret. However, it may be misleading when dataset is not totally balanced, as it is the case of the second approach tested. Thus, to better understand the performance of the AI model, precision, recall, and F1-score were also computed. These metrics are defined in the following equations, where TP, TN, FP, FN refer to the true/false positive/negative observations, and n represents the total number of classes (which is 4). Both micro- and macro-averages were computed for precision, recall, and F1-score, but the macro-average was preferred to consider the overall performance while taking into account the contribution of each class. Additionally, in cases where the dataset is not strictly balanced, namely when using U-Net, the weighted macro-average was computed instead.

$$\text{Accuracy} = \frac{\text{TP} + \text{TN}}{\text{TP} + \text{TN} + \text{FP} + \text{FN}} \tag{4.1}$$

$$\text{Precision} = \frac{1}{n}\sum_{i=1}^{n}\frac{\text{TP}_\text{i}}{\text{TP}_\text{i} + \text{FP}_\text{i}} \tag{4.2}$$

$$\text{Recall} = \frac{1}{n}\sum_{i=1}^{n}\frac{\text{TP}_\text{i}}{\text{TP}_\text{i} + \text{FN}_\text{i}} \tag{4.3}$$

$$\text{F1} - \text{score} = \frac{2 \times \text{Precision} \times \text{Recall}}{\text{Precision} + \text{Recall}} \tag{4.4}$$

4.7.2 Quantitative focus evaluation

Due to camera motion, background motion is also present in the input images, as shown in Figure 14, corresponding to the action performed by the SRW. This can compromise early action detection in real-time applications, as the model should focus on lower body features to predict walking directions, especially during their first occurrence, without overfitting to the background.

An algorithm for consistent quantitative evaluation of this focus has been implemented as part of explainable AI techniques. Following study [134], Grad-CAM heatmaps were generated for each input image, over the last convolutional layer of the model. These were then compared to the corresponding GT human masks, which were also used as segmentation labels. The model focus was evaluated by the similarity between the Grad-CAM heatmaps and the GT masks, using the *Dice* and IoU coefficients, as given in equations 4.5 and 4.6, considering two areas A and B:

$$\text{Dice} = \frac{2|A \cap B|}{|A| + |B|} \tag{4.5}$$

$$\text{IoU} = \frac{|A \cap B|}{|A \cup B|} \tag{4.6}$$

Ideally, these coefficients would be close to 100% in the case of a segmentation process. The purpose here is to obtain quantitative data that can indicate whether the focus is more on the person or the background. Thus, a value very close to 100% is not expected, nor is a value very close to 0%, which would indicate that the model focuses mostly on the background.

4.7.3 Trial simulations and Post-processing

The results of each approach were analyzed and compared to select the most promising model architecture and input form. The best approaches were then evaluated in experimental simulations, assessing their performance in online early action detection tasks.

To deal with the possible uncertainty of the model during prediction, a post-processing technique was designed and implemented. It assumes that each action should last at least 2 s, consisting of at least two complete steps, given the selected walking speeds. In addition, an online mode filter was used considering a sliding window of 5 frames. This post-processing technique reduces possible noise without introducing significant delays.

4.8 Results and Discussion

4.8.1 Multi-class classification

Table 8 shows the validation results for single frame classification using VGG16 and ResNet-50 neural networks. Different inputs were studied with two of the most widely used neural networks in the literature for activity classification, and the results obtained were quite high, with all metrics above 90%. These validation results were always consistent with learning curves from the training data, as evidenced by the loss and accuracy for each of the models tested (see Figures 68 and 69 of Appendix B.1).

Table 8: Validation results, in percentage, of the VGG16 and ResNet-50, as well as the training time, in hours

Input	Crop	Accuracy	F1-score	Precision	Recall	Training Time
VGG16						
DIF	False	97.02	96.80	97.38	96.23	4.45
DIF	True	94.76	95.02	95.66	94.37	4.47
ADD	False	95.50	96.28	97.79	94.82	4.44
ADD	True	94.48	94.53	94.99	94.03	4.54
ResNet-50						
DIF	False	98.42	98.27	98.52	98.03	4.45
DIF	True	94.37	94.34	95.24	93.47	4.47
ADD	False	96.34	96.26	96.65	95.83	4.44
ADD	True	94.87	95.76	97.05	94.48	4.46

Analyzing the results in detail in Table 8, it can be seen that on average ResNet-50 gives slightly better results than VGG16, but by a small margin (less than 2%). Thus, skip connections and a deeper network improved performance, though the difference was small (less than 1.47% in F1-score). An exception to this is when the input to the network is cropped *DIF* images, where VGG16 outperforms ResNet-50 by at least 0.4% on all metrics analyzed. This suggests that less deep models could also effectively recognize human motions.

Further analysis of Table 8 also shows that the *DIF* input metrics were generally better than the *ADD* input metrics for both VGG16 and ResNet-50, albeit by a small margin (2%), which may not be significant. An exception to this result is when cropping the *ADD* input to the ROI and using the ResNet-50 model,

where all metrics were higher by at least 0.5%. When cropping to the ROI, it was found that the performance of both models was lower for both *ADD* and *DIF* inputs. This result is expected, as it hinders the learning process by removing part of the image background, which may in fact contain relevant information to classify the type of activity.

Although the test metrics were not used as a way to decide on the best neural network (the validation split was used instead), the success percentage of each of the models was assessed for each of the inputs studied considering the test dataset. An analysis of the results, presented in Table 9, shows that for both models, the percentage of correct classifications reached 90%, as in validation (and as in training, as can be seen in the learning curves of Figures 68 and 69 of Appendix B.1). However, for the test data, the best form of input was the *ADD*, with a slightly higher percentage of correct classifications (minimum 0.9% increment). Cropping within the ROI gave the same result as the validation data, *i.e.* there was a lower accuracy percentage. Nevertheless, the accuracy value is over 93%.

Table 9: Percentage of correct classifications for both models (VGG16 and ResNet-50) and for each input regarding the test split

Input	Crop	VGG16	ResNet-50
DIF	False	96.21	97.94
DIF	True	93.69	95.03
ADD	False	97.51	98.84
ADD	True	95.66	96.43

To identify the focus of the neural network when classifying motion intention, the Grad-CAM of the last convolutional layer was generated and compared with the generated human masks. Table 10 shows the results obtained for the *Dice* and *IoU* metrics.

In contrast to the classification results, the cropped inputs presented better focus, meaning a higher similarity between the model's Grad-CAM and the GT masks. This increased *Dice* and *IoU* metrics in average by 4.72% and 3.16%, for the *DIF* input, and by 9.09% and 5.98%, for the *ADD* input, respectively. Additionally, ResNet-50 outperformed VGG16, with an average boost of 7.03% in *Dice* and 4.96% in *IoU*.

The model with the best focus was ResNet-50 with cropped *ADD* input. This indicates that although the learning process was hindered by the cropping of the image in the ROI, it allowed the model to focus better on the user, who is in fact the key actor in the context of assistance considering MI. This statement also holds for the *DIF* input: cropping the input image improved the model's focus. So one can conclude: **i)** background motion may contain features that are easier to extract, thus helping the classification task.

Table 10: Quantative evaluation results, in percentage, for validation Grad-CAM, when predicting with the VGG16 and ResNet-50 models

Input		VGG16		ResNet-50	
Type	**Crop**	**Dice (±std)**	**IoU (±std)**	**Dice (±std)**	**IoU (±std)**
DIF	False	16.16 (±9.64)	9.10 (±5.87)	29.06 (±13.26)	17.70 (±9.01)
DIF	True	22.57 (±14.26)	13.44 (±8.95)	32.09 (±11.57)	19.67 (±8.22)
ADD	False	20.19 (±6.84)	11.39 (±4.21)	22.10 (±16.00)	13.36 (±10.51)
ADD	True	**28.34** (±9.17)	**16.84** (±6.26)	**32.13** (±13.34)	**19.89** (±9.48)

However, this is not the goal, since these features are not reliable for detecting transitions in real-time contexts; **ii)** a careful performance evaluation is needed, since better classification results can sometimes be associated with non-ideal features that cause the model to overfit to the background; and **iii)** cropping the inputs was an effective way to redirect the model's focus to the user's lower limbs. For this reason, the *ADD* input was considered the best way to redirect the focus to the user, combined with cropping the image in the ROI. In fact, the *DIF* input makes it possible to visualize the differences between the initial and final image of the sliding window, while the *ADD* input makes it possible to visualize the drag of the movement, which can help the model to see the trajectory of the lower limbs and thus to classify the MI.

In an attempt to improve the model's focus to the user's lower limbs, ResNet-50 was tested with a CHATT mechanism, and the learning curves can be analyzed in Figure 70 of Appendix B.1. Table 11 shows the validation results of this approach, as well as the training time.

Table 11: Validation results, in percentage, of ResNet-50 with a CHATT mechanism, as well as the training time, in hours

ResNet-50 + CHATT						
Input Type	**Crop**	**Accuracy**	**F1-score**	**Precision**	**Recall**	**Training Time**
DIF	False	99.04	99.03	99.04	99.04	2.93
DIF	True	98.31	98.32	98.37	98.25	2.76
ADD	False	99.38	99.39	99.38	99.38	3.86
ADD	True	99.61	99.61	99.61	99.61	4.17

Analyzing Table 11, it can be seen that the inclusion of the attention mechanism increased all the previously obtained scores, with a minimum variation of 0.52% and a maximum of 5.13%. Furthermore, it was observed that the *ADD* input always showed better classification results, in each of the analyzed

metrics, which was increased by cropping the image to the ROI.

The cropped *ADD* input presented the best results, with an increase of 4.74% in accuracy, 3.85% in F1-score, 2.56% in precision and 5.13% in recall. However, the ability of the model to redirect the focus to the user's lower limbs needs to be evaluated, so the Grad-CAM was analyzed and the *Dice* and *IoU* scores were calculated. Table 12 shows the results obtained for the validation set.

Table 12: Quantative evaluation results, in percentage, for validation Grad-CAM, when predicting with the ResNet-50 model with the CHATT mechanism

Input		**Validation set**	
Type	**Crop**	**Dice (±std)**	**IoU (±std)**
DIF	False	30.37 (±12.86)	18.59 (±9.13)
DIF	True	32.90 (±9.13)	20.04 (±6.43)
ADD	False	26.30 (±14.71)	15.99 (±10.04)
ADD	True	31.79 (±8.54)	19.21 (±6.13)

Analyzing the model's focus results, there was a general increase in focus for all inputs, except for the cropped *ADD* input, which was lower on average by 0.34% for *Dice* and 0.68% for *IoU*, which may be marginal. The non-cropped *ADD* input showed the greatest improvement (4.20% in *Dice*), though it still performed worse than the non-cropped *DIF* input (4.07% higher). In contrast, cropped *DIF* achieved the highest focus, with only a small difference (1.11%) compared to cropped *ADD*. Additionally, it should be noted that the standard deviation also decreased for all inputs, both *Dice* and *IoU*, but this decrease was more significant for the cropped *ADD* input, indicating that the model's focus was more stable for this input. Nevertheless, the attention mechanism does not significantly outperform the baseline model, especially for cropped inputs, indicating that it does not completely correct its main focus. This was still below the established requirement of 50%, and this may be due to the focus evaluation algorithm itself, which uses the GT images that mark all human regions as 1 and background as 0. However, it is possible that not all regions of the lower limbs contain equally relevant information for MI decoding. For example, if the model does not focus on the thigh region, which may be more static from the camera's point of view, the algorithm will penalize the *Dice* and *IoU* values, which can be misleading.

This approach was tested on the test set and the accuracy percentage is shown in Table 13.

Table 13: Percentage of correct classifications for ResNet-50 with the CHATT mechanism and for each input regarding the test split

Input	Crop	ResNet-50 + CHATT
DIF	False	99.32
DIF	True	97.62
ADD	False	99.29
ADD	True	99.36

It was found that there was a significant increase in accuracy percentage on the test data, especially for the cropped *ADD* input. Given these results, it was considered that ResNet-50 with the CHATT and the cropped *ADD* input is the best approach so far for classifying motion intention, both in terms of classification and focus on the user's lower limbs. This result is also confirmed by the confusion matrix obtained for the test set, shown in Figure 19.

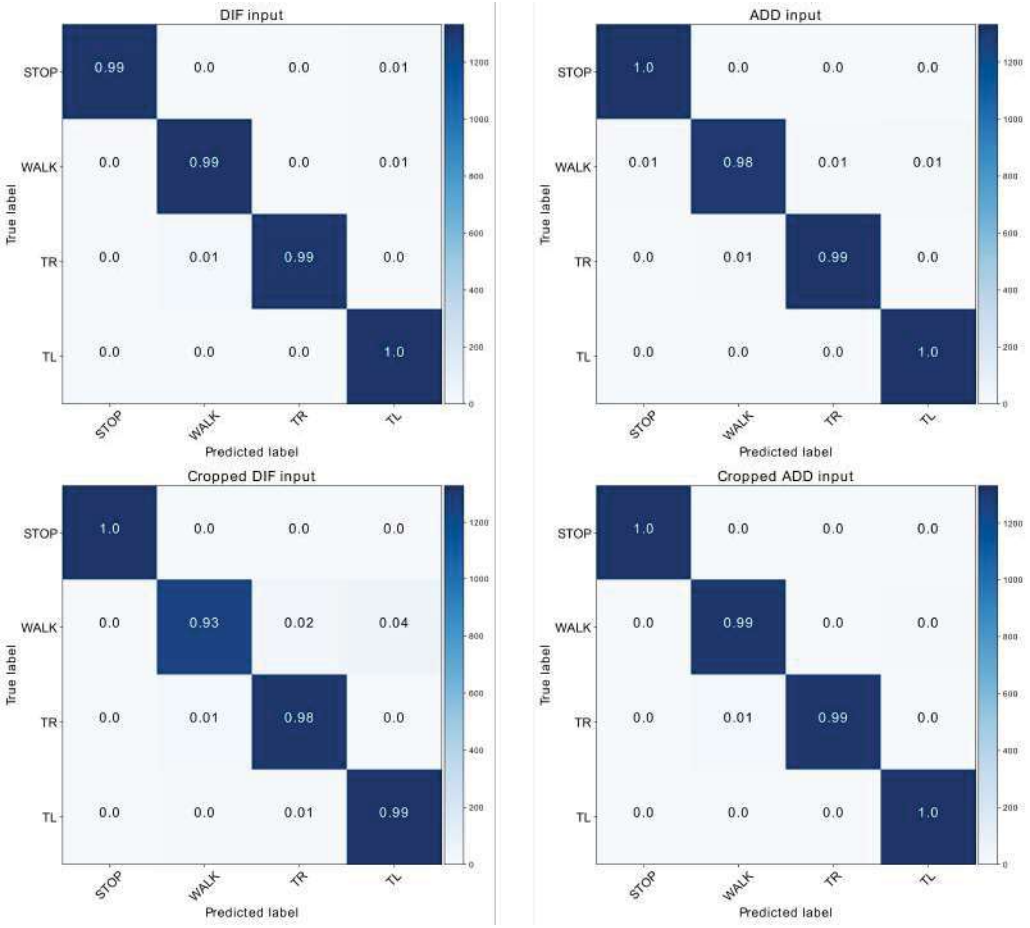


Figure 19: Confusion matrices for the ResNet-50 model with CHATT mechanism, over the four types of input and considering the test set.

Figure 20 and Figure 21 show the Grad-CAM visualization for two random trials **A** and **B** from different participants of the test set. Trial **A** corresponds to participant 11 performing a TL walk at 0.5 m/s, and trial **B** corresponds to participant 15 performing a TR walk at the fastest walking speed, 1.0 m/s. The Grad-CAM visualization provides relevant information about the focus of the model and gives insight into the reasons behind the values obtained for the *Dice* and *IoU* coefficients. Note that these frames of Figures 20 and 21 are not necessarily consecutive in the dataset. In addition, the predicted classes in these figures correspond to the predictions of the model.

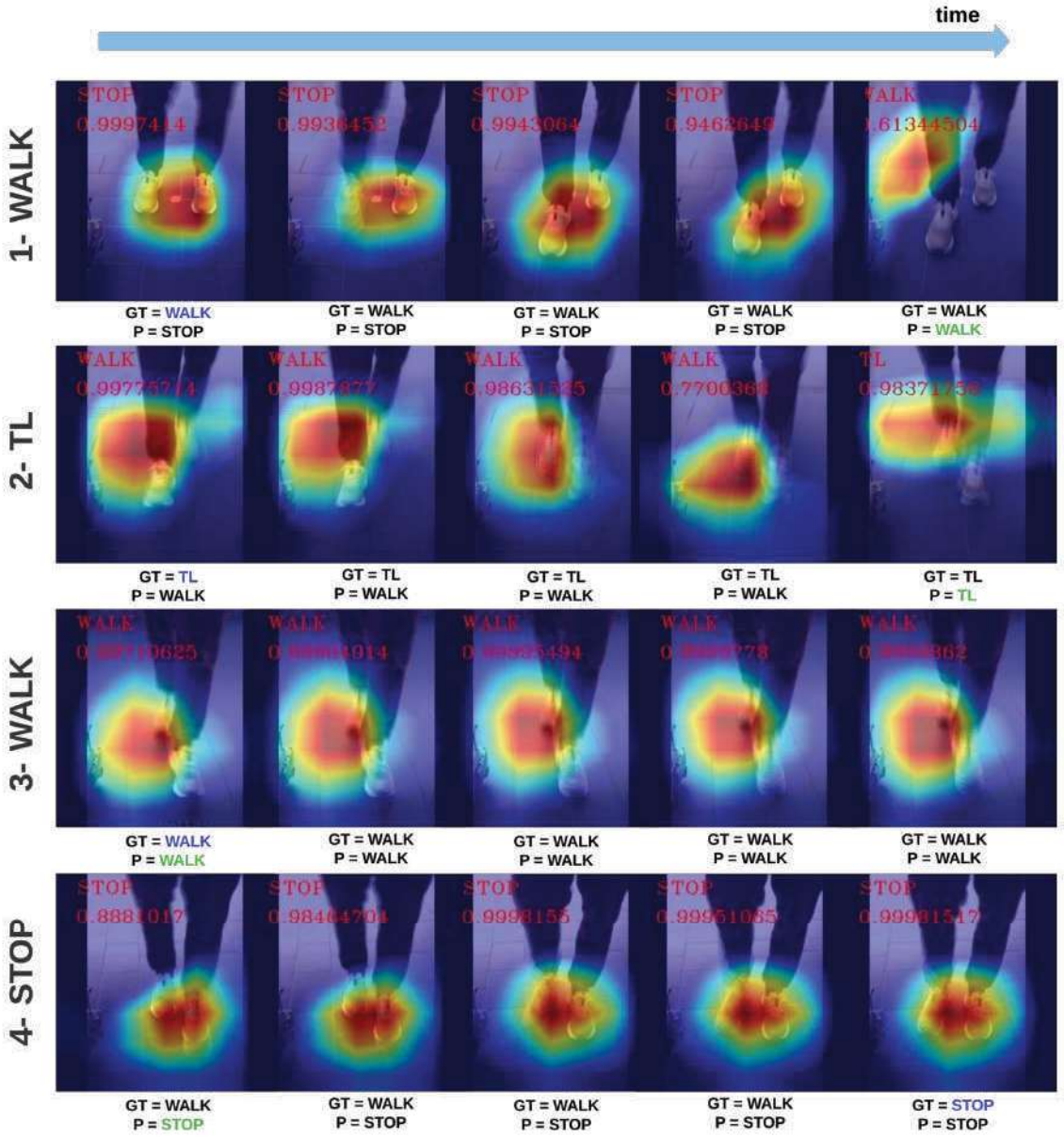


Figure 20: Grad-CAM visualization, temporally ordered, for each one of the transitions in the slow trial (trial A). The green and blue labels correspond to the first prediction and GT label, respectively, of the action that is beginning (P = predicted class).

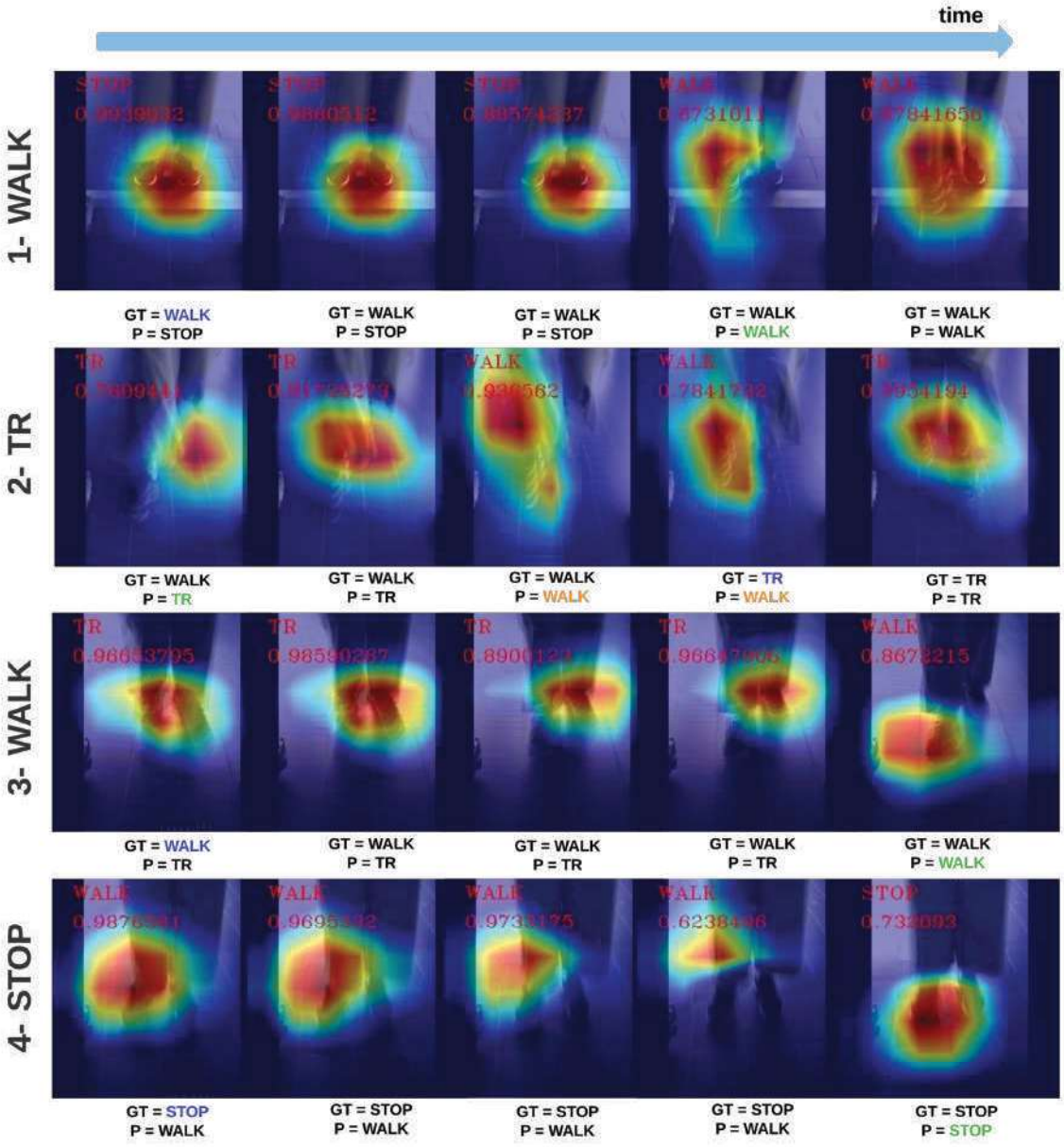


Figure 21: Grad-CAM visualization, temporally ordered, for each one of the transitions in the fast trial (trial B). The green and blue labels correspond to the first prediction and GT label, respectively, of the action that is beginning (P = predicted class). The orange ones correspond to the perturbations in the model's predictions that do not correspond to the post-processed predicted class.

In general, the model focus does not deviate too much from the human region, but sometimes shifts to the background, especially the visible motion of the ground stripes, which may explain the lower values of *Dice* and *IoU*. In fact, the ground of the data collection site was found to provide information that could be considered relevant for MI classification (the visible motion of the ground stripes). This is particularly visible in Figure 20, first row, during the walking event. In fact, the model initially correctly focused on the user's feet, even though it indicated that the user was still stationary. The user was indeed in the

same place, but the intention was given by the first step. Later, the model changes its prediction to WALK (first row, last image), but in this case the focus shifts mostly to the background, although not far from the human region. Subsequently, during the turn event, the model first decoded that the user intended to turn by focusing on the orientation of the lines on the ground (second row, last image). Then, during the walking activity, the model correctly decodes the activity, but one can see that the focus, although close to the human region, is mostly focused on the background.

The results also show that as the device slows down, the background motion becomes less evident and the model starts to focus on the user's feet (last row, first image). In this case, the stopping event was anticipated because the user's feet showed little motion.

Figure 21 illustrates another case where the model shifts its focus to the floor stripes. This is particularly evident but analyzing the second row of this image. On this specific row, there was some confusion by the model in decoding the intention to turn and walk forward. Moreover, the turning event was anticipated by the model, but the latter focused on the background.

These visualizations show that the model focus still needs to be improved in order to be integrated into a real-time control mechanism. Therefore, both a SE layer and a SPATT mechanism were tested for the best backbone found, *i.e.* ResNet-50, and the best input form so far, cropped *ADD*. The SE layer is still a CHATT mechanism, but instead of relying on convolutional operations, it squeezes the feature maps into a channel descriptor and then performs an excitation operation using dense layers to perform feature recalibration. This produces the weighted channel descriptor, which is then used to weight the feature maps. Regarding the SPATT, this layer creates a spatial map that is responsible for weighting each pixel of the feature maps, allowing to highlight those pixels with more information to predict the user's MI. Table 14 presents the results obtained for all the metrics related to ResNet50 with a SE layer, considering the best model (r=16), and with a SPATT mechanism (see learning curves of Figure 71 of Appendix B.1).

Table 14: Validation results, in percentage, of ResNet-50 with both SE layer and a SPATT mechanism, as well as the training time, in hours

Input	Crop	Accuracy	F1-score	Precision	Recall	Training Time
ResNet-50 + SE						
ADD	True	99.21	99.21	99.23	99.21	2.95
ResNet-50 + SPATT						
ADD	True	98.37	98.37	98.40	98.37	4.05

Analyzing Table 14, one can see that ResNet-50 achieved metrics above 98% with both the SE layer

and the SPATT mechanism. Nevertheless, a slight decrease was observed with respect to the CHATT mechanism, with a maximum residual decrease of 0.4% for the SE layer and 1.24% for the SPATT mechanism, considering all key performance indicators. Furthermore, the introduction of the SE layer, combined with the adaptive learning rate, allowed the neural network to converge faster. Analyzing the test set, one can see the generalization ability of the model, since the key performance indicators for the unseen data are above 98%, as shown in Table 15. This performance on the test data represents a maximum drop of 1.26% over the CHATT mechanism, which is consistent with the results obtained for the validation set.

Table 15: Test results, in percentage, of ResNet-50 with both the SE layer and the SPATT mechanism

Input	Crop	Accuracy	F1-score	Precision	Recall
ResNet-50 + SE					
ADD	True	98.35	98.35	99.38	99.35
ResNet-50 + SPATT					
ADD	True	98.10	98.10	98.13	98.10

Figure 22 provides a visualization of the confusion matrices for both attentional mechanisms under study. It can be seen that there is a clear distinction between the STOP class and the remaining classes, but there is confusion in the model when classifying WALK and TR/TL. For both models, it was found that the model confuses TR with WALK, *i.e.*, in images that the model should classify as TR, it actually classifies as WALK, and it confuses WALK with TL.

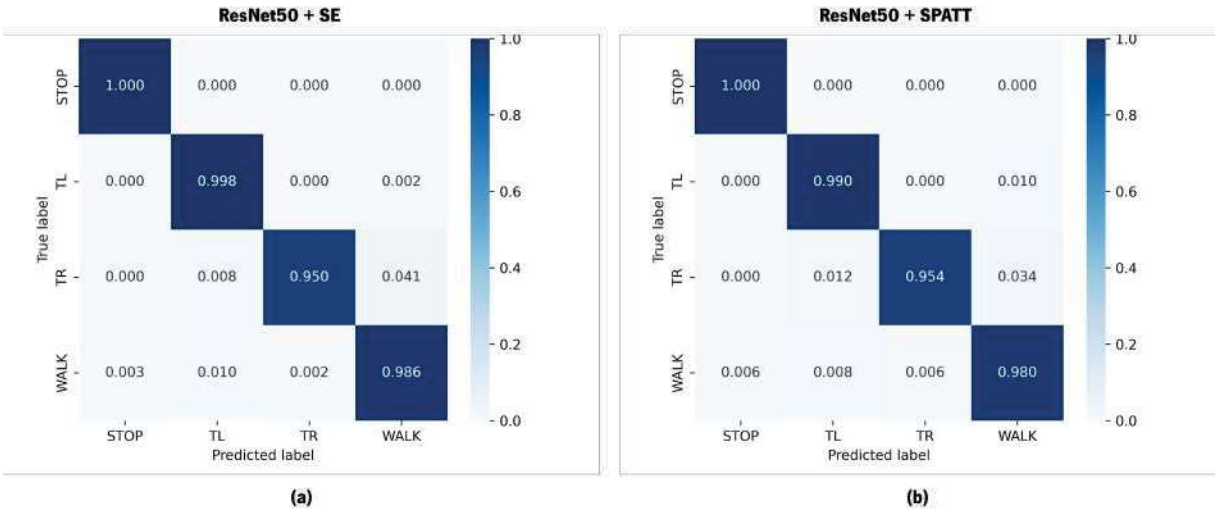


Figure 22: Confusion matrices for the ResNet-50 model with both: **(a)** SE and **(b)** SPATT mechanisms considering the test split.

Regarding the AI model focus on the human lower limb region, the explainable AI technique showed that the SE layer provided an improvement over the first CHATT mechanism tested. Table 16 shows the results obtained for the validation split. In fact, there was an improvement of 14.84% for the *Dice* coefficient and 12.43% for the *IoU* indicator. The same was not true for the SPATT mechanism, which shifted the model's focus to other areas outside the lower limbs, showing a 3.95% decrease in the *Dice* coefficient and a 1.94% decrease in the *IoU*, considering the validation set.

Table 16: Quantative evaluation results, in percentage, for validation Grad-CAM, when predicting with the ResNet-50 model with both the SE layer and the SPATT mechanism

Input		**Validation set**	
Type	**Crop**	**Dice (±std)**	**IoU (±std)**
ResNet-50 + SE			
ADD	True	46.63 (±15.06)	31.64 (±12.76)
ResNet-50 + SPATT			
ADD	True	27.84 (±16.44)	17.27 (±11.59)

Table 16 suggests that the background does indeed contain important information for decoding MI, since the SPATT mechanism caused the *Dice* and *IoU* values to decrease. In fact, the camera is stationary with respect to the device, but actually moves with the device, so both inputs also give an indication of the background movement. On the other hand, the SE layer has improved the focus on the person, albeit with some confusion between turning event and walking forward.

Regarding the quantitative focus evaluation for the test set, the ResNet-50 model with the SE layer produced a *Dice* of 43.87 ± 15.24% and a *IoU* of 29.35 ± 12.89%. These values were slightly lower than the validation set, but represented an improvement of 11.57% in *Dice* and 9.75% in *IoU* over ResNet-50 with the first CHATT tested (*Dice* of 32.30 ± 8.83 % and a *IoU* of 19.60 ± 6.37 % [135]). However, it can be seen that the standard deviation for ResNet-50 is slightly higher with SE, considering both the validation and test splits, indicating that the focus of the model is more spread out around the mean. Nevertheless, the lower bounds of both the *Dice* and *IoU* coefficients for ResNet-50 with SE layer are close to the average value found for the first CHATT mechanism tested.

Analyzing the focus of the model for ResNet-50 with the SPATT mechanism considering the test set, an improvement of 1.33% in *Dice* and 1.88% in *IoU* was found (*Dice* of 33.63 ± 16.78% and *IoU* of 21.48 ± 12.62%), considering our last published results [135], but this improvement may not be significant compared to those found for the SE layer. In addition, the standard deviation is again higher than that

registered for the first CHATT mechanism, indicating that there are images where the model is more focused in areas outside the user's ROI.

Figures 23 and 24 show examples of Grad-CAM obtained for the test set when adding a SE and the SPATT layers, respectively. A comparison between these two figures shows that the model with a SPATT mechanism does indeed tend to focus more on regions beyond the user (see Figures 24b, 24c, and 24d).

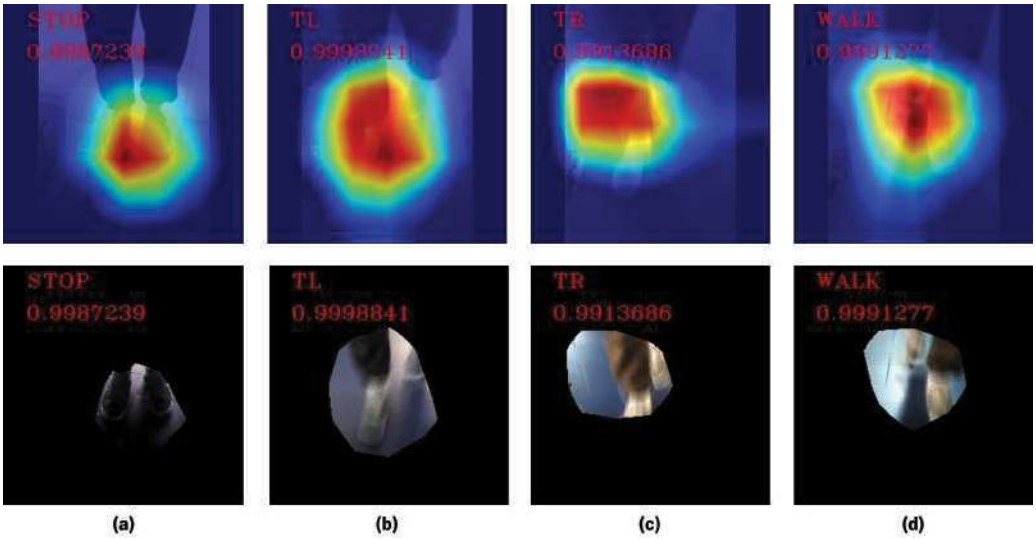


Figure 23: Examples of Grad-CAM for MI decoding considering ResNet-50 with the additional SE layer, considering: **(a)** STOP, **(b)** TL, **(c)** TR, and **(d)** WALK classes. Below it can be observed the segmented region of the heatmap with a threshold of 0.5.

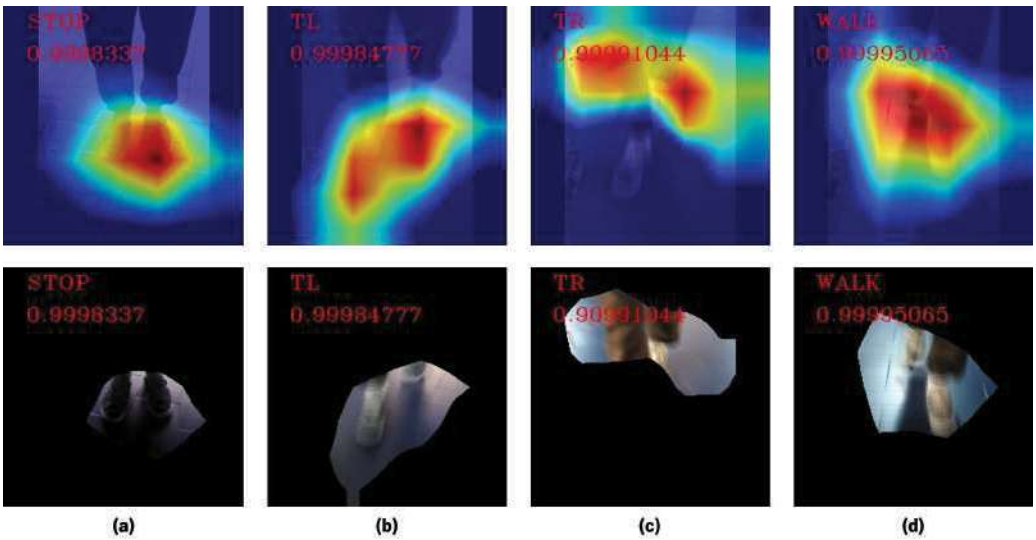


Figure 24: Examples of Grad-CAM for MI decoding considering ResNet-50 with the additional SPATT mechanism, considering: **(a)** STOP, **(b)** TL, **(c)** TR, and **(d)** WALK classes. Below it can be observed the segmented region of the heatmap with a threshold of 0.5.

4.8.2 Multi-class segmentation-classification

Regarding the second approach analyzed in this thesis, it consisted in adapting the U-Net neural network, commonly used for segmentation tasks, to classify the user's MI. In this case, the U-Net encoder, optimized to focus on the user's lower limbs, was used, followed by a classification block. For this, the U-Net neural network was first trained to segment the user's lower limbs. Table 17 shows the key performance indicators for the segmentation task.

Table 17: Validation results, in percentage, of the U-Net model, as well as the training time, in hours, for 30 epochs

Input Type	Crop	Accuracy	Loss	IoU (±std)	Dice (±std)	Training Time
DIF	False	98.80	0.02	93.81 (±1.96)	96.80 (±1.05)	1.37
DIF	True	98.36	0.03	93.85 (±1.95)	96.81 (±1.05)	1.37
ADD	False	98.94	0.02	94.34 (±1.71)	97.08 (±0.91)	1.38
ADD	True	98.57	0.03	94.52 (±1.71)	97.17 (±0.91)	1.37

Considering these results, all inputs seem to segment the human body region accurately, with *Dice* and *IoU* values higher than 93% and very low standard deviations, indicating that most of the coefficient values are close to the average. Among these inputs, the cropped *ADD* stood out, albeit by a small margin (less than 1%), with *IoU* and *Dice* values of 94.52% and 97.17%, respectively. However, one should note that there was an apparently small overfitting (Figure 72 of Appendix B.1), which can affect generalization in subsequent models. Still, note that the selected weights are not from the final epoch of training but from the epoch with the lowest validation loss.

Tables 18 and 19 present the classification validation results, as well as the training time for 100 epochs, and the quantitative evaluation of the model focus, respectively. The results reveal a decrease in the key performance indicators compared to those obtained previously. In this approach, the *DIF* input achieved the highest F1-score, namely 94.14% and 93.36% for non-cropped and cropped images, respectively. Furthermore, when analyzing the focus of the model, there is a decrease in focus, especially when compared to ResNet-50, as the *Dice* and *IoU* values are similar to those obtained with VGG16. Nevertheless, the best focus was achieved with the cropped *ADD* input (*Dice* values with an average of 28.17%).

Table 18: Validation results of the adapted U-Net classification model as well as the training time, in hours, for 100 epochs

Input Type	Crop	Accuracy	Loss	F1-score	Precision	Recall	Training Time
DIF	False	94.09	0.16	94.14	94.29	93.92	4.48
DIF	True	93.47	0.17	93.36	93.70	93.02	4.53
ADD	False	90.82	0.24	91.08	92.07	90.23	4.49
ADD	True	92.79	0.27	92.69	93.08	92.34	4.43

Table 19: Quantitative focus evaluation results, in percentage, of the validation Grad-CAM, when predicting with the adapted U-Net model for classification

Input Type	Crop	Dice (±std)	IoU (±std)
DIF	False	19.48 (±8.00)	11.01 (±5.06)
DIF	True	18.27 (±10.46)	10.44 (±6.80)
ADD	False	21.21 (±7.80)	12.08 (±4.88)
ADD	True	28.17 (±9.66)	16.75 (±6.35)

The results of the key performance indicators, together with the training curves (see learning curves of Figure 73 of the Appendix B.1), indicate that the adapted U-Net for the classification of MI showed problems of generalization. The classification metrics were worse than those obtained by the previously evaluated models, as the maximum F1-score, which is still above 90%, is 0.2% lower than the minimum registered for the previous models. Analyzing the loss curves, they show a slightly decreasing trend, which means that perhaps a larger number of epochs could give better results, but this hyperparameter was kept at 100 to ensure the comparison with the other approaches. Nevertheless, there was a significant gap between the training and validation losses, indicating that this approach has a weak generalization. Moreover, this approach has not fulfilled its purpose of increasing the model's focus towards human-centered features.

4.8.3 Trial Simulations

ResNet-50 with a CHATT mechanism showed higher performance in both classification metrics and focus on the user's lower body. This was particularly evident when using the cropped *ADD* input. The addition of another type of channel attention mechanism, the SE layer with r=16, improved the network's focus on the user, although with a residual decrease in classification performance. Therefore, considering

that the gain in focus on the user is higher than the loss of accuracy in the classification process, this new model was tested offline, in real-time simulations, considering the same participants of Figures 20 and 21, which belong to the test set. Figure 25 shows the offline simulation of the same trials **A** and **B**, but also two other trials for each participant, considering the remaining gait speeds.

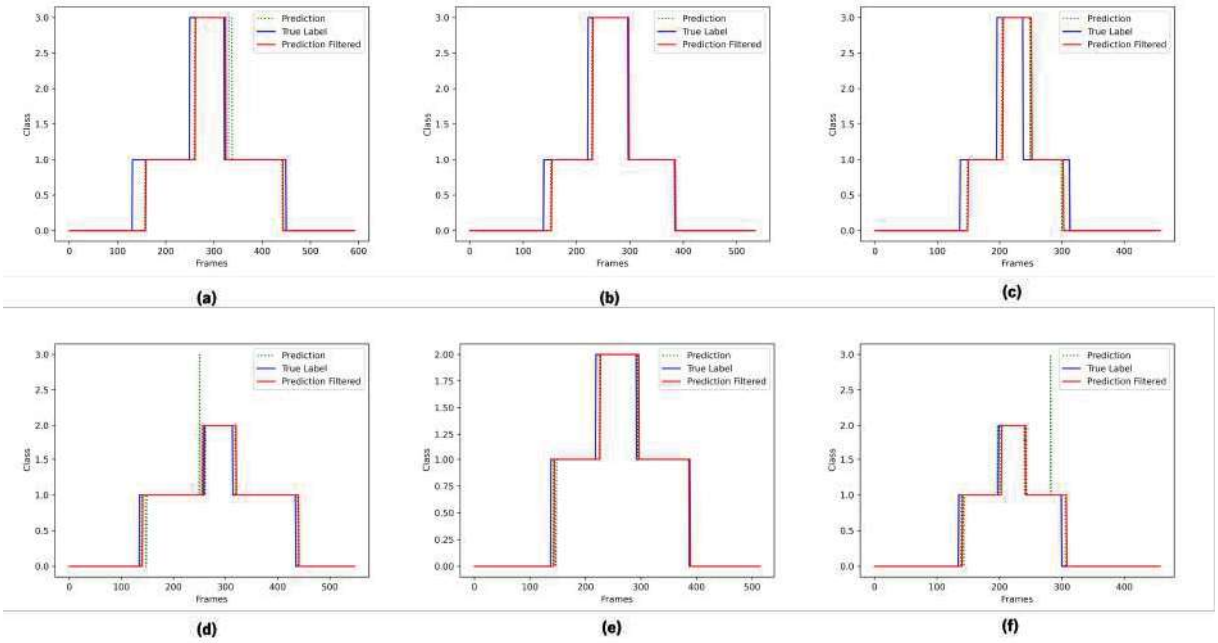


Figure 25: Plot of the GT (solid blue line), predicted (dotted green line) and post-processed predicted labels (solid red line) for **(a)** trial A - 0.5 m/s, **(b)** trial of participant 11, 0.7 m/s, **(c)** trial of participant 11, 1.0 m/s, **(d)** trial of participant 15, 0.5 m/s, **(e)** trial of participant 15, 0.7 m/s, and **(f)** trial B - 1.0 m/s. Class: 0 stands for STOP, 1 stands for WALK, 2 stands for TR and 3 stands for TL.

Analyzing the offline simulation of the trials, considering the test data, it reveals how the model will behave in a real context and with unknown data. It was found that the model has relatively high accuracy when simulating the real scenario, with an accuracy of 91.74% for trial **A** and 95.85% for trial **B**. Together, these particular trials had an average accuracy of 93.8%, which represents an increase of 0.8% when compared to ResNet-50 with a CHATT mechanism, as presented in our published study [135]. Table 20 shows the accuracy for all the trials shown in Figure 25.

Table 20: Accuracy value, in percentage, for the tested trials in offline simulations for both ResNet-50 with CHATT and the SE layer with r = 16

Trial	ResNet-50 + CHATT	ResNet-50 + SE
Participant 11		
0.5 m/s (Trial A)	91.06	91.74
0.7 m/s	94.40	94.96
1.0 m/s	89.32	89.76
Participant 15		
0.5 m/s	95.41	95.85
0.7 m/s	94.56	95.92
1.0 m/s (Trial B)	93.98	95.99

Analyzing Table 20, almost every trial showed an accuracy value above 90%, considering the post-processed label. In fact, the model showed some uncertainty, pronounced with ON-OFF noise, visible in the trials (mainly Figure 25a, 25d, and 25f), which was later removed by the post-processing technique. In addition, the model showed a delay in predicting the transitions, but this is to be expected since the model was not trained under transitions. According to Figure 25, there is a visible delay in predicting the intention of WALK, which was more pronounced in participant 11 and especially in trial **A**. In fact, analyzing Figure 26, the user gave his MI to walk in the second image of first row, visible by the slight drag on the user's legs (marked as green with GT label), but the model predicted WALK only after 1.87s (image marked with an orange rectangle). Moreover, it is shown that the model started by focusing on the user's feet and progressed to the user's legs.

For participant 15 this delay is not so pronounced. Regarding the curves, the delay was also observed in most cases, which was more pronounced for participant 11 than for participant 15, considering the three speeds tested. Moreover, Figure 26 suggests that in the curves, the model still has difficulty in decoding the user's intention just by analyzing the user's ROI, since, as can be seen, the model focuses on the background where it is likely that a change in the orientation of the ground stripes has occurred (second row, third image). However, the model then shifts its focus back to the user (second row, last image). On the other hand, during walking and the stopping condition, the model behaves as required, *i.e.*, it focuses mostly on the user's body (*e.g.* second row, first image of Figure 26, or last row, first image).

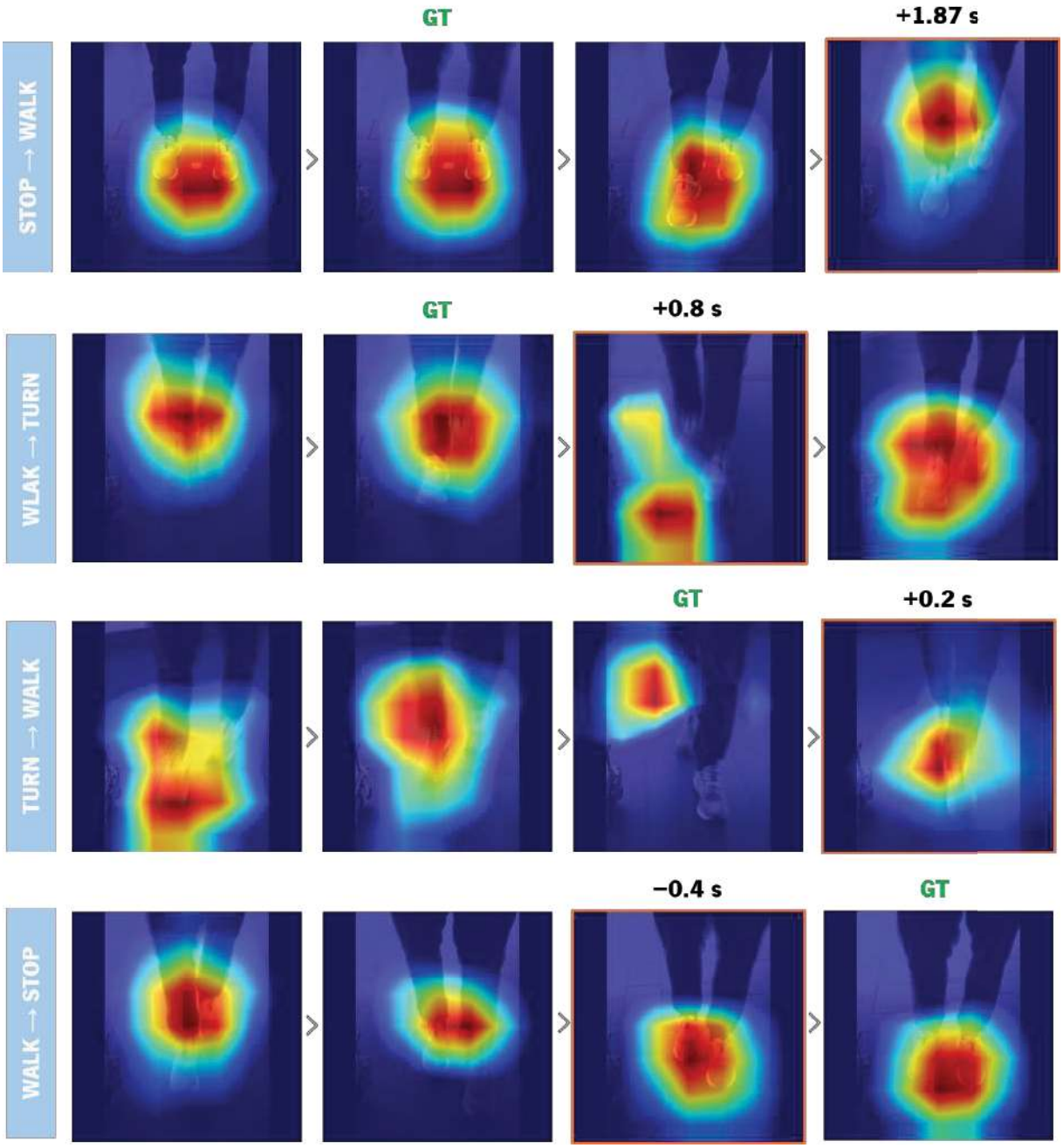


Figure 26: Grad-CAM of trial A - participant 11 walking with the SRW at 0.5 m/s - considering the ResNet50 with the SE layer. GT, marked in green, represents the true label. An indication is given of how long it took the model to correctly decode MI.

The results suggest that despite the improvement in the user's focus, the four-class classification model still needs to be improved before it can be used for control purposes. Additionally, the recognition of the prediction delay is also essential to verify that it does not compromise the viability of implementing this strategy in real time and that the overall delay is below the specified requirement (less than 0.64s, which is the step time while walking the device at a maximum speed of 1.0 m/s). Therefore, Table 21

shows the calculated delays for the two participants studied. Note that these calculated delays include the correct prediction delay plus the post-processing technique.

Table 21: Delays of the final predicted labels in relation to the respective GT labels, considering the specific trials of participants 11 and 15

Time delays (s)					
Trial	Walk	Turn	Walk	Stop	**Avg ($\pm std$)**
Figure 25a	1.87	0.80	0.20	-0.4	**0.62 ± 0.97**
Figure 25b	1.0	0.60	0.13	0.07	**0.45 ± 0.44**
Figure 25c	0.87	0.67	0.93	0.67	**0.79 ± 0.14**
Figure 25d	0.4	-0.20	0.47	0.40	**0.34 ± 0.38**
Figure 25e	0.4	0.53	0.33	0.13	**0.35 ± 0.17**
Figure 25f	0.4	0.33	0.00	0.53	**0.32 ± 0.23**
macro-average (±std)					**0.48 ± 0.18**

As can be seen, the calculated delays are variable, taking into account the different walking speeds and the different transitions. There are some trials where the delay was more expressive, but overall the delays were below the requirement of 0.64s, which corresponds to the average step time for the fastest allowed walking speed, *i.e.*, 1 m/s. The results are quite positive considering that the network was not trained with transitions, but it still needs further improvement. Therefore, future work should include a training procedure that considers transitions in the dataset and focuses on improving data quality with variable backgrounds. For example, one could consider replacing the *ADD* or *DIF* inputs by a 3D sliding window.

4.8.4 Ablation Study

In this thesis, three ablation studies were considered to determine their contribution to the model's learning process and, ultimately, to try to improve the results obtained. In a first approach, since the model often focuses on the background, the background was removed from the images. To avoid confusing the black background with the participants' clothing, the background was changed to green. The best model found without the attention mechanisms was then tested to see if the model's performance and focus improved. The second approach was to change the background with different backgrounds, especially hospital backgrounds, to emphasize that the information for motion decoding has to come from the user.

Since these models required the user's segmentation, the dataset used for the multi-class segmentation-classification approach was used (see Table 7).

Table 22 shows the weighted macro-average of the performance metrics considering these two first approaches. In this case, the key performance indicators were the weighted macro-averages because the dataset was not strictly balanced due to human mask corruption by intense sunlight. The learning curves of the ablation studies can be visualized in Figure 75 of Appendix B.1.

Table 22: Validation results, in percentage, of ResNet-50 with erased background and with a random background

Input	Crop	Accuracy	F1-score	Precision	Recall	Training Time
Erased Background						
ADD	True	98.53	98.54	98.56	98.53	1.61
Different Backgrounds						
ADD	True	98.07	98.07	98.07	98.07	2.31

According to the results, all classification metrics were high and above 98%. However, when the background was removed, a loss of performance was observed on the test data, whose metrics were around 90%, with a maximum drop of 8.62% for erased backgrounds and 9.54% for different background, when compared to the validation data (Table 23). This result indicates that by removing the background, the model may overfit to the training data, in which case the validation data may not be fully representative. In addition, the test data may be slightly different from the remaining data due to the segmentation quality of the algorithm [38]. Although the corrupted human masks have been removed and the remaining ones improved, there may be some frames that segment a little beyond the user, adding extra information that could confuse the model.

Table 23: Test results, in percentage, of ResNet-50 with erased background and with random hospital backgrounds

Input	Crop	Accuracy	F1-score	Precision	Recall
Erased Background					
ADD	True	89.91	89.97	90.10	89.91
Different Backgrounds					
ADD	True	88.60	88.53	88.70	88.60

Figure 27 shows the confusion matrices of the validation and test sets for the first two ablation studies.

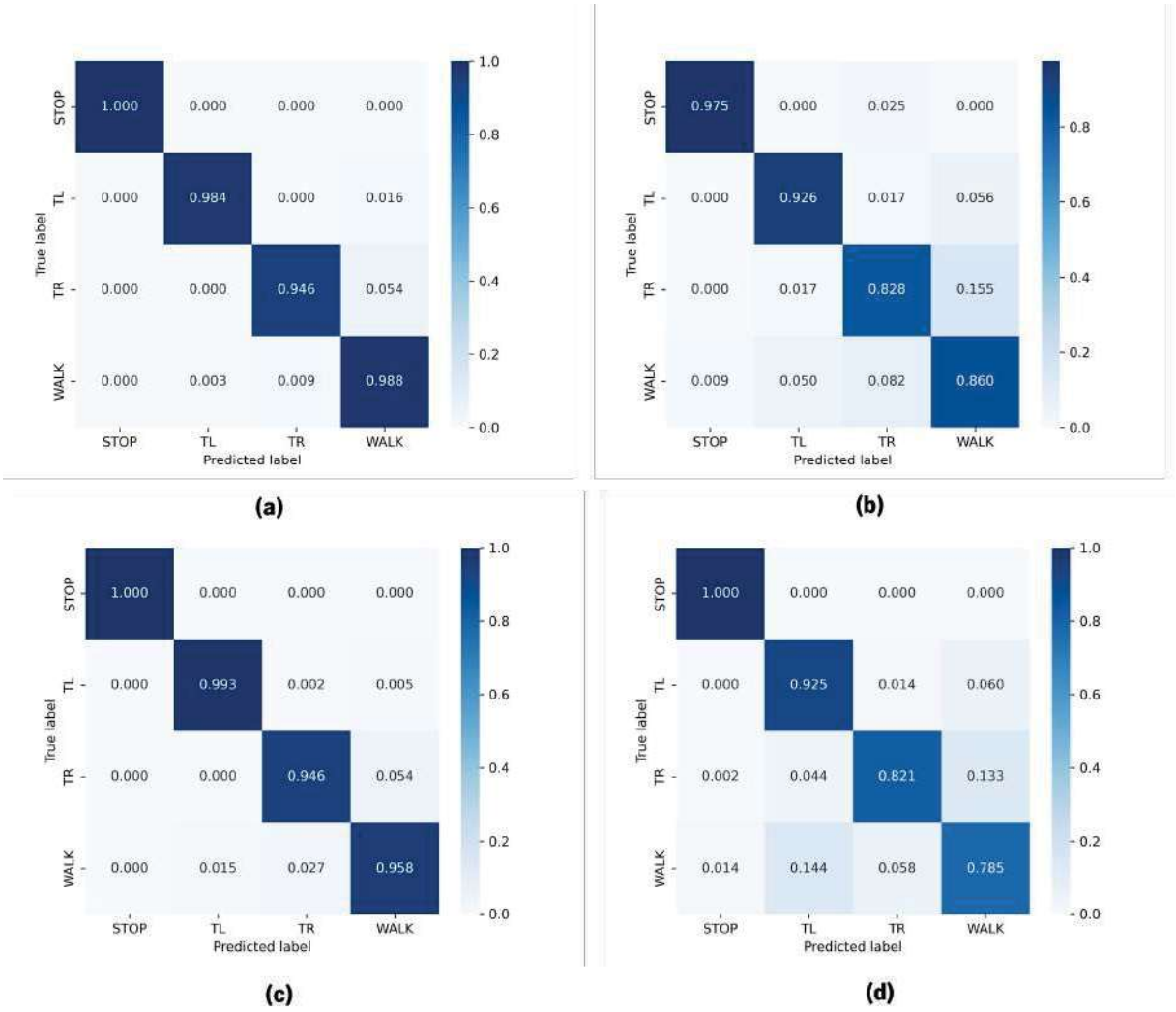


Figure 27: Confusion matrices of ResNet-50 considering validation and test sets with background removed (a and b), and validation and test sets with background changed (c and d).

Analyzing the test set when the background is removed (Figure 27a and 27b), it can be seen that the model shows some confusion in differentiating the TR class from WALK, as 16% of the true TR frames were classified as WALK in unseen data. Furthermore, when the model should classify as WALK, 5% of the frames are classified as TL and 8.2% are classified as TR. This confirms that the model does indeed have some difficulty in distinguishing curves from straight walking when the background is removed and only the user is analyzed. On the other hand, the model is very good at detecting STOP, as it gets 97.5% of the images correct when the user is actually stationary.

When the model is trained with images where the background is changed to a random one, the results show that it presents similar behavior. The model is therefore very good at distinguishing between when the user is stationary (100% correct) and when he/she is moving. However, it has particular difficulty

in differentiating between WALK and TR/TL: when the model should classify as TR, 13% of the frames are classified as WALK, and when it should classify as WALK, 14% of the frames are classified as TL and 6% are classified as TR. These results demonstrate that indeed the background has an influence on the model's learning and, considering the inputs analyzed, contains important features to decode motion.

However, the results show that the model is able to distinguish very well between when users are stationary and when they are walking. Thus, the third ablation study was performed. For this, the background-changed images were used to train a two-class classification model with the target classes STOP and WALK. In this case, the total dataset consisted of 10323 images, of which 703 were the validation set and 2368 were the test set. The results showed that, regardless of the background, distinguishing between the STOP and WALK classes is a fairly simple and easily detectable task, with a validation-weighted F1-score of 99.86%. Table 24 shows the overall results for both the validation and test sets.

Table 24: Validation and test results, in percentage, and training time, in hours, for dual-class classification model with different backgrounds

Input	Crop	Accuracy	F1-score	Precision	Recall	Training Time
Validation set						
ADD	True	99.86	99.86	99.86	99.86	1.33
Test set						
ADD	True	98.73	98.73	98.73	98.73	-

The test results followed the validation and training results quite well (see the learning curves in Figure 75c), even when the test set had only 50% of the data changed, confirming that the model was indeed able to generalize and perform well in real scenarios. These results are supported by the confusion matrices, which show the model's ability to generalize and easily discriminate between these two classes, making it a strong candidate for use in the development and proof-of-concept of the control strategy in the first stage, given the confusion the model occasionally has in discriminating the WALK class of TR/TL. Figure 28 illustrates the confusion matrices for both the validation and test sets considering the dual-class classification problem.

Regarding the model's focus on the user, an average validation *Dice* coefficient of 40.68% $\pm$ 16.67% and *IoU* of 26.93% $\pm$ 13.42% were observed. These results, although lower than those obtained for the SE layer, are higher than those obtained in our previous study [135], representing an improvement of 8.89% for *Dice* and 7.72% for *IoU*, which shows that the model has indeed become more user-focused. An individual analysis shows that the average is mainly influenced by the focus on the frames of the STOP

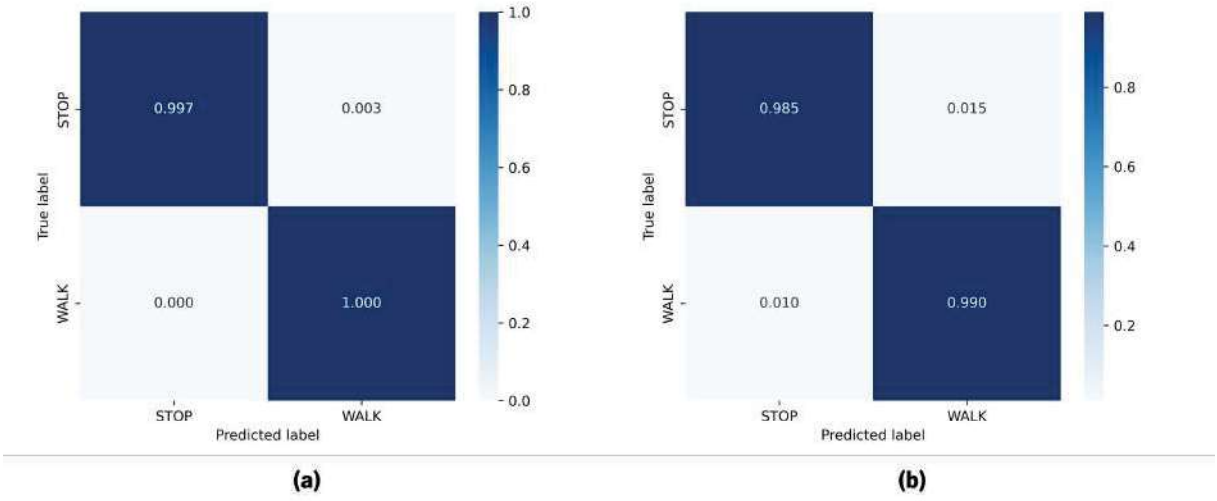


Figure 28: Confusion matrices for the dual-task classification approach considering: **(a)** validation set, and **(b)** test set.

class, which has an average *Dice* value of 30.71%, while the WALK class has an average value of 51.75%. This is because in the STOP class, the model focuses more on the feet region, while in the WALK class, the heatmap region extends beyond the user's feet to the leg region, as can be seen in Figures 29c and 29d. Regarding the test set, a *Dice* coefficient of 37.44% ± 17.82% and a *IoU* of 24.57% ± 14.17% were found, which is in agreement with the validation results, but slightly lower.

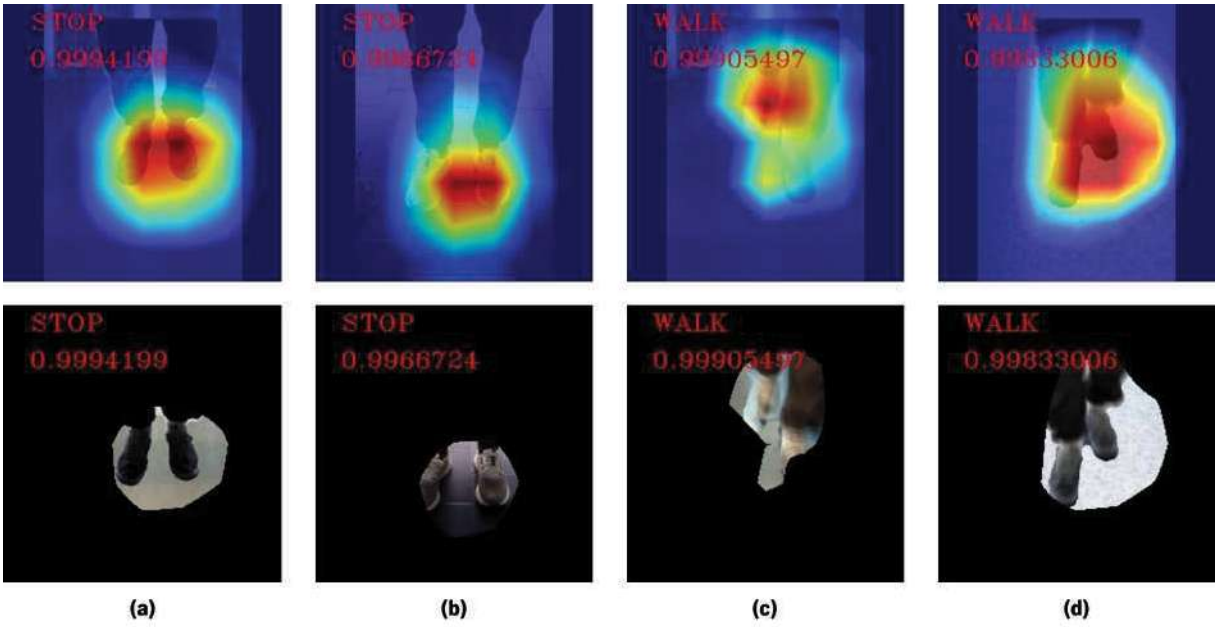


Figure 29: Examples of Grad-CAM for the two-class early recognition of MI: **(a)** and **(b)** STOP, **(c)** and **(d)** WALK. Below it can be observed the segmented region of the heatmap with a threshold of 0.5.

4.9 General conclusion

This chapter has provided an **in-depth study of several DL-based approaches to decoding the user's MI**. Both VGG16 and ResNet-50 were used as base models. To achieve better generalization, transfer learning was applied using the pre-trained weights from the ImageNet dataset. The results showed that the model is **able to detect human motion early, but sometimes extracts information from the background**. In order to improve the model's focus on the user, different attention mechanisms were investigated and improvements were observed compared to our previous study [135], especially for ResNet-50 with a SE layer. Three ablation studies were also performed to verify the effect of background on human motion detection and to increase the model's ability to generalize by changing the background using different hospital environments. It was found that the **model's ability to learn was indeed affected when the background was removed and modified**, as there was a noticeable decrease in performance in the test data. As for the two-class model, it showed positive results and generalized well. Given that the AI models sometimes redirect the focus to the background, it was realized that it could be difficult to quickly detect MI to turn, since in real time only the initial moments of the action can be detected and it is unknown what comes next. Since the models were not trained with transitions, it might have been difficult to detect the turns in the first moments. Thus, as a first step, the two-class model as used to test a new HIL control strategy.

The results enabled KPI 2 to be achieved, as the best model found to decode the intention to walk, turn and stop achieved metrics above 95%. However, in the trial simulations, there was a slight decrease in the model's accuracy, to values higher than 90%, but this result is justified by the inclusion of transitions in these simulations. With regard to the model's focus, it was found that the Dice metric was close to 45%, and IoU close to 30% for the best model, which reveals that the model still needs improvement.

Chapter V

Assistive Control Strategies

Chapter 5

Assistive Control Strategies

5.1 Introduction

Another goal of this thesis was to develop novel assistive control strategies to make the robotic walker **responsive and compliant** to the user's needs and intentions. Therefore, this chapter presents the development of a new control strategy, based on the HIL concept, in which the device is controlled from RGB images of gait using AI models. In this way, the human's interaction with the device is **natural, completely intuitive, allowing physical interaction to be reduced to a minimum**. Even so, in the case of ataxic patients, who have a more unsteady gait, it is necessary to endow the device with the necessary intelligence to understand when to assist the user in a hazardous situation or simply to reach a certain goal (*e.g.*, a location). Thus, this chapter also presents the validation of a RL-based AAN shared control strategy that **assists the user whenever necessary**. The strategy implements an ADS that is activated whenever necessary by a RL agent that evaluates the user's input and the environment.

The first section of this chapter will present the novel HIL control strategy based on user's MI decoding. The proposed strategy, methodology, validation protocol, results, and discussion will be presented. Then, the validation of the AAN shared control strategy will be addressed.

5.2 Human-in-the-loop Control of a Smart Walker through DL-based Human Motion Decoding

5.2.1 Proposed strategy

In order to provide a more engaging and adaptable therapy and to make the walker responsive to the user's needs, a novel HIL strategy is proposed in which the robotic device analyzes the user through the RGB-D camera of gait, decodes the MI, and generates velocity commands accordingly. This strategy

consists of three modules, as presented in Figure 30, namely: **i)** the user intention detector module, **ii)** the safety module, and **iii)** the velocity generator and adaptability module.

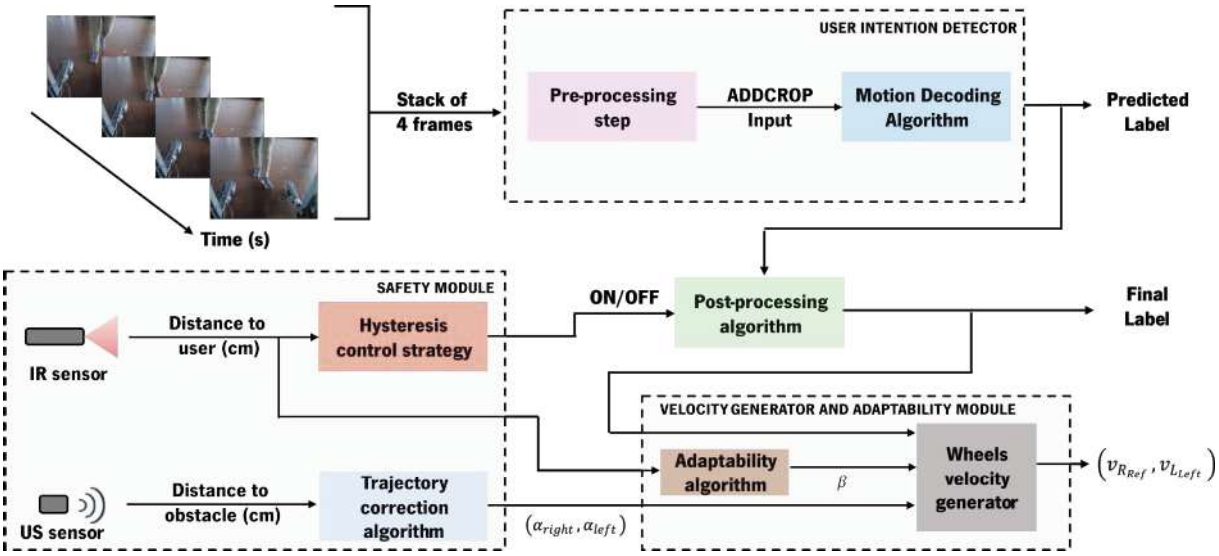


Figure 30: Overview of the proposed HIL control strategy.

The user intention detector module is responsible for reading the upcoming frames from the gait camera and performing a pre-processing algorithm that resizes the image to match the network input ($224 \times 224 \times 3$) and crops the image to match the user's ROI, as presented in Chapter 4. This image is then fed to the motion decoding algorithm, which predicts the probability associated with each class, from which the predicted class is taken as the label with the maximum probability. The predicted label is then filtered with a post-processing algorithm, which was previously presented in Chapter 4.

A safety module was also considered using the embedded infrared and ultrasonic sensors of WALKit SRW to assess the distance (cm) relative to the user and the surrounding obstacles (cm), respectively. The infrared sensor is used to implement a hysteresis control strategy that can override the motion decoding algorithm given the distance to the user to stop the device. The ultrasonic sensor, on the other hand, detects obstacles in the environment and, in the event of a potential collision, either immobilizes the device or performs a small trajectory correction to avoid the collision. This is accomplished by a trajectory correction algorithm that outputs an α factor for both the left and right wheel (α_{left}, α_{right}) based on WALKit's US readings, which is then used to change the reference speed for each of the device's wheels.

Finally, the infrared readings are used in a velocity generator and adaptability module to adjust the walker's speed based on a factor β. In this way, the walker's speed is adapted in real time to the user's needs, ensuring that the device maintains the average safety distance measured during the calibration period.

Strategy requirements

Some requirements were considered to implement this strategy on WALKit SRW, namely **i)** the proposed strategy should correctly detect the user's MI with at least a 95% accuracy rate and a maximum acceptable delay of 0.64s, which is the average step time when walking with WALKit SRW at 1.0 m/s; **ii)** it should operate in real time at a minimum frequency of 15 Hz, which is the frame rate used in the previous chapter to train the DL-based model and is a suitable operating frequency for control purposes; **iii)** it should allow real time speed adaptability to be more responsive to the user's needs, thus allowing a more user-centered assistance, considering a constant acceleration of 0.5 m/s^2; and **iv)** it should include small automatic trajectory corrections in the presence of obstacles.

5.2.2 Methodology

Reference velocity generator

According to Figure 30, the wheel speed commands are obtained by the fusion of three modules, as follows: **i)** the user intention detector module, which predicts the user's MI based on a single RGB frame that contains the information of a stack of four frames acquired at 15 Hz, which are later filtered by a post-processing algorithm; **ii)** the safety module, which adjusts the speed of the wheel according to a hysteresis control strategy considering the infrared readings, and performs small trajectory corrections using the device's US, and **iii)** the adaptability module which, when activated, implements a β factor responsible for adapting the linear speed, taking into account the user's requests expressed by their distance from the device.

The velocity command of the HIL control strategy is given by the Equation 5.1, where (v_{left}, v_{right}) are the linear velocity of the left and right wheel, in m/s, d_k and d_{k-1} are the current and previous distance, both measured in cm with the infrared sensor, v_{ref} is the reference linear velocity chosen by the clinician in the GUI, β is the adaptability factor, $(\alpha_{left}, \alpha_{right})$ are the factors applied for the trajectory correction, th_1 and th_2 are the two thresholds of the hysteresis control of the safety module, and $label_k$ and $label_{k-1}$ are the current and previous filtered label obtained with the post-processing algorithm. These labels can be 0, corresponding to STOP, or 1, corresponding to WALK.

The reference linear velocity, v_{ref}, of each wheel is then used to control the device with a proportional controller, where the loop is closed by measuring the actual linear speed of each wheel using a built-in encoder.

$$(v_{\text{left}}, v_{\text{right}}) = \begin{cases} 0 & \text{if } d \geq \text{th}_1 \\ 0 & \text{if label}_k = \text{STOP} \\ (v_{\text{ref}} \pm \beta) \times (\alpha_{\text{left}}, \alpha_{\text{right}}) & \text{if } d_{k-1} \geq \text{th}_1 \wedge \text{label}_k = \text{WALK} \wedge d_k \leq \text{th}_2 \\ (v_{\text{ref}} \pm \beta) \times (\alpha_{\text{left}}, \alpha_{\text{right}}) & \text{if label}_{k-1} = \text{label}_k = \text{WALK} \end{cases} \tag{5.1}$$

Regarding the hysteresis control, two thresholds (th) of the infrared sensor have been considered to implement the control strategy. These thresholds were obtained empirically and are related to the average distance of the user from the device, d_{avg}, considering a calibration period of 5s at the beginning of each session. The first threshold is $\text{th}_1 = d_{\text{avg}} \times$ 1.25, which represents a 25% increase in the user's average distance from the device. If the distance starts to increase and exceeds this threshold, the walker will stop. Once stopped, the walker will only accept new speed commands if the user's distance is less than $\text{th}_2 = d_{\text{avg}} \times$ 1.10, otherwise the reference linear velocity remains 0 m/s. The safety module's ultrasonic sensors also affect the velocity commands by applying a α factor whenever an obstacle is detected. This factor α can be one of four values, $\alpha \in \{0, 0.5, 0.75, 1\}$, taking into account a set of empirically defined distances.

Finally, the adaptability factor, β, is a constant value measured in m/s and obtained with Equation 5.2 considering an acceleration (a) of 0.5 m/s^2 and an operating frequency (f_{op}) of 15 Hz. This factor allows to increase or decrease the speed according to the user's intentions, while maintaining a constant acceleration, up to the maximum linear speed of the SRW, which is 1.0 m/s. To better adjust the linear velocity of the SRW when the adaptability module is enabled, th_1 has been increased to $d_{\text{avg}} \times$ 1.40.

$$\beta = \frac{a}{f_{\text{op}}} = \frac{0.5}{15} \approx 0.033[\text{m/s}] \tag{5.2}$$

Real-time integration in WALKit

After offline training with a Python environment using the TensorFlow platform in Chapter 4, the model loaded with the optimized weights was exported to Open Neural Network Exchange (ONNX), a widely supported framework that provides an open source format for AI models. The exported model was used and loaded into the device's embedded software using the ONNXRuntime library's C++ API.

A specific ROS package (C++) was created to subscribe to the camera's RGB+D streams, perform the pre-processing steps described in Chapter 4, the inference using the exported model, and generate the wheel velocity commands using the described modules presented in Figure 30 and Equation 5.1.

Experimental Protocol

A healthy male participant participated in the proof-of-concept validation of the novel HIL control strategy. Data collection was performed under the ethical procedures of Life and Health Sciences Ethics Committee (CEICVS 147/2021), according to the Declaration of Helsinki and the Oviedo Convention. Data were collected at the School of Engineering, University of Minho.

The participant performed a 20-Meter Walk Test (20-MWT) with WALKit SRW at three different walking speeds: 0.3 m/s, 0.5 m/s and 0.7 m/s. Each trial was repeated twice and consisted of: **i)** an initial 10-second stationary period, **ii)** a 20-MWT walking phase, and **iii)** a final 10-second stationary period. Additionally, a three-trial test was performed with the adaptive distance control enabled, considering a starting gait speed of 0.3 m/s. Finally, the participant performed another trial with the safety module activated, in which he performed the same 20-MWT, but encountered an obstacle on the left and later on the right.

Data Acquisition

Data acquisition included: **i)** the raw predicted class using the exported ONNX model; **ii)** the filtered class using the post-processing algorithm; **iii)** the reference linear velocity of each wheel in m/s; **iv)** the actual measured linear velocity of each wheel, in m/s; **v)** the user's average distance d_{avg}, in cm; the actual infrared reading **vi)**, in cm; the time, in ms, of both inference and post-processing algorithm; **vii)** and the GT class (STOP or WALK) which was obtained by visual inspection and using a remote control. Data acquisition was performed at 100 Hz.

Validation metrics

To verify that the proposed strategy meets the stated requirements, three relevant metrics were included, namely **i)** the overall precision and recall of the model, **ii)** the IA rate, which measures the rate of correct predictions while the predictions are being made, and **iii)** the delay between the GT class and the final class after the post-processing algorithm. Although this is a two-class problem, which is a binary classification in terms of training the model, there is not exactly one positive class and one negative class in this problem. Instead, there is a probability of being WALK or STOP, and both classes have meaning. Therefore, the overall metrics were calculated for each class independently. The IA rate was calculated using Equation 5.3, where K_t is the total number of observations between the start of the untrimmed video and time t [136].

$$IA = \sum_{i=1}^{K_t} \frac{TP + TN}{K_t} \tag{5.3}$$

5.2.3 Results and Discussion

Table 25 shows the overall classification metrics of the selected model considering the GT label for the 20-MWT without the adaptability and safety modules activated. The results have been divided into the two classes considered in order to obtain a more realistic and reliable view of the model's performance.

Table 25: Overall precision and recall for the AI-based model of the proposed HIL control strategy, considering the GT labels and the model's prediction after the post-processing algorithm

Gait Speed (m/s)	CLASS	Precision			Mean (std)	Recall			Mean (std)
		T1	T2	T3		T1	T2	T3	
0.3		0.979	0.988	0.985	**0.984±0.005**	0.958	0.963	0.961	**0.961±0.003**
0.5	**STOP**	0.982	0.987	0.970	**0.980±0.009**	0.990	0.974	0.981	**0.982±0.008**
0.7		0.982	0.970	0.991	**0.981±0.011**	0.979	0.996	0.978	**0.984±0.010**
0.3		0.986	0.986	0.985	**0.986±0.001**	0.993	0.995	0.994	**0.994±0.001**
0.5	**WALK**	0.993	0.985	0.987	**0.988±0.004**	0.987	0.993	0.980	**0.987±0.007**
0.7		0.982	0.997	0.983	**0.987±0.008**	0.984	0.980	0.993	**0.986±0.007**

The results show that the model chosen for the control strategy performs well in real time, with high precision and sensitivity (classification metrics above 95% in every case), which was consistent across all trials conducted for the three gait speeds tested. Figure 31 shows two trials representative of the slowest and fastest speeds tested with the proposed control strategy, presenting the GT label (0 for STOP and 1 for WALK) and both the predicted and filtered labels over time, the user's distance, in cm, relative to the device, and the reference and real linear velocity of each wheel.

In this figure it is possible to visualize an example trial performed by the participant. During the first 10 seconds, the participant remained still, and the model decoded the STOP intention (label at 0 coinciding with GT). Afterwards, the participant gave the intention to walk, visible in the graph with the transition from 0 to 1 (STOP $\rightarrow$WALK), in Figure 31a (first panel, at $t \approx 11$s). After walking the 20 meters, the participant stops, performing a transition from STOP to WALK (gray region of Figure 31a) and remains stationary for 10 seconds. The same explanation is valid for the trial with the higher gait velocity (Figure 31b).

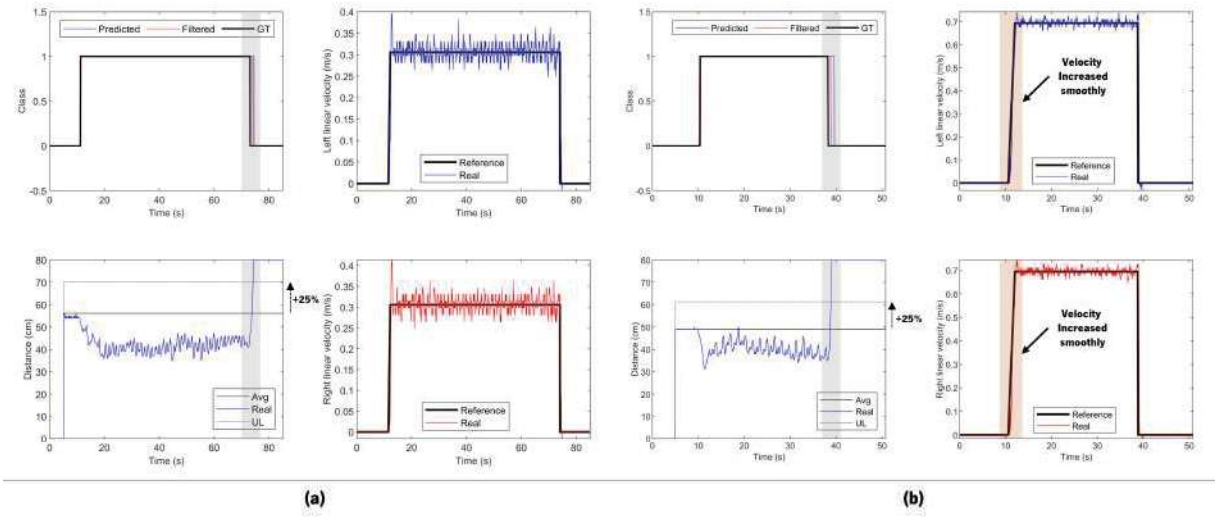


Figure 31: Representative trials of the experimental validation of the proposed HIL control strategy considering: **(a)** 0.3 m/s and **(b)** 0.7 m/s. GT and UL stand for Ground Truth and Upper Limit, respectively.

The results of Figure 31 show that the model correctly decodes the user's MI over time, since the filtered label (after post-processing) is mostly coincident with the GT label. This result is emphasized by the IA metric, which shows values above 97% over time, as shown in Figure 32.

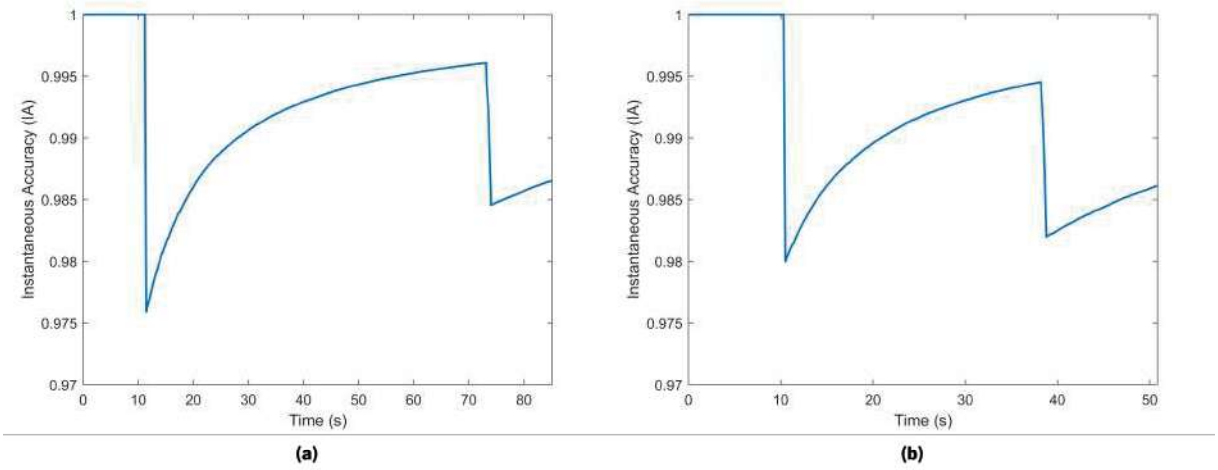


Figure 32: Instantaneous Accuracy (IA) of the two representative trials considering the lowest and fastest gait speeds, namely: **(a)** 0.3 m/s and **(b)** 0.7 m/s.

However, Figure 31 also shows that the model exhibited some delay in decoding the user's MI in transitions, especially in the transition WALK → STOP, emphasized by the gray box of Figure 31. These delays are also visible in the IA plots, where a drop in the model's performance can be seen. Indeed, in the real-time simulations shown in the previous chapter, the model showed some delay in decoding

the intention to stop, but this was no more than 0.64s considering the trials presented. However, in the dataset collected in the previous chapter, the device was in active mode with a predefined trajectory, meaning that the device would stop or walk regardless of the user's intention to move. This is not the case in the real-time tests because the device now reacts according to the user's intentions. The fact that the device does not stop when the user has actually stopped may be due to the parallax effect, where the model understands that the user intends to walk because it still "sees" him/her in the camera's FOV. In addition, due to the drag caused by the sum of the frames, there is the perception that the user is moving, when in fact he/she is not. Thus, the device only stopped when the user's distance increased to values greater than 25% of the user's average distance from the walker (see Figure 31a and 31b gray regions), measured over the calibration period. The fact that the user exceeded this threshold (th_1) activated the infrared controller, that overrode the AI model and instructed the device to stop (reference velocity became 0 m/s, see Figure 31a and 31b gray regions).

Table 26 shows the delay values recorded for the STOP $\rightarrow$ WALK and WALK $\rightarrow$ STOP transitions.

Table 26: Delay estimated between the GT labels, obtained with a remote control and by visual inspection, and the raw prediction of the model (D_1) and the final label after post-processing (D_2), considering the STOP to WALK and WALK to STOP transitions

Gait Speed (m/s)	Trial	STOP TO WALK		WALK TO STOP	
		D_1	D_2	D_1	D_2
0.3	1	0.259	0.394	1.163	0.918
	2	0.132	0.270	1.368	0.967
	3	0.194	0.325	1.191	0.861
Average $\pm$ STD		**0.195 $\pm$ 0.052**	**0.330 $\pm$ 0.051**	**1.241 $\pm$ 0.091**	**0.915 $\pm$ 0.043**
0.5	1	0.336	0.473	0.899	0.379
	2	0.133	0.265	1.160	0.565
	3	0.196	0.329	1.039	0.568
Average $\pm$ STD		**0.222 $\pm$ 0.085**	**0.356 $\pm$ 0.087**	**1.033 $\pm$ 0.107**	**0.504 $\pm$ 0.088**
0.7	1	0.260	0.484	1.181	0.443
	2	0.456	0.673	0.697	0.092
	3	0.065	0.198	1.364	0.562
Average $\pm$ STD		**0.260 $\pm$ 0.160**	**0.452 $\pm$ 0.195**	**1.081 $\pm$ 0.281**	**0.366 $\pm$ 0.200**

Based on results, the model decodes the intention to walk well, with a delay of no more than 0.3s considering the raw prediction (D_1), which is 53% lower than the proposed requirement of 0.64s. However, since the post-processing algorithm needs at least more than 50% of the buffer of frames with the same class to change the mode, there is an additional delay (D_2). Nevertheless, this delay was consistent

from trial to trial and never exceeded the requirement of 0.64s (the time of a step for the highest walking speed). Interestingly, it was found that the delay for this particular transition increased as the speed also increased, but regardless, it always remained below the defined requirement (at most 29.4% lower, considering the delay observed for the maximum velocity tested, 0.7 m/s). This result emphasizes the ability of the proposed strategy to timely react to the MI, making it possible to control the robotic walker without giving the perception of delay, since the delays observed are below the average step time for maximum speed.

Regarding the WALK $\rightarrow$ STOP transition, it can be seen that the model does not consider the user to be stopped until 1s after the user actually stops (see Figure 33, timestamp 3). The hysteresis control with the infrared sensor made it possible to reduce the response delay of the device to less than 0.64s, since the user passed the $(d_{\text{avg}} \times 1.25)$ cm threshold (Figure 33a and 33b, timestamp 2). However, this did not occur for the slowest speed, 0.3 m/s, because the device takes a little longer to cross the upper limit threshold and therefore does not meet the time requirement for this particular speed. This observation is also valid when comparing the post-processed prediction of Figures 33a and 33b (red solid line), where the delay with respect to the GT label is lower for the fastest walking speed. Nevertheless, the results show that future work should include training the model with transitions and possibly include the infrared sensor as an additional input.

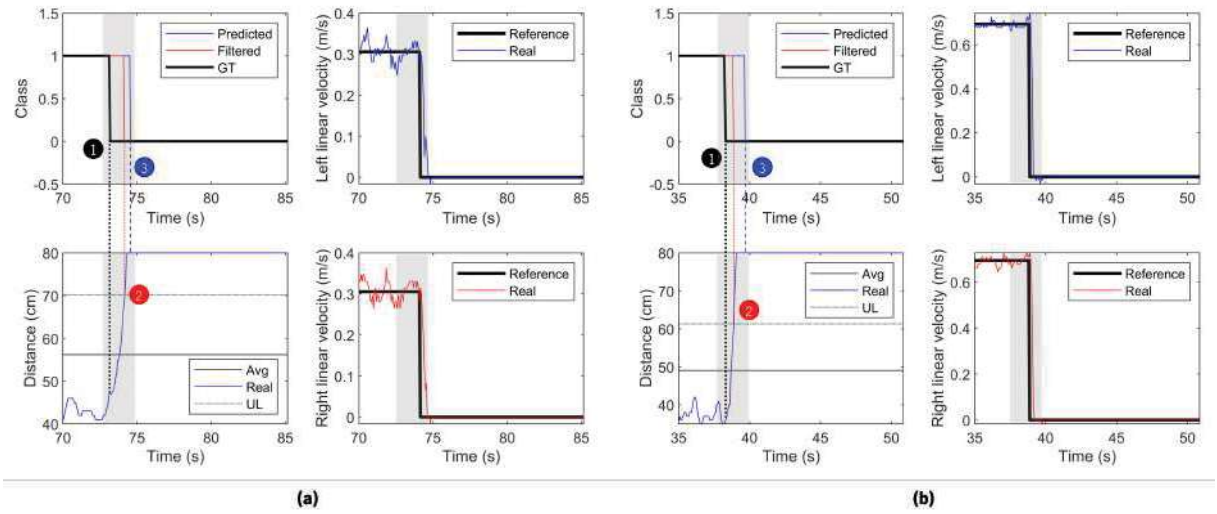


Figure 33: Zoom of transition WALK $\rightarrow$ STOP considering the representative trial of: **(a)** 0.3 m/s and **(b)** 0.7 m/s. GT and UL stand for Ground Truth and Upper Limit, respectively.

To increase the adaptability and compliance of the device with the user, a speed adaptation mechanism has been implemented based on the user's distance from the device. In this way, the walker detects

the user's intention to accelerate or decelerate and acts accordingly. This algorithm was designed with the assumption that the user moves at the same speed as the walker, since the device imposes a certain speed. However, given the user's distance from the device's platform, it is possible to make some adjustments to the speed. This adjustment was made gradually with the β factor, allowing the linear speed of the device to be optimized smoothly. Figure 34 shows two representative trials of the proposed HIL strategy with the adaptability module enabled.

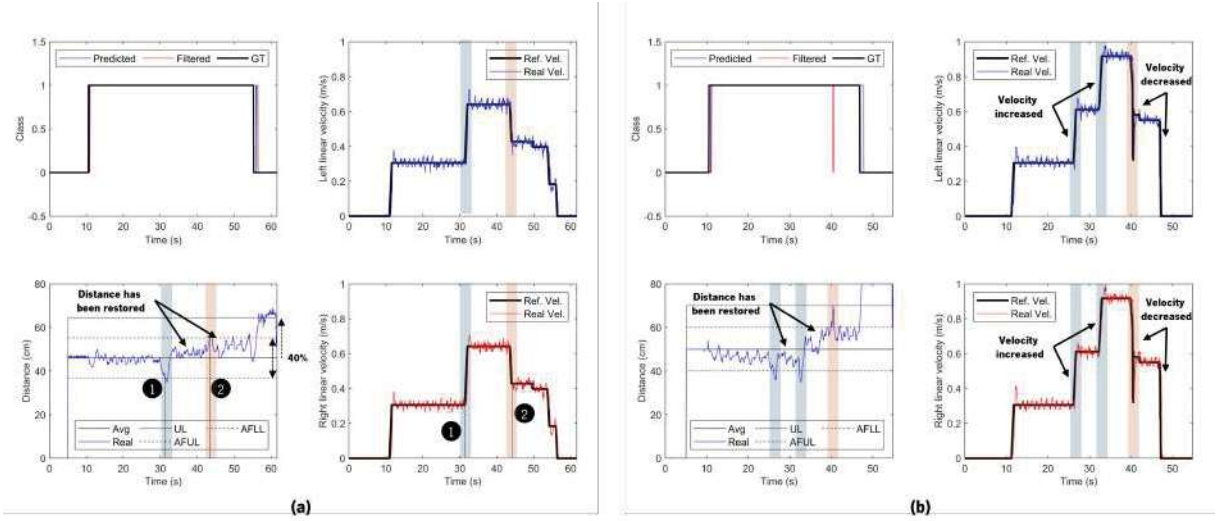


Figure 34: Representative trials of the proposed HIL control strategy with the adaptability module activated, considering an initial walking speed of 0.3 m/s. GT, UL, AFLL, AFUL stand for Ground Truth, Upper Limit, Adaptability Factor Lower Limit, and Adaptability Factor Upper Limit, respectively.

The results show that the proposed strategy allows the adaptation of the proportional controller's reference speed to maintain a fixed distance from the user (*i.e.*, the average distance measured during the calibration period). This is demonstrated in Figure 34a at timestamp 1. At this point, the user approached the device's platform and exceeded the lower limit of the adaptability module. This triggered the adaptability module, which activated the β factor at a rate of 15 Hz, allowing it to increase the real linear velocity of the SRW, as seen in the highlighted region at timestamp 1. This made it possible to restore the average distance of the user from the device, as can be seen in the trial section between timestamps 1 and 2 in Figure 34a, where the linear velocity remained constant. On the other hand, at timestamp 2, the user crossed the dead zone boundary, but this time the user increased the distance from the device, indicating an intention to slow down. Therefore, the adaptability module was activated and the device slowed down. Note, however, that the user's average distance was later not completely restored, indicating that the user was still slowing down and may have wanted to stop. Thus, the β factor continued to decrease the linear velocity until the user finally stopped, exceeding the upper limit (th_1). As a result, the linear velocity

decreased to 0 m/s. From the moment the device stops, the linear velocity is reset to the value initially set by the physiotherapist using the GUI.

Figure 35 illustrates the behavior of the robotic walker when an obstacle is detected by the ultrasonic sensors and while the safety module is activated. The proposed strategy is not yet developed to provide assistance during turning but rather to make small adjustments to the trajectory or even to stop when in the presence of an obstacle, so as to avoid collision.

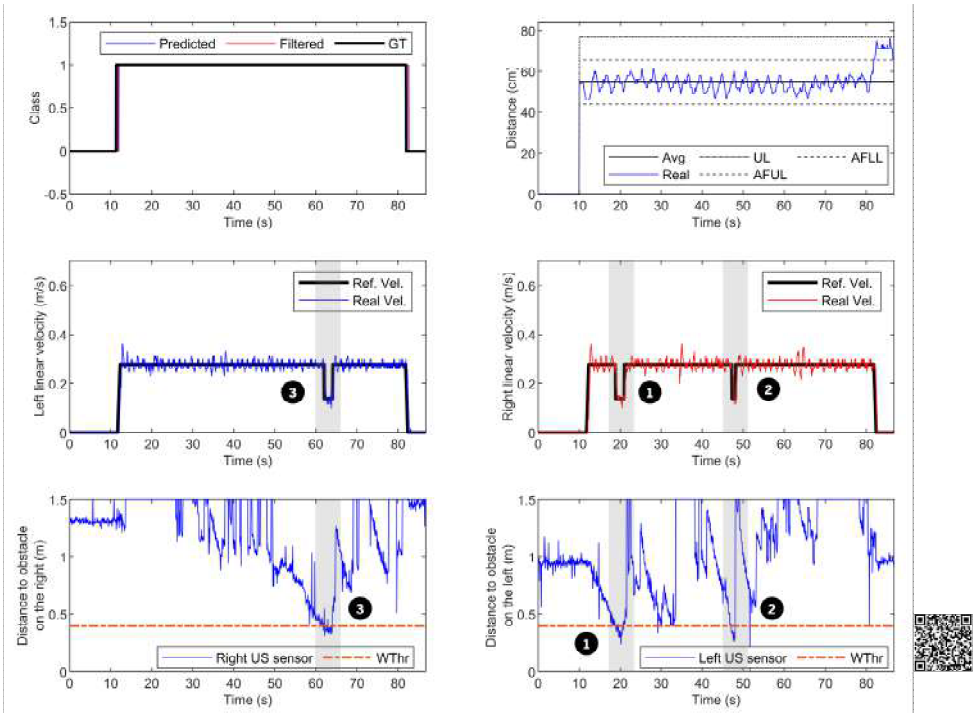


Figure 35: Representative trials of the proposed HIL control strategy with the adaptability and safety modules activated, considering an initial walking speed of 0.3 m/s. GT, UL, AFLL, AFUL, WThr stand for Ground Truth, Upper Limit, Adaptability Factor Lower Limit, Adaptability Factor Upper Limit, and Warning Threshold, respectively.

The results show that the device reacts immediately when an obstacle is detected at a distance of 40 cm or less from the device, which is the case for regions 1, 2 and 3 in Figure 35. Analyzing region 1, it can be seen that an obstacle is detected on the left side of the robot, since from $t = [10,20]$ s the distance detected by the ultrasonic sensor decreases linearly. As a result, the speed command for the right wheel has been reduced and is lower than the speed command for the left wheel. This difference allowed the robotic walker to deviate from the obstacle by changing its orientation.

The change in course is maintained as long as an obstacle is detected below the set limit. According to the results, immediately after correcting the speed of the right wheel in region 1, there is an increase in the distance measured by the ultrasonic sensor on the left. Later, in zone 2, the left ultrasonic sensor

again detects an obstacle and the device reacts by reducing the right wheel speed command. Finally, in region 3, the user encounters an obstacle, but this time on the right side of the device. The results show that the robotic walker has adjusted its trajectory to avoid a possible collision. This specific trial can be visualized using the QR code shown in Figure 35.

In terms of operating times, Table 27 shows the pre-processing time and the prediction time for the corresponding class, given the hardware of the robotic device presented in Chapter 3. Considering the hardware, the proposed HIL strategy requires a total time close to 44 ms, taking into account all the trials of the different walking speeds, thus fulfilling the requirement of 15 Hz. This time is mostly explained by the inference time of the model, which represents on average 96.23% of the total time. Therefore, future research should include reducing the computational burden of the implemented AI model through knowledge distillation, for instance.

Table 27: Operation times, in ms, of the proposed HIL control strategy with WALK and STOP classes. The pre-process time corresponds to the time of preparing the input frame

Gait Speed (m/s)	Trial	Pre-Process Time (ms)	Predict Time (ms)	Final Time (ms)
0.3	**T1**	1.68	41.77	**43.45**
	T2	1.80	41.64	**43.45**
	T3	1.76	41.07	**42.83**
0.5	**T1**	1.70	41.14	**42.84**
	T2	1.51	42.03	**43.55**
	T3	1.65	41.71	**43.35**
0.7	**T1**	1.49	43.03	**44.51**
	T2	1.47	42.29	**43.76**
	T3	1.65	40.94	**42.60**

5.3 Deep Reinforcement Learning based Shared Control Strategy for Robotic Walkers

To cope with the unpredictability of ataxic gait, this thesis also aimed to validate an AAN control strategy, based on RL, in which the robotic walker, in addition to perceiving the user's MI, is able to analyze the environment and decide whether it should assist the user by sharing the user's control with an ADS. The primary goal of this based strategy is to provide the robotic walker with the intelligence to analyze all the user's movements and verify that they do not compromise his/her safety. If the commands

are considered safe, the RL agent gives the user complete freedom, increasing his/her participation and involvement in controlling the robotic walker. On the other hand, if the commands are considered unsafe, the agent activates the ADS and no longer responds to the user's commands. This subsection briefly introduces the control strategy and presents its validation with healthy participants.

5.3.1 Proposed strategy

This strategy consists of four modules, as shown in Figure 36: **i)** the User Intention Detector, **ii)** the ADS, **iii)** the prioritizer, and **iv)** the controller.

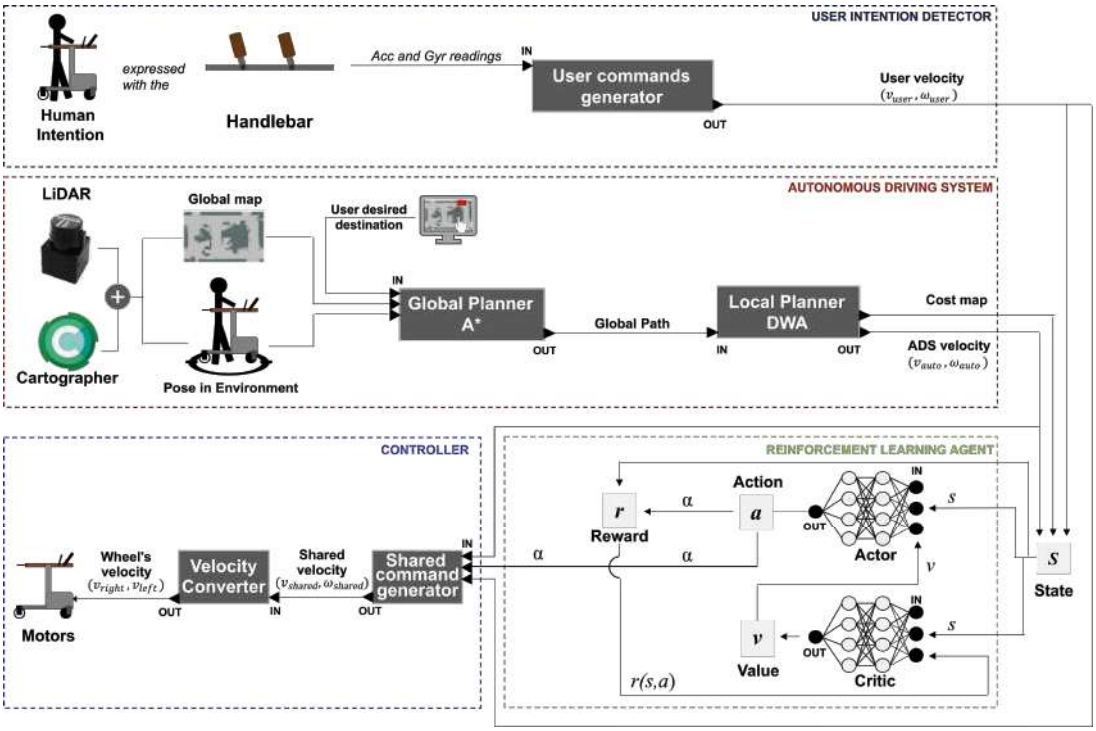


Figure 36: Overview of the implemented RL-based shared control strategy.

Regarding the first module, the User Intention Detector, this is responsible to directly perceive the user's intention to go forward, right and left, or to stop, and to generate the user's velocity command ($v_{\text{user}}, \omega_{\text{user}}$). As for the second module, the Autonomous Driving System, this is responsible for creating the map of the environment, taking into account permanent and dynamic obstacles, using Simultaneous Localization and Mapping (SLAM) with 2D laser technology. It is also responsible for generating the ADS velocity ($v_{\text{auto}}, \omega_{\text{auto}}$), assisting or overriding the user's commands if necessary, according to the instructions of the prioritizer, the third module. This third module is based on RL and is responsible for analyzing the user and ADS velocity commands and analyzing the environment. Based on this evaluation, and taking into account a target defined by the clinician using the device's GUI, the agent makes decisions

about who should control the device. For the proposed strategy, the agent estimates a α parameter, known as the sharing factor, which results in a shared velocity command ($v_{\text{shared}}, \omega_{\text{shared}}$) that is used to control the device. Finally, the fourth module corresponds to the controller module and is responsible for converting the shared velocity command into specific linear velocities for the two wheels of the device.

Strategy Requirements

Three key requirements were considered to implement this strategy on WALKit SRW, namely **i)** the proposed strategy should be able to safely guide the Human-Robot System (HRS) without registering collisions, given the fall risk associated with ataxia; **ii)** it should operate at a minimum frequency of 4 Hz, which was empirically determined to be acceptable; and **iii)** should give the user maximum freedom and activate the ADS whenever the user is in danger or not approaching the rehabilitation goal. A control frequency of 4 Hz was chosen to ensure safe braking, given the walker's maximum speed of 1 m/s and a acceleration of 2 m/s^2. These parameters allow the robotic walker to come to a complete stop from full speed in 0.5 s (*i.e.*, 2 Hz).

5.3.2 User Intention Detector

Although novel ways of controlling the device through early detection of MI have been studied in this doctoral thesis, this control strategy was first tested considering the direct MI obtained using WALKit's user-friendly handlebar. This handlebar moves forwards or sideways according to the desired movement, and its excursion is computed by means of a Complementary Filter (CF). This information is then translated into linear velocity commands of both right and left wheels (v_{R}, v_{L}). Under manual control of the device, v_{R} and v_{L} act as reference linear velocity command for a proportional controller implemented in the walker's low-level control. Then, since WALKit use the differential drive mechanism, the total linear velocity from the user's command (v_{user}) and the angular velocity from the user's command (ω_{user}) are derived as follows, where d is the distance between wheels:

$$v_{\text{user}} = \frac{v_{\text{R}} + v_{\text{L}}}{2} \tag{5.4}$$

$$\omega_{\text{user}} = \frac{v_{\text{R}} - v_{\text{L}}}{d} \tag{5.5}$$

5.3.3 Autonomous Driving System

The ADS is intended to assist the user when needed or to override the user's intentions in dangerous situations. It has been implemented with a URG-04LX-UG01 LFR (Hokuyo Automatic Co., Ltd., Osaka, Japan) placed at the front of the walker's chassis so that the sensor's FOV is not obstructed. The laser does not allow the presence of obstacles behind the device to be assessed in real time, but this was not considered relevant since it has a wide FOV (240° scanning range) and the walker is not allowed to move backwards as this could cause the user to fall.

Google's Cartographer, an open source real-time SLAM library with ROS support [137], was used for indoor mapping. SLAM is widely used in robotics, especially in indoor environments, because it allows to simultaneously map the environment and localize the robot in real time [138]. After obtaining the map of the environment and the current position of the robotic walker, the path planning process is performed [139], which is divided into global and local planners [138], responsible for creating a path between the robot's current position and the destination, and for translating this path into velocity commands, respectively.

To obtain the map of the environment, the *costmap_2d* package of ROS was used to create a map with: **i)** the static layer, which is the map of the environment; **ii)** the obstacle layer, which tracks the obstacles directly from the laser; and **iii)** the inflation layer, which fills the area near the obstacles. Two parameters of the inflation layer, the *inflation_radius* and the *cost_scaling_factor*, were empirically set to 0.6 and 10, respectively. The *inflation_radius* was chosen based on the space occupied by WALKit SRW, and the *cost_scaling_factor* was chosen based on providing a smooth gradient of cost values to the inflation process. When a destination is selected on the map, the global planner calculates the shortest path between the walker's current position and the destination [138] using the A* algorithm of the *global_planner* package of ROS [139] due to its computational efficiency.

Once the global path is created, it is translated into velocity commands by the local planner, taking into account both linear and angular velocities. This conversion is done using the *base_local_planner* package of ROS, which uses a 5×5 meter submap surrounding the robot walker and implements a DWA algorithm. The local planner should operate at a higher frequency than the global planner, since it is responsible for constantly simulating possible trajectories given the walker's current position.

The *base_local_planner* package publishes a cost cloud that is created and used when estimating the velocity commands. It consists of a point cloud representation of the cost map, where each pixel contains the cost of moving from one point to another. High cost values often correspond to obstacles, forcing the robotic walker to minimize the cost of the path. Some parameters were tuned empirically, namely

sim_time, *sim_granularity*, *vx_samples*, *vtheta_samples*, *pdist_scale*, *gdist_scale*, and *occdist_scale*. For most parameters, the default value was considered sufficient; only *sim_granularity* was set to 0.2 seconds, and *vx_samples* and *vtheta_samples* were set to 5. The output of the local planner is a vector of linear (v_{auto}) and angular velocities (ω_{auto}), representing the ADS velocity commands.

5.3.4 RL-based control strategy

Regarding the novel control strategy, the ultimate goal is to give users the freedom to walk and steer the device according to their intentions and needs, but in case of dangerous situations, the proposed strategy should assist users as needed or override their commands. Four components of the system were considered, as shown in Figure 36: **i)** the state space, **ii)** the action, **iii)** the reward, and **iv)** the policy. This subsection presents an overview to each of the four components that comprise the proposed strategy.

State and Action Space

The state space s is the representation of the current environment and should be fully observable. It needs to have the full description of the environment so that the agent can make the decision whether the user or the ADS will have more control over the walker. In this work, the state space includes the target velocities from the ADS (v_{auto}, ω_{auto}) and the user (v_{user}, ω_{user}), the latter obtained by the user intention detector module, and the cost map published by the local planner.

Regarding the action space, the action a is a one-dimensional vector that contains the sharing factor, which ranges between 0 and 1. This factor expresses the contribution of both the ADS and the user intention module, culminating into the shared speed command, (v_{shared}, ω_{shared}), as shown in Equation 5.6. As α increases towards 1, the robotic walker becomes autonomous and does not react to the user's intentions. On the other hand, as the value approaches 0, the robotic walker will be complacent to the user's commands. In this way, this strategy will provide only the necessary amount of assistance given the context and the defined goal.

$$(v_{\text{shared}}, \omega_{\text{shared}}) = \alpha(v_{\text{auto}}, \omega_{\text{auto}}) + (1 - \alpha)(v_{\text{user}}, \omega_{\text{user}}) \tag{5.6}$$

This shared velocity is then converted into linear velocities for each wheel using Equation 5.7 and following the differential drive kinematics, where (v_{left}, v_{right}) represents the linear velocity of the left/right wheel, in m/s; v_{shared} and ω_{shared} represent the total linear and angular velocities of the robot, in m/s and rad/s, respectively; and d is the distance between the wheels (80 cm).

$$(v_{\text{left}}, v_{\text{right}}) = \left(v_{\text{shared}} - \omega_{\text{shared}} \frac{d}{2}, v_{\text{shared}} + \omega_{\text{shared}} \frac{d}{2} \right) \tag{5.7}$$

Reward

To learn the policy, the RL agent needs a reward. The purpose of the reward is to provide feedback to the agent about how good or bad its actions are. It serves as a guiding signal to drive the agent's learning process, helping it to learn behaviors that maximize the cumulative reward over time. Equation 5.8 represents the reward function *r* given the state space *s* and the action a. To create the reward function, three aspects were considered: **i)** the risk of falling associated with ataxics in the event of a collision; **ii)** the concept of assist when and as needed strategy, in the sense that the ADS should only be activated when the user is not driving the robotic walker safely; and **iii)** the need to converge to the specific target goal defined by the clinician using the GUI.

$$r(s,a) = \begin{cases} -1 & \text{if collision} \\ 10 & \text{if goal achieved} \\ -1 \times |\text{dist}_{\text{factor}} + \alpha - 1| + 1 & \text{otherwise} \end{cases} \tag{5.8}$$

To ensure the safety of the ataxic patient, the robotic walker must receive a penalty whenever a collision is detected. So if a collision is detected, a reward of -1 is given. In addition, even if the robotic device does not collide, but approaches both permanent and dynamic obstacles, thus compromising the safety of ataxic users, the reward should not be identical to a collision, but should vary according to a distance factor, $dist_{factor}$, obtained by taking into account the minimum distance to a detected obstacle. In this case, the reward should increase as the robotic walker gets further away from obstacles to ensure patient safety. The distance factor is a developed heuristic calculated by Equation 5.9, where $obst_{distance}$ is the array of distances measured in real time with the 2D laser:

$$\text{dist}_{\text{factor}} = \max\left(\min\left(2.5 \times \min\left(\text{obst}_{\text{distance}}\right) - 1.5, 1\right), 0\right) \tag{5.9}$$

A collision is considered to occur at a minimum distance to an obstacle of 0.6 m. For a minimum distance of 0.6 m or less, the $dist_{factor}$ is clipped to 0. On the other hand, for a minimum distance of 1 m or more, the $dist_{factor}$ is clipped to 1. When the minimum distance to an obstacle is 1 m or more, the shared strategy should output low values of α to give more priority to the user, since there is no risk of collision. According to equations 5.8 and 5.9, the reward function will be $r = (1 - \alpha)$, since α is always a positive value. Therefore, to maximize the given reward, the agent is encouraged to generate low values

of α. On the other hand, for a minimum distance of 0.6 m, the reward will be $r = 1 - |\alpha - 1|$. In this case, the reward will be maximized if the system considers high values of α rather than low ones, thus giving more weight to the ADS.

The concept of AAN is given by introducing the sharing factor α into the reward itself. Since $\alpha \in [0, 1]$, the proposed control strategy will only provide the necessary assistance to the user by controlling the contribution of ADS, as shown in Equation 5.6. Finally, in order to give an additional incentive to the agent when reaching the predefined goal, a higher reward is given, in this case 10.

Policy and State-Value Networks

To train the RL agent, the Proximal Policy Optimization (PPO) algorithm was used in its Actor-Critic configuration. Two Deep Neural Networks (DNN) have been developed in [140] to act as Actor and Critic. The structure of both networks is similar, but their outputs differ: the Actor generates the action a, which includes the α factor used to compute the shared velocity commands. The Critic, on the other hand, outputs the value $v(s)$ of the state-action pair, evaluating the Actor's decisions based on the reward function and state space. This evaluation guides the Actor in learning to improve its policy.

Figure 37 illustrates the structure of the Actor implemented in this work. The structure can be divided into two parts: **i)** the cost map feature detection and **ii)** the shared command regression. The Cost Map Feature Detection is composed of three CNN layers, where the output of each layer is followed by a ReLU activation function and produces 10 channels, as proposed in [141]. The first CNN layer uses a kernel of size 7 and stride 2, and the following ones use a kernel of size 10 and stride 1, which were found empirically. The shared command regression is composed of two FC layers of size 256 and one FC layer of size 1. Finally, a logistic function (sigmoid) was applied to scale the output of the last FC layer in the interval [0, 1], which are the allowable values of α.

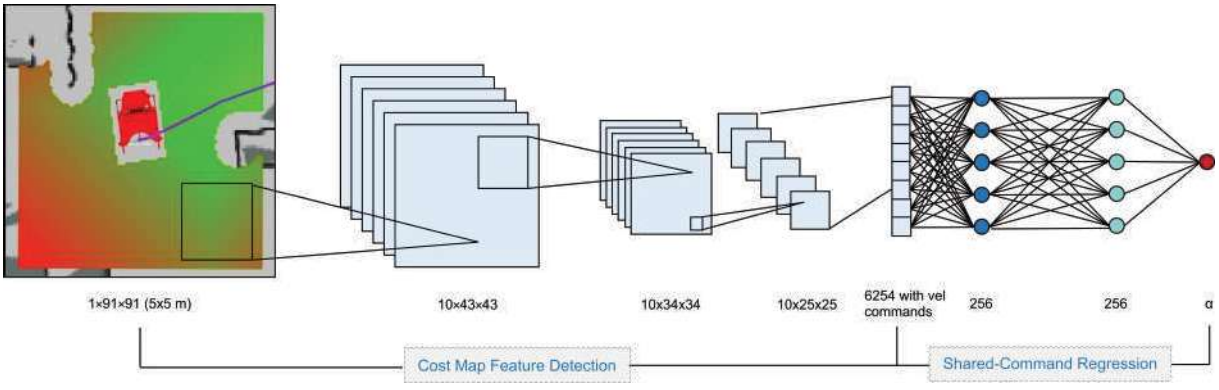


Figure 37: A representation of the deep neural network used as policy function. The number of entries (inputs/outputs) in this figure is not representative of the actual number present in the network.

5.3.5 Experimental Protocol

To validate the control strategy, three healthy participants were invited to participate. Data collection was carried out under the procedures of the Life and Health Sciences Ethics Committee of the University of Minho (CEICVS 147/2021), in accordance with the Declaration of Helsinki and the Oviedo Convention.

Five scenarios were considered, repeated three times, similar to those performed by real users of WALKit during therapy sessions, namely **i)** 5−meter straight ahead (scenario 0); **ii)** 5−meter with the destination behind the walker (scenario 1); **iii)** 8−meter to the right (90° corner) with a static obstacle (scenario 2); **iv)** 8−meter to the left (90° corner) with a static obstacle (scenario 3); and **v)** 8−meter ahead with a dynamic obstacle (person walking perpendicular to the walker's trajectory) (scenario 4). In these scenarios, users were instructed to perform different actions besides driving the device correctly, namely trying to collide with obstacles and increasing the distance to the target, to simulate the possible actions of end users of WALKit who may have limited driving skills due to some possible upper limb incoordination.

Validation metrics

To evaluate the proposed RL-based strategy, two common metrics in the literature were considered: **i)** the number of collisions registered, as it indicates whether the robotic walker can successfully detect and avoid static or dynamic obstacles with the proposed strategy; and **ii)** the KTE, as addressed in [51]. The KTE was computed with Equation 5.10, where x_{actual} and x_{global} path represent the actual and global path coordinates, respectively. This metric was chosen because it allows to verify how close the walker is to the path planned by the ADS, evaluated in all scenarios considering both the ADS and the proposed shared control strategy, to verify the impact of the proposed strategy regarding the ADS.

$$\text{KTE} = \sqrt{\frac{1}{n}\sum(x_{\text{actual}} - x_{\text{global path}})^2 + \text{Var}[x_{\text{actual}} - x_{\text{global path}}]} \tag{5.10}$$

In addition, this work proposes a new metric, the URC metric, expressed as a percentage, which gives an idea of how much the user controls the walker. The URC metric was estimated using Equation 5.11, where N is the total number of samples in the trial and α is the sharing factor. Considering 5.6, the user is mostly in control when $1 - \alpha$ is greater than 0.5, and in full control when it is progressively closer to 1. In this case, the values of the sharing factor are low, and thus the shared control strategy will prioritize the user commands over the ADS commands. Therefore, a URC of at least 50% is expected. However, as a key requirement, it is proposed to achieve at least 70%, indicating a high level of user involvement.

$$\text{URC} = 100\frac{1}{N}\sum_{n=0}^{N}(1-\alpha_n) \tag{5.11}$$

5.3.6 Results and Discussion

Table 28 presents the KTE values of the HRS when guided by the ADS and the proposed shared control strategy. Evaluating the difference in KTE values between the ADS and the proposed strategy is quite relevant, as it allows one to see whether the strategy actually gives the user the expected freedom in controlling the device, while at the same time verifying that the outlined goal is being met and that the user is driving safely.

Table 28: KTE values (m) registered for the both the ADS and the proposed strategy

Scenario No.	KTE (m)	
	Autonomous Driving System	**RL-based control strategy**
0	0.19 ± 0.12	0.48 ± 0.32
1	0.78 ± 0.33	0.99 ± 0.47
2	0.17 ± 0.09	0.85 ± 0.44
3	0.16 ± 0.09	0.69 ± 0.11
4	0.25 ± 0.15	0.17 ± 0.10

Regarding the ADS, Table 28 shows that the robotic walker followed the path accurately, especially in scenarios where the device had to move forward or make slight deviations (scenarios 0, 2, and 3). In these scenarios, the KTE values were found to be below 0.2 m, on average, which indicates the path take by the HRS is mostly coincident with that proposed by the global planner of the ADS. This would be expected since, as the HRS is controlled by ADS, the user does not have an input into the device's control. In addition, in these specific scenarios, no permanent or dynamic obstacles were presented to the HRS, so there was no need to change the walker's trajectory in regard to the global path. This result is actually consistent with Figure 38, which presents a representative trial, showing the paths taken by the HRS following the specific velocity commands of the implemented ADS. Scenario 0, 2, and 3 corresponds to Figure 38a, c, and d, respectively. As one can observe, the actual path, represented as red, is mostly coincident with the planned path, shown in green.

Scenario 1 the presented the higher value of KTE, with an average value of 0.78 ± 0.33 m. This higher value, which is at least three times higher in comparison with the remaining scenarios, is explained by

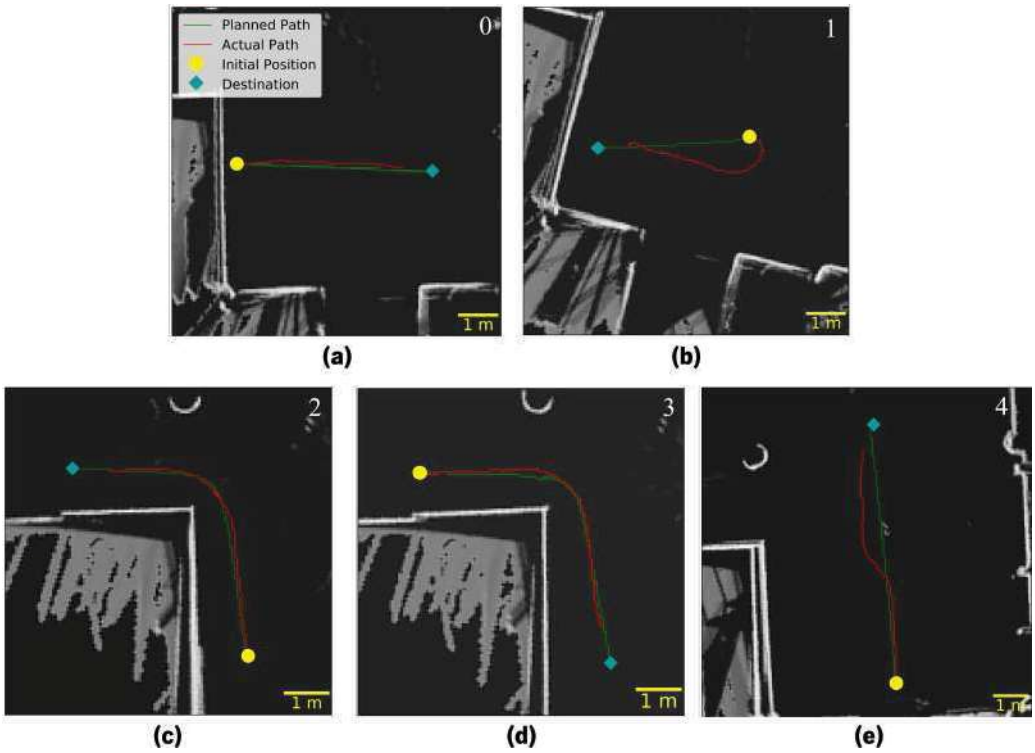


Figure 38: Representative trials of the path taken by the HRS with the ADS (red trajectory) in comparison to the planned paths (green trajectory) considering the five scenarios tested considering the ADS: **(a)** scenario 0, **(b)** scenario 1, **(c)** scenario 2, **(d)** scenario 3, and **(e)** scenario 4.

the wide turn the device made, as exemplified in Figure 38b. In fact, the walker is not allowed to move backwards (*i.e.* both wheels have negative speed). However, since the goal of the scenario was to reach a target that was 5 meters behind the device, the device would have to turn 180°, which in the case of a holonomic robot would make it stay in the same place. However, WALKit is not a holonomic robot, nor is its footprint centered on the device, so this behavior would not be feasible. In addition, this could compromise the user's instability, especially for users with CA, as it is not a natural rotation. Therefore, the actual path of the HRS (see red trajectory of Figure 38b) is not coincident with the planned one (green trajectory of Figure 38b), explaining the higher KTE.

As for scenario 4, an average KTE value of 0.25 ± 0.15 m was found. This is not as higher as scenario 1, but it represents a minimum average increase of 31.6% in comparison with scenarios 0, 2, and 3. In this specific scenario, as exemplified in Figure 38d, the HRS encountered an dynamic obstacle in its path. Thus, the local planner of the ADS changed the velocity command in order to deviate from the obstacle. This result is quite positive, as it shows that the ADS implemented in this work responds well and promptly to obstacles, without registering collisions, which is essential to ensure the safety of ataxic patients.

When comparing the the ADS with the proposed shared control strategy considering Table 28, the latter

presents higher values of KTE, with a global average value of 0.63 m, in comparison with the ADS that presents 0.31 m. This result was expected, but it is relevant, as it shows that, under the proposed shared control strategy, the HRS did not strictly follow the ideal path recommended by the ADS. This suggests that, indeed, users mostly command the device and, thus, the proposed strategy strongly appeals to their interaction and engagement. Specifically for scenarios 2 and 3, the KTE values were expressively higher (at least four times higher), as it can also be inferred in Figure 39c and d. In these specific scenarios, there is a considerable deviation from the trajectory proposed by the ADS (green path in Figure 39), and this is only possible because the sharing factor, α, is mostly low, below 0.5 (see heatmap of Figure 39), which causes the control to prioritize the user's commands.

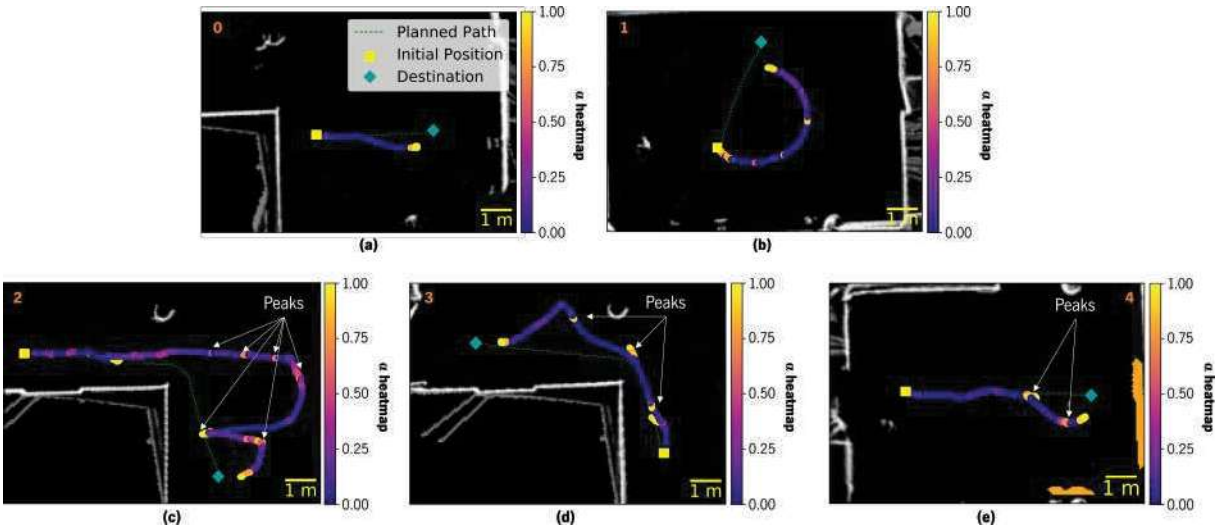


Figure 39: Representative trials of the path taken by the HRS with the proposed shared control strategy (trajectory with heatmap) in comparison with the planned path by the global planner (green trajectory) in the five scenarios tested: **(a)** scenario 0, **(b)** scenario 1, **(c)** scenario 2, **(d)** scenario 3, and **(e)** scenario 4.

Regarding scenario 1, the KTE is also higher, 0.99 m, in comparison with 0.78 m for the ADS, but the difference is not so expressive. This result was obtained since the target goal of the HRS is 5-meters behind the actual position of the system. Figure 39b exemplifies the HRS trajectory for a representative trial. It can be seen from the presented heatmap that the α values at the start are higher than 0.75, which causes the control strategy to prioritize the velocity commands of the ADS. The agent reacted in this way because it considered that it would be difficult for the user to reach the target goal while facing the opposite direction. However, as soon as the orientation was corrected, the α values dropped drastically, to below 0.25 (see trajectory's heatmap), which indicates that from that moment on, the strategy prioritized the user's intention to move.

By the other hand, analyzing scenario 4, the proposed strategy presented an average KTE 32% lower than that registered for the ADS. Although this is not expected at first analysis, it can be explained by the fact that ADS, as exemplified in Figure 38e, seems to start correcting the trajectory earlier in the presence of the dynamic obstacle, when compared to Figure 39e, which shows the same scenario but considering the proposed shared based control strategy. This event, combined with the fact that the user's trajectory in Figure 39e is mostly coincident with that proposed by the ADS, contributed to the lower KTE value observed.

For scenarios 2, 3, and 4, Figure 39c, 39d, and 39e) illustrates the existence of peaks in the α factors, *i.e.*, high values of α in specific zones of the trial, usually above 0.5. For example, in scenario 2, the heatmap shows that the value of α gradually increases as the user begins to move significantly away from the path defined by the global planner (green trajectory). When the HRS reaches the maximum distance from the goal (see Figure 39c), the α value increases (see heatmap of α in the system's trajectory), introducing some contribution from the ADS to correct the HRS trajectory towards the goal. As the system starts to move toward the goal, the α decreases, noticed by the purple-to-blue color of the heatmap, that indicates an α below 0.25. Still in this scenario, Figure 39c shows that the HRS intercepts the planned path (green trajectory) and, at this time, the α value has a peak of 1.0. This is probably because the user changed to walker's orientation in regard to the target goal, and since the HRS was close to the target goal, the RL agent is motivated to finish the episode to obtain a higher reward. Even so, the agent realized that the user's intention was not to reach the destination immediately, so it reduced the α value again and prioritized the user's velocity commands. This result shows the adaptability of the strategy in real time and the strategy's ability to give the user freedom. However, when the user moves further away from the target, the strategy increases the α value again in order to adjust the user's strategy slightly and to encourage the user to meet the target.

The results also show that when the HRS is close to the target, the α value increases to a high value, close to 1. This is due to the fact that the reward implemented gives a great incentive when the system finishes the episode, *i.e.* fulfills the proposed goal. In this way, and to ensure that the episode is finished, the strategy prioritizes the ADS commands. Although this is not necessarily a negative result, since it encourages and helps the user to fulfill the proposed goal, the reward obtained by completing the episode could be slightly lower so that the strategy also takes the user's intentions into consideration.

Alongside these results, the URC metric also shows this strategy's ability to prioritize user motion intentions. According to Table 29, it can be seen that the metric reaches average values above 60% in all the scenarios tested, which shows that, most of the time, the α values are low.

Table 29: URC, in percentage, registered all over the five scenarios tested with the shared control strategy

Scenario No.	URC (%)
0	84.93 ± 6.04
1	73.27 ± 4.37
2	67.66 ± 7.32
3	62.71 ± 7.63
4	65.06 ± 7.26

Scenario 0 presented the highest value among the five scenarios, which is confirmed by Figure 39a, which shows that the α values were uniformly low (between 0 and 0.25, see heatmap). The highest URC obtained in this scenario compared to the others, and the higher KTE values compared to the ADS, suggest that the proposed control strategy can prioritize the user's intentions when there are no obstacles and the path is straight. In addition, the results suggest that the prioritizer, although aiming to provide the user with maximum freedom, does not allow the user to fully control the robotic walker, since the URC values are not 100%, although close to 85%. This indicates that the proposed strategy also takes into account the ADS advice to converge to the goal. However, if the user is not progressing towards the desired goal, the strategy should gradually intervene and help the HRS to reach the desired goal. This is also evidenced by the fact that the user never had 100% control in the scenarios tested.

As for scenarios 2, 3 and 4, the URC value was similar and corroborates with Figure 39c, 39d and 39e, where low values of α were mostly obtained throughout the HRS trajectory. In these specific scenarios, the standard deviation is slightly higher compared to scenarios 0 and 1, probably motivated by the observed peaks. As for scenario 1, as shown in Table 29, the URC value is the second highest. In this scenario there are no obstacles, but the target is 5 m behind the robotic walker. As shown in Figure 39b, the proposed strategy produced a high value of α, close to 0.75, just in the first meters of the trial, and then prioritized the user's commands, since the probability of reaching the goal had increased.

Regarding collisions, no collisions were verified while performing the validation of the proposed strategy. Finally, in terms of operating frequency, it was observed that the proposed control strategy operates in the interval of $4.5-10$ Hz. The median was found to be approximately 5.5 Hz, as illustrated in Figure 40. Therefore, it can be concluded that the minimum requirement of 4 Hz was met.

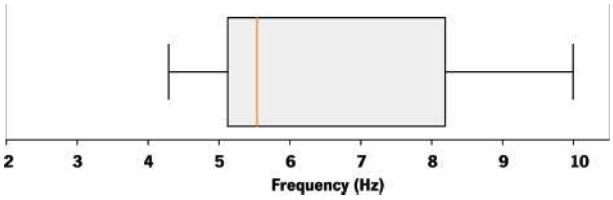


Figure 40: Operating frequency box plot of the proposed shared control strategy.

Overall, the results show that the proposed strategy does indeed provide the user with freedom, but whenever necessary, the proposed strategy assists and with the required amount, by varying the α value in real time. In addition, the use of a RL algorithm (PPO), with trial-and-error optimization, allowed the agent to express a behavior that considered a full range of possibilities, instead of using heuristics with hard constraints to solve the problem, as presented in the literature. Thus, this strategy allows for an essential HRC, which will be important for ensuring the safety of ataxic patients. In the future, this strategy will be linked to the HIL strategy proposed previously, allowing ataxic patients to control the device in a natural and intuitive way without additional cognitive effort or unnecessary additional physical interaction, always maintaining therapy closely supervised by the robot. This AAN strategy will be of great importance in helping patients to focus on their gait and on ways to improve their walking pattern, without having to deal with obstacles that may appear along the way.

5.4 General Conclusion

In this chapter, two control strategies based on AI are presented in order to increase the device's compliance with the user's needs and intentions.

The first control strategy consists of a **HIL approach in which the user interacts with the device and the latter reacts according to the user's MI**. This strategy uses DL neural network, which analyzes single RGB frame that comprises a stack of 4 frames focused on the user's lower limbs, acquired at 15 *fps*, corresponding to 0.27s of action. As a first approach and proof of concept, the control strategy was tested considering only the WALK and STOP classes, since the model revealed confused in distinguishing between curves and forward motion. It was found that the model was able to correctly distinguish the two classes with an **IA of over 97%** and overall **precision and recall above 98%**. Furthermore, an average prediction delay of less than the required 0.64s was observed, and the control strategy was found to meet the 15 Hz operating frequency. In addition, considering an average step time of 0.64s, this AI model detects the user's intention to walk before the user finishes his/her step, enabling the device to be controlled in with no sense of delay for the user. These results enabled to achieve KPI 5.

As for the second control strategy, this consists of an AAN shared control strategy. This approach focuses on understanding the user's MI, in a first approach using the user-friendly handlebar, and combining this input with autonomous navigation support, **aiming to ensure safety while encouraging the user's active participation and autonomy in the therapy**. In particular, the RL agent monitors the user's decision and decides whether to follow the user's intention or to combine with an ADS that can override the user if the walker is being driven unsafely or assist if the target goal is not being approached. This strategy represents a system that learns and evolves in response to the user's specific intentions and the environment context. In addition, it prioritizes ease of use for ataxic patients, while ensuring that WALKit is not only a physical support tool. The results allowed to partially achieve KPI 6, with higher KTE values in comparison with the ADS, and average URC of 70%. The 10 Hz frequency was not achieved, but a lower limit of 4 Hz was guaranteed, which is sufficient when using the handlebar.

Chapter VI

Human-Robot Interaction Strategies

Chapter 6

Human-Robot Interaction strategies for balance and posture rehabilitation

6.1 Introduction

Another key aspect of this thesis was to integrate different interaction strategies into the device to maximize the user's involvement in the therapy, making it more **motivating, collaborative, and engaging**. Therefore, this thesis proposes the integration and exploration of BS and SG in the WALKit Smart Walker, which are **fully adaptable to the user** and can be used in the rehabilitation of different gait disorders. These systems and games have been designed taking into account the main impairment observed in ataxic patients, which is balance. This chapter presents the development of these HRI strategies as well as their validation in terms of functionality, *i.e.* whether they operate technically as expected, and usability, which has been assessed with both healthy and pathological participants. With regard to its effectiveness in the rehabilitation of ataxic patients, this topic will be addressed in the following chapter, which presents several case studies resulting from the use of the WALKit Smart Walker in the rehabilitation of patients with cerebellar ataxia.

6.2 Audiovisual Biofeedback Strategy

A systematic review published in 2016 by Ma *et al.* [142] discusses the use of BS integrated with wearable sensors. The authors report that "evidence supports the effectiveness of biofeedback systems in improving static and dynamic balance" in patients with balance disorders. In the case of CA, biofeedback is **still being explored** [85], but so far these HRI strategies are showing promising results. For example, Fleszar *et al.* [86] observed that real-time use of audio biofeedback can improved postural sway control in degenerative ataxia. An older study [102] also concluded that tongue electrotactile biofeedback

can improved bipedal postural control in patients with degenerative CA. However, **there is still a gap in the integration of these systems into robotic walkers**, which has already been seen in other robotic devices such as exoskeletons [143]. Their integration into the WALKit SRW would make this device multifunctional, capable of being used for gait rehabilitation as well as for dynamic and static balance. This would further increase the rehabilitative capacity of this device, making it capable of providing the user with information about their performance in real time, allowing for **greater motor awareness and promoting self-correction**.

6.2.1 Proposal

This thesis proposes the integration of an audiovisual BS in WALKit SRW, as shown in Figure 41. Biofeedback is given in real time, through the walker's GUI, using the device's monitor (see Chapter 3), which is easily visible by the user.

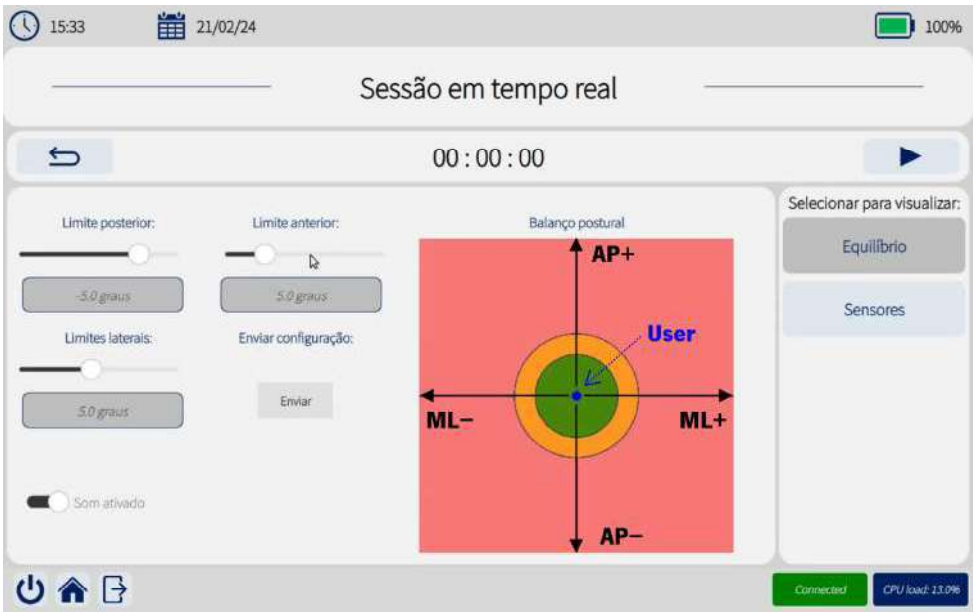


Figure 41: Biofeedback system embeeded in WALKit Smart Walker proposed to control the postural sway of ataxic patients.

A square is shown to the patient and is composed by three regions: **i)** green, which defines a safety region, **ii)** orange, which defines a warning region, and **iii)** red, which defines a danger region. These regions are created as a function of the green region, which is fully adaptable to the user, through the modification of the AP and ML limits in real time by a physiotherapist. The blue sphere represents the user and moves along these regions according to the user's torso orientation, estimated through a sensor fusion algorithm and an IMU placed closer to the user's CoM. Moreover, an audible warning is given whenever

the user goes beyond the green or orange regions. This warning is emitted at a different frequency and with a different sound, so that the user can intuitively recognize which limit has been exceeded. The two types of biofeedback proposed, audible or visual, can be additive or given independently. Figure 42 shows a short video demonstration of the novel BS embedded in WALKit SRW.



Figure 42: Video demonstration of the novel BS embedded in WALKit SRW.

6.2.2 Methodology

Orientation estimation

In order to estimate the orientation of the user's torso, a IMU was placed near the location of the CoM, more specifically in the L3-L5 vertebrae, following literature considerations [86, 106, 144]. Sensor fusion algorithms, namely the CF [145] and the Kalman Filter (KF) [146] as described in [147, 148] have been implemented in the WALKit SRW software using the C++ language.

Regarding CF, it is a computationally efficient sensor fusion algorithm that combines a low-pass and a high pass filter to refine orientation estimates (roll, pitch, yaw) from the accelerometer and the integration of angular velocity, respectively [145]. Let $\hat{\theta}$ represent the orientation estimate obtained with the CF, ω the gyroscope measurements (angular velocity), and θ_a the orientation estimated from the accelerometer, the CF is given by Equation 6.1:

$$\hat{\theta} = \alpha \int \omega dt + (1 - \alpha)\theta_a \tag{6.1}$$

The parameter α, which varies between 0 and 1, determines the corresponding weight for the gyroscope and accelerometer estimates. The purpose of this is to filter out the drift introduced by the integration of ω and to eliminate the high frequency noise of θ_a. In this work, α was set to 0.98, which was empirically obtained.

To obtain the torso's orientation using the accelerometer, trigonometric equations were developed using the Earth's gravity vector ($\vec{g}$). For the BS, only the roll and pitch angles are estimated, representing the orientation with respect to the mediolateral and anteroposterior axes, respectively. Roll (θ_z) and pitch

(θ_y) can be obtained using the following equations:

$$\theta_z = -\arctan(\frac{a_y}{a_x}) \tag{6.2}$$

$$\theta_y = \arctan(\frac{a_z}{(\text{sign}(a_x) \times \sqrt{(a_x)^2 + (a_y)^2}}) \tag{6.3}$$

Regarding the KF, this is an optimal state observer algorithm that predicts a parameter of interest from indirect, noisy and uncertain observations. It is a more computational complex algorithm, but it is a widely adopted sensor fusion algorithm for orientation estimation [145]. The KF is used to provide estimates of x_k at time k, *i.e.*, $\hat{x}_k$, given an initial estimate, x_0, and a measurement z_k [149]. It is as two-stage process that involve the time update ("prediction") and the measurement update ("correction"). In the "prediction" step, an a $priori$ state estimation, $\hat{x}_k^-$, is predicted, along with the error covariance, P_k^-, as follows:

$$\hat{x}_k^- = A\hat{x}_k^+ + Bu_k \tag{6.4}$$

$$P_k^- = AP_{k-1}^+A^T + Q \tag{6.5}$$

In the previous equations, $\hat{x}_k^-$ is the *a priori* state estimate (the predicted, *i.e.*, before the correction step) at time k, A is the state transition matrix, $\hat{x}_{k-1}$ is the state estimate from the previous time step, B is the control input matrix, u_k is the control input applied at the time k, P is the state error covariance, and Q is the process noise covariance matrix.

Afterwards, the correction step is performed. In this step, the measurement residual, $\tilde{y}_k$, is calculated, along with the Kalman gain, K, as follows, where H is the measurement matrix, and R is the measurement noise covariance matrix:

$$\tilde{y}_k = z_k - H\hat{x}_k^- \tag{6.6}$$

$$K = P_k^-H^T(HP_k^-H^T + R)^{-1} \tag{6.7}$$

The residual, $\tilde{y}_k$, is then multiplied by the Kalman gain, K, to provide the correction to the predicted estimate $\hat{x}_k^-$, obtaining the updated state estimate (*a posteriori* update), $\hat{x}_k^+$. Then, the error covariance, P, is updated to be used in the next time step. This culminates in P_k^+ and is obtained as follows, where I is the identity matrix:

$$\hat{x}_k^+ = \hat{x}_k^- + K\tilde{y}_k \tag{6.8}$$

$$P_k^+ = (I - KH)P_k^- \tag{6.9}$$

Equation 6.8 gives the updated state estimate, which is the optimal state estimation, *i.e.*, the output of the KF. This process is then repeated for the following time steps, enabling to obtain the user's orientation estimates in real time considering a reference frame. In the case of this specific problem, the Kalman Filter uses the estimates from the accelerometer (which is extremely noisy) and the integration of the gyroscope (that presents drift) to estimate the optimal state of the user at each of time step k.

Real-time integration in WALKit

In order to integrate this algorithm into WALKit's software, a specific ROS package was created. The code was developed in C++, based on the previous formulations and as described in [148]. This package is responsible for subscribing to the ROS topic, which publishes the message containing data from the smart walker's low-level sensors. The accelerometer and gyroscope data are then used to estimate the user's orientation using the sensor fusion algorithms presented in the previous subsection.

Visual biofeedback

Regarding the visual biofeedback, the user's orientation estimated by the previous sensor fusion algorithms is processed and translated into an (x, y) position on the screen, and this information is then processed by the walker's frontend to move the blue dot around the regions, accordingly. When the user enters the red region, a danger sign appears in the upper-right corner of the square.

Three regions have been empirically defined as the safe region (green area), the warning region (orange area), and the danger region (red area). These regions are created using two ellipses centered on the point (h, s) on the screen, which corresponds to the starting position of the blue ball (as shown in Figure 41). If the limits are the same, then the two ellipses together form a circumference. To set the limits, the physiotherapist can configure the strategy in a user-friendly way using the new GUI. The strategy has a small menu on the left side, shown in Figure 43, which shows three QML sliders representing the anterior, posterior and lateral limits. These limits are fully customizable by the user, allowing for more focused and targeted therapy. The strategy allows the anterior and posterior limits to be adjusted because, anatomically, the human body has different limits of movement in the AP axis. In the case of the ML axis,

considering a healthy individual, it is expected that he/she will have the same limit of movement for the right side as for the left side.



Figure 43: Example of the configuration of the biofeedback strategy.

To move the blue ball, a multiplicative factor for both axes has been empirically derived, which is then multiplied by the width and height of the parent window containing the biofeedback strategy. The result of this multiplication is then added to the initial position of the blue ball on the screen, allowing it to move according to the user's orientation. The multiplicative factor is derived through cubic interpolation, based on the estimated user orientation and the maximum allowable AP and ML limits defined in the GUI menu for the biofeedback strategy. Figure 44 illustrates snapshots of a user using the BS.

Audio biofeedback

Regarding audio biofeedback, this is provided directly through the backend of the device's software, taking into account the user's orientation estimate. Two half-ellipses, one for the 1^{st} and 2^{nd} quadrants, and another for the 3^{rd} and 4^{th} quadrants, as shown in Figure 45. Considering (h, s) as the center of the ellipses and a, b and c as the semi-axes of the ellipses obtained from the limits set by the physiotherapist, one can write the equation of the ellipses.



Figure 44: Snapshots of a user using the BS developed in this doctoral thesis and the corresponding visual biofeedback.

In this case, $h = s = 0$. If $a = b = c$, then the ellipses form a circumference.

$$\frac{(x-h)^2}{b^2} + \frac{(y-s)^2}{a^2} = 1 \tag{6.10}$$

$$\frac{(x-h)^2}{b^2} + \frac{(y-s)^2}{c^2} = 1 \tag{6.11}$$

These semi-ellipses are generated for both the green and orange regions. If the user's posture results in an orientation (roll, pitch) that is within the limits of the green region, audio biofeedback is not activated. If it exceeds this range and is within the orange range, a sound will be emitted. If the (roll, pitch) pair is neither in the green nor the orange range, then the user is in the danger range and a different, more intense, higher frequency tone will be emitted.

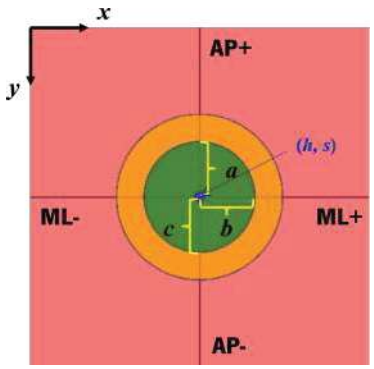


Figure 45: Ellipses created for audio biofeedback.

6.2.3 Validation Protocol

The validation of the biofeedback strategy consisted of two different protocols. The first protocol related to the validation of the sensor fusion algorithms for the estimation of the user's pose, *i.e.* the orientation of the torso using the IMU. As for the second validation protocol, this consisted of the strategy validation considering functionality and usability with healthy individuals. The BS is also being tested with pathological participants, but the results of this validation will be discussed in the following Chapter 7.

Data collection was performed under the ethical procedures of the Life and Health Sciences Ethics Committee (CEICVS 147/2021), according to the Declaration of Helsinki and the Oviedo Convention. Data were collected at the School of Engineering, University of Minho.

Participants

Regarding the first protocol, six healthy participants (3F, 3M, age of 25.1 $\pm$ 2.6 years, height of 170 $\pm$ 6 cm, and body mass of 67.9 $\pm$ 8.2 kg), without evidence of motor disorders, voluntarily agreed to participate in this validation study. The second protocol involved seven healthy participants (4F, 3M, age 24.0 $\pm$ 1.2 years, height 172.3 $\pm$ 9.6 cm, and body mass 72.4 $\pm$ 15.9 kg), without any evidence of motor disorders, some of whom participated in the first round of validation.

Experimental proceedings

The first validation protocol was divided into two steps, as follows. The first step consisted in performing a static validation, only with the IMU. Several movements were performed with the sensor, namely **i)** 90° rotation to the right (positive roll), **ii)** 90° rotation to the left (negative roll), **iii)** 90° rotation forward (positive pitch), and **iv)** 90° rotation backward (negative pitch). The second step involved user participation. Here, participants were instrumented with a single sensor from the Xsens Awinda motion capture system (Xsens Technologies B.V., The Netherlands) and the robotic walker's IMU. Each participant performed both static (no walking activity) and dynamic (with walking activity) trials. The static trials consisted of a sequence of movements that the participants had to perform, namely **i)** leaning forward, backward, right and left in a continuous motion, **ii)** remaining in a quiet standing position, **iii)** sitting down, and **iv)** standing up. Participants were then instructed to walk with the robotic device and complete 60 steps. Four speeds were tested, namely: 0.3, 0.5, 0.7, and 1.0 m/s. All trials were performed three times for better statistical power.

As for the second validation protocol, this served three main purposes: **i)** to verify whether the biofeed-

back strategy enables compensatory user responses, validating its functionality; **ii)** to assess whether the strategy indirectly controls the sway of the CoM; and **iii)** to evaluate user perception and the overall usability of the strategy. For that, participants followed a two-day protocol: one day with the biofeedback strategy enabled and the another day without it. Therefore, two random groups were created.

Each participant performed a 15-minute protocol, which comprised three tasks of 5-minutes each, as illustrated in Figure 46. These activities consisted of static exercises, as follows: **i)** bipedal stance, *i.e.*, standing in a stance position with the feet together; **ii)** tandem stance position, with the dominant leg holding the weight; and **iii)** unipedal stance with the dominant leg held the participant's weight. In each exercise, 3 trials of 60 seconds each were conducted with a 45-second break within. Since these were healthy and young participants with no reported balance issues, a foam platform was used to further challenge their balance, following literature considerations [102, 106, 150]. To set the AP and ML limits of the BS, each participant performed a trial of 60s for each exercise prior to the experimental study. The 90% range of values was found, similar to studies [106, 151], considering the 5^{th} and 95^{th} percentiles, in both axes. Since it is required both a positive and negative value for AP and ML limits, the largest absolute value was used.

An extra trial for each activity was performed considering the lowest absolute values of the AP and ML limits, to challenge more the user. Note that these values can be adjusted in real time for each user, and the goal is for them to be modified by the physiotherapist so that the therapy is more targeted and focused on the real needs of the patient.

Participant instrumentation

In addition to the robotic walker's IMU, the participants were instrumented with Xsens Awinda (Movella, USA, validated in [152]). For the first validation protocol, one IMU was placed at L3-L5 vertebrae. For the second protocol, 17 sensors were placed on head, both shoulder, sternum, upper arms, forearms, wrist, pelvis, upper leg, lower leg, and feet. Each of these sensors were positioned according to the manufacturers' guidelines [153] and were placed by the same researcher.

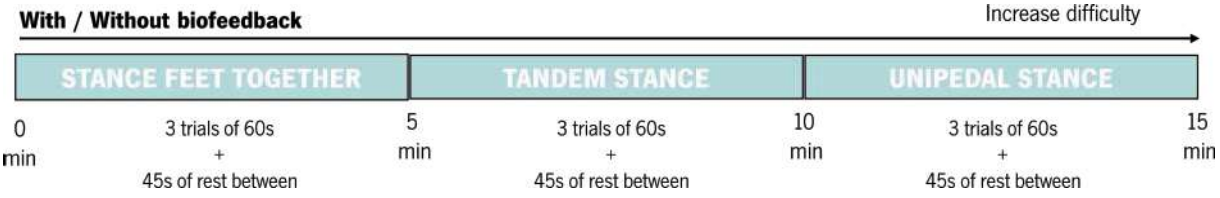


Figure 46: Diagram of the experimental protocol for the technical and usability validation of the BS.

Data acquisition

Regarding the first protocol, data acquisition from WALKit's IMU included acceleration, in m/s^2, and angular velocity, in °/s, collected at 50 Hz. As for the Xsens Awinda sensor, data was acquired at 100 Hz using the MT Manager software (version 2021.4.0) and included acceleration in m/s^2, angular velocity in rad/s, and both roll and pitch angles in degrees.

As for the second validation protocol, the data acquisition included the acceleration, in m/s^2, the angular velocity, in °/s, and both the pitch and roll angles, acquired with the ROS package responsible for the implementation of the biofeedback strategy, collected at 100 Hz, and the CoM position obtained with the Xsens Awinda motion capture system, collected at 60 Hz. The goal was to verify if the biofeedback strategy has any effect on the variation of the CoM.

Validation metrics

The validation metrics were different depending on the validation protocol. With regard to the validation of the user's torso orientation estimation, the RMSE was used, as presented in Equation 6.12, where N is the number of observations, y_i are the observed values (true values), and $\hat{y}_i$ are the predicted values, taking into account the sensor fusion algorithms.

$$\text{RMSE} = \sqrt{\frac{\sum_{i=0}^{N}(y_i - \hat{y}_i)^2}{N}} \tag{6.12}$$

In addition, to verify the monotonic relationship between the implemented algorithms and the orientation measured with Xsens Awinda, the Spearman correlation coefficient (r_s) was calculated as follows, where d is the difference between the two ranks of each observation and n is the number of observations:

$$r_s = 1 - \frac{6\sum d_i^2}{n(n^2-1)} \tag{6.13}$$

As for the second protocol, the percentage of activation (A) of the strategy. This was calculated using the following equation, where K is the number of samples of a trial in which the biofeedback strategy was activated and N is the total number of observations over a trial:

$$A = 100 \times \frac{K}{N} \tag{6.14}$$

Additionally, the CoM displacement in position was calculated using data gathered from the Xsens Awinda motion capture system, considering both AP and ML axes [144]. The total ROM was calculated considering both maximum and minimum values of position, as follows:

$$\text{ROM} = \max(\text{CoM}_i) - \min(\text{CoM}_i), i = \text{AP, ML} \tag{6.15}$$

Lastly, the usability of the biofeedback strategy was evaluated using the SUS [118].

Data processing and analysis

All raw data were filtered with a 4th order low-pass Butterworth filter with a cut-off frequency of 5 Hz [154, 155]. Data were processed with MATLAB R2023b (MathWorks®, California, USA). Statistical analysis was performed on ROM in both AP and ML axes using IBM SPSS Statistics 26 (IBM, New York, USA) to assess whether the proposed strategy affected CoM variation. The data were therefore tested for normality using both the Shapiro-Wilk and Kolmogorov-Smirnov tests. If the data followed a normal distribution, a paired *t*-test was performed considering the three types of activities (*i.e.*, bipedal stance, tandem stance, and unipedal stance). On the other hand, if the data did not follow a normal distribution, the Wilcoxon signed-rank test was performed. G* Power 3.1.7 software (University of Kiel, Kiel, Germany) was used to calculate effect sizes and to determine the power of the analysis using Cohen's *d* interpretation (small: $>$0.2; moderate: $>$0.50; large: $>$0.80) [156]. All statistical analyses were performed using IBM SPSS Statistics 26 (IBM, New York, USA) with a significance level of α =0.05.

6.2.4 Results and Discussion

This section presents and discusses the main results regarding the estimation of the user's torso orientation using the inertial system embedded in the robotic device, as well as the functionality and usability of the audiovisual biofeedback strategy evaluated by healthy participants.

User's torso orientation

Figure 47 shows the results obtained for each of the three trials carried out for the static tests with the IMU. In this case, it was decided to use the inertial sensor of the Xsens Awinda motion capture system, so that the calculated error only takes into account the algorithms implemented and not the fact that it is also a different sensor. In this way it was possible to make a direct comparison with the algorithm used by Xsens, which is the Xsens Kalman Filter 3 DOF for Human Motion [157].

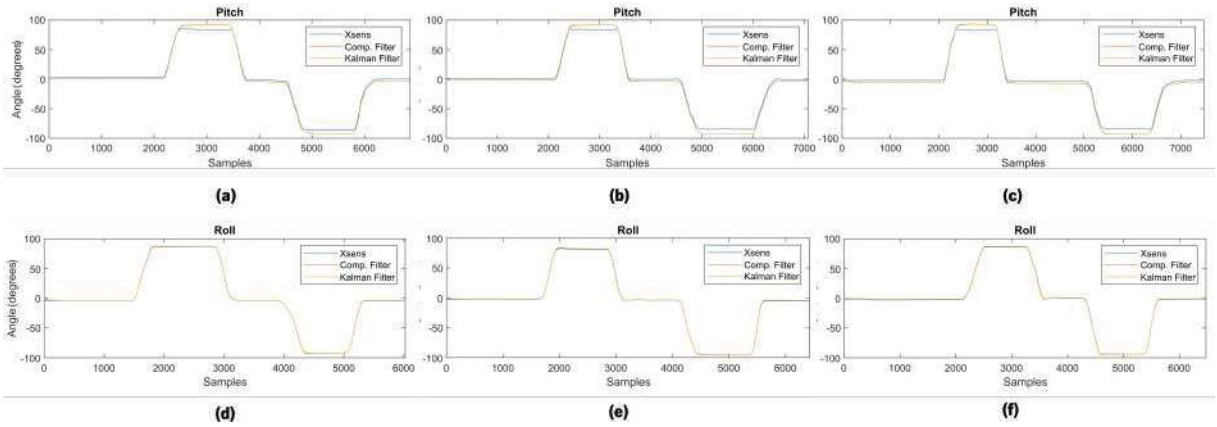


Figure 47: Representative illustration for the estimated pitch and roll of static trials: **(a)** trial 1, **(b)** trial 2, and **(c)** trial 3.

Both orientation estimation algorithms showed similar errors close to 5 – 6°, considering Xsens as GT, as shown in Table 30. Considering the observed ROM in Figure 47, the error was found to be on average less than 4% of the total ROM. Therefore, under static conditions, each of the algorithms used gives quite reasonable results.

Table 30: RMSE of both sensor fusion algorithms considering static trials

Trial	Pitch		Roll	
	CF	KF	CF	KF
T1	5.61	5.64	6.71	6.77
T2	6.43	6.48	5.29	5.37
T3	6.35	6.40	5.36	5.27
Average	**6.13**	**6.17**	**5.79**	**5.80**
STD	**0.45**	**0.46**	**0.80**	**0.83**

Regarding the validation trials with healthy participants, Figures 48, 49 and 50 show the three trials of a representative participant considering the different activities. Figure 48 shows the results obtained for the tilt activity, where participants leaned forward and backward (pitch), right and left (roll); Figure 49 shows the quiet standing activity, sitting down and then standing up; and Figure 50 shows an example of the walking activity.

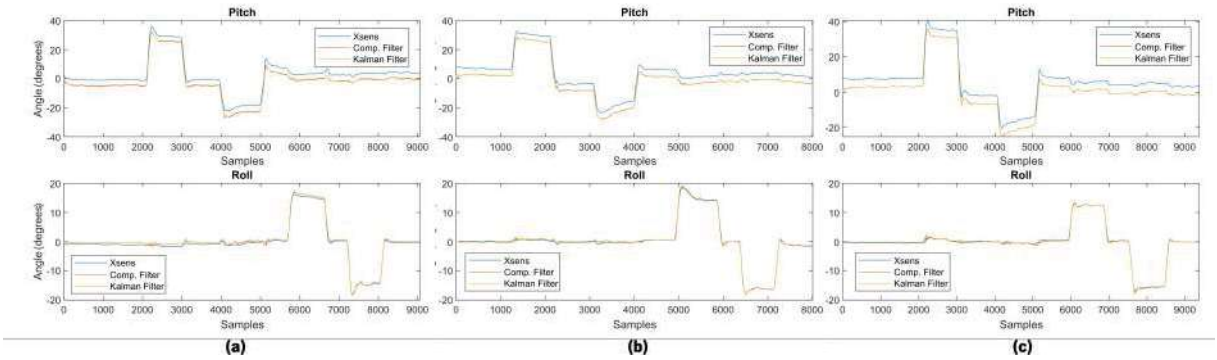


Figure 48: Representative illustration for the estimated pitch and roll of stance trials: **(a)** trial 1, **(b)** trial 2, and **(c)** trial 3.

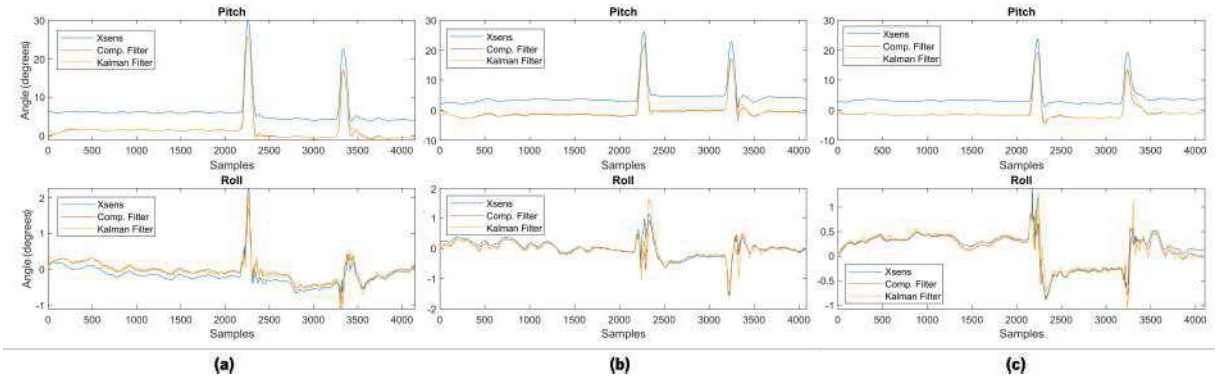


Figure 49: Representative illustration for the estimated pitch and roll of sit-to-stand trials: **(a)** trial 1, **(b)** trial 2, and **(c)** trial 3.

The results show that both algorithms performed reasonably well, especially for the roll angle. For pitch estimation, an offset of less than 5° was observed, which can be improved with more precise tuning of the algorithms. Analysing the results for all participants, as shown in Table 31, the results suggest that, overall and for the dynamic trials, *i.e.*, where the participants walked at different speeds, the CF filter gives slightly better results compared to the KF. As for the static trials (*i.e.*, leaning on the AP and ML axes, and quiet standing and sitting), it can be seen that the error was roughly similar.

A comparative analysis of the pitch and roll angles shows a lower error for the roll angle, as verified in Figures 48, 49 and 50, with average values of less than 2.5° for each of the algorithms. The pitch angle, on the other hand, has a higher error, close to 4.5°, which, when analysing Table 31, quickly shows that the main error is not due to the variation of the angle, but to an introduced offset. This conclusion can also be seen in Figures 48, 49 and 50, where it can be seen that the pattern of variation is roughly similar, although there is an offset.

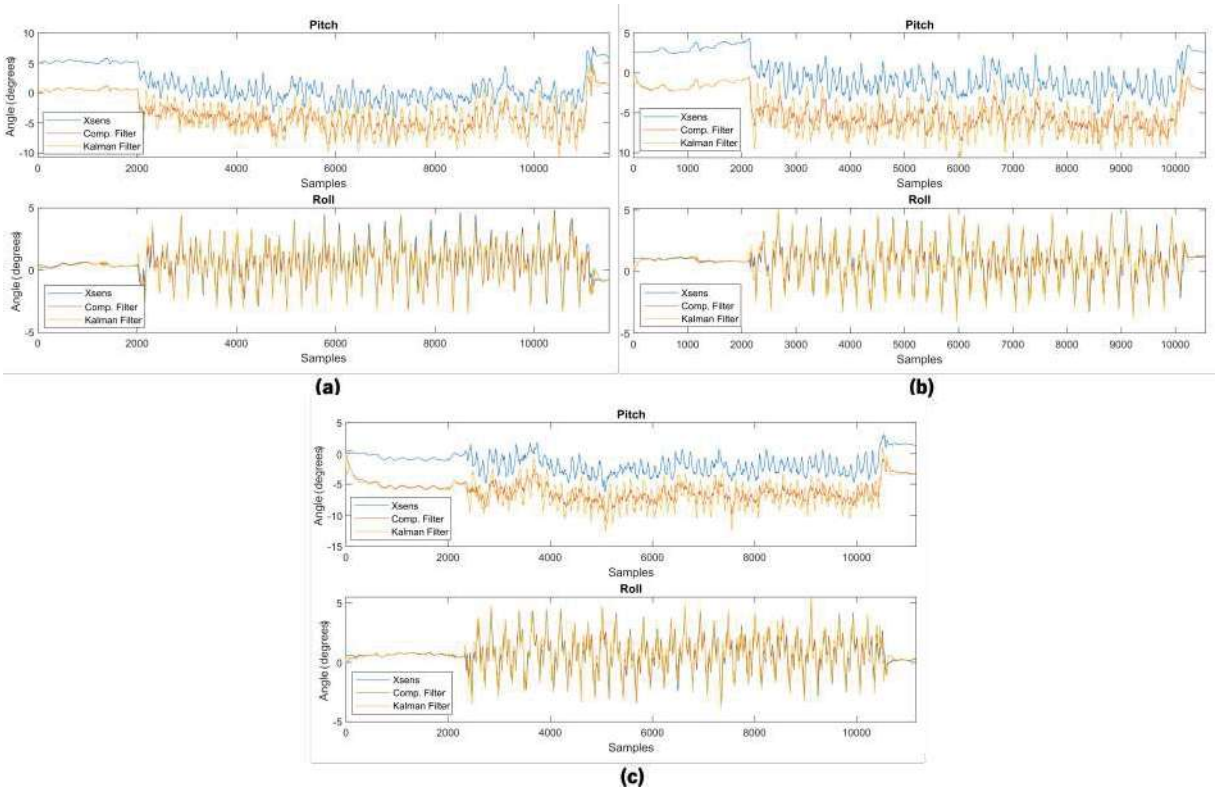


Figure 50: Representative illustration for the estimated pitch and roll of walk trials at 0.3 m/s: **(a)** trial 1, **(b)** trial 2, and **(c)** trial 3.

Table 31: RMSE for the different activities that healthy individuals performed and considering both the KF and CF and AP (pitch) and ML (roll) axes

Filter	Action	Roll (with DC)	Roll (without DC)	Pitch (with DC)	Pitch (without DC)
KF	Inclination	2.54 ± 3.61	2.33 ± 3.40	4.54 ± 0.64	0.95 ± 0.76
	Quiet standing and sit down	1.40 ± 1.84	1.31 ± 1.74	4.54 ± 0.65	0.71 ± 0.14
	Gait (0.3 m/s)	1.28 ± 0.41	1.22 ± 0.41	4.62 ± 0.88	1.69 ± 0.21
	Gait (0.5 m/s)	1.57 ± 0.49	1.52 ± 0.51	4.76 ± 0.92	2.08 ± 0.27
	Gait (0.7 m/s)	1.74 ± 0.36	1.56 ± 0.39	4.58 ± 1.07	2.19 ± 0.26
	Gait (1.0 m/s)	1.99 ± 0.28	1.75 ± 0.27	4.58 ± 1.20	2.21 ± 0.25
CF	Inclination	2.58 ± 3.54	2.37 ± 3.34	4.52 ± 0.63	1.01 ± 0.71
	Quiet standing and sit down	1.47 ± 1.80	1.37 ± 1.72	4.55 ± 0.73	0.64 ± 0.24
	Gait (0.3 m/s)	0.82 ± 0.33	0.72 ± 0.32	4.26 ± 1.08	0.80 ± 0.13
	Gait (0.5 m/s)	0.91 ± 0.37	0.82 ± 0.37	4.27 ± 1.08	0.98 ± 0.15
	Gait (0.7 m/s)	1.05 ± 0.46	0.78 ± 0.35	4.41 ± 2.02	1.08 ± 0.13
	Gait (1.0 m/s)	1.33 ± 1.33	0.87 ± 0.33	4.05 ± 1.34	1.24 ± 0.18

Indeed, analyzing at the error without the offset (DC component, see Table 31), it is generally between

0.6° and 2.4°. Furthermore, the KF algorithm shows a slightly higher error compared to CF, which can probably be explained by the tuning process of the filter, which could be further improved. However, considering that the biofeedback strategy only shows variations in movement, the error without offset is the most important, as this offset can be removed by an initial calibration period.

Figure 51 shows a heatmap of Spearman's correlation coefficient between the orientation estimated by both sensor fusion algorithms and the orientation measured by Xsens Awinda. This value corresponds to the average of the observations, taking into account the average coefficient for each participant. Indeed, there is a positive monotonic relationship between the estimated orientation and GT, although it varies in strength. In general, CF shows stronger monotonic correlation values, with values always above 0.6, which, according to the grading rate presented in study [158], corresponds to a strong to very strong positive correlation. For KF, lower correlation values were found, especially for dynamic walking activities, where there was generally a moderate-strong correlation. However, for a walking speed of 0.5 m/s, the results show a weak monotonic correlation. For static activities, a positive and strong to very strong correlation was found for KF, similar for CF, although higher for pitch estimate.

	Roll		Pitch	
W1	0.8466	0.6135	0.8636	0.4624
W2	0.7827	0.5660	0.7923	0.3785
W3	0.7544	0.5471	0.7609	0.4491
W4	0.7542	0.4505	0.7883	0.6020
INC	0.7766	0.7695	0.9287	0.9266
QS+SD	0.6290	0.6249	0.9352	0.9396
	CF	KF	CF	KF

Figure 51: Heatmap of the Spearman's correlation coefficient considering both sensor fusion algorithms, roll and pitch angles, and the different activities (Wx stands for each walking activity considering each gait speed, QS stands for quiet standing, and SD stands for sitting down and standing up activity).

Overall, the results obtained indicate that both sensor fusion algorithms are suitable for use in the biofeedback strategy, specially during static activities. Nevertheless, the CF showed slightly better results, but this could be related to the tuning process of the KF, which can be improved with a more thorough tuning process. The use of the CF may be advantageous in part due to its lower computational cost and ease of implementation and tuning. Nevertheless, the KF is generally considered to be a more accurate algorithm, although it is more computationally expensive [154].

Functionality and usability

A second validation protocol was carried out with healthy participants in order to validate the proposed BS in terms of functionality and technological usability. Although this validation protocol was conducted

with healthy individuals, an intervention protocol is currently in progress to validate the proposed system with end users, namely patients with CA.

To assess the functionality of the system, each participant performed a short 15-minute protocol over two days, during which they had to complete three balance training exercises with and without the biofeedback strategy. As these were healthy, young participants with good balance, a foam platform was used to further challenge the participants' balance. The aim was to check whether the strategy allowed the participants to stay within the defined boundary region and, if they left the region, whether the stimulus they received triggered a compensatory response. In addition, as this strategy limits the orientation of the trunk, which may influence the position of the CoM, this protocol aimed to determine whether there was any change in the variation of the CoM with and without biofeedback by analyzing its displacement, similar to study [159].

Figure 52 illustrates example cases of two participants performing the bipedal stance activity, where: (a) and (b) represents the participant with the highest percentage of biofeedback activation, 10.40±3.30%, and 80.66% for the extra trial with the stricter limits; and (c) and (d) represents the participant with the lowest percentage of biofeedback activation, with an average activation of 0.36±0.33%, and 57.78% for the extra trial with the stricter limits.

As can be observed, the proposed biofeedback strategy does in fact promote a compensatory response in the user, particularly visible in trial 1 of Figure 52a, *e.g.* in zones A, B, and C, where there is an oscillation in pitch and roll in response to the visual and auditory stimuli received. This oscillation actually consists of the user searching for the best posture to stay within the defined range. After some time of searching for the best posture, the user controls his/her postural oscillation within the predefined threshold limits, specially for pitch after zone A. It would be interesting to analyze the user's muscular activity in response to the stimuli received. It is possible that there would be greater muscle activation in an attempt to maintain a more upright posture. The foam platform also challenges the user's balance and muscle activity could also be seen in response to small imbalances. Despite this, the participant was able to maintain his/her orientation within the limits set.

The compensatory response is also visible in the extra trial of bipedal stance, where the limits were much stricter. In fact, the limits set are very small and close to 0°, which hinders the user's ability to stay within the limits, since small imbalances resulting from the use of the foam platform are enough to trigger the activation of the biofeedback strategy. Nevertheless, Figure 52b shows that the user's pitch varies close to the defined limits after zone D, and that the biofeedback activation is mainly caused by the roll angle, which is mostly outside the defined range. However, noted that the limits set for roll are

in fact extremely strict. In the context of rehabilitation, these limits will be adjusted in real time by the physiotherapist through continuous monitoring of the patient and analysis of the compensatory response. In fact, the intervention should be challenging but also motivating, so the limits set should always be adaptable and adjusted in real time. If the limits are extremely strict, this can also increase the patient's frustration and consequently reduce his/her motivation in the therapy.

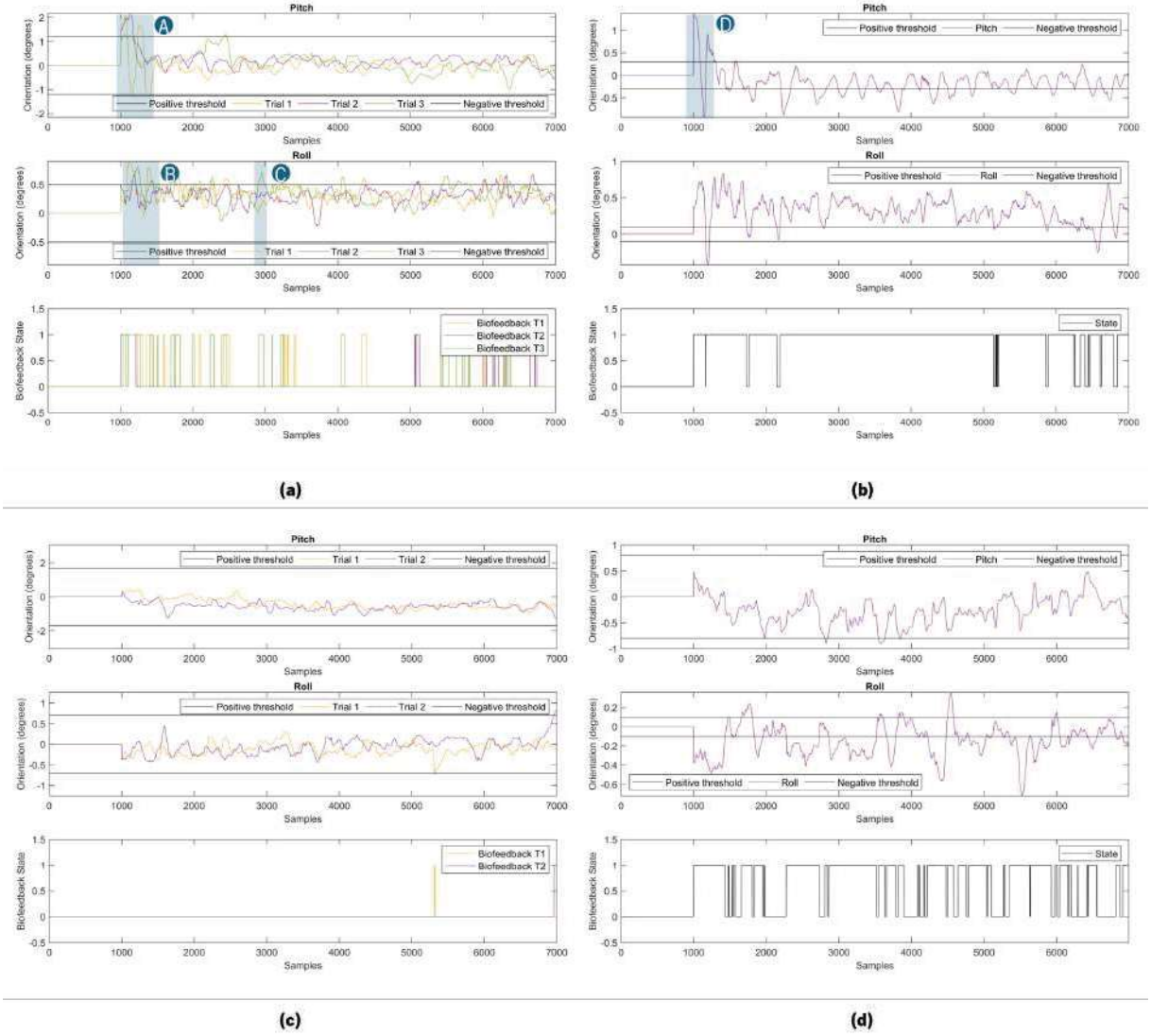


Figure 52: Example of users' compensatory response for bipedal stance, considering: **(a)** the participant with the highest activation (AP limit: ±1.2°, ML limit: ±0.5°), **(b)** extra bipedal stance (AP limit: ±0.3°, ML limit: ±0.1°), **(c)** bipedal stance for the participant with the lowest activation (AP limit: ±1.8°, ML limit: ±0.7°), and **(d)** extra bipedal stance (AP limit: ±0.9°, ML limit: ±0.5°).

Figure 53 gives an example of the results obtained for the tandem stance and unipedal stance activities, considering the participant with the highest percentage of biofeedback activation in each of the

activities (4.49±3.30% for tandem stance and 39.41% for the extra trial, and 1.75±1.73% for unipedal stance and 40.89% for the extra trial). Participants again responded in a compensatory manner, visible in Figure 53d, through zones A to G. However, this compensatory response was particularly visible in zones F and G of Figure 53d. In this period of time, the user had an imbalance, but quickly compensated and maintained his/her posture close to the established limit.

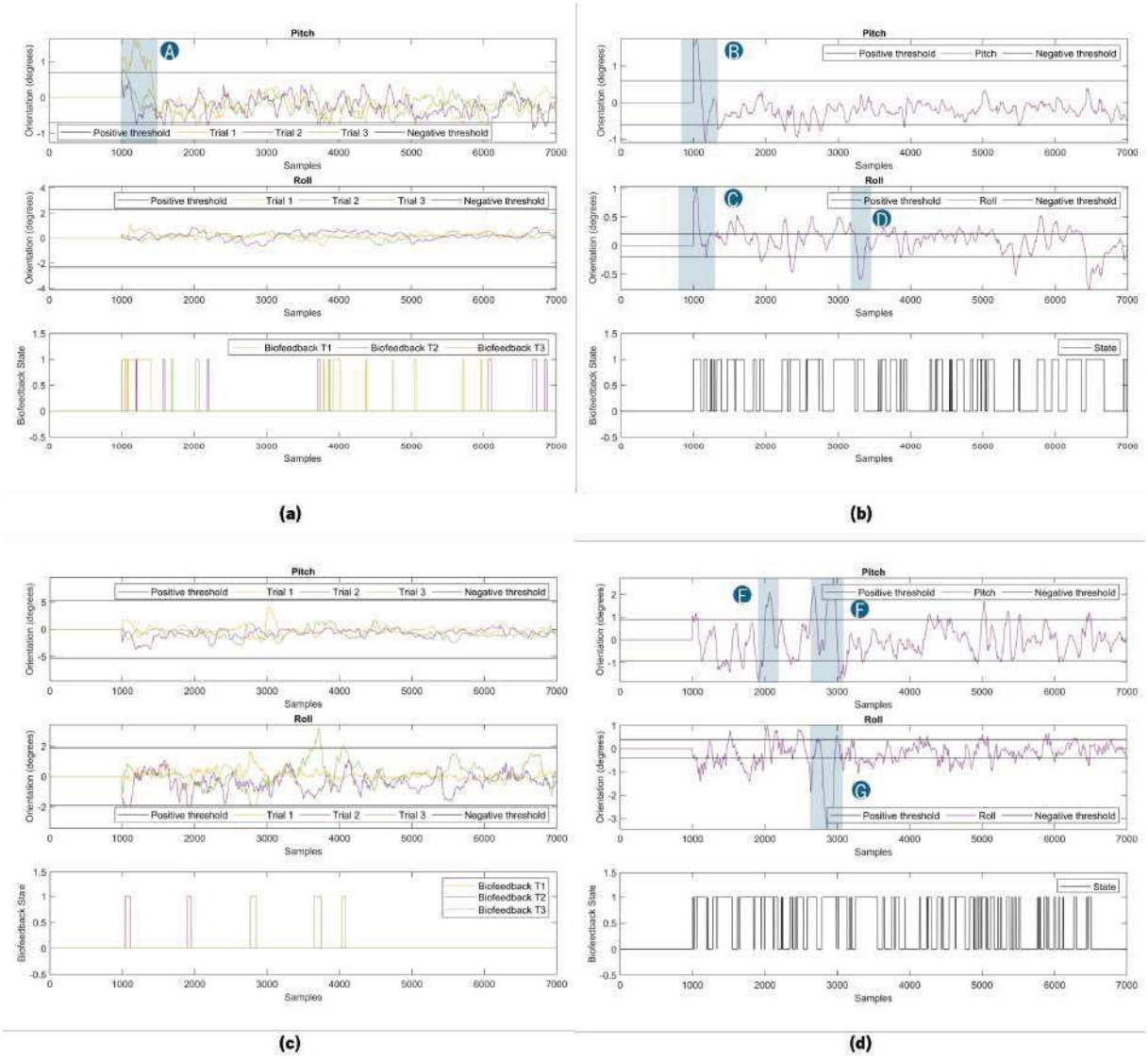


Figure 53: Example of users' compensatory response considering: **(a)** tandem stance for the participant with the highest activation (AP limit: ±0.7°, ML limit: ±2.3°), **(b)** extra tandem stance (AP limit: ±0.6°, ML limit: ±0.2°), **(c)** unipedal stance for the participant with the highest activation (AP limit: ±5.3°, ML limit: ±1.9°), and **(d)** extra unipedal stance (AP limit: ±0.9°, ML limit: ±0.4°).

According to these results, the proposed biofeedback strategy is capable of producing compensatory responses to maintain an ideal posture. Furthermore, during the validation protocol, it was found that the

compensatory responses were also reinforced by the audio stimulus, which prompted the user to find the correct posture. The audio stimulus was actually a negative reinforcement cue, as it reinforced the user in realising that they were wrong. The visual biofeedback, on the other hand, helped the user to return to the position that was considered safe and "correct".

To verify whether the proposed strategy could reduce the CoM displacement, the position of the CoM with and without biofeedback was assessed. Then the ROM of the user's CoM was calculated according to Equation 6.15, in both AP and ML axes, and the difference between trials with and without biofeedback was calculated. Table 32 shows the difference in CoM variation between trials with and without biofeedback. This was calculated for all participants across the three different activities. Table 33 shows the same analysis for the extra trials.

Table 32: Difference in ROM of the CoM position between trials with and without biofeedback, the corresponding mean, standard-deviation, and *p*-value, considering the different activities and participants

Type	Participant	ΔAP (cm)	ΔML (cm)	AP axis				ML axis			
				Mean	STD	Median	p-value	Mean	STD	Median	p-value
Bipedal stance	P01	-0.66	-0.41	-0.39	0.35	-0.55	**0.043 ***	-0.65	0.64	-0.41	**0.046 ***
	P02	-0.55	-1.05								
	P03	-0.08	-1.61								
	P04	-0.15	0.00								
	P05	-0.79	-1.20								
	P06	0.12	0.08								
	P07	-0.65	-0.39								
Tandem stance	P01	-1.42	-0.95	-0.78	0.42	-0.83	**0.003 ***	-1.09	0.47	-0.93	**0.018 ***
	P02	-0.67	-0.84								
	P03	-0.02	-0.84								
	P04	-0.87	-0.65								
	P05	-0.95	-2.00								
	P06	-0.68	-1.42								
	P07	-0.83	-0.93								
Unipedal Stance	P01	-1.05	-1.40	-0.63	0.95	-1.05	0.130	-1.31	1.72	-1.51	0.091
	P02	-1.34	-1.95								
	P03	-1.80	-1.51								
	P04	-1.05	-0.61								
	P05	-0.37	-3.52								
	P06	0.37	-2.17								
	P07	0.83	2.02								

Table 33: Difference in ROM of the CoM position between trials with and without biofeedback, the corresponding mean, standard-deviation, and *p*-value, considering the extra trials

Type	Participant	ΔAP (cm)	ΔML (cm)	AP axis				ML axis			
				Mean	STD	Median	p-value	Mean	STD	Median	p-value
Bipedal stance	P01	n/a	n/a	-0.20	0.51	-0.20	0.463	-0.87	0.81	-0.63	**0.046 ***
	P02	-0.11	-0.82								
	P03	0.12	-2.22								
	P04	0.47	-0.01								
	P05	-1.06	-1.40								
	P06	-0.29	-0.43								
	P07	-0.31	-0.36								
Tandem stance	P01	n/a	n/a	0.08	0.90	-0.09	0.753	-1.02	0.52	-0.85	**0.028 ***
	P02	-1.02	-1.56								
	P03	0.21	-0.55								
	P04	-0.15	-0.64								
	P05	-0.02	-1.71								
	P06	1.72	-1.05								
	P07	-0.25	-0.58								
Unipedal Stance	P01	2.05	1.55	-0.22	2.08	-0.16	0.735	-0.22	2.22	-1.11	1.000
	P02	-0.16	-2.14								
	P03	-2.44	-1.36								
	P04	-2.21	-1.11								
	P05	-2.12	-3.08								
	P06	0.89	2.31								
	P07	2.46	2.26								

By calculating the CoM variation between trials with and without biofeeback enables to directly verify an increase or decrease in the total ROM of the CoM if the difference is positive or negative, respectively. However, according to the proposed strategy, whose aim is to control the user's postural sway, it is indirectly intended to minimise the CoM displacement. According to the findings, it can be seen that most of the participants showed a decrease in ROM of the CoM position, as the values obtained were mostly negative. This difference is considered significant for the bipedal stance ($W=2.0$, p-value$=0.043$, $dz=1.03$ for AP, $W=1.0$, p-value$=0.046$, $dz=1.16$ for ML) and the tandem stance ($t(6)=4.906$, p-value$=0.003$, $dz=1.85$ for AP, $W=0$, p-value$=0.018$, $dz=1.47$ for ML) tasks, which reveals positive results in terms of the functionality of the proposed strategy. With regard to the unipedal stance exercise, there is a mean difference of -0.63 cm between the trials with and without biofeedback, indicating a decrease in the ROM of the CoM position, but this result is not considered statistically significant on either the AP or the ML axis (p-value>0.05). Nevertheless, it should be noted that the statistical tests

were only applied because the participants are healthy and the groups are not heterogeneous in terms of balance control, but their statistical power may be reduced because the validation protocol included only seven participants. Therefore, future perspectives should include a larger study with more participants. Overall, the results obtained indicate that the proposed biofeedback strategy tends to control and reduce the swaying of the CoM.

An analysis between the extra trials performed by the participants, the results of which can be seen in Table 33, shows a general decrease in CoM variation for most participants, but on average the variation was close to 0 cm for the AP axis, without statistical significance, and higher for the ML axis. For the ML axis, there was an average decrease in CoM variation, and this decrease was significant for bipedal stance ($t(6)=2.642$, p-value$=0.046$, $dz=1.08$) and tandem stance ($W=-2.201$, p-value$=0.028$, $dz=1.96$). Overall, the results suggest that the proposed BS is effective in reducing postural sway in healthy participants, which may therefore benefit patients with CA.

Regarding the usability of the system, Table 34 shows that most users scored the BS above 85 points on the SUS scale ($n=4$, 57.1%), with an average of 85.36 ± 12.62 points. The results suggest that: **i)** the BS is generally easy to use (Q2: 1.71 points, Q3: 4.71, Q8: 1.14 points); **ii)** all features of the BS were well integrated (Q5: 4.57 points); **iii)** the BS is easy to learn (Q7: 4.71 points, Q10: 1.43 points); and **iv)** users reveal confident while using the BS (Q9: 4.43 points). This classifies the proposed biofeedback strategy as acceptable (maximum on the acceptability scale), with a rating between "excellent" and "best imaginable" according to [47].

Table 34: SUS scores of the proposed biofeedback system

Question	Participants							Mean	Std
	P1	P2	P3	P4	P5	P6	P7		
Acho que gostaria de utilizar este produto com frequência.	4	4	5	4	4	4	3	**4.00**	**0.58**
Considerei o produto mais complexo do que o necessário.	2	1	1	1	3	2	2	**1.71**	**0.76**
Achei o produto fácil de utilizar.	5	5	5	5	4	4	5	**4.71**	**0.49**
Acho que necessitaria de ajuda de um técnico para conseguir utilizar este produto.	1	2	1	2	5	4	3	**2.57**	**1.51**
Considerei que as várias funcionalidades deste produto estavam bem integradas.	5	5	5	4	5	4	4	**4.57**	**0.53**
Achei que este produto tinha muitas inconsistências.	1	1	1	1	2	2	2	**1.43**	**0.53**
Suponho que a maioria das pessoas aprenderia a utilizar rapidamente este produto.	5	5	5	5	5	4	4	**4.71**	**0.49**
Considerei o produto muito complicado de utilizar.	1	1	1	1	1	2	1	**1.14**	**0.38**
Senti-me muito confiante a utilizar este produto.	5	4	5	5	4	4	4	**4.43**	**0.53**
Tive que aprender muito antes de conseguir lidar com este produto.	1	1	1	1	2	3	1	**1.43**	**0.79**
	95	**92.5**	**100**	**92.5**	**72.5**	**67.5**	**77.5**		

To complement the SUS scale, the participants were asked to provide a short comment on their experience with the strategy. Based on the comments received, the participants found the strategy intuitive,

encouraging, interactive, effective, but also challenging, as follows: **i)** *"I considered the strategy to be well implemented, as it encouraged me to keep my balance and was simple enough for me to realize where I was failing. One possible area for improvement would be to perhaps increase the size of the window with the circles and the ball."*; **ii)** *"I think the biofeedback strategy is quite intuitive. When the thresholds are smaller, it becomes more difficult to understand how to adjust the balance in certain movements, due to the high sensitivity when moving, however it has always remained intuitive during the exercises to correct the body position."*; **iii)** *"The biofeedback system helped me perceive my posture during the exercise and was also very useful in correcting it. The presence of both visual and auditory feedback made the tool more effective during the exercises."*; **iv)** *"It is easy to understand in which direction we have to move our bodies in order to return to the balance zone. When the limits were reduced, it became more difficult to stay within the green zone and when I went out into the yellow/red zone it was also more difficult to return. I think the strategy allowed me to have a good spatial awareness of my body and kept me motivated to stay in the green zone."*; **v)** *"It was a very interactive experience, being able to understand the positioning of my body in order to find balance. The first round of each strategy was the most complex, but by the time I reached the last round I was able to position my body in the most appropriate position to maintain balance, and it was also easier to stay within the limits as the rounds progressed. In the more restricted round, for all positions, the beginning proved to be more complex, however, balance was quickly restored within the limits, with the exception of the position of one foot in front of the other where balance during the more restricted round became more complex. In terms of sensitivity, both the position with the feet sideways and one foot in front of the other showed a lot of sensitivity. In the case of balancing on just one leg, I felt that the system was not as sensitive, but I do not think that it worsened performance, with the progression of confidence and balance being similar to the previous ones."*; **vi)** *"Effective and responsive strategy."*; and **vii)** *"The biofeedback experience was very positive, although challenging. It was easy to understand and the biofeedback made it easier to achieve balance most of the time. Small delays in the movement of the blue dot and perhaps the necessary attention to placement and ensuring the sensor does not move are the only notes I have regarding the biofeedback strategy."*.

6.3 Non-immersive Virtual Reality based Exergame

Recent research has focused on the use of SG, particularly video exergames, in cognitive and motor rehabilitation [43]. The need to ensure that therapy is **effective as well as motivating, interactive and encouraging** has been a challenge for researchers and novel ways of making these therapies more

engaging are being explored. The use of SG and VR is being used because of their effectiveness in motor learning and recovery [43]. In the case of hereditary ataxia, their use has shown improvements, although the gain from this type of therapy compared to conventional therapy is still not significant [99, 100, 103, 160]. Nevertheless, their continued development has been remarkable because they are highly interactive, encourage active user participation, are motivating, easy to use and also fun [161], which may reduce the dropout rate from therapy. Additionally, similarly to BS, SG **are not usually integrated into robotic walkers**. Its development would therefore provide the device with cutting-edge technology, maximizing its usability and making it an attractive device from a rehabilitative point of view.

6.3.1 Proposal

This thesis proposes a novel SG integrated into the WALKit SRW, specifically designed for balance rehabilitation in patients with ataxia. This game consists of an additional non-immersive VR component to the therapy already performed with the robotic device, in an attempt to improve the balance performance of ataxic patients. The game consists of an avatar that moves according to the user's orientation, estimated by the sensor fusion algorithms presented and validated in the previous section. The primary goal of the game is to exercise postural control, *i.e.* swaying in the AP and ML axes, as well as balance by shifting weight sideways, forwards and backwards.

As shown in Figure 54, the game features an avatar holding two buckets of water. The primary goal is for the user to hold the buckets of water by controlling their posture while walking with the robotic device. In this case, the user has to walk while holding the rear handles of the device (see Figure 4) when necessary. In addition, short games have been integrated into the main game to train the weight transfer process, which is affected in ataxic patients due to their constant loss of balance [5, 8, 85, 162]. These short games appear randomly and are different from each other, allowing the user to experience different stimuli in order to stay motivated during rehabilitation.

6.3.2 Methodology

Game Engine

When developing the game, the solution would have to be integrated into the device's software to ensure that it could be widely used during rehabilitation sessions with the device, but also to reduce the amount of unnecessary equipment. However, since the frontend of the new walker application is based on QML, it would be complex to idealize 3D scenarios and its performance would not be the best.



Figure 54: Screenshot of the novel SG proposed for WALKit SRW.

Therefore, it was decided to develop the game as an external application and then communicate with WALKit's own application. Unity (Unity Software Inc., Califronia, USA) was used to develop the game as it is a powerful cross-platform engine that allows the development of dynamic animations and realistic scenarios. It consists of both a visual editor and a Integrated Development Environment (IDE) that allows for rapid prototyping and game development [163].

Connection to WALKit Smart Walker

Since the game was developed using the Unity engine, it consisted of a third-party application that required bi-directional communication with the WALKit software in order to **i)** know if the user has started or stopped a new session, or **ii)** send relevant information from the game to the WALKit software, such as the user's performance. Therefore, a WebSocket protocol was established between the game and the WALKit's high-level software. To access sensor data, the ROSBridge package from ROS was used to forward topic values, enabling Unity to retrieve them via the ROS# library.

Avatar controlling

To control the avatar, a sensor fusion algorithm, namely the CF filter presented in the previous section, was first used to estimate the user's torso orientation, taking into account both pitch and roll. Then, this information was published as a message in a ROS topic, which was then accessible to the game application via the ROSBridge package. These values are then normalized by the maximum angle obtained with a calibration routine. This is done for each new user to record the maximum roll and pitch (considering left/right and forward/backward, respectively) the user can do without losing balance. A 2D *Blend Tree*

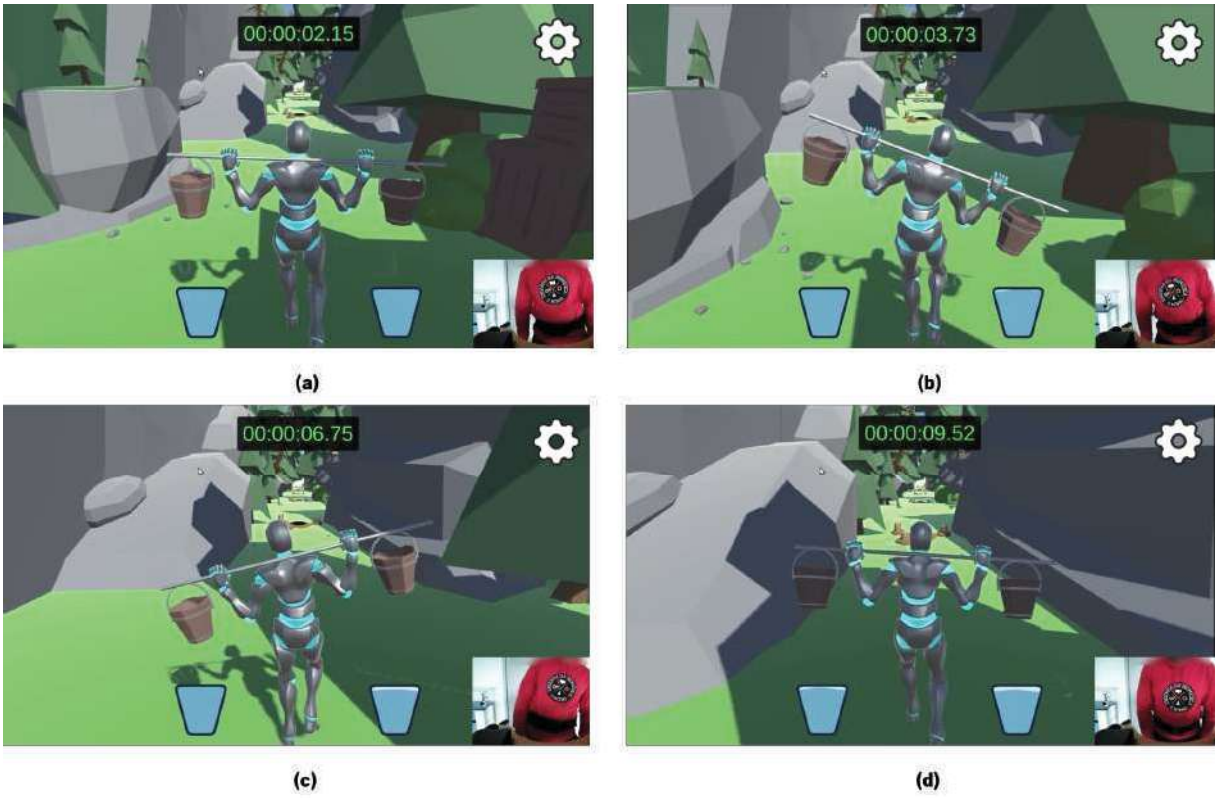


Figure 55: Example of controlling the tilt of the avatar through the user's motion.

feature of Unity's animation system was then used to interpolate between the animations. Similarly, the linear velocity information obtained from each motor's encoder was used to interpolate between the avatar's idle and walking animations. Figure 55 illustrates an example of the avatar's tilt control using the user's motion as seen in the image captured by the robotic walker's embedded camera.

Weight-transfer short games

Short games that challenge weight transfer have been developed and integrated as events throughout the main game. These short games always require the user to lean right, left, forward, or backward in order to **i)** put out a fire; **ii)** open a door to get through a level; **iii)** hit moles; or **iv)** steer a flying carpet to grab the golden rings. Figure 56 illustrates an example of these small events that appear randomly throughout the game, namely the activity of hitting moles. The main goal is to complete the task correctly. However, the game records the total time the user has needed to complete this short event, and provides feedback to the user. Besides the time, the game provides other statistics, such as the number of moles hit, serving as an incentive.

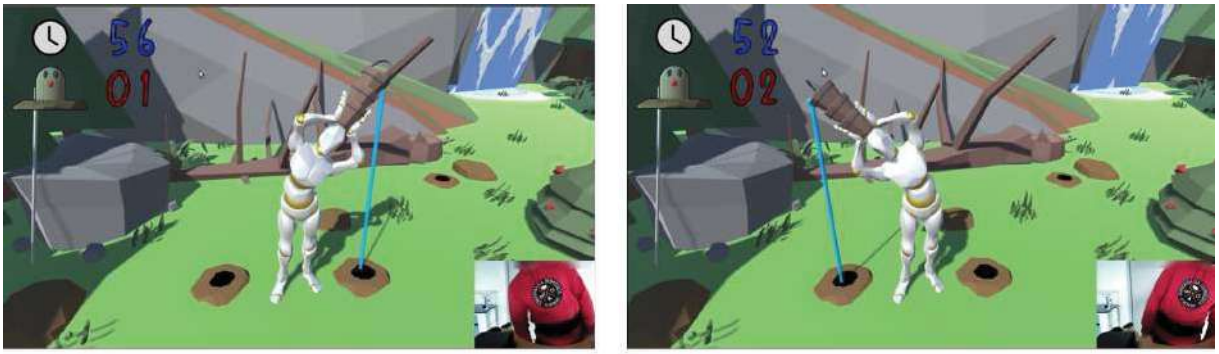


Figure 56: Example of hitting mole event.

Levels and user-adaptability

A key aspect of this thesis was to introduce the concept of adaptability of the device to the user, *i.e.* to ensure that the robotic walker is highly user-specific and targeted to real clinical needs. In this way, the exergame includes 4 levels of execution, which vary in difficulty and therefore can be used at different levels of rehabilitation. These 4 levels include **i)** postural control without weight transfer events, **ii)** postural control with AP weight transfer events, **iii)** postural control with ML weight transfer events, and **iv)** postural control with both AP and ML weight transfer events. The first level is specifically designed for postural control training. In this case, the user's main goal is to keep the buckets filled with water while receiving real-time visual biofeedback through the avatar's movements. This training can be done either in static mode, *i.e.* with the robotic walker stationary, or in dynamic mode, during gait training. Furthermore, this first level can also be used with load cells instead of the IMU on the user's torso, and in this case the main goal of the strategy is to improve posture by correctly distributing the load on the device's platform. Levels 2 and 3 include small events that challenge balance through weight transfer training. In this case, the physiotherapist can choose which of the movements to train, AP or ML. Finally, level 4 is a combination of levels 2 and 3, with weight transfer events on both axes. Figure 57 presents a short video demonstration of the novel non-immersive VR-based exergame of WALKit SRW.

Figure 57: Video demonstration of the novel exergame of WALKit SRW.

6.3.3 Validation Protocol

As an initial step, the game was validated with healthy participants. From a technical point of view, the algorithm used to control the avatar through the inertial sensor is the same one that was previously implemented for the biofeedback strategy, so it was already tested and validated. In this sense, the usability and intuitiveness of the game were evaluated. Regarding the capacity for motor rehabilitation, the clinical study is currently in progress at 2CA-Braga, therefore some preliminary results will be discussed in Chapter 7. Data acquisition was conducted under the ethical procedures of the Life and Health Sciences Ethics Committee (CEICVS 147/2021), following the Declaration of Helsinki and the Oviedo Convention. Data were collected at the School of Engineering of University of Minho.

Participants

Ten healthy participants (4F, 6M, age of 26.9 $\pm$ 2.73 years old), without evidence of motor disorders, accepted to participate in the usability validation protocol of the proposed non-immersive VR exergame. Each participant experienced the SG and were asked regarding its functionality, intuitiveness, and sense of challenge.

Experimental proceedings

The protocol consisted of a 5-minute walking test with WALKit SRW at a walking speed of 0.5 m/s. The device was remotely controlled by the investigator so that the user did not take their attention away from their gait and the SG itself. For this purpose, the participants grasped the rear handles of the device. First, a calibration routine was performed to adapt the exergame to each participant, namely the maximum angle they could perform considering both the AP and ML axes. This was done so that the avatar could respond correctly to the user's movements. This calibration routine was built into the game itself, and is responsible for subscribing to the ROS messages published by the WALKit backend via the ROSBridge package. After this calibration routine, the game was ready to start. Before starting the test session, the participant was given a familiarization test.

Validation metrics

After the 5-minute trial, each participant was asked to answer the SUS questionnaire, as presented in Appendix A.1, and a some specific questions, namely:

- Was the game fun? If not, where?

- Did you consider the game challenging?
- Did walking and playing simultaneously make the game more difficult?
- Do you think the movement of the walker translates well into the avatar's movement?
- Did it feel natural to control the avatar with the inertial sensor?

6.3.4 Results and Discussion

Table 35 shows the main results obtained regarding the usability of the system. The results from healthy users indicate that the exergame is well-received across several key dimensions: **i)** ease of use (Q2: 1.10 points, Q3: 4.40 points, Q8: 1.10 points); **ii)** seamless integration of features (Q5: 4.50 points); **iii)** ease of learning (Q7: 4.60 points, Q10: 1.70 points); and **iv)** user confidence while playing (Q9: 4.80 points). Overall, the majority of participants ($n = 8, 80\%$) rated the exergame with at least 85 points, and more than 50% of the participants scored with at least 90 points, which indicates that the game is intuitive. Scores ranged from 75 to 100 points, with an average of 89.50 ± 7.43 points, which rates the proposed non-immersive VR-based SG from excellent to best imaginable, according to the grading scale presented in [47].

Table 35: SUS scores for the proposed postural control and weight transfer game

Question	Participants										Mean	Std
	P1	P2	P3	P4	P5	P6	P7	P8	P9	P10		
Acho que gostaria de utilizar este produto com frequência.	5	5	5	4	3	5	5	5	4	5	**4.60**	**0.70**
Considerei o produto mais complexo do que o necessário.	1	1	1	2	1	1	1	1	1	1	**1.10**	**0.32**
Achei o produto fácil de utilizar.	5	5	5	5	5	5	5	4	1	4	**4.40**	**1.26**
Acho que necessitaria de ajuda de um técnico para conseguir utilizar este produto.	2	1	1	2	2	4	1	4	1	2	**2.00**	**1.15**
Considerei que as várias funcionalidades deste produto estavam bem integradas.	4	5	3	5	5	5	5	4	4	5	**4.50**	**0.71**
Achei que este produto tinha muitas inconsistências.	2	1	1	1	1	1	1	2	1	1	**1.20**	**0.42**
Suponho que a maioria das pessoas aprenderia a utilizar rapidamente este produto.	5	5	4	5	4	5	5	4	5	4	**4.60**	**0.52**
Considerei o produto muito complicado de utilizar.	1	1	1	2	1	1	1	1	1	1	**1.10**	**0.32**
Senti-me muito confiante a utilizar este produto.	5	5	4	5	5	5	5	5	4	5	**4.80**	**0.42**
Tive que aprender muito antes de conseguir lidar com este produto.	2	1	1	2	1	3	1	1	4	1	**1.70**	**1.06**
	90	**100**	**90**	**87.5**	**90**	**87.5**	**100**	**82.5**	**75**	**92.5**		

Regarding the participants' answers to the questions, all of them found the exergame fun and appealing. In addition, the vast majority found it challenging (n =9, 90%), even though they were healthy individuals. One participant, however, noted a lack of challenge in the sense that there was no time limit to complete the tasks. Indeed, the main goal is not to perform the balance exercises in the shortest possible time, but to do them consciously, with controlled movements to optimize postural stability. If the

user manages to reduce the time needed to complete the task while maintaining postural control, this is considered an improvement.

Participants also felt that, overall, the multitask of walking and balance training using the exergame was not a difficult task. However, one participant felt that it required more cognitive effort. The exergame offers 4 difficulty levels and can be played in either static or dynamic modes, allowing physiotherapists to tailor the experience to each patient's motor abilities. In dynamic mode, the exergame acts more as a visual biofeedback strategy for postural stability, encouraging users to analyze and adjust their posture to keep the virtual buckets filled with water while walking. As the levels increase, so does the difficulty, making it more challenging for the user, but this challenge is essential for the patient's rehabilitation. When small weight transfer games are introduced, they are performed in static mode, requiring the user to stop walking and complete the challenge. Finally, this challenge can be completed in either bipedal or tandem stance, depending on the user's level of motor disability.

Finally, regarding the avatar's control, either through the IMU or the movement of the walker, all healthy users reported that it was a natural and intuitive HRI. Therefore, it can be concluded that the non-immersive VR-based exergame for postural stability and balance training is intuitive, challenging, interactive, and fun.

6.4 General conclusions

Overall, this chapter has presented **two HRI strategies designed for the rehabilitation of postural control and balance in ataxic patients using robotic walkers**. These novel strategies, consisting of a postural sway BS and a non-immersive VR-based exergame for postural control and balance training, have been embedded in WALKit SRW, transforming this device into a multifunctional robot to complement conventional physiotherapy.

For the first HRI strategy, it was necessary to implement a sensor fusion algorithm to estimate the user's pose based on the orientation of the torso. For this, sensor fusion algorithms were implemented and both achieved reasonable results for use in the audiovisual biofeedback strategy, although CF performed better. Furthermore, there was a moderate to very strong monotonic correlation between the estimated orientation by both algorithms and the considered GT obtained with the Xsens Awinda motion capture system. The technical validation with healthy participants showed that the **audiovisual biofeedback strategy is interactive, intuitive and challenging**. The strategy **induced compensatory responses in the participant's posture** in order to stay within the range considered safe according to the set limits. Furthermore, it was found that with the biofeedback strategy, the user showed a **significant**

reduction in CoM total ROM, partially achieving KPI 7, particularly in the bipedal stance and tandem stance exercises. Therefore, these results are promising to validate the novel BS with ataxic patients.

The second HRI strategy was to develop a SG based on non-immersive VR. The exergame uses the torso orientation estimation algorithm to control an avatar carrying two buckets of water to train the user's postural stability. Additionally, the exergame includes small challenges/events that aim to train the user's balance through weight transfer activities. The validation with healthy participants showed a **very high usability**, partially achieving KPI 8, so the next step is to validate the game with ataxic patients to assess its effectiveness in motor rehabilitation.

Chapter VII

Robot-Assisted Gait Training in Ataxia

Chapter 7

Introducing WALKit Smart Walker in Ataxia Rehabilitation

7.1 Introduction

This chapter presents the main results of a **intervention study to evaluate the effectiveness of WALKit SRW in gait and balance rehabilitation of patients with CA**. The study is part of the clinical validation project of the robotic walker, entitled *Smart Walker gait training: a contribution to the assessment and rehabilitation of patients with balance disorders*, initiated in 2016 and approved by the Ethics Committee of the Braga Hospital under reference CESHB-135/2016, according to the Declaration of Helsinki and the Oviedo Convention. The project has undergone successive addenda, extending the study until 2025 (CEHB 48/2021), and is currently in its final form under addendum CEHB 216/2023. First, the participants are described, followed by the experimental protocol and the key indicators evaluated. The methods used to process and analyze the data collected are then presented. Finally, the main results obtained are presented and discussed.

7.2 Ataxia treatment: current status

CA can be considered as a pathology, as in the inherited CA, or as a symptom resulting from another disorder [8, 85]. In both cases, however, it is very disabling, causing gait impairment and loss of balance. Given that pharmacological options are limited [10, 85, 164], **rehabilitation becomes the mainstay of treatment**, aiming to improve the symptoms or slow their worsening if CA is hereditary and progressive. Evidence-based recommendations suggests that ataxic patients should undergo an intensive rehabilitation program to alleviate their symptoms [10, 85]. This rehabilitation program is multidisciplinary and usually includes motor and respiratory physiotherapy, occupational therapy and speech therapy [85].

Regarding physical therapy, the literature suggests that it should be **adaptive and explore the patient's potential to be more effective**. Coordination and balance training exercises should be considered as suggested by [165] and reported in study [85]. In addition, Marquer *et al.* [16] presented a literature review in which they concluded that intensive rehabilitation programs with balance and coordination exercises are necessary and that more technological interventions, namely the use of VR or biofeedback, appear to add value, **but further studies should be conducted to verify their efficacy**. Milne *et al.* [17] also presented a literature review in which the included studies presented rehabilitation programs that included coordination and balance exercises, cycling, balance training with biofeedback, muscle training, and treadmill training. The authors found that rehabilitation improved mobility and balance. Regarding postural training with biofeedback reported in study [17], the authors reported a significant improvement in stability limits, BBS, and Sensory Organization Test score after a 2-week protocol giving biofeedback of Centre-of-Gravity (CoG) [166].

New technological interventions are also being studied, namely the use of exergames involving coordination training, weight transfer and balance training [85]. Moreover, the literature has reported an added value for patients with ataxia [87]. In fact, Synofzik *et al.* [87] reported that an exergame-based training strategy has benefits, particularly when used in the long term with patients with chronic disease. They also reported that even patients with severe ataxia may benefit from these more technical interventions. Nevertheless, **further studies should be conducted to strengthen these findings** [16].

The use of RAGT has also recently been employed for CA rehabilitation, mainly using exoskeletons [20–24]. The first results are encouraging, justifying its further development and applicability in healthcare services, namely rehabilitation centers and hospitals. Robotic walkers show great potential to provide effective rehabilitation treatments for the ataxic population [48], particularly in the most severe cases where patients are unable to walk independently or require the full support of a physiotherapist. In these specific cases, patients benefit from the full BWS of the device, relieving the therapist of the burden of simultaneously assisting, monitoring and correcting.

7.3 Intervention Study

This study had two main objectives: **i)** the first was to evaluate the motor effect of using WALKit SRW without an additional HRI strategy and compare the results with treadmill-assisted gait training; **ii)** the second goal was to evaluate the effects of WALKit SRW with an additional BS or SG on balance and postural control. The hypothesis associated with each goal were as follows:

Hypothesis A: There are no differences in gait training between the treadmill and the WALKit Smart Walker.

Hypothesis B: The combined effect of WALKit SRW and a HRI does not improve balance and postural control.

7.3.1 Participants

Seven participants (3 male, 4 female) agreed to participate in the clinical validation of WALKit SRW. At the start of the study, the participants had a mean age of 59.3 $\pm$ 14.1 years, with ages ranging from 37 to 80 years, an average height of 161.9$\pm$7.3 cm, and a mean body mass of 66.2$\pm$9.1 kg (average Body Mass Index of 25.3$\pm$3.7 kg/m^2). The participants had ataxia of different etiologies, whose detailed description is given below. It is noteworthy that participants were not required to suspend their usual treatments, in accordance with ethical considerations.

The study was presented to all participants by the medical team. Patients were identified based on the inclusion criteria, namely **i)** having been diagnosed with CA for more than 3 months; **ii)** having gait ataxia; **iii)** having muscle strength of at least 3 according to the Medical Research Council scale in the hip flexor, knee extensor and ankle dorsiflexor muscles. Patients were excluded if **i)** they were unable to understand or cooperate in the study; **ii)** they had other orthopedic or neurological pathologies that affected their gait; **iii)** they had cardiovascular or respiratory pathologies that contraindicated physical exercise; and **iv)** they were unable to maintain the orthostatic position or gait.

Participant 1

Male patient, 59 years old, diagnosed with acquired ataxia due to ischemic stroke in the cerebellum (1 year after stroke). After suffering the ischaemic stroke, the participant underwent daily rehabilitation therapy first in the Physical Medicine and Rehabilitation Department of Braga's Hospital and later was transferred to The Northern Rehabilitation Centre. After being medically discharged, he agreed to participate in this research study and did not receive any additional physiotherapy during the participation period. During the study, the patient used a two-wheeled walker on the daily basis.

Participant 2

Female patient, 66 years old, initially diagnosed with Idiopathic Late Onset Cerebellar Ataxia (ILOCA) with signs of Parkinson's disease. With the progression of symptoms, the diagnosis was revised to Multiple

System Atrophy (MSA) (cerebellar type). MSA is a rare condition that causes loss of coordination and balance, and may also causes changes in speech and loss of control of other body functions [167]. The participant did not receive any additional therapy. She uses a wheelchair for mobility on the daily living, but she is able to walk with the help of a standard walker. At home, she walks by holding onto furniture.

Participant 3

Female patient, 37 years old, diagnosed with acquired cerebellar ataxia due to a surgically removed cerebellar tumor (Pilocytic Astrocytoma (PCA)). This is the most common pediatric brain tumor that causes peripheral ataxia, dysmetria, tremor, nystagmus (uncontrolled eye movements), and dysarthria [168]. The patient's gait is severely impaired, with marked loss of balance when BoS is restricted and constant tremor. She uses a wheelchair for mobility on the daily living, but she is able to walk with the assistance of crutches or strong support of a third person.

Participant 4

Male patient, 80 years old, diagnosed with cerebellar atrophy. This consists of a degeneration process of neurons in the cerebellum [169], responsible for slow and unsteady movements of arms and legs, slowed and slurred speech and nystagmus. The patient exhibited loss of balance with impaired gait and required an assistive device, namely a standard walker, for mobility. The patient did not receive any additional conventional therapy during the study.

Participant 5

Female patient, 55 years old, diagnosed with autosomal recessive SCA type 8. This is a slowly progressive cerebellar ataxia that causes gait and limb ataxia, dysarthria characterized by slowness of speech, among other clinical findings, typically in adulthood [170]. The patient presented nystagmus, dysmetria, dysarthria, gait ataxia and recurrent falls. The participant is able to ambulate without the use of a walking aid.

Participant 6

Female patient, 49 years old, diagnosed with CA caused by mitochondrial cytopathy [171]. CA is a possible consequence of these disorders. In this case, the ataxia is often progressive. The patient presented dysarthria, dysphagia, dysmetria, and ataxia. She requires an assistive walking aid for locomotion, namely a four-wheeled walker. She presents impaired gait and a marked loss of balance, with a predom-

inantly AP sway. In addition, the patient tends to position her CoM close to the posterior limit of the BoS. The patient maintained her usual physiotherapy throughout the study.

Participant 7

Male patient, 69 years old, diagnosed with acquired ataxia caused by Traumatic Brain Injury (TBI) and Spinal Cord Injury (SCI) due to a motor vehicle accident on March 2022. He was then admitted to the Physical Medicine and Rehabilitation Department at Braga's Hospital and transferred to the Northern Rehabilitation Centre. After this period, he was discharged home. The patient presents with marked loss of balance while walking and requires a wheelchair on the daily living. He is able to walk with one-sided assistance and has recently started using a walking stick. He regularly attends conventional physiotherapy and continued to do so during the trial.

Table 36 provides a general overview of all volunteers who participated in this study.

Table 36: General overview of all participants of this intervention study

Characteristic	Participants							Mean (±std)
	P1	P2	P3	P4	P5	P6	P7	
Gender	Male	Female	Female	Male	Female	Female	Male	
Age	59	66	37	80	55	49	69	59.29±14.08
Body height (cm)	169	158	160	164	160	150	172	161.86±7.31
Body mass (kg)	69	50	72	68	79	61	64.4	66.20±9.14
BMI (kg/m2)	24.2	20	28.1	25.3	30.9	27.1	21.8	25.34±3.74
Diagnose	Ischemic stroke	MSA-C	PA	Cerebellar Atrophy	SCA 8	CA by mitocondrial cytopathy	TBI and SCI	-

7.3.2 Clinical Protocol

The intervention study involved seven participants enrolled in a randomized crossover trial. The study was designed in this way because CA is a rare condition, being notoriously difficult to recruit patients for the study. The crossover design reduces this difficulty as each participant will be his/her own control. This allows a controlled trial to be conducted with a smaller number of participants, and also allows for the assessment of the individual participant's response to the application of a particular treatment [172].

Figure 58 illustrates the design of the experimental protocol. This was divided into two main phases, Phase 1 and Phase 2. **Phase 1** consisted of a block of sessions to compare rehabilitation gains with WALKit SRW *vs* treadmill. At this stage, and due to a notable scarcity of participants, the first participant was randomly assigned to start therapy with either the walker or the treadmill. Subsequently, each new participant would undergo the opposite intervention. **Phase 2** consisted of several blocks of sessions in

which each participant was assigned a random sequence of HRI strategies. The study was conducted at the Clinical Academic Center of Braga, 2CA-Braga.

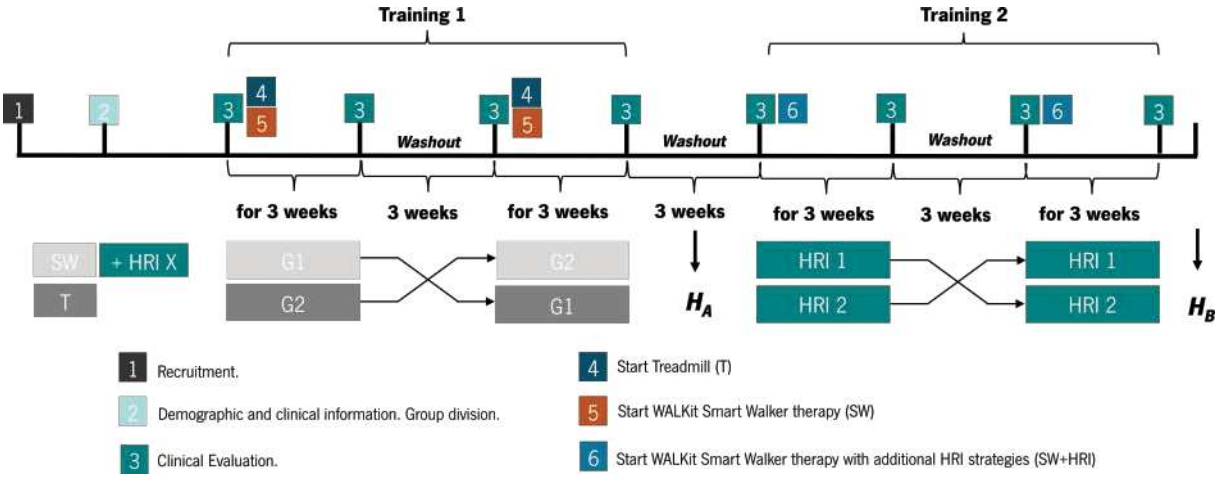


Figure 58: Experimental protocol design of the intervention study.

In light of these considerations, the protocol was implemented as follows: **i)** first, a personal visit was scheduled to present the study to the participant, including the robotic walker and, if he/she agreed to participate voluntarily; **ii)** upon acceptance, an evaluation session (pre-training) was scheduled to assess all the rehabilitation outcomes explained in the following subsection; **iii)** then the intervention phase began, consisting of several blocks of 15 daily sessions, each lasting a maximum of 30 minutes; and **iv)** after each block of sessions, the patients underwent another evaluation session (post-training). An equal period of washout (at least) was introduced between each block of 15 sessions in order to reduce the carry-over effect, which is a concern in crossover studies [172]. Although the device was introduced alongside the study, the first day of the intervention was more focused on familiarizing the participant with the device.

Table 37 shows the treatment program assigned to each participant, considering Phase 1. For gait training with both WALKit and treadmill, gait speed was user-adapted and adjusted if necessary by the therapist in charge.

Table 37: Intervention programme of training phase 1

Intervention program (phase 1)		
P1	Smart Walker	Treadmill
P2	Treadmill	Smart Walker
P3	Smart Walker	Treadmill
P4	Treadmill	Smart Walker
P5	Smart Walker	Treadmill
P6	Treadmill	Smart Walker
P7	Smart Walker	Treadmill

For Phase 2 of the study, each participant was assigned a random sequence of HRI strategies in order to study the effect of the different strategies presented in Chapter 6 (Table 38). As a result, a biofeedback strategy to control postural sway, an exergame based on non-immersive VR, and a cognitive game to evaluate the effect of multitasking during therapy were included. In this thesis, however, only the HRI strategies described in the previous chapter were evaluated. When assigning the random sequences, care was taken to generate the sequences in such a way as to minimize the effect of starting with one of the strategies.

Table 38: Intervention programme of training phase 2

Intervention program (phase 2)		
P3	Exergame	Biofeedback
P5	Biofeedback	Exergame
P6	Biofeedback	Exergame
P7	Exergame	Biofeedback

Regarding the clinical protocol of Phase 2, and particularly the protocol for validating the biofeedback strategy, the 30 minutes of training were divided into two parts. The first part, which lasted 15 minutes, involved static training with the biofeedback enabled. This training included 5 minutes of bipedal stance training, 5 minutes of tandem stance training and 5 minutes of unipedal stance training. Whenever necessary, users used the rear handles of the device for support. The second part involved 15 minutes of gait training with the robotic walker. Both the AP and ML limits of the biofeedback strategy and the device's velocity were user dependent and adapted, if necessary, by the physiotherapist. As for the exergame, the

protocol consisted of 30 minutes of gait training combined with the game. The device's linear velocity was adapted by the physiotherapist for each participant. Figure 59 shows examples of participants taking part in interventions using WALKit SRW for both Phase 1 and 2.



Figure 59: Example of participants with CA during the interventions sessions.

7.3.3 Participant Instrumentation

Before and after each block of sessions, participants were evaluated to further assess their gain from the intervention. For this purpose, the participants were instrumented with an inertial motion capture system, the Xsens Awinda (Movella, USA, validated in [152]), in a full-body configuration with seventeen IMU placed on the head, both shoulders, sternum, upper arms, forearms, wrist, pelvis, thigh, shin, and feet. Each of these sensors was positioned according to the manufacturer's guidelines [153], as shown in Figure 60, and were placed by the same researcher. Data collection was performed at 60 Hz.



Figure 60: Inertial sensors placement following Xsens guidelines. Note that each sensor was placed in the inner part of the strap to better secure the sensors.

7.3.4 Rehabilitation outcomes

Participants were evaluated on day 0 (**pre-training**) and day 16 (**post-training**) for each intervention they received. At these evaluations, both clinical scales and gait-related spatiotemporal parameters were assessed.

Phase 1 specific outcomes

Regarding Phase 1 of the training, and considering specific clinical scales, the SARA score (see Appendix A.2) was primarily evaluated [173]. This clinical test was used because it is a short clinical scale designed specifically for ataxia and allows the participant to be evaluated taking into account gait, stance, sitting, speech, finger chase, nose-finger test, rapid alternating hand movements, and the heel-shin exercise [174]. Although all exercises were evaluated, this study focused more on evaluating the sub-scores of gait, stance, and sitting that are trained during gait training with the robotic walker and treadmill. SARA scale presents a maximum score of 40 points and indicates more severe ataxia. Regarding the specific sub-scores, gait sub-score presents a maximum of 8 points (more severe), stance sub-score presents a maximum of 6 points (more severe), and the sitting sub-score presents a maximum of 4 points (more severe). SARA scale was applied by blind residents of the research team, belonging to the Physical Medicine and Rehabilitation Service of the Hospital of Braga.

Participants were also evaluated considering both the 10-MWT test and the TUG test, as recommended in [175]. For these two tests, participants used their assistive walking aid as needed and completed three valid trials at their comfortable walking speed. Regarding the 10-MWT, this test was employed to measure gait speed and calculate gait-related spatiotemporal parameters, which were divided into temporal and spatial parameters as shown in Table 39. For this, specific marks were placed on the floor, marking the 0, 2, 8, and 10 meters. The participant was instructed to walk at a comfortable pace while the researcher recorded the time the participant took between the 2 and 8 meter markers. For the TUG test, participants were instructed to sit in a chair, stand up, walk three meters forward, turn 180°, and return to the chair. The test ended when the participant sat down. At the same time, the investigator measured the time it took the patient to get up and sit down. This is a reliable scale for assessing mobility and measuring fall risk [176].

Gait-related spatiotemporal parameters were calculated using data acquired with Xsens MTW Awinda and data from the 10-MWT. Both spatial and temporal parameters were calculated, as presented in Table 39, that also presents brief definition of how they were obtained.

Table 39: Gait-related spatiotemporal outcomes that were evaluated in this study

Type of parameter	Name	Unit [SI]	Definition
Temporal	Stride time	*s*	Time between consecutive initial contacts of the same foot
	Step time	*s*	Time between the initial contact of the current foot and the immediately preceding initial contact of the opposite foot
	Stance time	*s*	Time between the initial contact and final contact of the same foot
	Swing time	*s*	Time between the final contact and the immediately afterwards initial contact of the same foot
Spatial	Stride excursion	*m*	Distance traveled during a complete gait cycle (between consecutive initial contacts of the same foot)
	Step excursion	*m*	Total distance traveled between the foot contact of one foot to initial contact of the contralateral foot

Phase 2 specific outcomes

For the **Phase 2** of the training, in which the participants received gait training with WALKit SRW with an additional HRI strategy, other outcomes were considered. Since these patients suffer from CA, either acquired or hereditary, and therefore present balance issues, the use of the BBS scale was later considered. The BBS is a widely used clinical scale (see Appendix A.3) to assess functional balance [177], taking into account both static and dynamic balance [175, 178]. It is a 14-item list with each task ranging from 0 to 4 points, the latter indicating the highest level of function. Thus, it presents a maximum score of 56 points, indicating functional balance. Although extremely useful, the BBS was not used immediately in Phase 1 because it is more time consuming and can cause some fatigue in the participant. Instead, participants' balance was assessed using the specific sub-score of SARA, which gives an idea of how it is affected and whether or not there has been progress. As Phase 2 of training included balance-specific exercises, the BBS was introduced.

Besides the overall BBS score, specific exercises of BBS scale were evaluated considering the two HRI strategies presented in Chapter 6. Regarding the BS for postural sway control, the following specific exercises from the BBS were evaluated: **i)** exercise 2, in which patients stand in their natural position with eyes open for 2 minutes, **ii)** exercise 7, in which patients stand with feet together for 1 minute with eyes open, and **iii)** exercise 13, in which patients stand in a tandem stance position. These last two exercises were only evaluated for P5, who was able to perform the exercise without help from the therapist to maintain balance. As for the non-immersive VR exergame, the following specific exercises of BBS involving weight transfer were evaluated: **i)** exercise 8, in which patients bend and reach forward with an outstretched arm, **ii)** exercise 9, in which patients bend to pick up an object from the floor, and **iii)** exercise 10, in which patients turn to look behind them.

Specific outcomes obtained with Xsens Awinda were also considered for this specific phase, con-

sidering both day 0 and day 16. In order to validate the proposed biofeedback strategy, the CoM total displacement (ROM) [144] was calculated on both AP and ML axes, considering the above mentioned exercises 2, 7 and 13 of the BBS. As for the non-immersive VR-based exergame, the forward ROM of the right arm, in cm, was obtained until a loss of balance was detected. This ROM was calculated considering the maximum displacement of the arm and the initial position (*i.e.*, arms at a 90° angle with the torso). Additionally, the maximum inclination of the torso was calculated and subtracted from the initial position to obtain the total pitch movement. Regarding exercise 9 of BBS, the time taken to grasp the object was calculated in seconds. Considering exercise 10 of BBS, the lateral rotation of the pelvis (yaw), for both the left and right side was calculated. Lastly, all participants were evaluated considering the TUG test.

7.3.5 Usability and functionality

The robotic walker and the HRI strategies were evaluated for usability and functionality. After each block of 15 daily sessions, participants were asked to evaluate their experience during the intervention study by answering the SUS questionnaire, translated and validated into Portuguese language [119].

7.3.6 Data Processing and Analysis

Regarding the clinical scale questionnaires, namely SARA, the variation between day 0 and day 16 was evaluated. For the 10-MWT test, the walking speed, in m/s, was calculated considering the central 6 meters of the test and the time measured within, as presented by [175]. For both 10-MWT and TUG times and gait speed, the mean and standard-deviation of the three trials, in seconds, was calculated. Then, to minimize the effect of heterogeneity in the population, these data were normalized to day 0, which was considered the baseline and equal to 1.0. Therefore, a value on day 16 of 1.0 indicates that there was no change, below 1.0 indicates that there was a decrease on day 16 compared to day 0, and above 1.0 indicates that there was an increase on day 16 compared to day 0.

For the evaluation of the gait-related spatiotemporal parameters, the data collected with the Xsens Awinda were used. Since Xsens Awinda is occasionally corrupted by electromagnetic interference, this may affect the absolute position of the segments relative to the world axis, sometimes causing cumulative horizontal drift. This effect has been minimized by calibrating the system in the evaluation environment. However, in order to account for some possible horizontal drift, the spatial parameters were not evaluated as usually reported in the literature. Instead of considering only the forward axis of each segment data, the total excursion of both stride and step, computed as euclidean distances, was considered instead. This represents the total distance traveled in a stride and for each step, taking into account the variation

of both forward ($x-$) and lateral ($y-$) axes. Step width, although of high relevance in ataxic gait, was not evaluated because this metric depends on y position. Nevertheless, this metric was indirectly analyzed when calculating the step excursion. To do so, first, the position of each foot was divided into gait cycles, taking into account the initial contact of each foot (the heel strike event). Then, only the forward and lateral movements were used to calculate the spatial parameters explained in Table 39.

After the calculation of spatiotemporal parameters of gait, gait symmetry was analyzed (*i.e.*, the inter-limb difference) by calculating the inter-limb Symmetry Ratio (SR) [179, 180] for both day 0 and day 16. Although this metric is widely used, it leads to different interpretations of the result, depending on whether the higher value of the parameter is used as the numerator or denominator [179]. Therefore, following the standardization technique proposed by Patterson *et al.* [180], the SR was calculated using the highest value as the numerator and a positive or negative sign as a convention to indicate which of the measures is higher, whether the measure obtained for the right foot (positive) or the left foot (negative). Thus, a value of 1.0 indicates "perfect symmetry" and an absolute value much higher than 1.0 indicates asymmetry. In this thesis, only the absolute value was evaluated.

Regarding the specific outcomes of Phase 2, namely for the audiovisual biofeedback strategy, the CoM sway, in cm, was presented similarly to a statokinesiogram [97], providing a two-dimensional view of the sway considering AP and ML movement. Additionally, the ellipse that best described the data was calculated and the ratio between day 16 and day 0 was assessed considering the total ROM. Regarding the specific outcomes of the non-immersive VR-based exergame, a ratio between day 16 and day 0 was also assessed. A ratio of 1.0 indicates no change and a value below or above 1.0 indicate a decrease or an increase, respectively.

All data were processed in MATLAB R2023b (MathWorks®, California, USA) and analyzed using GraphPad Prism 8.4 (GraphPad Software, Inc., Massachusetts, USA). Although the study included two research hypotheses, these were not tested with appropriate statistical tests due to the heterogeneity of the population and the limited number of participants.

7.4 Results

This section presents the main findings of the clinical intervention study being implemented at Braga Hospital. The first phase of this study consisted of evaluating the rehabilitative effects of WALKit SRW and compare it with treadmill gait training. On the second phase, two HRI strategies were introduced, discussed in Chapter 6, and the rehabilitative gain in terms of balance and CoM sway control was evaluated.

This section is therefore divided into: **i) training Phase 1**, where a comparison between RAGT with WALKit SRW and Treadmill-Assisted Gait Training (TAGT) will be performed to assess hypothesis A, and **ii) training Phase 2**, where the previously detailed HRI strategies (see Chapter 6), namely the biofeedback strategy for CoM's sway control and the non-immersive VR-based exergame for balance and weight shift training, will be evaluated to assess hypothesis B.

Of the seven participants, one participant (14.3%), P2, was excluded from the study because she revealed behavior changes due to the progression of her condition, which sometimes made it impossible for her to cooperate properly, two participants completed training Phase 1 (28.6%) but they did not continue to Phase 2, and the remaining participants (57.1%) continued to training Phase 2, in which one patient is still in therapy.

7.4.1 Training Phase 1

Clinical Scales

Table 40 present the SARA specific sub-scores obtained for the six participants considering both assessment days and for both RAGT and TAGT. To further clarify the findings, the table display the variations observed between assessment days.

Table 40: SARA sub-scores of gait, stance, and sitting balance for both RAGT and TAGT. A negative variation represents improvement on day 16

Participant	Intervention	Gait		Variation	Stance		Variation	Sitting		Variation
		Day 0	Day 16		Day 0	Day 16		Day 0	Day 16	
P1	RAGT	4	4	0	2	2	0	0	0	0
	TAGT	3	2	-1	2	2	0	0	0	0
P3	RAGT	6	6	0	4	5	1	0	0	0
	TAGT	6	6	0	2	3	1	1	0	-1
P4	RAGT	6	6	0	2	2	0	0	1	1
	TAGT	6	6	0	4	4	0	0	0	0
P5	RAGT	2	3	1	1	1	0	0	0	0
	TAGT	2	2	0	1	1	0	0	0	0
P6	RAGT	6	5	-1	4	3	-1	1	0	-1
	TAGT	6	6	0	1	3	2	1	0	-1
P7	RAGT	6	5	-1	3	3	0	0	0	0
	TAGT	6	6	0	2	3	1	0	0	0

Considering RAGT, overall, differences between assessment days have been reported, with improve-

ments for two participants, while the remaining participants either presented no change, or presented an increase of 1 point. Regarding P1, the results of Table 40 shows that either no improvement or worsening was verified regarding sub-scores of gait, stance, and sitting after RAGT with WALKit SRW. Regarding P3, both gait and balance sub-scores maintained on day 16, while an increase of 1 point (from 4 to 5) was observed regarding stance sub-score. The same conclusion applies to P4, where no change was observed regarding gait and stance sub-scores, but an increase of 1 point in sitting sub-score (from 0 to 1) was verified. As for P5, a slight increase in gait sub-score, from 2 to 3 points, was observed on day 16, while stance and sitting sub-scores maintained. By the other side, training with WALKit SRW seems to had more effect on P6 and P7, who presented a decrease of 1 point in SARA's gait sub-score after training with the device, from 6 to 5 points, implying a slight improvement on day 16. In addition, P6 also revealed improvements in both stance and sitting sub-scores, decreasing 1 point in each one. As for P7, these scores maintained on day 16.

As for TAGT, Table 40 shows that this type of intervention appeared to be benefic for participants P1, P3, and P6, but only considering gait sub-score for P1 and sitting sub-scores for P3 and P6. However, P3 reported an increase of 1 point in stance sub-score, from 2 to 3 points, and P6 presented an increase of 2 points on stance sub-score. Finally, P7 maintained his scores of gait and sitting, but an increase of 1 point was observed in stance sub-score.

Comparing RAGT and TAGT, the results suggest that: **i)** WALKit SW seems to be more effective than treadmill for participants P6 and P7 regarding gait sub-score, while P5 showed a slight deterioration on day 16; **ii)** in cases where an improvement or no change was found in stance sub-score after RAGT (P6 and P7), these patients presented a deterioration in treadmill training; and **iii)** treadmill appeared to be slightly better than RAGT regarding sitting sub-score. However, the reported differences were not so pronounced (usually 1 point), which can represent a clinically relevant improvement/decline, but may also be affected by the inter-rater variability. Indeed, clinicians did not know what type of intervention the participant had undergone, which is positive, but patients were not assessed by the same evaluator at both assessment times. This, in a way, may have introduced some variability into the assessment. Actually, it would be optimal to have different assessments of the SARA scale, conducted by different blind clinicians, and then consider an average score. Furthermore, reported declines may also be related with the symptomatic variability shown by patients on different days, which is influenced by their state of mind or tiredness. Future research should consider an intermediate assessment (on day 7), and short daily assessments to analyze the participant's progress throughout training, thereby minimizing eventual fluctuations that may influence results.

To further assess the motor effects of both RAGT with WALKit SRW and TAGT, the 10-MWT was applied. This test is extremely useful and objective because it measures the patient's walking speed in m/s [175]. In this case, the test was applied considering the participant's comfortable speed, and only the central six meters were considered for the gait speed measurement, following the recommendation of [175], since the first and last two meters were assumed to be the period of acceleration and deceleration, which was thought to influence the participant's effective walking speed. All participants were able to complete the test when prompted, but some participants required the use of walking aid. Specifically, P3 used crutches as this is the only assistive device that provides her with walking stability, P4 used a standard walker, and P6 used her usual four-wheeled walker. As for P1, although he usually walks with a two-wheeled walker, he was able to complete the test without the assistive device. Finally, P7 did not use an assistive device but walked with support from one arm. In this case, the participant was assisted by the team's physiotherapist, but the latter always stayed on the side and followed the cadence set by the participant.

Results of day 16 have been normalized to day 0, expressing a ratio. A ratio lower than 1.0 for the time needed to complete the test indicates that participants were able to complete the test more quickly, thus increasing their walking speed (considering the same six meters). Figure 61 presents the 10-MWT and gait speed ratios obtained for each participant and considering both RAGT and TAGT. Absolute average values can be found in Table 52.

Results suggest that both interventions promoted an improvement in the time to complete the 10-MWT. Regarding the intervention phase with WALKit SRW, the ratio between day 16 and day 0 **was below 1.0 for most participants** (average ratio of 0.88 $\pm$ 0.08). No improvement was found for P1, with a ratio of 1.00, and a maximum improvement was observed for P4, with a ratio of 0.78. As for participants P3, P5, P6, and P7, ratios of 0.95, 0.88, 0.90, and 0.80 were observed, respectively. As for TAGT, all participants reported a decrease in time to complete the 10-MWT, except for P4, who maintained the mean time on day 16. Regarding P1, P3, P5, P6, and P7, ratios of 0.87, 0.93, 0.92, 0.97, and 0.69 were reported, respectively. This resulted in an average ratio of 0.90$\pm$0.11 for TAGT.

The decrease in time to complete the 10-MWT resulted in an increase in gait speed. In fact, the **gain in speed was notorious after training with WALKit SRW**. As Figure 61 shows, all participants except P1 showed an increase in gait speed after RAGT that was larger than 5%. Participants P3, P4, P5, P6, and P7 presented ratios of 1.05, 1.28, 1.14, 1.12, and 1.25. As for TAGT, only participants P1 and P7 reported a ratio considerably higher than that obtained for RAGT, presenting ratios of 1.14 and 1.43, respectively. The remaining participants, namely P3, P4, P5, and P6 reported ratios of 1.08, 1.00, 1.09, and 1.03, respectively.

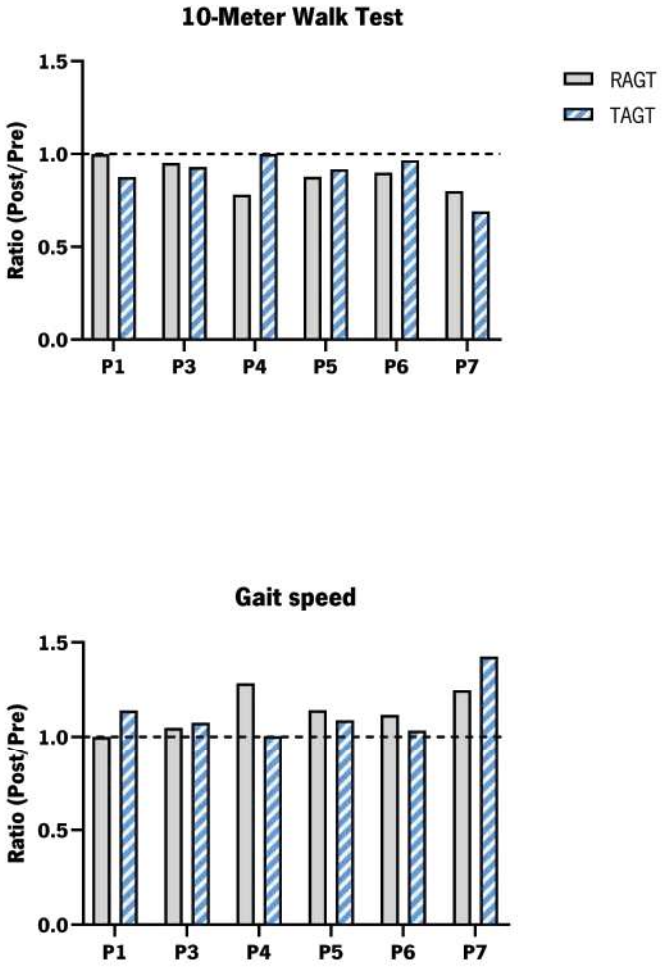


Figure 61: Ratio of time to complete the 10-MWT and ratio of gait speed, considering post-training with WALKit SRW and treadmill.

As for TUG test, this was another clinical test used to assess functional mobility and balance, as proposed by Podsiadlo, D. and Richardson, S. [181]. Similar to 10-MWT time and gait speed, the time taken to perform the TUG test on day 16 was normalized to day 0. Therefore, a value below 1.0 on day 16 represents an improvement in mobility. Figure 62 illustrates the gain observed after RAGT and TAGT.

Most participants reported an improvement on this test considering RAGT, with improvements that range from 8% to 28%, except for P3, who maintained her score on day 16. Participants P1, P4, P5, P6, and P7 presented ratios of 0.91, 0.72, 0.80, 0.92, and 0.85. TAGT proved to be more effective in terms of TUG test for participants P1 and P7, similarly to what has been observed in gait speed, presenting ratios of 0.69 and 0.78 respectively. Moreover, P3 also reported a slight improvement, with a ratio of 0.97. As for participants P4 and P5 these reported a slight increase in ratio (1.03 and 1.01, respectively), while P6 reported a more evident increase (1.15). Overall, the results suggest that **WALKit**

SRW was more effective than treadmill for participants P4, P5, and P6. Furthermore, considering an average result, despite the fact that both treatments generally promoted a decrease in the time to complete the TUG test, this decrease was **more evident after training with the robotic walker** (ratio of 0.87±0.10 for RAGT and 0.94±0.17 for treadmill).

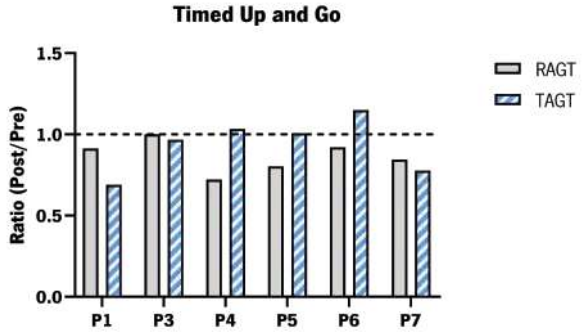


Figure 62: Ratio of time to complete TUG test considering post-training with WALKit SRW and treadmill.

Gait quality

Although improvements were seen in gait speed, inter-limb gait symmetry should be analyzed, as it is considered an indicator of gait quality [182]. For example, the literature has shown that step length asymmetry plays an important role in postural balance, which is impaired in patients with CA [183].

Different ways of quantifying the difference between the two limbs have been proposed in the literature, as presented by Patterson *et al.* [180], but the authors state that the SR is easier to interpret. A "perfect" SR is obtained when the ratio is 1.0, but not even healthy individuals present this value [183]. In fact, Patterson *et al.* [180] defines normative symmetry values by considering the 95% confidence interval for each metric calculated for a healthy group [183]. In this case, a threshold of 1.08 was defined for step length, and 1.05 and 1.06 for stance and swing phase durations, respectively [180, 183].

A. Temporal parameters

Temporal metrics were assessed with data acquired with Xsens Awinda. These included stride time, step time, and stance and swing times. Figure 63 summarizes the overall results. Although participants P1 and P4 completed Phase 1, technical problems were identified with the data from at least one intervention period, so these patients were not included in this analysis.

Regarding stride time, the results show a symmetry between the right and left foot at both day 0 and day 16, and this was consistent across participants. Moreover, this conclusion is valid either for RAGT (day 0: 1.01±0.005, day 16: 1.01±0.003) and TAGT (day 0 and day 16: 1.01±0.002). All participants

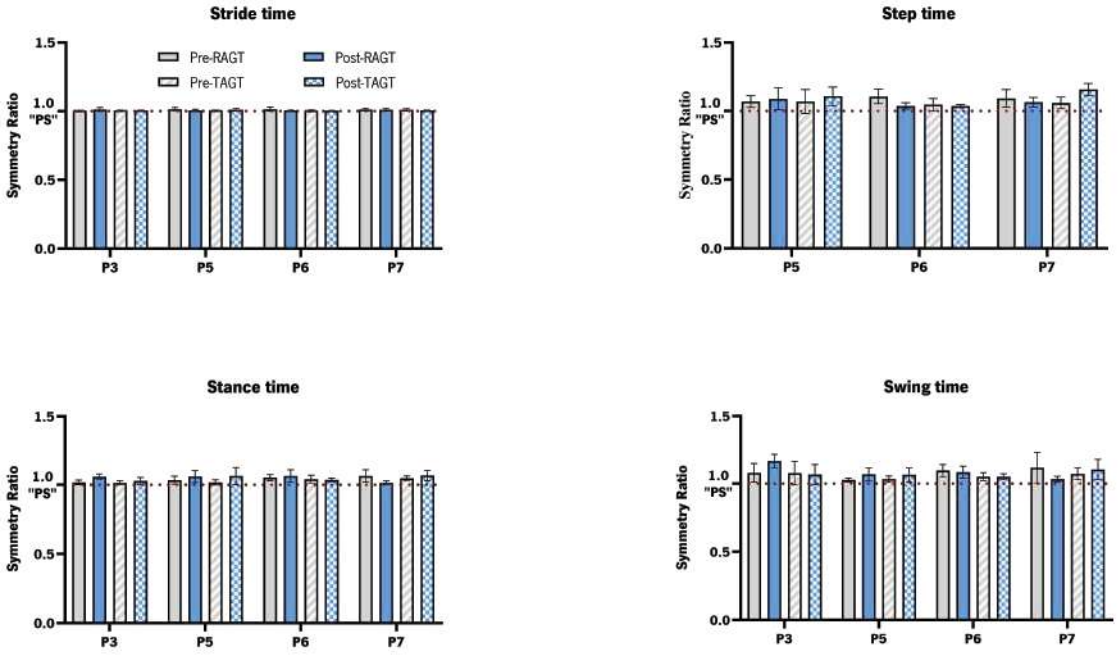


Figure 63: Symmetry Ratio of temporal gait metrics: stride time, step time, stance and swing times, considering both day 0 and day 16 for RAGT with the robotic walker and for treadmill training.

reported similar stride times for both feet, as also can be observed in Table 52 of Appendix C.1. In terms of absolute values, all participants except for P7 presented decreases on stride time, ranging from 1% to 7%, that is consistent with the observed increase in gait speed. This result, together with the fact that most participants showed an increase in gait speed, suggests that stride length probably increased or was maintained over a shorter period of time.

The same analysis was performed for step time. However, for this analysis, only participants P5, P6, and P7 were included. P3 was not included since the step time of the right foot is affected by the time it takes to project the crutches forward. Therefore, considering this time for the symmetry analysis would completely affect the results and would always indicate an asymmetric time, as can be seen from Table 52 provided in Appendix C.1. Although this is a systematic factor, the time needed to project the crutches forward is variable, thus removing this time would introduce additional error. Regarding the remaining participants, P6 and P7 showed improvements in the SR after RAGT: **i)** P6 presented a decrease from 1.11 ± 0.04 to 1.04 ± 0.02, and **ii)** P7 presented a decrease from 1.09 ± 0.05 to 1.06 ± 0.03. As for P5, a slight increase of the SR was observed, from 1.07 ± 0.03 to 1.09 ± 0.07.

Regarding TAGT, two participants (P5 and P7) reported an increase in the SR. P5 presented an increase of SR from 1.07 ± 0.07 to 1.11 ± 0.06. As for P7, a more notorious increase from 1.06 ± 0.03 to 1.16 ± 0.04 was observed. Finally, for P6, the SR was practically maintained. These results suggest that

WALKit SRW was more effective in terms of improving step time symmetry ratio for participants P6 and P7. As for P5, both interventions appeared to worse the SR, but this was more evident for TAGT.

Figure 63 also presents the SR considering the stance and swing times. According to these results, all participants, with the exception of P7, increased their SR of stance time, to values close to 1.06/1.07, after RAGT. P3 reported an increase in her SR from 1.02±0.01 to 1.06±0.02, P5 from 1.03±0.02 to 1.06±0.02, and P6 from 1.05±0.02 to 1.07±0.04. On the other hand, P7 revealed an improvement in stance time SR, from 1.07±0.04 to 1.02±0.01. Table 52 (Appendix C.1) shows a generalized decrease in stance time on day 16, which aligns with the observed increase in speed but may have contributed to unexpected variations in SR. Regarding TAGT, shown in Figure 63, P5 and P7 reported an increase of stance time SR, from 1.02±0.01 to 1.06±0.05 for P5, and from 1.05±0.01 to 1.07±0.03 for P7. The remaining participants maintained their inter-limb SR for this specific temporal parameter.

Overall, the results suggest that WALKit SRW was beneficial for P7, and for the remaining participants, although slight increases were observed for both interventions, the value remains close to the threshold for symmetry (1.05) [180], though it is unclear whether the slight deviation holds clinical significance.

The SR of swing time was also evaluated. The results, presented in Figure 63, shows that RAGT was beneficial for participants P6 and P7, since both decrease their SR. However, for P6, swing time remained asymmetric (day 0: 1.10±0.04, day 16: 1.08±0.04) considering the threshold proposed by [180], although close to be considered symmetric. Regarding P7, training with WALKit SRW was more effective to improve the swing time SR, since the participant's gait was asymmetric on day 0 (1.12±0.09) and become symmetric on day 16 (1.03±0.02). On the other hand, P5 revealed an increase in the swing time SR (day 0: 1.03±0.01, day 16: 1.07±0.04), although close to the limit proposed in [180] (1.06). Lastly, P3 revealed a more expressive increase in the SR for the swing time, which was already considered asymmetrical on day 0 (day 0: 1.08±0.06, day 16: 1.16±0.04). Analyzing data shown in Table 52, it can be seen that the average swing time of the left foot is shorter than that of the right foot, and this difference became more pronounced on day 16, perhaps motivated by the increase in gait speed. This difference may also be related to the way the participant walks with the crutches, as the left foot is in the air much less time than the right foot.

The results obtained for the TAGT, shown in Figure 63, reveal that P3 registered practically no change in the swing time SR (day 0: 1.08±0.07, day 16: 1.07±0.06), P5 slightly increased the SR (day 0: 1.03±0.02, day 16: 1.06±0.04), similarly to what was found after training with the robotic walker, P6 maintained her SR (day 0: 1.05±0.02, day 16: 1.05±0.02), and P7 slightly increased the SR that was already above the limit (day 0: 1.07±0.04, day 16: 1.10±0.06). For this particular participant, the re-

ported increase was justified by a difference in average time of 58 ms, which contrasts with that obtained on day 0 (around 18 ms, see Table 52). Indeed, for P7, the treadmill training, despite a marked increase in walking speed, seems not to have been as effective in terms of improving gait quality.

B. Spatial parameters

Gait symmetry was also evaluated considering spatial metrics, namely stride and step excursion. The absolute values are presented in Table 52 of Appendix C.1. Figure 64 presents the SR obtained for P3, P5, P6, and P7, considering the parameters previously explained in Table 39. Similarly to the temporal parameters, although P1 and P4 completed training Phase 1, there have been identified technical issues with the data from at least one intervention period, therefore these patients were not considered for this analysis.

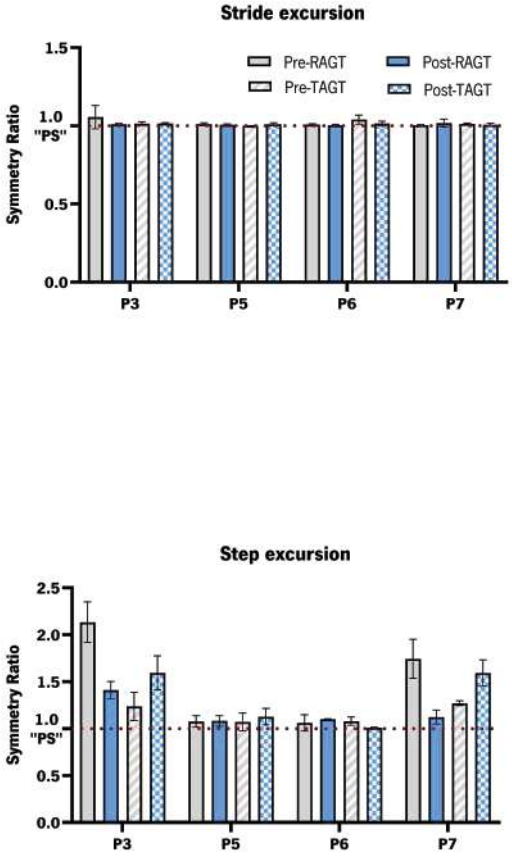


Figure 64: Symmetry Ratio of spatial gait metrics: stride and step excursion, considering both day 0 and day 16 for RAGT with the robotic walker and for treadmill training.

As shown in Figure 64, stride excursion of both legs was considered symmetrical, and this result is consistent for all participants, allowing a global analysis to be performed. An average SR of 1.02 ± 0.02 and

1.01±0.01 were found for day 0 and day 16, respectively, considering RAGT. A careful analysis to Figure 64 reveals that the overall decrease was motivated by an improvement observed for P3 who presented a SR of 1.06±0.06 on day 0 and 1.01±0.003 on day 16. As for TAGT, the SR of stride excursion was also similar between day 0 and day 16, except for P6 who decreased her SR from 1.04±0.02 to 1.02±0.01.

Step excursion was also evaluated for both interventions. Analyzing step excursion is extremely relevant if one aims to assess gait quality. For instance, data from Table 52 reveals that, for P3, gait is symmetrical in terms of stride excursion, but asymmetrical in terms of the step, partially explained by the use of crutches. The results of P3 demonstrates that the step excursion expressively improved after RAGT (day 0: 2.13±0.18, day 16: 1.41±0.08). Although the SR maintained certainly asymmetric, the robotic walker proved to be effective in decreasing the existing asymmetry. P7 also revealed an important improvement in step excursion on day 16 (day 0: 1.74±0.17, day 16: 1.12±0.06). As for participants P5 and P6, P5 revealed no change (day 0: 1.08±0.05, day 16: 1.08±0.05) and P6 revealed a slight increase on day 16 (day 0: 1.06±0.07, day 16: 1.10).

Regarding TAGT, there was an overall increase in the SR. In fact, only P6 revealed a decrease in the SR and for a value very close to 1.0 (day 0: 1.08±0.04; day 16: 1.01±0.01). This result suggests that, for P6, treadmill training was beneficial in terms of step excursion.

C. Gait Speed and Gait Symmetry

Although most of the participants reported an increase in gait speed, which may be positive, this increase in speed should be compared with gait quality [182], measured by the inter-limb SR [180]. Clinically, it may be more relevant to improve gait quality rather than to have a significant increase in speed, although this is also relevant as it allows the patient to move more easily, thereby increasing functional ambulation [184].

Looking specifically at the results obtained for training with the robotic walker, two participants, P3 and P7, **reduced expressively the existing asymmetry in step excursion while increasing their gait speed**. As for P5, the inter-limb SR of **step excursion maintained, while an increase in speed was reported**. For P6, the increase in speed was accompanied by a slight increase in the step excursion ratio. The difference between feet was less than 5 cm, approximately 10% of the total step excursion. Although the value obtained may include changes in step width and length, its clinical significance is not known. With regard to the SR of step time, participants P6 and P7 **revealed improvements after training with WALKit SRW**. P5, on the other hand, presented a slight increase on day 16. Regarding stance and swing times SR, these did not benefit from increased gait speed, except for P7, who revealed improvements in

all temporal parameters after training with WALKit SRW.

As for TAGT, three participants (P3, P5, P7) revealed increases in SR of step excursion, especially for P3 and P7 whose increase was more expressive. Additionally, P7 presented a marked increase in speed after TAGT (43%), but the ratio in step excursion worsened considerably. As for P6, she revealed an improvement in step excursion after treadmill training, which was beneficial alongside her improvement in gait speed. In terms of step time, P5 and P7 increased their SR, while P6 revealed no change.

7.4.2 Training Phase 2

Biofeedback for postural sway control

The main goal of the biofeedback strategy is to improve postural control and indirectly reduce CoM movement in the AP and ML axes. During the validation with healthy individuals, in Chapter 6, it was observed that activating the strategy reduced the total ROM in both AP and ML axes while performing specific stance exercises (bipedal, tandem, and unipedal stance). However, participants were assessed only to determine whether ROM decreased during the biofeedback use, not to evaluate potential learning effects. Therefore, another validation protocol was conducted to assess the effectiveness of training in pathological individuals. For this purpose, the variation of the CoM in both the AP and ML axes on day 0 and day 16 was assessed using specific exercises of the BBS scale, namely exercise 2, 7, and 13.

Regarding the biofeedback strategy, three participants completed the protocol (P3, P5, P6), while P7 is still in progress. For this specific validation, it was decided to reduce the gait training by 15 minutes and to introduce 15 minutes of static training, using the same exercises as for healthy individuals, *i.e.* bipedal stance, tandem stance and unipedal stance, at the beginning of the session. Biofeedback was only used for the first 15 minutes of training, and then participants performed 15 minutes of gait training on the robotic walker. Regarding the AP and ML limits, these were adjusted by the physiotherapist in charge.

To assess the effect of the proposed BS, it was considered to plot AP displacement as a function of ML displacement, similar to a statokinesiogram. Figure 65 shows the results for participants P3, P5, and P6 while performing BBS 2. Table 41 presents the total ROM calculated for both AP and ML axes, considering BBS 2, 7, and 13, as well as the specific score for each exercise.

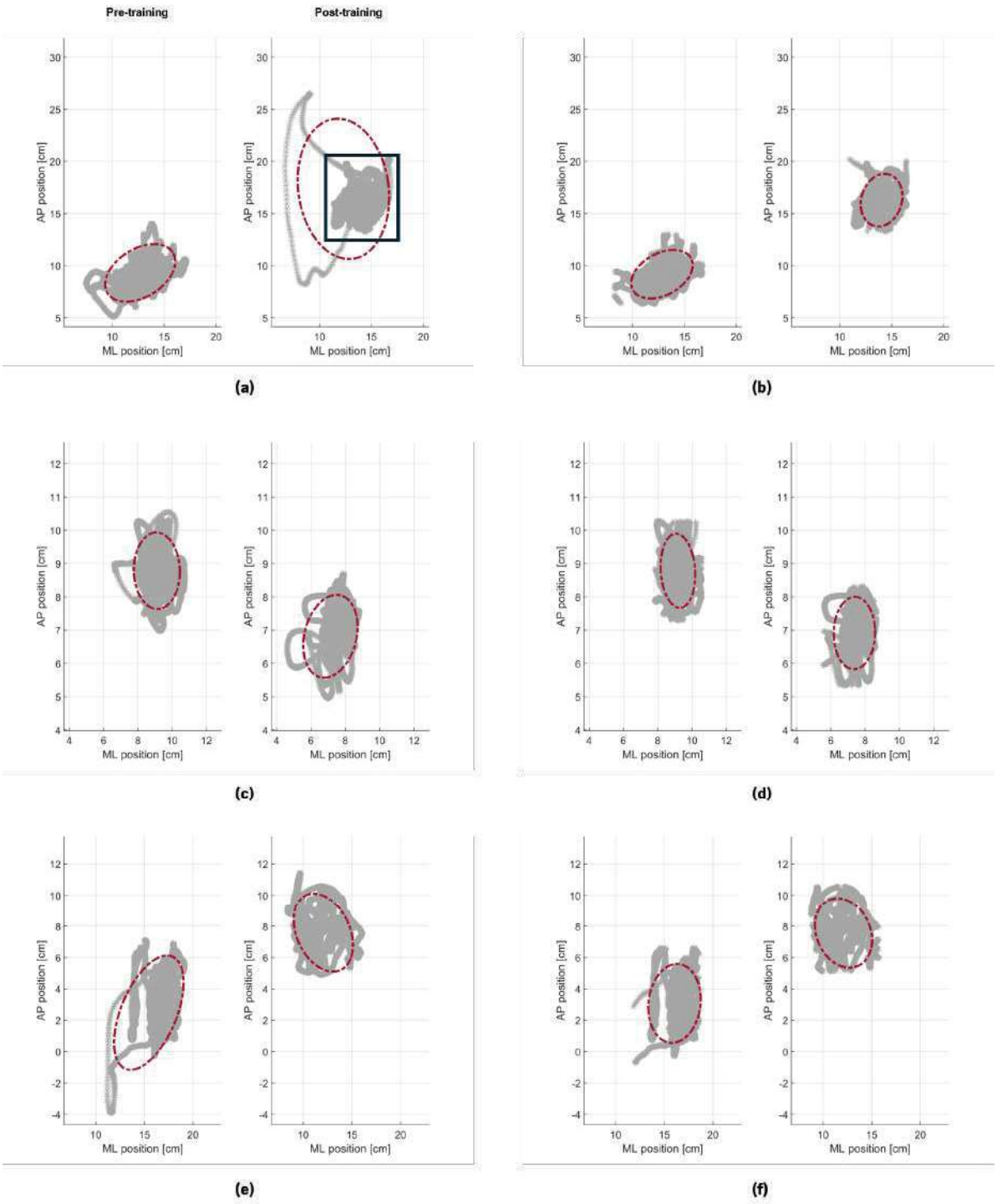


Figure 65: CoM displacement considering AP and ML axes for for P3 (a and b), P5 (c and d), and P6 (e and f); panels a, c and e consider all data, and b, d, f consider the 98% most representative data.

As shown in Figure 65, P3 had an imbalance on day 16 while performing exercise 2 of BBS (score of 4 on day 0 and 3 on day 16, motivated by the imbalance). This imbalance caused a larger ROM considering the AP and ML axes, but it was more pronounced on the AP axis. However, if one analyzes Figure 65, it can be seen that P3 remains within the region bounded by the blue rectangle most of the time, as there is

Table 41: Total ROM and gain on day 16 obtained for all participants, considering BBS 2, 7, and 13, both day 0 and day 16, and the 98% most representative data

Participant	BBS	ROM AP (cm)		ROM ML (cm)		Ratio AP	Ratio ML	BBS sub-score	
		Day 0	Day 16	Day 0	Day 16			Day 0	Day 16
P3	2	6.68	6.93	8.41	5.53	**1.04**	**0.66**	4	3
P5		2.97	2.97	2.71	3.10	**1.00**	**1.14**	4	4
P6		7.34	5.41	6.72	6.96	**0.74**	**1.04**	4	4
P5	7	3.08	2.91	2.86	3.57	**0.94**	**1.25**	4	4
P5	13 LFF	4.16	3.75	4.41	4.69	**0.90**	**1.06**	2	3
P5	13 RFF	3.09	2.09	4.29	3.76	**0.68**	**0.88**		

a large accumulation of points in this region. Therefore, the 98% most representative data were calculated, excluding the 1% higher and lower values, that were considered outliers for this analysis.

The results show that P3 revealed a **decrease in the CoM's sway considering the ML axis**, as evidenced by the lower ROM of Table 41. This **represented a 34% drop regarding day 0**, which is positive. However, a 4% increase was observed for the AP axis, representing an increase of 2.5 mm. This result is also visible in the ellipse of Figure 65, whose ML projection difference is notorious, while AP projection difference appears similar.

As for P5, no improvement was observed on day 16, maintaining the AP ROM. However, an increase of 14% on the ML axis was observed, representing an increase of 4 mm. This is also notorious on the ellipse, whose ML projection difference is slightly larger. External factors may explain this result, since P5 maintained a level of 4 points (total functional): recordings from the Xsens Awinda reveal that the participant probably coughed, moved her arm, and sometimes interacted with the therapist.

Lastly, P6 revealed **a 26% reduction of the AP ROM** (ROM of 7.34 cm on day 0 and 5.41 cm on day 16), while a 4% increase was observed for ML axis (6.72 cm compared to 6.96 cm, 2.4 mm of difference). Despite this increase, P6 maintained a level of 4 points (total functional). Additionally, the decrease in AP ROM is encouraging, given that this particular patient has instability at the AP level, especially at the posterior limit.

Overall, evidence of BBS 2 suggests that the biofeedback strategy had a positive effect for P3 and P6 considering the ML and AP movements, respectively. No effect was observed for P5 regarding the AP axis, while a 4 mm increase was observed regarding the ML, which can be due to external factors given the overall level of functional balance of this participant.

BBS 7 was also analyzed for P5. Figure 66 shows the observed variation in the CoM.

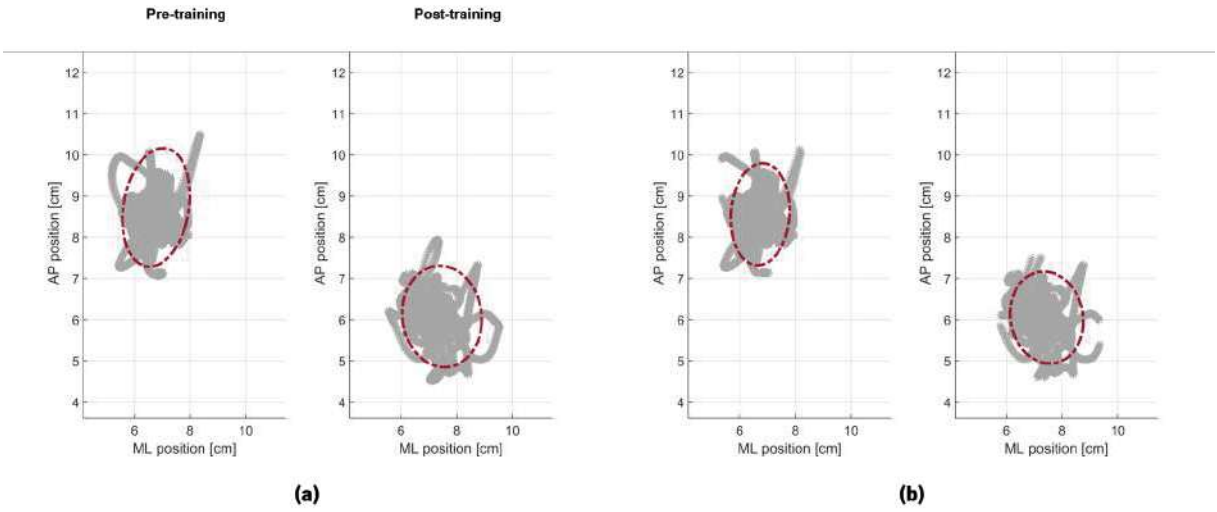


Figure 66: CoM variation during execution of BBS 7 for P5, considering day 0 and day 16: **(a)** total data, **(b)** 98% most representative data.

These findings suggest that P5 revealed the same behavior as that demonstrated in BBS 2 regarding the ML axis. An increase of 7 mm (25%) on the CoM ROM for the ML axis was observed. Analyzing the records performed with Xsens Awinda, it was verified that the participant involuntarily jerked her hands and interacted with the therapist. However, additional studies are needed to determine whether this increase was influenced by external factors or resulted from training, as P5 achieved the maximum score in exercise 7 of the BBS on both assessment days (4 points), indicating full functionality. Still, the biofeedback strategy **promoted a decrease of 6%** regarding the total ROM for the AP axis. Regarding the BBS sub-score, P5 scored 4 in both days.

BBS 13 was also assessed for P5. Although this participant needed slight support to maintain balance in the first moments of the exercise, the participant eventually reached an equilibrium state. Thus, the CoM ROM was analyzed from that moment on. Figure 67 illustrates the results obtained, considering RFF - Right Foot Front, and LFF - Left Foot Front. In the first case, P5 was holding her weight mostly on the left leg. By the other side, for the second case, the participant hold her weight mostly on the right leg.

The findings of both Figure 67 and Table 41 show that the proposed biofeedback strategy was **important in reducing the CoM total ROM**, especially for the AP axis, with an **average decrease of 21±15.6%** (10% for AP LFF and 32% for AP RFF). Regarding the ML axis, a small increase of 2.8 mm (6% worsening) was observed considering LFF, while a decrease of 4.1 mm (12% improvement) was obtained for RFF, resulting in an average decrease of 3%. In addition, the results suggest that P5 revealed a stronger ability to hold the weight on her left leg, having reported **decreases in the CoM total ROM,**

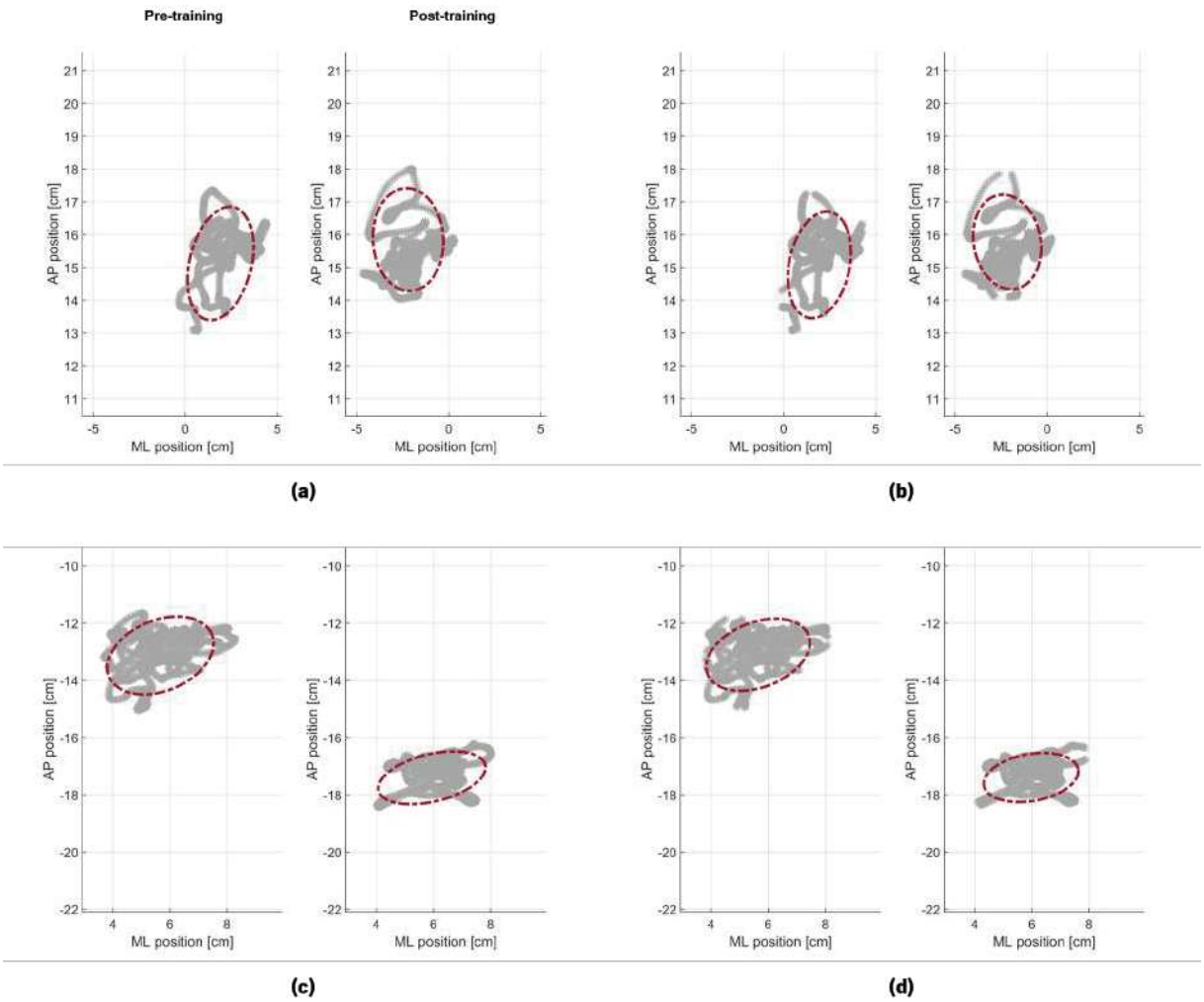


Figure 67: CoM variation during execution of BBS 13 for P5, considering day 0 and day 16: **(a)** total data of Left Foot Front (LFF), **(b)** 98% most representative data of LFF, **(c)** total data of Right Foot Front (RFF), and **(d)** 98% most representative data of RFF.

both in the AP and ML axes. Regarding the BBS sub-score, P5 reported an **improvement of score**, from 2 points on day 0 to 3 points on day 16.

Regarding the BBS total score, only P6 increased her score from 34 points on day 0 to 40 on day 16, representing an **improvement of 18%**. The participant improved in BBS 6 for bipedal stance with eyes closed and BBS 7 for standing with feet together, but her score decreased in BBS 11, requiring assistance for full rotation. P3 and P5 maintained scores of 25 and 51 points, respectively.

Lastly, TUG test was also evaluated at both assessment days to verify any progress. According to the absolute values (see Appendix C.2), P3 decreased her time, albeit slightly (3%), P5 increased her time by 3%, and P6 decreased her time by 1%. When comparing the ratio for participants P5 and P6 after RAGT in Phase 1, the decrease is lower (P5 had decreased by 20% and P6 by 8%). P3, on the other

hand, decreased her time after this new training while in Phase 1 she maintained her time. However, the absolute time increased after phase 1.

Overall, the results suggest that the combined effect of gait training with WALKit SRW and the integrated BS may be effective in controlling the CoM displacement, although more evident for the AP axis. These results are encouraging to continue the development of assistive robots as a complement to rehabilitation therapies and to urge the integration of biofeedback strategies.

Non-immersive VR-based exergame for balance training

The second HRI strategy to be tested was the integration of the non-immersive VR-based exergame. In this case, the main goal of the protocol was to complete 30 minutes of gait training supported by WALKit SRW, while participants played an exergame that mainly involved ML weight transfers (simpler levels) and both AP and ML weight transfers (higher levels). Levels were assigned by the physiotherapist and were adjusted as needed throughout the protocol. All participants started therapy at level 2 (ML training) and progressed to level 4 (ML and AP training).

After the training program, participants were assessed using the BBS. P3 showed a 11-point improvement (20 to 31), reflecting gains in standing safely (BBS 1), in quiet standing (BBS 2), sitting control (BBS 4), transfers (BBS 5), standing with eyes closed (BBS 6), object pickup (BBS 9), and turning to one side without supervision (BBS 10). Despite these improvements, P3 remained at high fall risk [178]. P5 improved by 2 points (48 to 50), with better full rotation performance (BBS 11). Lastly, P7 gained 2 points (33 to 35), with improvements in independent standing (BBS 1), standing with feet together (BBS 7), object pickup (BBS 9), and slight rotation improvement (BBS 11). However, P7's score dropped in BBS 8, indicating he needed supervision while leaning forward.

Specific exercises from the BBS were evaluated, namely BBS 8, 9, and 10, as these exercises challenge balance by shifting the CoM and CoG while the user remains stationary. These were chosen as they reflect the balance training that was performed while experiencing the exergame. Regarding BBS 8, Table 42 and 43 present the main results for participants P3, P5, and P7.

Table 42: Forward displacement of right arm considering exercise 8 of BBS

Participant	D0	D16	Ratio	BBS sub-score	
	Arm ROM [cm]	Arm ROM [cm]		D0	D16
P3	14.63	18.34	**1.25**	1	1
P5	18.45	22.71	**1.23**	4	4
P7	17.04	20.66	**1.21**	3	1

Table 43: Torso inclination (pitch) considering exercise 8 of BBS

Participant	D0	D16	Ratio	BBS sub-score	
	Torso pitch [deg]	Torso pitch [deg]		D0	D16
P3	23.50	28.42	**1.21**	1	1
P5	48.17	49.96	**1.04**	4	4
P7	30.14	30.66	**1.02**	3	1

The results suggest that there is an **increase in total trunk forward displacement** on day 16, and this increase is consistent for all three participants. P3 revealed an **improvement of 25%** on day 16. However, it is noteworthy that this participant had a score of 1 on day 0 and maintained this score on day 16, suggesting that she is able to lean forward but still needs supervision. As for P5, she revealed an **improvement of 23%**, and maintained her score of 4 points on both assessment days. Finally, P7 reported an **increase of 21%**, but he ended up unbalanced, causing his score to worse from 3 to 1 point. However, before losing his balance, the participant was able to control his CoM and achieve a higher distance. Regarding trunk inclination, an expressive increase was only observed for P3, with an **increase of 21% on day 16**. Participants P5 and P7, although it was reported an increase on day 16, this was marginal (4% for P3 and 2% for P7).

Regarding BBS 9, the time to complete the task was assessed as well as the vertical variation of the CoM. Regarding the vertical variation, it was found that it did not exceed a maximum of 2.7 cm between assessment days and considering the three participants, but the time to complete the task was variable. Table 44 shows the results obtained for the three subjects analyzed.

Table 44: Time, in seconds, to complete exercise 9 of BBS

Participant	Time [s]		Ratio	BBS sub-score	
	D0	D16		D0	D16
P3	5.32	6.53	**1.23**	3	4
P5	4.22	4.17	**0.99**	4	4
P7	20.20	20.83	**1.03**	3	4

The results suggest that, considering practically the same vertical variation in CoM (maximum variation of 2.7 cm), P3 increased her time by 23%, and both P5 and P7 approximately maintained their time. Two different behaviors for the same exercise were observed, and yet both can be positive. As for P3, she scored 3 points on BBS 9 of day 0 but **improved her score on day 16**, achieving 4 points. Therefore, one can conclude that the increase in the time taken to perform the task may suggest that she tried to do

it in a **more controlled way so as not to lose her balance**. As for P5 and P7, by analyzing only the overall time, it is not possible to infer whether the participants completed the task in a more controlled way or not. Therefore, the descent time and ascent time were calculated and presented in Table 45.

Table 45: Descent and ascent time, in seconds, to complete exercise 9 of BBS

Participant	Time [s]					
	Descent time		Ratio	Ascent time		Ratio
	D0	D16		D0	D16	
P3	2.65	3.52	**1.33**	2.67	3.02	**1.13**
P5	2.07	1.73	**0.84**	2.15	2.43	**1.13**
P7	10.93	13.83	**1.27**	9.27	7.00	**0.76**

The results show that P3 spends much more time descending (an increase of 33% compared to day 0) than she does ascending, whose time increases not so expressively (close to 13%). This result suggests that, in fact, on the descent, the participant was **more cautious so as not to lose her balance**. P5, on the other hand, decreased her descent time by 16%, which shows that she was quicker to pick up the object, but ended up taking longer to ascend, around 13%. Considering her score of 4 points on BBS 9, this result suggests that she had **more confidence** in completing the task, since during the descent there is always the fear of unbalancing and falling. Lastly, P7 also increased his descent time by 27%, which means that he performed the movement in a **slower and more controlled way**. After picking the object, he ascended faster, with a 24% decrease in time. P7 also **improved his score of BBS 9**, from 3 to 4 points, indicating that he can pick the object **autonomously and safely**.

As a last objective assessment from Xsens Awinda data, BBS 10 was evaluated. The total ROM of torso rotation (yaw) was measured for both left and right sides while participants were performing the weight-transfer task. Table 46 presents the results.

Table 46: Torso rotation, in degrees, while performing exercise 10 of BBS

Participant	Torso Left Rotation [deg]		Ratio	Torso Right Rotation [deg]		Ratio	BBS sub-score	
	Day 0	Day 16	D16/D0	Day 0	Day 16	D16/D0	Day 0	Day 16
P3	32.54	24.10	**0.74**	43.94	8.98	**0.20**	1	3
P5	71.35	72.90	**1.02**	69.49	69.88	**1.01**	4	4
P7	38.03	45.05	**1.18**	35.26	43.40	**1.23**	4	4

The results show that P5 has roughly the same rotation from day 0 to day 16, and rotates with approximately the same magnitude on both the left and right sides. This result is consistent with her

score of BBS 10, that maintained on 4 points. As for P7, an improvement was observed, **increasing 18% on the left and 23% on the right, while maintaining balance**. This result was also consistent with his score of 4 points on both day 0 and day 16. Lastly, for P3, she presented a decrease in rotation to the left side, but expressively to the right side, with a decrease of 80%. Analyzing the recordings of the Xsens Awinda, it is clear that the participant only looked backwards and did not rotate, which actually explains her score of 3 points on day 16. However, although a decrease in excursion was found, her score of the BBS 10 **increased on day 16**, from 1 to 3 points, as she revealed loss of balance on day 0.

Lastly, participants were evaluated considering the TUG scale. The average times and scores are presented in Appendix C.2. P5 and P7 revealed improvements, presenting, respectively, a **14% and 6% decrease**, revealing improvements in general mobility and functional balance. As for P3, she slightly increased her time by 4%. The ratios obtained are positive for P5 and P7, but not better than those obtained in phase 1. Nevertheless, for P7, the absolute result obtained on day 16 is slightly lower than that obtained after training with WALKit SRW (see Appendix C.1 and C.2).

7.4.3 Usability and functionality

In addition to assessing the potential gain in motor rehabilitation, the device and the proposed novel HRI strategies were evaluated for their usability and functionality using the SUS questionnaire [118], translated and validated into Portuguese [119]. Table 47 presents the results of the questionnaire for all the participants who completed phase 1 of training with the robotic walker.

The results reveal that participants felt confident using the system (Q9: 4.5 points), and they found easy to use and well integrated (Q3: 4.5 points, Q7: 4.33 points). However, users tended to be neutral when asked if the system was more complex than necessary (Q2: 2.83 points), if they would need help from a technician to use the system (Q4: 3.33 points), or if they had to learn a lot before being able to handle the system (Q10: 2.5 points). The overall results reveal that participants found the device **functional**, with scores ranging from 57.5 points ("Ok", considering the grading scale proposed in [47]) to 90 points (between "Excellent" and "Best imaginable"). The average score was 75.42 ± 11.00 points, **classifying the device as as "Good" and acceptable** (maximum of the acceptability grade), considering the acceptability scale proposed in [47].

Table 47: SUS scores for the experimental validation of WALKit SRW with pathological users

Question	Participants						Mean	Std
	P1	P3	P4	P5	P6	P7		
Acho que gostaria de utilizar este produto com frequência.	5	5	5	4	5	3	**4.50**	**0.84**
Considerei o produto mais complexo do que o necessário.	2	5	3	3	1	3	**2.83**	**1.33**
Achei o produto fácil de utilizar.	5	5	4	4	5	4	**4.50**	**0.55**
Acho que necessitaria de ajuda de um técnico para conseguir utilizar este produto.	2	5	2	2	5	4	**3.33**	**1.51**
Considerei que as várias funcionalidades deste produto estavam bem integradas.	5	5	4	5	5	4	**4.67**	**0.52**
Achei que este produto tinha muitas inconsistências.	2	2	1	3	2	3	**2.17**	**0.75**
Suponho que a maioria das pessoas aprenderia a utilizar rapidamente este produto.	4	4	4	5	5	4	**4.33**	**0.52**
Considerei o produto muito complicado de utilizar.	1	1	1	3	1	2	**1.50**	**0.84**
Senti-me muito confiante a utilizar este produto.	5	5	4	5	5	3	**4.50**	**0.84**
Tive que aprender muito antes de conseguir lidar com este produto.	1	1	2	4	4	3	**2.50**	**1.38**
	90	**75**	**80**	**70**	**80**	**57.5**		

Regarding the inclusion of the biofeedback strategy, users P3, P5 and P6 considered the biofeedback strategy easy to use (Q3: 4.33 points, Q8: 1.67 points), although they were neutral about its complexity (Q2: 3.00 points). They also felt that its features were well integrated (Q5: 4.00 points), and it is easy to learn (Q7: 4.00 points, Q10: 2.33 points). Furthermore, they felt confident while using the proposed BS (Q9: 4.67 points). Overall, participants rated the strategy overall with 70.83±16.65 points (see Table 48), considering it **acceptable (maximum acceptability scale) and almost as "Good"**. The scores per participant were 90 points, 60 points and 62.5 points, respectively. Thus, two participants considered the strategy to be between "Ok" and "Good", while P3 considered the strategy to be "Excellent" [47].

Table 48: SUS scores for the experimental validation of the proposed BS with pathological users

Question	Participants			Mean	Std
	P3	P5	P6		
Acho que gostaria de utilizar este produto com frequência.	5	3	5	**4.33**	**1.15**
Considerei o produto mais complexo do que o necessário.	3	2	4	**3.00**	**1.00**
Achei o produto fácil de utilizar.	5	3	5	**4.33**	**1.15**
Acho que necessitaria de ajuda de um técnico para conseguir utilizar este produto.	3	3	4	**3.33**	**0.58**
Considerei que as várias funcionalidades deste produto estavam bem integradas.	5	3	4	**4.00**	**1.00**
Achei que este produto tinha muitas inconsistências.	1	2	5	**2.67**	**2.08**
Suponho que a maioria das pessoas aprenderia a utilizar rapidamente este produto.	5	2	5	**4.00**	**1.73**
Considerei o produto muito complicado de utilizar.	1	2	2	**1.67**	**0.58**
Senti-me muito confiante a utilizar este produto.	5	4	5	**4.67**	**0.58**
Tive que aprender muito antes de conseguir lidar com este produto.	1	2	4	**2.33**	**1.53**
	90	**60**	**62.5**		

Lastly, the average score was slightly higher for the exergame, with participants P3, P5 and P7 giving

72.50±2.50 points on the SUS scale (see Table 49). In this case, P3 gave a score of 75 points, P5 gave a score of 70 points and P7 gave 72.5 points, **classifying the exergame as "Good"**. Overall, participants considered the exergame easy to use (Q3: 4.33 points, Q8: 1.33 points), although they were neutral about its complexity (Q2: 3.33 points). They also tend to agree that its features were well integrated (Q5: 3.67 points), and it is easy to learn (Q7: 4.67 points, Q10: 1.67 points). Furthermore, they felt confident while using the proposed exergame (Q9: 4.33 points).

Table 49: SUS scores for the experimental validation of the proposed non-immersive VR-based exergame with pathological users

Question	Participants			Mean	Std
	P3	P5	P7		
Acho que gostaria de utilizar este produto com frequência.	5	3	4	**4.00**	**1.00**
Considerei o produto mais complexo do que o necessário.	5	2	3	**3.33**	**1.53**
Achei o produto fácil de utilizar.	5	4	4	**4.33**	**0.58**
Acho que necessitaria de ajuda de um técnico para conseguir utilizar este produto.	4	2	4	**3.33**	**1.15**
Considerei que as várias funcionalidades deste produto estavam bem integradas.	4	3	4	**3.67**	**0.58**
Achei que este produto tinha muitas inconsistências.	3	2	2	**2.33**	**0.58**
Suponho que a maioria das pessoas aprenderia a utilizar rapidamente este produto.	5	4	5	**4.67**	**0.58**
Considerei o produto muito complicado de utilizar.	1	2	1	**1.33**	**0.58**
Senti-me muito confiante a utilizar este produto.	5	4	4	**4.33**	**0.58**
Tive que aprender muito antes de conseguir lidar com este produto.	1	2	2	**1.67**	**0.58**
	75	**70**	**72.5**		

7.5 Discussion

The use of RAGT in the rehabilitation of patients with impaired mobility is still a topic of modern times, since there is still no consensus on its real application in a clinical context [185]. RAGT is widely used in the rehabilitation of patients with mobility disorders [3, 19], including patients diagnosed with CA [20–24]. So far, the results are being promising, but further studies are needed to establish RAGT as a complement to conventional therapy, as some studies are still case reports [20, 23], single-arm studies [24], or retrospective studies [186]. Thus, randomized controlled trials, as presented in [21], are still needed to demonstrate the efficacy of this assisted therapy. In addition, most of the studies are related to acquired CA, so there is still a need to verify if this is also beneficial for patients with inherited CA, which is characterized by progressive motor impairment. To address this issue, this work reports the findings of RAGT in individuals with either acquired or inherited CA. Due to the low number of participants and their heterogeneity, and in order to consolidate the rehabilitation gains obtained from the two interventions,

a patient-by-patient analysis was deemed appropriate to interpret the results in order to draw overall conclusions.

7.5.1 Motor rehabilitation

Participant 1

Participant 1 is a case of acquired ataxia due to ischemic stroke in the cerebellum. Although the participant completed Phase 1 of training, the data collected with the Xsens Awinda system showed issues in at least one of the stages of training, so the main outcomes assessed for this participant were the SARA scale, 10-MWT, TUG and walking speed. This participant first started gait training with the walker and, after the washout, switched to the treadmill. The results show that, for this particular patient, treadmill training was more effective as it led to a decrease in the gait sub-score of the SARA scale, an improvement of in 31% in TUG time and 13% in 10-MWT, as well as an improvement of 14% in gait speed. It is not known whether this increase in gait speed was coupled with an improvement in gait quality, but given the results of the SARA scale, one speculates that it was. With regard to training with the robotic walker, there was a 9% decrease in the TUG scale. This result, considering that no improvement in walking speed was reported, may suggest that the walker enabled an improvement in the process of standing up, sitting down or turning, suggesting a reduction in the risk of falling.

Participant 3

P3 is a case of acquired ataxia due to a tumor in the cerebellum that was surgically removed. The tumor left the participant with balance difficulties, ataxic gait and constant tremors. In terms of locomotion, the participant is unable to walk alone without the strong support of crutches, and has an asymmetrical and very slow gait. She therefore usually uses a wheelchair to move around more quickly.

The participant completed Phase 1 of training, having started with the robotic walker. In addition, she proceeded to Phase 2, having tested the biofeedback strategy and the VR-based exergame. The results of Phase 1 revealed that training with WALKit **was effective** and led to a 5% decrease in the 10-MWT time and a 5% increase in gait speed. This increase in gait speed was accompanied by an expressive improvement in the SR of the step excursion, although still asymmetric. Motion analysis using Xsens Awinda revealed that the participant's asymmetrical gait is linked to her crutch-assisted walking pattern. Specifically, she takes a larger step with her right foot, as she first moves her crutches forward one at a time. This results in a shorter left step. Additionally, a pelvic rotation to the right was observed on day

16, which may have contributed to an increase in left step excursion and a subsequent decrease in SR. The results also showed an increase in both stance and swing time SR. The more evident change in swing time SR may also be linked to the observed pelvic rotation, which increased the left foot's step excursion but simultaneously reduced swing time, as shown in Table 52. With regard to the TUG test, no change was reported on day 16. Comparing gait training on WALKit with treadmill, the latter allowed for a greater increase in gait speed (7.5%), but this increase was accompanied by a worsening in the symmetry of the step excursion, which is not positive. In this case, the pelvic rotation to the right was also detected. An improvement of 3% was also seen in the TUG time.

As for Phase 2, specifically in relation to the biofeedback strategy, the participant showed **improvements in controlling the CoM ML sway**, with a 34% improvement. In fact, the participant showed an imbalance when performing the BBS exercise, but for the great majority of the trial time she managed to control the CoM and reduce the total ROM. In turn, the AP sway increased slightly (4%), which can be a consequence of the more pronounced decrease at ML level. Additionally, she **improved her TUG time** by 3%, while the BBS score remained similar. With regard to the effects of the exergame, it was found that training on the robotic walker and the inclusion of the exergame led to an improvement in exercise 8 of the BBS, even though the participant maintained her score of 1 point. The score did not change because the participant actually needed supervision, both on day 0 and day 16, as she showed tremors that could result in a momentary loss of balance. As for BBS 9, she scored 3 points on day 0, which means that she is able to pick up the object but needs supervision. The fact that the participant reduced the time taken to perform the task may suggest that she tried to do it in a more controlled way so as not to lose her balance. Therefore, on day 16, an improvement in her score of BBS 9 was reported, which suggests that she is able to pick up the object successfully and safely. BBS 10 showed an expressive decrease in rotation to the right side. This behavior can be explained by the fact that on day 0 the participant showed imbalance (an overshoot on vertical acceleration was observed, as suggested by the total ROM of vertical acceleration on day 0, 2.6 m/s^2, in comparison to day 16, 1.2 m/s^2) after rotating from the right side, which led to a score of 1 point on day 0. Thus, on day 16, the participant was perhaps more cautious, only rotating to the left side. Still, this allowed her sub-score improve to 3 points.

Participant 4

Participant 4 is a case of cerebellar atrophy. This participant completed Phase 1, but decided not to continue to Phase 2. In Phase 1, the participant began therapy with treadmill and then switched to WALKit after the washout period. Although it was not possible to evaluate spatiotemporal gait parameters,

the robotic walker proved to be more effective than the treadmill for this particular patient. The results show that **gait speed increased expressively** (29%) post-training with WALKit SRW, while practically no change was observed post-treadmill. Furthermore, this improvement was accompanied by a **marked decrease in TUG time** (28%). Despite requiring a walking aid during both interventions (stable 6-point of SARA gait sub-score), the improvements after training with WALKit SRW suggest increased gait confidence. Moreover, **these results reinforce the robotic walker's ability to improve walking speed and mobility** in general.

Participant 5

P5 is a case of hereditary ataxia (SCA type 8). This participant completed Phase 1 of training and went on to Phase 2, where she tested the biofeedback strategy and the VR-based exergame. The results of Phase 1 showed that WALKit SRW was more effective in terms of reducing the 10-MWT time (12% improvement), TUG (20% improvement) and improving walking speed (14.2%). Moreover, gait quality in terms of spatial metrics did not change between assessment days. Nevertheless, there was a slight worsening in the SR of the step time (from 1.07 to 1.09), but, on average, the step time between feet was closer on day 16, which suggests intra-trial gait variability, typical in ataxic gait [5, 9, 10]. A slight increase in the SR of the stance and swing times was also reported, due to an average difference between feet of 35 ms in the stance time and 28 ms in the swing time. As for TAGT, P5 revealed a decrease of 10-MWT time, but lower in comparison with RAGT (8%), TUG time was similar, and gait speed improved 9%. However, this improvement in gait speed was coupled with an increase of the inter-limb SR of step excursion (from 1.07 to 1.13). As for the temporal parameters, TAGT revealed the same behavior as training with the robotic device. This latter result may suggest that the observed slight increase may not be related to the type of intervention, but perhaps a compensatory mechanism to deal with the increase in speed.

Phase 2 **demonstrated the ability of the biofeedback strategy to improve postural control in tandem stance**. P5 showed an improvement in the CoM ROM, particularly in the AP axis (12% improvement), while in the ML axis there was only an overall improvement of 3%. However, the bipedal stance results show a worsening of the ML ROM, which was probably influenced by external factors, such as occasional interaction with the therapist or involuntary movements by the participant since P5 maintained her score of 4 points (the maximum of BBS 2 and 7).

Improvements were also identified in the participant's balance after training with the VR-based exergame, especially in BBS 8, where a 23% increase was reported on the distance the participant was able to reach. In addition, she obtained a score of 4 on both day 0 and day 16. Although she was not able to

reach 25 cm on either day 0 or day 16, she received a score of 4 instead of 3 because she has always been autonomous, confident, and does not need supervision or assistance. The participant reported a ruptured ligament in her shoulder at that time, which made it impossible for her to reach a higher distance due to some pain. However, it was considered that without the ruptured shoulder ligament, the participant would be able to complete exercise 8 of the BBS with a score of 4. Lastly, there were also improvements in TUG time (−14%) and an overall improvement of 2 points in BBS, **revealing improvements on balance**.

Participant 6

P6 is a case of CA caused by mychondrial cytopathy, which is a hereditary condition. The participant completed Phase 1 and began the training with the treadmill. She then proceeded to Phase 2 training in which she experienced the biofeedback strategy for postural control.

With regard to the results of Phase 1, the robotic walker led to a more marked improvement in the 10-MWT (−10%), the TUG (−8%) and gait speed (12%). As for TAGT, 10-MWT reduced 3%, TUG increased 15%, and gait speed increased 3%. The increase in walking speed after RAGT was accompanied by an improvement in the SR of the step time, but the SR of the step excursion increased slightly, motivated by a difference of almost 5 cm. Indeed, analyzing the average step excursion presented in Appendix C.1, the increase in the SR was motivated by a larger increase in the left step excursion (8.49% on average) compared to the right step (+3.83% on average). This result, together with the increase in overall walking speed, suggests that P6 may have created a compensatory mechanism that negatively influenced the SR for step excursion. Perhaps this could be motivated by the participant's instability on the AP axis (mainly posterior), which affects the way she walks with her walking aid.

With regard to Phase 2, it was found that the **biofeedback strategy was effective in reducing the total ROM of the CoM in the AP axis** (−26%), where the participant reveals more imbalances. However, a slight increase was reported for the ML axis. Still, the strong result for the AP axis, together with the results of P5, suggests that gait and balance rehabilitation with the robotic walker is **suggestive of improvement for patients with CA of hereditary etiology**.

Participant 7

P7 is a case of gait ataxia acquired as a result of traumatic brain injury and spinal cord injury. This participant started Phase 1 on the robotic walker and then continued to Phase 2, where he tested the VR-based exergame. He is currently in an intervention phase with the biofeedback strategy for postural control.

Regarding Phase 1, P7 showed more substantial improvements in the 10-MWT (−31%) and TUG (−22%) times, considering the TAGT. In addition, there was a considerable increase in speed of nearly 43%. However, this increase in speed was not beneficial as the participant showed a more asymmetrical gait in terms of step excursion after TAGT. Furthermore, he also exhibited an increase in step time asymmetry, which indicates that post-TAGT gait quality was not achieved. The same did not happen in post-RAGT. Although the increase in speed was more modest, **but still substantial** (25%), there was a **marked improvement in asymmetry of step excursion** (day 0: 1.74 ± 0.17; day 16: 1.12 ± 0.06) and a slight improvement regarding step time (day 0: 1.09 ± 0.05; day 16: 1.06 ± 0.03). Although the latter decrease is small, the average step time for both feet, as presented in Table 52 of Appendix C.1, show that on day 0, the step time of the right foot was larger than that of the left foot. After training with the robotic walker, there was a decrease in the right step time of -4.6%, while the average left step time increased by $+5.3\%$. This brought the times closer together, explaining the slight decrease in the SR. In addition, considering the SR obtained by the average step times, the gait is suggestive of being symmetrical, so the result obtained for the average SR may also be at the limit of what is considered symmetrical.

Regarding Phase 2, the results suggest that the use of the exergame was positive. The participant showed an **improvement in BBS 8 (21%)**, in BBS 9 by performing the movement in a **slower and more controlled way which allowed the score to increase to 4 points**, and in **BBS 10 (20.5% on average)**. Additionally, the overall BBS score increased 2 points (6%), proving a **slight improvement in balance**.

7.5.2 Usability and acceptability

Usability scores showed high acceptance, with average SUS scores above 70 points, classifying the device as "Good" and "Acceptable" [47]. Participants found the device and HRI strategies intuitive, though patients reported some shortcomings: **i)** hard elbow pads, **ii)** handlebars causing hand discomfort, and **iii)** difficulty seeing the biofeedback blue dot due to limited screen coverage. Addressing these issues could boost usability above 85, rating the device as "excellent."

7.6 General Conclusion

This chapter presents a clinical study to validate the use of WALKit SRW as rehabilitation device for patients with balance disorders, in particular patients diagnosed with CA, either acquired or hereditary. To do so, a clinical protocol was implemented considering a total of six ataxic patients, divided into two

phases. The main goal of the first phase was to validate the robotic walker as a rehabilitation device and compare the gain obtained with treadmill-assisted gait training. The second phase consisted of validating a biofeedback strategy developed specifically to train postural control, and a non-immersive VR-based exergame whose aim is to train posture and balance by encouraging weight transfer along the AP and ML axes.

With regard to phase 1 of training, it was found that the robotic walker led to an **increase in gait speed combined with an improvement in gait quality** for most of participants, considering specific spatial and temporal gait metrics. Gait quality was not as noticeable after treadmill training, especially considering the SR of the step excursion. Additionally, an improvement in the TUG scale was reported for both RAGT with WALKit and TAGT, but this was more evident during training with the robotic walker. Overall, the results of this clinical intervention allowed to achieve KPI 9, mainly due to the improvements observed in 10-MWT, TUG, gait speed, and gait quality after training with WALKit SRW.

As for phase 2 of the training, it was found that the combined use of the robotic walker and the biofeedback strategy **enabled to control the movement of the CoM**, especially in the ML axis for P3 (while a small increase was observed in the AP axis) and in the AP axis for P6 (while a small increase as observed in the ML axis). Regarding P5, the biofeedback strategy was found to be important in **improving the tandem stance**, where there was an average decrease in CoM sway in both axes, although more pronounced in the AP axis. Regarding the exergame, it was found that all three participants improved the overall BBS score. Moreover, they managed to reach a greater distance in BBS 8, which shows **an improvement in the AP weight transfer**. In addition, in BBS 9, participants P3 and P7 tried to control the movement, which explains the increase in time to pick up the object, while P5, who is autonomous, was able to pick up the object more quickly. Finally, in BBS 10, only P7 showed improvements in backward trunk rotation. With regard to usability and acceptability, the results showed that, in general, the participants considered the device **to be acceptable (maximum on the acceptability scale)**, as well as for the biofeedback strategy and the exergame, with **usability scores above 70 points on average**. Overall, these results allowed to achieve KPI 7 and 8.

Chapter VIII

General Overview

Chapter 8

Main Conclusions

This doctoral thesis presents the work performed over the last four years on the robotic walker formerly known as the ASBGo Smart Walker. This walker, started in 2011 and funded through the EML R&D project, consists of a multi-functional assistive device whose main goal is to help rehabilitate individuals with CA. Depending on the severity and type of ataxia, these patients suffer from a variety of symptoms, including speech and vision difficulties, tremors, lack of motor coordination and balance disorders, greatly reducing their QoL [5, 8–11, 14]. Additionally, in severe cases of degenerative ataxia, patients end up in wheelchairs, strongly restricting their autonomy. Currently, there is no approved pharmacological treatment for inherited ataxia [15], while acquired ataxia can generally be improved with a long rehabilitation process. Patients therefore require intensive physical intervention to maintain motor function [10, 16]. RAGT is being introduced in the rehabilitation of patients with CA [20–24], and the results are encouraging to pursue its development. Therefore, the ultimate goal of this doctoral thesis was to present the next generation of ASBGo Smart Walker, presently known as WALKit Smart Walker. This new device, with renewed and innovative software and features, aims to establish itself as a high-tech device to complement the rehabilitation programs of individuals with CA by analyzing the user's gait, posture and balance.

This doctoral thesis allowed for the reformulation of the device's software (OB. 2), especially a new GUI, which proved to be very important in allowing the device to be easily and intuitively used by clinicians. This step was crucial to enable the device to be used in a clinical setting (OB. 6) and to integrate new functionalities in a modular and more intuitive way. The software redesign was based on the best practices of software development processes that are reported in literature (Chapter 3). Furthermore, this doctoral thesis enabled to develop an intuitive clinical support and feedback tool for clinicians, which can be used to manage the rehabilitation programs involving the robotic walker and to analyze the data collected using the many different sensors that the device includes in its structure (Chapter 3 and OB. 2).

Moreover, this doctoral thesis focused on making this device more user-compliant, attempting to give the device the intellect to detect the user's MI (Chapter 4 and OB. 3) in order to provide seamless

assistance based on intuitive HRC. The purpose was to devise novel control strategies based on the HIL concept, in which the human has a major role in controlling the device solely through his/her gait, thus allowing the user to focus on his/her therapy and attempt to improve and optimize torso and gait posture (Chapter 5 and OB. 4). Therefore, this thesis allowed to study different DL-based approaches to decode the intention of walk, stop and turn using real-time RGB frames of gait, seeking to obtain a model with high accuracy, precision and sensitivity (Chapter 4 and OB. 3). Although the results proved it is possible to early recognize the MI with an accuracy of over 90% across all the models studied, it was found that these models have some difficulty in detecting the intention to curve solely by analyzing the user's gait, sometimes diverting the focus to the background. It was therefore realized that it would be difficult to detect the turn event in real-time so, as a first phase, gait images were used to only detect the intent of walk and stop. Using this information, a HIL control strategy was developed whose primary goal was to set velocity commands that serve as the reference of a proportional controller that is responsible for controlling the device's wheels velocity. Although the strategy is functional and does not present a significant delay ($<$0.64s on average), which is positive, it still does not provide assistance to the user in turning events. Thus, in future, new ways of detecting the MI should be investigated, using, for example, the integration of other sensors, such as the RGB posture camera or the device's load cells, although load cells present similar difficulties to force sensors.

Given that WALKit users are mostly individuals who present poor motor coordination, this doctoral thesis also presents the validation of a novel RL-based shared control strategy, based on the concept of AAN, in which the walker analyzes the user's MI and the environment in general with a 2D laser, and uses a RL-based model to decide whether or not to activate an ADS to help users achieve a predefined goal or simply because it considers that they are not safe (Chapter 5). The novelty of this approach lies in its ability to continuously learn and optimize from each user interaction and make intelligent decisions about when and how to assist the user. The validation proved that the proposed control strategy is effective and enables a closer and intuitive HRI and HRC, with URC values above 60%, which reveals an active participation of the user in the device's control.

This doctoral thesis also focused on integrating novel, more technological functionalities, namely biofeedback strategies to control the CoM's movement and an non-immersive VR-based exergame to improve users' balance (Chapter 6 and OB. 5). The biofeedback strategy integrates sensor fusion monitoring algorithms to estimate the orientation of the user's torso, using data collected in real time by a single inertial device (IMU) placed at the L3—L5 lumbar vertebra. The strategy was validated with 7 healthy participants, analyzing the effect of biofeedback when it is enabled. For this purpose, it was assessed whether

the proposed strategy generates any compensatory mechanism in the user so as to correct his/her posture and whether it is also capable of reducing the CoM's sway. Additionally, users considered the strategy functional and easy-to-use, with an averaging score of 85 points considering SUS. As for the non-immersive VR-based exergame, this HRI strategy aims to increase the users balance, but also can be used as a BS of posture, using the IMU or load cells. The exergame, created in the Unity engine and integrated into the robotic walker, was validated with 10 healthy participants to assess mainly usability and functionality. Users found the exergame fun and appealing. Furthermore, a large majority found it challenging. Both the interactive game and the biofeedback strategy are completely adaptable in real time and can be used with a wide range of users. The adjustment is performed by the physiotherapist in charge, based on the patient's progress throughout the rehabilitation process.

Lastly, the new generation of the robotic walker was tested in a real-life context with end users, namely six pathological individuals diagnosed with CA (Chapter 7 and OB. 6). The experimental protocol, which was accepted by the Ethics Committee of Braga Hospital (CESHB-135/2016, final form under addendum CEHB 216/2023), was performed at 2CA-Braga, and consisted of two training blocks, designated phase 1 and phase 2.

Phase 1 validated gait training with the robotic device and compared the gain/loss in rehabilitation with treadmill gait training. The results demonstrated that the robotic walker enabled an increase in gait speed for five of the six participants. Furthermore, three participants (of the four analyzed regarding the spatiotemporal parameters) maintained or reduced the existing asymmetry in step excursion while increasing their gait speed. However, for one participant, the increase in gait speed was associated with a slight increase in the step excursion ratio. Additionally, an improvement in the TUG scale was reported after gait training with both interventions, but this was more evident during RAGT with WALKit SRW.

Phase 2 consisted of validating two HRI strategies, namely the biofeedback strategy for postural control and the exergame for balance training, with three pathological individuals. Overall, the combined effect of RAGT with WALKit and the biofeedback strategy generally led to a post-training decrease in CoM sway, although some situations of no change or a slight increase were also reported. However, only one participant increased the BBS score, while the others maintained. Regarding the TUG time, two participants slightly decreased their time by a maximum of 3%. Regarding the combined effect of RAGT and the exergame for balance training, this intervention enabled the participants to perform the weight transfer more safely, improving the overall BBS score and allowing an overall decrease in the TUG time.

8.1 Research Questions

The work presented in this doctoral thesis made it possible to answer the six research questions presented in Chapter 1.

RQ. 1: How can the motion intention be decoded in a more intuitive way and be used to foster personalized assistance?

Chapter 4 approaches this research question by presenting several DL-based approaches for early detection of the user's MI in real time while walking with WALKit SRW. In fact, direct and indirect ways of decoding MI are reported in the literature. Usually, direct ways involve user-specific interaction by applying force (physical interaction [48]), considering force or pressure sensors, while indirect ways analyze human motion, either with IMU, laser technology, cameras, or proximity sensors. In this thesis, an indirect method was used to decode the MI, using a camera to analyze the user's gait in real time. Different DL-based approaches have been studied, using CNNs that have been widely studied in the literature for activity classification, namely ResNet-50 and an adaptation of VGG16. Furthermore, different inputs were studied, namely *DIF* and *ADD*, optionally cropped to a human ROI, considering a stack of 4 RGB frames. The first highlights the main differences between the last and first frames of the stack, using CNN networks (ResNet-50 and adapted VGG16) as feature extractors to further classify the walking, stopping, and turning activities. The second allows for the creation of a kind of drag image that allows the user's movements to be perceived. This technique was chosen to incorporate the information from 4 frames into a single RGB frame in order to reduce the computational complexity of the AI model. In this way, the model would be provided with spatial and temporal gait information considering a single RGB frame, which was considered essential for decoding intention.

Although results were favorable for rapid recognition of MI, it was found that the model sometimes focuses on background information. Indeed, the background also proved to be important, which makes sense because the walker is not static, only the camera is in relation to the device's structure. Therefore, this chapter also presented the study of two channel-wise attention mechanisms and a spatial attention mechanism. Additionally, it also investigates the use of an adapted U-Net to classify activities. Furthermore, it presents ablation studies, one in which the background was removed, and another in which the background was replaced by random backgrounds of hospital environments. The results showed a greater ability to focus on the user, but still insufficient to distinguish the events of turning and walking forward without resorting to additional information. Even so, the results showed that using cameras, it is possible to distinguish the different activities, but ways of redirecting the model's focus solely to the user should

be investigated. The integration of such a model would be relevant because it would allow the user to intuitively drive the device without additional cognitive effort as the MI is provided by their natural gait. Moreover, by assessing human gait, this strategy would encourage the users' active participation in therapy, would increase their autonomy and sense of involvement and control of the device, and would enable them to fully concentrate on their gait performance.

Chapter 5 also addresses this research question by proposing a HIL control strategy to control WALKit SRW using an AI model to detect the user MI. However, while testing the integration of the model into the robotic device, it was found that, although the model was able to classify activities with high accuracy, detecting curves revealed difficult in real-time. This is because the model sometimes confuses walk and turn activities by only analyzing the user's gait. Furthermore, the fact that the model sometimes uses the background to classify the activity also makes the task of detecting the curves more difficult since, in real time, it is only possible to obtain the first moments of the activity, which is where the intention is firstly provided. During the training process, the first 40 frames of the action were given, but transitions were avoided so as not to mislead the model when classifying the activity. Although MI is given at every moment while a certain activity is being undertaken, the set of initial frames that differentiate the turn from the straight walk are dubious to the model, which is why there was some delay in detecting the intention. In addition, it was found that the model sometimes focuses on the orientation of the floor lines to confirm the turning action, but besides this is not extracted from the user, it is only valid offline and is not obtained in real time during the first moments of the activity.

Additionally, this chapter presents the validation of a RL-based control strategy that aims to ensure the user's safety by analyzing their MI and the surrounding environment. The strategy implements the PPO algorithm, based on the Actor-Critic configuration, to estimate an α parameter responsible for sharing control between the human and the user. In situations of danger and insecurity for the user, or when the user is not fulfilling a defined goal, the value of α increases, activating the autonomous mode. Whenever the RL model considers that the user's movement intentions are safe and enable the proposed goal to be achieved, the α levels decrease, emphasizing manual control. In this way, this strategy follows closely the AAN concept, assisting the user whenever necessary and with the required amount by varying α in real time. The validation was performed against the use of autonomous mode, and it was found that the implemented control strategy gives users more freedom while ensuring their safety at all times. The strategy was found to be able to divert the walker away from permanent and dynamic obstacles by activating the autonomous driving mode. Even so, this control strategy has only been tested when the motion intentions are provided directly by the user via the handlebar specially designed for ataxic patients. Once it

is possible to ensure full assistance by indirectly decoding motion intentions, it will be possible to combine the proposed HIL strategy with the AAN shared control strategy.

RQ. 2: How to encourage the user's active participation in therapy while reducing the workload of the physiotherapist?

This research question was addressed in Chapters 5 and 6. In fact, besides the main goal of developing a multi-functional and effective device for the rehabilitation of ataxic patients, another goal is to reduce the burden of physical therapy. This can be achieved by introducing robot-assisted therapy as a complement to conventional therapies. Furthermore, the use of HRI and HRC strategies could be extremely helpful in captivating the patient's attention, encouraging active participation in therapy, and stimulating movement perception and self-correction. Therefore, this doctoral thesis presents two control strategies that collect the user's intention to move and analyze whether their behavior is safe and correct. The physiotherapist only needs to designate a location goal and the user can freely perform their gait training, always having the autonomous mode on standby in case of need. This control strategy can be combined with the use of those HRI strategies presented in Chapter 6, namely the biofeedback strategy or the non-immersive VR-based exergame. Both strategies allow users to have a visual perception of their movement, knowing if they are performing it correctly, which stimulates their self-correction. In addition to the possible advantages for patients, these novel strategies implemented in WALKit SRW highlight this device as a valuable complementary tool to standard of care, relieving the pressure on healthcare systems and improving the clinicians' well-being.

RQ. 3: How does multimodal biofeedback affect postural sway control of users?

This research question was addressed in Chapters 6 and 7. Chapter 6 presents a research study involving healthy users on the use of the biofeedback strategy to control postural sway and indirectly decrease the CoM sway. The results with seven individuals suggested that the proposed biofeedback strategy was indeed capable of controlling users' postural sway by creating compensatory mechanisms in order to maintain within the predefined safety region. Additionally, it was found that the proposed strategy enabled a significant decrease on the CoM's AP and ML sway considering data acquired with Xsens MVN Awinda, specially for bipedal and tandem stance exercises.

Since this validation involved healthy individuals, the post-training effect was not verified, but rather the effect during training. However, in the validation study with three ataxic patients, the combined effect of the biofeedback strategy and gait training provided by the robotic walker was studied. The results varied

from patient to patient. With regard to the bipedal stance exercise, there was a marked decrease in the CoM sway at the ML level for participant P3, while for the AP axis, there was a slight increase of 4%; and a marked decrease in the CoM AP sway for participant P6, while for the ML axis a slight increase was observed. With regard to the participant P5, this maintained the AP sway, but increased slightly at ML level, possibly explained by other factors (communication, hand movement, etc). Even so, the participant revealed the same behavior for bipedal stance with her feet together, again possibly justified by other factors. Regarding tandem stance, participant P5 showed very positive results, with a decrease in the CoM sway, both AP and ML, but more expressive when the participant holds her weight on her left leg. Overall, the results are positive but need to be further validated with a more homogeneous and larger population.

RQ. 4: How usable and functional is WALKit Smart Walker?

This research question was addressed in Chapters 3 and 7. Chapter 3 presents the validation of the robotic walker in terms of software, involving stakeholders from the Braga and Guimarães hospitals. The results showed that the renewed graphic interface achieved high levels of acceptability and usability, with an average score of 84 points (out of 100) on the SUS scale. The clinical support and feedback tool achieved almost 96 points on the SUS scale. The results therefore allow one to conclude that the robotic walker, in terms of software, was considered intuitive and easy to use.

Regarding the use of the device by patients with CA, the results of Chapter 7 reveal high levels of usability and technology acceptability, with an average score of 75 points (out of 100) on the SUS scale. Patients reported some shortcomings, but not related to the renovated software, but regarding the structure of the device, namely: **i)** the elbow pads that they found to be very hard, causing discomfort with prolonged use, and **ii)** they considered that the handlebar occasionally began to cause discomfort to the hands. Regarding the handlebar, the complaints were occasional, however the strategy of indirectly decoding MI could mitigate this issue.

Participants also evaluated their experience with the new HRI and HRC strategies, and the results were also positive, with an average score of 71 points for the biofeedback strategy and 73 points for the exergame.

RQ. 5: How does RAGT with WALKit Smart Walker affects motor rehabilitation of patients with cerebellar ataxia?

This research question was addressed in Chapter 7. This doctoral thesis enabled the implementation of a clinical intervention protocol at 2CA-Braga to validate the robotic walker in terms of usability and

functionality. A longitudinal randomized crossover study was implemented to compare the effects of RAGT with treadmill-assisted gait training in a first phase, and to validate the proposed HRI strategies presented and discussed in Chapter 7, as a second phase.

Regarding the first phase of the study, the SARA scale was evaluated, along with the 10-MWT and TUG tests. From the 10-MWT test, spatial and temporal gait parameters were assessed. With the regard to the SARA scale, only the sub-scale of gait, stance, and sitting were evaluated since these are directly trained during the rehabilitation sessions with WALKit SRW. The findings suggest that, overall, there seems to be no difference between RAGT with the robotic walker and treadmill training. However, these are not very conclusive, so the gain in speed and gait quality was verified. Regarding gait speed, the gain was notorious after training with WALKit SRW. Additionally, two participants reduced the existing asymmetry in step excursion, while another one maintained the ratio for a higher gait speed, and another one slight increased the step excursion ratio, although it is not known if it holds clinical significance. Regarding the step time, results also suggest that RAGT with WALKit SRW was benefic for two patients that decreased their average symmetry ratio while increasing gait speed. As for the TUG test, improvements on day 16 were found for both RAGT and treadmill-assisted training, although the decrease with WALKit SRW was more evident.

Concerning to phase two of the intervention protocol, the BBS score and TUG time were evaluated for both the biofeedback strategy and the serious exergame. Additionally, strategy-specific exercises were evaluated considering the BBS scale. The results suggest that the BS was indeed benefic to decrease the overall sway of the CoM, although not consistent across participants. P3 revealed a decrease in terms of ML axis, while no improvement was verified regarding the AP axis. As for P6, a marked improvement was verified considering the AP axis which is, in fact, the primary axis of the patient's imbalance. Regarding P5, no change was found for the AP axis, although slight increases were found for the ML axis, but this could be due to external sources of distracting since this patient is completely autonomous. A marked difference was found on tandem stance for this particular participant, with improvements regarding both AP and ML axes. As for the serious exergame, results were also positive, with improvements on the specific exercises 8, 9, and 10 of BBS. Furthermore, regarding the overall BBS score, this has increased for all three participants on day 16, which indicates that the proposed strategy improved the participants' balance. Although the results are positive, a more in-depth study needs to be performed, with a more homogeneous population and considering a larger number of ataxic participants.

8.2 Future Perspectives

In terms of future work, there are several next steps. First, an attempt should be made to improve the AI model to decode the MI so that it focuses only on the user. To do this, a new dataset should be created with more participants, including pathological participants, with different backgrounds. The possibility of sensory fusion should be explored to distinguish between turning and walking forward, allowing full assistance in real time. Furthermore, although the AI model runs on the hardware of the robotic walker, the use of knowledge distillation should be considered to reduce the complexity of the neural network, allowing other models or algorithms to work effectively in parallel.

In terms of control strategies, the fusion of HIL and AAN shared control strategies should be investigated, allowing for a complete assistance tailored to the real needs of the user, in a more intuitive way, with low cognitive effort and without additional tasks. In addition, further HRI and HRC strategies should be developed to maximize the user's active participation in the therapy while reducing the monotony sometimes felt by the user. In particular, a visual biofeedback strategy should be developed for gait training that provides the user with spatial awareness and allows them to engage in other tasks such as proper foot positioning and orientation to control step length and width.

Finally, the intervention study should be continued and a multicenter approach should be attempted to maximize the recruitment of participants with hereditary ataxia into the study. Efforts should be made to homogenize the group of patients recruited so that it is possible to perform not only an individual analysis but also a group analysis, thus increasing the strength of the results and the conclusions drawn.

Bibliography

[1] World Health Organization. Disability – a global picture. In *World Report on Disability*, pages 19–55. 2011. Available online: `https://www.who.int/publications/i/item/9789241564182` (accessed on 2025-01-23).

[2] World Health Organization. Disability and Health, 2024. Available online: `https://www.who.int/news-room/fact-sheets/detail/disability-and-health` (accessed on 2025-01-23).

[3] Tadeusz Mikolajczyk, Ileana Ciobanu, Doina Ioana Badea, Alina Iliescu, Sara Pizzamiglio, Thomas Schauer, Thomas Seel, Petre Lucian Seiciu, Duncan L. Turner, and Mihai Berteanu. Advanced technology for gait rehabilitation: An overview. *Advances in Mechanical Engineering*, 10(7), jul 2018.

[4] Walter Pirker and Regina Katzenschlager. Gait disorders in adults and the elderly. *Wiener klinische Wochenschrift*, 129(3-4):81–95, feb 2017.

[5] Winfried Ilg and Dagmar Timmann. Gait ataxia—specific cerebellar influences and their rehabilitation. *Movement Disorders*, 28(11):1566–1575, sep 2013.

[6] Tiago Gomes, Joana Guimarães, Miguel Leão, Carla Moura, Carolina Garrett, Elsa Azevedo, João Massano, and João Paulo Oliveira. Investigation of Genetic Aetiology in Neurodegenerative Ataxias: Recommendations from the Group of Neurogenetics of Centro Hospitalar São João, Portugal. *Acta Medica Portuguesa*, 30(6):502–512, 2017.

[7] Luis Ruano, Claudia Melo, M. Carolina Silva, and Paula Coutinho. The Global Epidemiology of Hereditary Ataxia and Spastic Paraplegia: A Systematic Review of Prevalence Studies. *Neuroepidemiology*, 42(3):174–183, 2014.

[8] Ellen Buckley, Claudia Mazzà, and Alisdair McNeill. A systematic review of the gait characteristics associated with Cerebellar Ataxia. *Gait & Posture*, 60(November 2017):154–163, feb 2018.

[9] Carmela Conte, Francesco Pierelli, Carlo Casali, Alberto Ranavolo, Francesco Draicchio, Giovanni Martino, Mahmoud Harfoush, Luca Padua, Gianluca Coppola, Giorgio Sandrini, and Mariano Serrao. Upper Body Kinematics in Patients with Cerebellar Ataxia. *Cerebellum*, 13(6):689–697, 2014.

[10] Jonathan F. Marsden. Cerebellar ataxia. In *Handbook of Clinical Neurology*, volume 159, pages 261–281. Elsevier B.V., 1 edition, 2018.

[11] Dung Phan, Nhan Nguyen, Pubudu N. Pathirana, Malcolm Horne, Laura Power, and David Szmulewicz. Quantitative Assessment of Ataxic Gait using Inertial Sensing at Different Walking Speeds. In *2019 41st Annual International Conference of the IEEE Engineering in Medicine and Biology Society (EMBC)*, pages 4600–4603. IEEE, jul 2019.

[12] Mariano Serrao and Carmela Conte. Detecting and measuring ataxia in gait. In *Handbook of Human Motion*, pages 937–954. Springer International Publishing, Cham, 2018.

[13] Bart P.C. van de Warrenburg, Janneke A.G. Steijns, Marten Munneke, Berry P.H. Kremer, and Bastiaan R. Bloem. Falls in degenerative cerebellar ataxias. *Movement Disorders*, 20(4):497–500, apr 2005.

[14] Rui Moreira, Joana Alves, Ana Matias, and Cristina Santos. Smart and Assistive Walker – ASBGo: Rehabilitation Robotics: A Smart– Walker to Assist Ataxic Patients. In John M. Archibald, Alastair G.B. Simpson, Claudio H. Slamovits, Lynn Margulis, Michael Melkonian, David J. Chapman, and John O. Corliss, editors, *Robotics in Healthcare. Advances in Experimental Medicine and Biology.*, pages 37–68. Springer International Publishing, Cham, 2016.

[15] Geneieve Tai, Louise A. Corben, Eppie M. Yiu, Sarah C. Milne, and Martin B. Delatycki. Progress in the treatment of Friedreich ataxia. *Neurologia i Neurochirurgia Polska*, 52(2):129–139, 2018.

[16] A. Marquer, G. Barbieri, and D. Pérennou. The assessment and treatment of postural disorders in cerebellar ataxia: A systematic review. *Annals of Physical and Rehabilitation Medicine*, 57(2):67–78, mar 2014.

[17] Sarah C. Milne, Louise A. Corben, Nellie Georgiou-Karistianis, Martin B. Delatycki, and Eppie M. Yiu. Rehabilitation for Individuals with Genetic Degenerative Ataxia: A Systematic Review. *Neurorehabilitation and Neural Repair*, 31(7):609–622, 2017.

[18] Karla Tercero-Pérez, Hernán Cortés, Yessica Torres-Ramos, Roberto Rodríguez-Labrada, César M. Cerecedo-Zapata, Oscar Hernández-Hernández, Nelson Pérez-González, Rigoberto González-Piña,

Norberto Leyva-García, Bulmaro Cisneros, Luis Velázquez-Pérez, and Jonathan J. Magaña. Effects of Physical Rehabilitation in Patients with Spinocerebellar Ataxia Type 7. *The Cerebellum*, 18(3):397–405, jun 2019.

[19] Eva Swinnen, David Beckwée, Romain Meeusen, Jean-Pierre Baeyens, and Eric Kerckhofs. Does Robot-Assisted Gait Rehabilitation Improve Balance in Stroke Patients? A Systematic Review. *Topics in Stroke Rehabilitation*, 21(2):87–100, mar 2014.

[20] Gianfranco Lamberti, Gianluca Sesenna, Martina Marina, Emanuela Ricci, and Gianluca Ciardi. Robot Assisted Gait Training in a Patient with Ataxia. *Neurology International*, 14(3):561–573, jun 2022.

[21] Marcia Belas dos Santos, Clarissa Barros de Oliveira, Arly dos Santos, Cristhiane Garabello Pires, Viviana Dylewski, and Ricardo Mario Arida. A Comparative Study of Conventional Physiotherapy versus Robot-Assisted Gait Training Associated to Physiotherapy in Individuals with Ataxia after Stroke. *Behavioural Neurology*, 2018:1–6, 2018.

[22] Juntaek Hong, Jongweon Lee, Taeyoung Choi, Wooin Choi, Taeyong Kim, Kyuwan Kwak, Seongjun Kim, Kyeongyeol Kim, and Daehyun Kim. Feasibility of Overground Gait Training Using a Joint-Torque-Assisting Wearable Exoskeletal Robot in Children with Static Brain Injury. *Sensors*, 22(10):3870, may 2022.

[23] Myungeun Yoo, Jeong Hyeon Ahn, and Eun Sook Park. The Effects of Over-Ground Robot-Assisted Gait Training for Children with Ataxic Cerebral Palsy: A Case Report. *Sensors*, 21(23):7875, nov 2021.

[24] Akira Matsushima, Yoichi Maruyama, Noriaki Mizukami, Mikio Tetsuya, Minoru Hashimoto, and Kunihiro Yoshida. Gait training with a wearable curara® robot for cerebellar ataxia: a single-arm study. *BioMedical Engineering OnLine*, 20(1):90, dec 2021.

[25] Anselmo Frizera Neto, Arlindo Elias, Carlos Cifuentes, Camilo Rodriguez, Teodiano Bastos, and Ricardo Carelli. Smart Walkers: Advanced Robotic Human Walking-Aid Systems. In Samer Mohammed, Juan C. Moreno, Kyoungchul Kong, and Yacine Amirat, editors, *Intelligent Assistive Robots*, volume 106 of *Springer Tracts in Advanced Robotics*, pages 103–131. Springer International Publishing, Cham, 2015.

[26] Sara M. Bradley and Cameron R. Hernandez. Geriatric assistive devices. *American Family Physician*, 84(4):405–411, 2011.

[27] Gerard J. Lacey and Diego Rodriguez-Losada. The Evolution of Guido. *IEEE Robotics & Automation Magazine*, 15(4):75–83, dec 2008.

[28] Andrew J. Rentschler, Richard Simpson, Rory A. Cooper, and Michael L. Boninger. Clinical evaluation of Guido robotic walker. *The Journal of Rehabilitation Research and Development*, 45(9):1281, 2008.

[29] C. Barrué, R. Annicchiarico, U. Cortés, A. Martínez-Velasco, E. X. Martín, F. Campana, and C. Caltagirone. The i-walker: An intelligent pedestrian mobility aid. In Isabelle Bichindaritz, Sachin Vaidya, Ashlesha Jain, and Lakhmi C. Jain, editors, *Computational Intelligence in Healthcare 4: Advanced Methodologies*, pages 103–123. Springer Berlin Heidelberg, Berlin, Heidelberg, 2010.

[30] U. Cortés, A. Martínez-Velasco, C. Barrué, E. X. Martín, F. Campana, R. Annicchiarico, and C. Caltagirone. Towards an intelligent service to elders mobility using the i-Walker. *AAAI Fall Symposium - Technical Report*, FS-08-02:32–38, 2008.

[31] Geunho Lee, Takanori Ohnuma, and Nak Young Chong. Design and control of JAIST active robotic walker. *Intelligent Service Robotics*, 3(3):125–135, jul 2010.

[32] Geunho Lee, Eui-Jung Jung, Takanori Ohnuma, Nak Young Chong, and Byung-Ju Yi. Jaist robotic walker control based on a two-layered kalman filter. In *2011 IEEE International Conference on Robotics and Automation*, pages 3682–3687, 2011.

[33] Ming-Fang Chang, Wei-Hao Mou, Chien-Ke Liao, and Li-Chen Fu. Design and implementation of an active robotic walker for parkinson's patients. In *2012 Proceedings of SICE Annual Conference (SICE)*, pages 2068–2073, 2012.

[34] Eleni Efthimiou, Stavroula-Evita Fotinea, Theodore Goulas, Athanasia-Lida Dimou, Maria Koutsombogera, Vassilis Pitsikalis, Petros Maragos, and Costas Tzafestas. The mobot platform – showcasing multimodality in human-assistive robot interaction. In Margherita Antona and Constantine Stephanidis, editors, *Universal Access in Human-Computer Interaction. Interaction Techniques and Environments*, pages 382–391, Cham, 2016. Springer International Publishing.

[35] João Paulo, Paulo Peixoto, and Urbano J. Nunes. ISR-AIWALKER: Robotic Walker for Intuitive and Safe Mobility Assistance and Gait Analysis. *IEEE Transactions on Human-Machine Systems*, 47(6):1110–1122, dec 2017.

[36] Sergio D. Sierra, Juan F. Molina, Daniel A. Gómez, Marcela C. Múnera, and Carlos A. Cifuentes. Development of an interface for human-robot interaction on a robotic platform for gait assistance: Agora smart walker. In *2018 IEEE ANDESCON*, pages 1–7, 2018.

[37] Sergio D. Sierra M., Mario Garzón, Marcela Múnera, and Carlos A. Cifuentes. Human–Robot–environment interaction interface for smart walker assisted gait: AGoRA walker. *Sensors (Switzerland)*, 19(13):1–29, 2019.

[38] João André, João Lopes, Manuel Palermo, Diogo Gonçalves, Ana Matias, Fátima Pereira, José Afonso, Eurico Seabra, João Cerqueira, and Cristina Santos. Markerless gait analysis vision system for real-time gait monitoring. In *2020 IEEE International Conference on Autonomous Robot Systems and Competitions (ICARSC)*, pages 269–274, 2020.

[39] Martins Martins, Cristina P Santos, Solenne Page, Ludovic Saint-Bauzel, Viviane Pasqui, and Anthony Mézière. Real-time gait assessment with an active depth sensor placed in a walker. In *2015 IEEE International Conference on Rehabilitation Robotics (ICORR)*, pages 690–695, 2015.

[40] Chung Dial Lim, Chia-Ming Wang, Ching-Ying Cheng, Yen Chao, Shih-Huan Tseng, and Li-Chen Fu. Sensory cues guided rehabilitation robotic walker realized by depth image-based gait analysis. *IEEE Transactions on Automation Science and Engineering*, 13(1):171–180, 2016.

[41] João Paulo, Alireza Asvadi, Paulo Peixoto, and Paula Amorim. Human gait pattern changes detection system: A multimodal vision-based and novelty detection learning approach. *Biocybernetics and Biomedical Engineering*, 37(4):701–717, 2017.

[42] Rosalyn Stanton, Louise Ada, Catherine M Dean, and Elisabeth Preston. Biofeedback improves performance in lower limb activities more than usual therapy in people following stroke: a systematic review. *Journal of Physiotherapy*, 63(1):11–16, 2017.

[43] Giovanni Morone, Grazia Fernanda Spitoni, Daniela De Bartolo, Sheida Ghanbari Ghooshchy, Fulvia Di Iulio, Stefano Paolucci, Pierluigi Zoccolotti, and Marco Iosa. Rehabilitative devices for a top-down approach. *Expert Review of Medical Devices*, 16(3):187–195, 2019. PMID: 30677307.

[44] Linda M.A. van Gelder, Andrew Barnes, Jonathan S. Wheat, and Ben W. Heller. The use of biofeedback for gait retraining: A mapping review. *Clinical Biomechanics*, 59:159–166, 2018.

[45] J. Sauro and J. R. Lewis. *Quantifying the User Experience*. Elsevier, 2nd editio edition, 2012.

[46] Ana Isabel Martins, Ana Filipa Rosa, Alexandra Queirós, Anabela Silva, and Nelson Pacheco Rocha. European portuguese validation of the system usability scale (sus). *Procedia Computer Science*, 67:293–300, 2015. Proceedings of the 6th International Conference on Software Development and Technologies for Enhancing Accessibility and Fighting Info-exclusion.

[47] Aaron Bangor, Philip Kortum, and James Miller. Determining what individual sus scores mean: adding an adjective rating scale. *J. Usability Studies*, 4(3):114–123, may 2009.

[48] Maria M. Martins, Cristina P. Santos, Anselmo Frizera-Neto, and Ramón Ceres. Assistive mobility devices focusing on Smart Walkers: Classification and review. *Robotics and Autonomous Systems*, 60(4):548–562, apr 2012.

[49] M. Spenko, H. Yu, and S. Dubowsky. Robotic personal aids for mobility and monitoring for the elderly. *IEEE Transactions on Neural Systems and Rehabilitation Engineering*, 14(3):344–351, 2006.

[50] Anselmo Frizera-Neto, Ramón Ceres, Eduardo Rocon, and José Luis Pons. Empowering and assisting natural human mobility: The simbiosis walker. *International Journal of Advanced Robotic Systems*, 8(3):29, 2011.

[51] Mario F. Jiménez, Matias Monllor, Anselmo Frizera, Teodiano Bastos, Flavio Roberti, and Ricardo Carelli. Admittance Controller with Spatial Modulation for Assisted Locomotion using a Smart Walker. *Journal of Intelligent & Robotic Systems*, 94(3-4):621–637, jun 2019.

[52] Jianyu Ye, Jian Huang, Jiping He, Chunjing Tao, and Xitai Wang. Development of a width-changeable intelligent walking-aid robot. In *2012 International Symposium on Micro-NanoMechatronics and Human Science (MHS)*, pages 358–363, 2012.

[53] Jian Huang, Wenxia Xu, Samer Mohammed, and Zhen Shu. Posture estimation and human support using wearable sensors and walking-aid robot. *Robotics and Autonomous Systems*, 73:24–43, 2015. Wearable Robotics.

[54] Francesco Ferrari, Stefano Divan, Cristina Guerrero, Fabiano Zenatti, Roberta Guidolin, Luigi Palopoli, and Daniele Fontanelli. Human–Robot Interaction Analysis for a Smart Walker for Elderly: The ACANTO Interactive Guidance System. *International Journal of Social Robotics*, 12(2):479–492, may 2020.

[55] Luís Garrote, João Paulo, and Urbano J. Nunes. Reinforcement Learning Aided Robot-Assisted Navigation: A Utility and RRT Two-Stage Approach. *International Journal of Social Robotics*, 12(3):689–707, jul 2020.

[56] Abdullah Yeaser, James Tung, Jan Huissoon, and Ehsan Hashemi. Learning-aided user intent estimation for smart rollators. In *2020 42nd Annual International Conference of the IEEE Engineering in Medicine & Biology Society (EMBC)*, pages 3178–3183, 2020.

[57] Tao Shen, Md Rayhan Afsar, He Zhang, Cang Ye, and Xiangrong Shen. A 3D Computer Vision-Guided Robotic Companion for Non-Contact Human Assistance and Rehabilitation. *Journal of Intelligent and Robotic Systems: Theory and Applications*, 100(3-4):911–923, 2020.

[58] Xiaoyang Zhao, Zhi Zhu, Mingshan Liu, Chongyu Zhao, Yafei Zhao, Jia Pan, Zheng Wang, and Chuan Wu. A Smart Robotic Walker With Intelligent Close-Proximity Interaction Capabilities for Elderly Mobility Safety. *Frontiers in Neurorobotics*, 14(October):1–17, 2020.

[59] Lili Lv, Junyou Yang, Donghui Zhao, and Shuoyu Wang. A Novel Non-contact Recognition Approach of Walking Intention Based on Long Short-Term Memory Network. *Qian J., Liu H., Cao J., Zhou D. (eds) Robotics and Rehabilitation Intelligence. ICRRI 2020. Communications in Computer and Information Science*, 1335, 2020.

[60] Ji Ho Park, Bi Oh Park, and Won Gu Lee. Parametric Design and Analysis of the Arc Motion of a User-Interactive Rollator Handlebar with Hall Sensors. *International Journal of Precision Engineering and Manufacturing*, 20(11):1979–1988, nov 2019.

[61] Jiancheng (Charles) Ji, Shuai Guo, Fengfeng (Jeff) Xi, and Leigang Zhang. Design and Analysis of a Smart Rehabilitation Walker With Passive Pelvic Mechanism. *Journal of Mechanisms and Robotics*, 12(3):031007, 01 2020.

[62] Georgia Chalvatzaki, Xanthi S. Papageorgiou, Petros Maragos, and Costas S. Tzafestas. Learn to Adapt to Human Walking: A Model-Based Reinforcement Learning Approach for a Robotic Assistant Rollator. *IEEE Robotics and Automation Letters*, 4(4):3774–3781, 2019.

[63] Lei Wang, Jingang Yi, and Tao Liu. Gait adaptable human-robot interaction system and its application to a robotic walker. In *2018 IEEE 8th Annual International Conference on CYBER Technology in Automation, Control, and Intelligent Systems (CYBER)*, pages 707–712, 2018.

[64] Ihn-Sik Weon and Soon-Geul Lee. Intelligent robotic walker with actively controlled human interaction. *ETRI Journal*, 40(4):522–530, aug 2018.

[65] Wen-Chang Cheng and Yan-Zhi Wu. A user's intention detection method for smart walker. In *2017 IEEE 8th International Conference on Awareness Science and Technology (iCAST)*, pages 35–39, 2017.

[66] Maria Martins, Cristina Santos, Anselmo Frizera, and Ramón Ceres. Real time control of the asbgo walker through a physical human–robot interface. *Measurement*, 48:77–86, 2014.

[67] Kai-Tai Song and Sin-Yi Jiang. Force-cooperative guidance design of an omni-directional walking assistive robot. In *2011 IEEE International Conference on Mechatronics and Automation*, pages 1258–1263, 2011.

[68] Fei Shi, Qixin Cao, Chuntao Leng, and Hongbing Tan. Based on force sensing-controlled human-machine interaction system for walking assistant robot. In *2010 8th World Congress on Intelligent Control and Automation*, pages 6528–6533, 2010.

[69] Anselmo Frizera Neto, Juan A. Gallego, Eduardo Rocon, José L. Pons, and Ramón Ceres. Extraction of user's navigation commands from upper body force interaction in walker assisted gait. *BioMedical Engineering OnLine*, 9(1):37, dec 2010.

[70] Masayoshi Wada, Ken Ichiryu, Takeyoshi Iguchi, and Ryuta Yoshida. Design and control of an active-caster electric walker with a walk sensing system (smart walker). *2016 IEEE International Conference on Advanced Intelligent Mechatronics (AIM)*, pages 258–263, 2016.

[71] Limin Wang, Yuanjun Xiong, Zhe Wang, Yu Qiao, Dahua Lin, Xiaoou Tang, and Luc Van Gool. Temporal segment networks: Towards good practices for deep action recognition. In Bastian Leibe, Jiri Matas, Nicu Sebe, and Max Welling, editors, *Computer Vision – ECCV 2016*, pages 20–36, Cham, 2016. Springer International Publishing.

[72] Wen Liang Yeoh, Ryosuke Miyata, Osamu Fukuda, Nobuhiko Yamaguchi, and Hiroshi Okumura. Development of a person-following robotic assist walker with compliant-control arbitrated role-switching. *Artif. Life Robot.*, 28(3):553–559, mar 2023.

[73] A. Morris, R. Donamukkala, A. Kapuria, A. Steinfeld, J.T. Matthews, J. Dunbar-Jacob, and S. Thrun. A robotic walker that provides guidance. In *2003 IEEE International Conference on Robotics and Automation (Cat. No.03CH37422)*, volume 1, pages 25–30 vol.1, 2003.

[74] Cunjun Huang, Glenn Wasson, Majd Alwan, Pradip Sheth, and Alexandre Ledoux. Shared navigational control and user intent detection in an intelligent walker. *AAAI Fall Symposium - Technical Report*, FS-05-02:59–66, 2005.

[75] Birgit Graf and Rolf D. Schraft. Behavior-based path modification for shared control of robotic walking aids. In *2007 IEEE 10th International Conference on Rehabilitation Robotics*, pages 317–322, 2007.

[76] Milad Geravand, Christian Werner, Klaus Hauer, and Angelika Peer. An Integrated Decision Making Approach for Adaptive Shared Control of Mobility Assistance Robots. *International Journal of Social Robotics*, 8(5):631–648, nov 2016.

[77] Luís Garrote, João Paulo, João Perdiz, Paulo Peixoto, and Urbano J. Nunes. Robot-assisted navigation for a robotic walker with aided user intent. In *2018 27th IEEE International Symposium on Robot and Human Interactive Communication (RO-MAN)*, pages 348–355, 2018.

[78] Marco Andreetto, Stefano Divan, Francesco Ferrari, Daniele Fontanelli, Luigi Palopoli, and Fabiano Zenatti. Simulating Passivity for Robotic Walkers via Authority-Sharing. *IEEE Robotics and Automation Letters*, 3(2):1306–1313, apr 2018.

[79] Wenxia Xu, Jian Huang, Yongji Wang, Chunjing Tao, and Lei Cheng. Reinforcement learning-based shared control for walking-aid robot and its experimental verification. *Advanced Robotics*, 29(22):1463–1481, 2015.

[80] Joseph Redmon and Ali Farhadi. Yolo9000: Better, faster, stronger. *2017 IEEE Conference on Computer Vision and Pattern Recognition (CVPR)*, pages 6517–6525, 2016.

[81] Sergio D. Sierra M., Mario F. Jimenez, Marcela Múnera, Carlos A. Cifuentes, and Anselmo Frizera. Haptic Human-Robot Collaboration for Walker-Assisted Navigation Based on Admittance Controllers. *IEEE Robotics and Automation Letters*, 8(5):2622–2628, may 2023.

[82] Oonagh M Giggins, Ulrik Persson, and Brian Caulfield. Biofeedback in rehabilitation. *Journal of NeuroEngineering and Rehabilitation*, 10(1):60, 2013.

[83] Dorothea Sze Min Ong, Melvyn Zhang Weibin, and Ranganath Vallabhajosyula. Serious games as rehabilitation tools in neurological conditions: A comprehensive review. *Technol. Health Care*, 29(1):15–31, jan 2021.

[84] C Vieira, C Ferreira da Silva Pais-Vieira, J Novais, and A Perrotta. Serious game design and clinical improvement in physical rehabilitation: Systematic review. *JMIR Serious Games*, 9(3):e20066, 2021.

[85] Hsin Fen Chien, Marise Bueno Zonta, Janini Chen, Giovana Diaferia, Celiana Figueiredo Viana, Hélio Afonso Ghizoni Teive, José Luiz Pedroso, and Orlando Graziani Povoas Barsottini. Rehabilitation in patients with cerebellar ataxias. *Arquivos de Neuro-Psiquiatria*, 80(3):306–315, mar 2022.

[86] Zofia Fleszar, Sabato Mellone, Martin Giese, Carlo Tacconi, Clemens Becker, Ludger Schöls, Matthis Synofzik, and Winfried Ilg. Real-time use of audio-biofeedback can improve postural sway in patients with degenerative ataxia. *Annals of Clinical and Translational Neurology*, 6(2):285–294, feb 2019.

[87] Matthis Synofzik and Winfried Ilg. Motor Training in Degenerative Spinocerebellar Disease: Ataxia-Specific Improvements by Intensive Physiotherapy and Exergames. *BioMed Research International*, 2014:1–11, 2014.

[88] Ana Rojo, Arantxa Castrillo Calvillo, Cristina López, Rafael Raya, and Juan C. Moreno. Effects of a Virtual Reality Cycling Platform on Lower Limb Rehabilitation in Patients With Ataxia and Hemiparesis: Pilot Randomized Controlled Trial. *JMIR Serious Games*, 12:e39286–e39286, jan 2024.

[89] Hanady A. Mouhamed, Nehad A. Abo-Zaid, Heba A. Khalifa, Mohammed E. Ali, Noha S. Elserty, Mohamed A. Behiry, and Walaa E. Heneidy. Efficacy of virtual reality on balance impairment in ataxic cerebral palsy children: randomized controlled trial. *European Journal of Physical and Rehabilitation Medicine*, 60(6):949–955, dec 2024.

[90] Mirjam Bonanno, Paolo De Pasquale, Cristiano De Marchis, Antonino Lombardo Facciale, Giuseppe Paladina, Bartolo Fonti, Angelo Quartarone, and Rocco Salvatore Calabrò. Might patients with cerebellar ataxia benefit from the Computer Assisted Rehabilitation ENvironment (CAREN)? A pilot study focusing on gait and balance. *Frontiers in Bioengineering and Biotechnology*, 12(June):1–16, jun 2024.

[91] Telerehabilitation versus virtual reality supported task-oriented circuit therapy on upper limbs and trunk functions in patients with multiple sclerosis: A randomized controlled study. *Multiple Sclerosis and Related Disorders*, 71(February):104558, mar 2023.

[92] Alberto Romano, Martina Favetta, Susanna Summa, Tommaso Schirinzi, Enrico Silvio Bertini, Enrico Castelli, Gessica Vasco, and Maurizio Petrarca. Upper Body Physical Rehabilitation for Children with Ataxia through IMU-Based Exergame. *Journal of Clinical Medicine*, 11(4):1065, feb 2022.

[93] Ender Ayvat, Özge Onursal Kılınç, Fatma Ayvat, Cevher Savcun Demirci, Sibel Aksu Yıldırım, Oğuzhan Kurşun, and Muhammed Kılınç. The Effects of Exergame on Postural Control in Individuals with Ataxia: a Rater-Blinded, Randomized Controlled, Cross-over Study. *The Cerebellum*, 21(1):64–72, feb 2022.

[94] Ben Naets, Evelien De wachter, Rik Lambrechts, Joris Vaneyghen, Maaike Fobelets, Catherine Middag, Ruben Debeuf, Eva Swinnen, and Ben Minnaert. Smart Walker Design for Clinical Rehabilitation. In *2022 2nd International Conference on Innovative Research in Applied Science, Engineering and Technology (IRASET)*, pages 1–5. IEEE, mar 2022.

[95] Emanuele Lo Voi, Giorgio Carmelo Basile, Alessia Bramanti, Giuseppe Paladina, Annalisa Militi, Daniele Bruschetta, Angelo Alito, Filippo Cavallaro, Salvatore Bertino, and Demetrio Milardi. Cerebellar Atrophy Associated with Primary Sjögren's Syndrome: Diagnosis, Therapy, and Virtual Reality Rehabilitation: A Case Report. *Innovations in clinical neuroscience*, 18(7-9):11–17, 2021.

[96] Kazuhiro Takimoto, Kyohei Omon, Yuichiro Murakawa, and Hideo Ishikawa. Case of cerebellar ataxia successfully treated by virtual reality-guided rehabilitation. *BMJ Case Reports*, 14(5):e242287, may 2021.

[97] Oliwer Kahl, Ewelina Wierzbicka, Magdalena De□bińska, Maciej Mraz, and Małgorzata Mraz. Compensatory image of the stability of people with multiple sclerosis and atrial vertigo based on posturography examination. *Scientific Reports*, 11(1):7027, mar 2021.

[98] Elisabetta Peri, Daniele Panzeri, Elena Beretta, Gianluigi Reni, Sandra Strazzer, and Emilia Biffi. Motor Improvement in Adolescents Affected by Ataxia Secondary to Acquired Brain Injury: A Pilot Study. *BioMed Research International*, 2019:1–8, nov 2019.

[99] Feasibility of virtual reality-based balance rehabilitation in adults with spinocerebellar ataxia: a prospective observational study. *Hearing, Balance and Communication*, 15(4):244–251, oct 2017.

[100] Cornelia Schatton, Matthis Synofzik, Zofia Fleszar, Martin A. Giese, Ludger Schöls, and Winfried Ilg. Individualized exergame training improves postural control in advanced degenerative spinocerebellar ataxia: A rater-blinded, intra-individually controlled trial. *Parkinsonism and Related Disorders*, 39:80–84, 2017.

[101] Inês Caetano, Joana Alves, José Gonçalves, Maria Martins, and Cristina P. Santos. Development of a biofeedback approach using body tracking with active depth sensor in asbgo smart walker. In *2016 International Conference on Autonomous Robot Systems and Competitions (ICARSC)*, pages 241–246, 2016.

[102] Ondřej Čakrt, Martin Vyhnálek, Kryštof Slabý, Tomáš Funda, Nicolas Vuillerme, Pavel Kolář, and Jaroslav Jeřábek. Balance rehabilitation therapy by tongue electrotactile biofeedback in patients with degenerative cerebellar disease. *NeuroRehabilitation*, 31(4):429–434, nov 2012.

[103] Winfried Ilg, Cornelia Schatton, Julia Schicks, Martin A. Giese, Ludger Schöls, and Matthis Synofzik. Video game–based coordinative training improves ataxia in children with degenerative ataxia. *Neurology*, 79(20):2056–2060, nov 2012.

[104] Filipa Januário, Inês Campos, and Carla Amaral. Rehabilitation of postural stability in ataxic/hemiplegic patients after stroke. *Disability and Rehabilitation*, 32(21):1775–1779, jan 2010.

[105] Kentaro Kodama, Kazuhiro Yasuda, Nikita A. Kuznetsov, Yuki Hayashi, and Hiroyasu Iwata. Balance training with a vibrotactile biofeedback system affects the dynamical structure of the center of pressure trajectories in chronic stroke patients. *Frontiers in Human Neuroscience*, 13, 2019.

[106] R.P. van der Logt, O. Findling, H. Rust, O. Yaldizli, and J.H.J. Allum. The effect of vibrotactile biofeedback of trunk sway on balance control in multiple sclerosis. *Multiple Sclerosis and Related Disorders*, 8:58–63, jul 2016.

[107] Carlos Cruz-Montecinos, Antonio Cuesta-Vargas, Cristian Muñoz, Dante Flores, Joseph Ellsworth, Carlos De la Fuente, Joaquín Calatayud, Gonzalo Rivera-Lillo, Verónica Soto-Arellano, Claudio Tapia, and Xavier García-Massó. Impact of visual biofeedback of trunk sway smoothness on motor learning during unipedal stance. *Sensors*, 20(9), 2020.

[108] Janusz Maciaszek. Effects of Posturographic Platform Biofeedback Training on the Static and Dynamic Balance of Older Stroke Patients. *Journal of Stroke and Cerebrovascular Diseases*, 27(7):1969–1974, jul 2018.

[109] Adam T. Booth, Annemieke I. Buizer, Jaap Harlaar, Frans Steenbrink, and Marjolein M. van der Krogt. Immediate effects of immersive biofeedback on gait in children with cerebral palsy. *Archives of Physical Medicine and Rehabilitation*, 100(4):598–605, 2019.

[110] Hamed Ghomashchi. Investigating the effects of visual biofeedback therapy on recovery of postural balance in stroke patients using a complexity measure. *Topics in Stroke Rehabilitation*, 23(3):178–183, 2016. PMID: 27077976.

[111] Siddharth Bhardwaj, Abid Ali Khan, and Mohammad Muzammil. Lower limb rehabilitation robotics: The current understanding and technology. *Work*, 69(3):775–793, jul 2021.

[112] João M. Lopes, João André, António Pereira, Manuel Palermo, Nuno Ribeiro, João Cerqueira, and Cristina P. Santos. ASBGo: A Smart Walker for Ataxic Gait and Posture Assessment, Monitoring, and Rehabilitation. *Robotic Technologies in Biomedical and Healthcare Engineering*, pages 51–86, 2021.

[113] Michael R. Tucker, Jeremy Olivier, Anna Pagel, Hannes Bleuler, Mohamed Bouri, Olivier Lambercy, José del R. Millán, Robert Riener, Heike Vallery, and Roger Gassert. Control strategies for active lower extremity prosthetics and orthotics: a review. *Journal of NeuroEngineering and Rehabilitation*, 12, 2015.

[114] Vishwas Massey and K. J. Satao. Evolving a new software development life cycle model (sdlc) incorporated with release management. 2012.

[115] T. Saravanan, Sumit Jha, Gautam Sabharwal, and Shubham Narayan. Comparative analysis of software life cycle models. In *2020 2nd International Conference on Advances in Computing, Communication Control and Networking (ICACCCN)*, pages 906–909, 2020.

[116] Srikrishna Prasad and S B Avinash. Application of polyglot persistence to enhance performance of the energy data management systems. In *2014 International Conference on Advances in Electronics Computers and Communications*, pages 1–6, 2014.

[117] Kathy Baxter, Catherine Courage, and Kelly Caine. Chapter 7 - during your user research activity. In Kathy Baxter, Catherine Courage, and Kelly Caine, editors, *Understanding your Users (Second Edition)*, Interactive Technologies, pages 158–189. Morgan Kaufmann, Boston, second edition edition, 2015.

[118] John Brooke. SUS: A 'Quick and Dirty' Usability Scale. In Patrick W. Jordan, B. Thomas, Ian Lyall McClelland, and Bernard Weerdmeester, editors, *Usability Evaluation In Industry*. CRC Press, London, 1st editio edition, 1996.

[119] Ana Isabel Martins, Ana Filipa Rosa, Alexandra Queirós, Anabela Silva, and Nelson Pacheco Rocha. European portuguese validation of the system usability scale (sus). *Procedia Computer Science*, 67:293–300, 2015. Proceedings of the 6th International Conference on Software Development and Technologies for Enhancing Accessibility and Fighting Info-exclusion.

[120] Mohamed A. Ben-Zahia and Ibrahim Jaluta. Criteria for selecting software development models. In *2014 Global Summit on Computer & Information Technology (GSCIT)*, pages 1–6, 2014.

[121] Muhammad Junaid Aamir and Arshad Mansoor. Testing web application from usability perspective. In *2013 3rd IEEE International Conference on Computer, Control and Communication (IC4)*, pages 1–7, 2013.

[122] Joana Figueiredo, Simao P. Carvalho, Diogo Goncalve, Juan C. Moreno, and Cristina P. Santos. Daily Locomotion Recognition and Prediction: A Kinematic Data-Based Machine Learning Approach. *IEEE Access*, 8:33250–33262, 2020.

[123] Takafumi Kurai, Yutaro Shioi, Yasutoshi Makino, and Hiroyuki Shinoda. Temporal conditions suitable for predicting human motion in walking. *Conference Proceedings - IEEE International Conference on Systems, Man and Cybernetics*, 2019-Octob:2986–2991, 2019.

[124] Ben P.F. O'Callaghan, Emer P. Doheny, Cathy Goulding, Emma Fortune, and Madeleine M. Lowery. Adaptive gait segmentation algorithm for walking bout detection using tri-axial accelerometers. *Proceedings of the Annual International Conference of the IEEE Engineering in Medicine and Biology Society, EMBS*, 2020-July:4592–4595, 2020.

[125] Argyro Pachi and Tianjian Ji. Frequency and velocity of people walking. *The Structural engineer*, 83, 2005.

[126] Daniele Berardini, Sara Moccia, Lucia Migliorelli, Iacopo Pacifici, Paolo di Massimo, Marina Paolanti, and Emanuele Frontoni. Fall detection for elderly-people monitoring using learned features and recurrent neural networks. *Experimental Results*, 1:1–9, 2020.

[127] Hanbo Wu, Xin Ma, and Yibin Li. Convolutional Networks with Channel and STIPs Attention Model for Action Recognition in Videos. *IEEE Transactions on Multimedia*, 22(9):2293–2306, 2020.

[128] Kaiming He, Xiangyu Zhang, Shaoqing Ren, and Jian Sun. Deep residual learning for image recognition. *Proceedings of the IEEE Computer Society Conference on Computer Vision and Pattern Recognition*, 2016-Decem:770–778, 2016.

[129] Jie Hu, Li Shen, and Gang Sun. Squeeze-and-excitation networks. In *2018 IEEE/CVF Conference on Computer Vision and Pattern Recognition*, pages 7132–7141, 2018.

[130] Jia Deng, Wei Dong, Richard Socher, Li-Jia Li, Kai Li, and Li Fei-Fei. ImageNet: A large-scale hierarchical image database. (May 2014):248–255, 2010.

[131] Olaf Ronneberger, Philipp Fischer, and Thomas Brox. U-Net : Convolutional Networks for Biomedical Image Segmentation. In *Medical Image Computing and Computer-Assisted Intervention (MICCAI)*, volume 9351 LNCS, pages 234–241. Springer, 2015.

[132] Clebeson Canuto, Plinio Moreno, Jorge Samatelo, Raquel Vassallo, and José Santos-Victor. Action anticipation for collaborative environments: The impact of contextual information and uncertainty-based prediction. *Neurocomputing*, 444(xxxx):301–318, 2021.

[133] Mohammad Sadegh Aliakbarian, Fatemeh Sadat Saleh, Mathieu Salzmann, Basura Fernando, Lars Petersson, and Lars Andersson. Encouraging LSTMs to Anticipate Actions Very Early. *Proceedings of the IEEE International Conference on Computer Vision*, 2017-Octob:280–289, 2017.

[134] Ramprasaath R. Selvaraju, Michael Cogswell, Abhishek Das, Ramakrishna Vedantam, Devi Parikh, and Dhruv Batra. Grad-CAM: Visual Explanations from Deep Networks via Gradient-Based Localization. *International Journal of Computer Vision*, 128(2):336–359, 2019.

[135] Carolina Gonçalves, João M. Lopes, Sara Moccia, Daniele Berardini, Lucia Migliorelli, and Cristina P. Santos. Deep learning-based approaches for human motion decoding in smart walkers for rehabilitation. *Expert Systems with Applications*, 228:120288, 2023.

[136] Marcos Baptista-Ríos, Roberto J. López-Sastre, Fabian Caba Heilbron, Jan C. Van Gemert, F. Javier Acevedo-Rodríguez, and Saturnino Maldonado-Bascón. Rethinking online action detection in untrimmed videos: A novel online evaluation protocol. *IEEE Access*, 8:5139–5146, 2020.

[137] Wolfgang Hess, Damon Kohler, Holger Rapp, and Daniel Andor. Real-time loop closure in 2d lidar slam. In *2016 IEEE International Conference on Robotics and Automation (ICRA)*, pages 1271–1278, 2016.

[138] Ekim Yurtsever, Jacob Lambert, Alexander Carballo, and Kazuya Takeda. A survey of autonomous driving: Common practices and emerging technologies. *IEEE Access*, 8:58443–58469, 2020.

[139] František Duchoň, Andrej Babinec, Martin Kajan, Peter Beňo, Martin Florek, Tomáš Fico, and Ladislav Jurišica. Path planning with modified a star algorithm for a mobile robot. *Procedia Engineering*, 96:59–69, 2014. Modelling of Mechanical and Mechatronic Systems.

[140] António Manuel Moreira Pereira. *Adaptive shared-control of a robotic walker to improve human-robot cooperation in gait biomechanical rehabilitation*. Master thesis, University of Minho, 2021.

[141] Yuanzhi Li and Yang Yuan. Convergence analysis of two-layer neural networks with relu activation. In *Proceedings of the 31st International Conference on Neural Information Processing Systems*, NIPS'17, page 597–607, Red Hook, NY, USA, 2017. Curran Associates Inc.

[142] Christina Ma, Duo Wong, Wing Lam, Anson Wan, and Winson Lee. Balance Improvement Effects of Biofeedback Systems with State-of-the-Art Wearable Sensors: A Systematic Review. *Sensors*, 16(4):434, mar 2016.

[143] Federica Tamburella, Juan C. Moreno, Diana Sofía Herrera Valenzuela, Iolanda Pisotta, Marco Iosa, Febo Cincotti, Donatella Mattia, José L. Pons, and Marco Molinari. Influences of the biofeedback content on robotic post-stroke gait rehabilitation: electromyographic vs joint torque biofeedback. *Journal of NeuroEngineering and Rehabilitation*, 16(1):95, dec 2019.

[144] Marco Ghislieri, Laura Gastaldi, Stefano Pastorelli, Shigeru Tadano, and Valentina Agostini. Wearable inertial sensors to assess standing balance: A systematic review. *Sensors*, 19(19), 2019.

[145] Parag Narkhede, Shashi Poddar, Rahee Walambe, George Ghinea, and Ketan Kotecha. Cascaded Complementary Filter Architecture for Sensor Fusion in Attitude Estimation. *Sensors*, 21(6):1937, mar 2021.

[146] R E Kalman. A New Approach to Linear Filtering and Prediction Problems. *Journal of Basic Engineering*, 82(1):35–45, mar 1960.

[147] Thomas Jespersen. A practical approach to kalman filter and how to implement it, 2012. Available online: `https://blog.tkjelectronics.dk/2012/09/a-practical-approach-to-kalman-filter-and-how-to-implement-it/` (accessed: 2024-09-03).

[148] Brandon Mccarron. Low-Cost IMU Implementation via Sensor Fusion Algorithms in the Arduino Environment. *California Polytechnic State University*, (June):1–17, 2013.

[149] Youngjoo Kim and Hyochoong Bang. Introduction to kalman filter and its applications. In Felix Govaers, editor, *Introduction and Implementations of the Kalman Filter*, chapter 2. IntechOpen, Rijeka, 2018.

[150] Zuzana Halická, Jana Lobotková, Kristína Bučková, and František Hlavačka. Effectiveness of different visual biofeedback signals for human balance improvement. *Gait & Posture*, 39(1):410–414, jan 2014.

[151] W. Nanhoe-Mahabier, J.H. Allum, E.P. Pasman, S. Overeem, and B.R. Bloem. The effects of vibrotactile biofeedback training on trunk sway in Parkinson's disease patients. *Parkinsonism & Related Disorders*, 18(9):1017–1021, nov 2012.

[152] Mohammad Al-Amri, Kevin Nicholas, Kate Button, Valerie Sparkes, Liba Sheeran, and Jennifer L Davies. Inertial measurement units for clinical movement analysis: Reliability and concurrent validity. *Sensors*, 18(3), 2018.

[153] Movella. Sensor placement in xsens awinda system, 2022. Available online: `https://base.movella.com/s/article/Sensor-Placement-in-Xsens-Awinda-System?language=en_US` (accessed on 2024-07-18).

[154] Dhruv Parikh, Sajil Vohra, and Maryam Kaveshgar. Comparison of Attitude Estimation Algorithms With IMU Under External Acceleration. In *2021 IEEE International Symposium on Smart Electronic Systems (iSES)*, pages 123–126. IEEE, dec 2021.

[155] David A. Winter. *Biomechanics and Motor Control of Human Movement*, volume 2nd. Wiley, Hoboken, New Jersey, 4th editio edition, sep 2009.

[156] Jacob Cohen. *Statistical Power Analysis for the Behavioral Sciences*. Lawrence Erlbaum Associates Inc., 1988.

[157] Xsens. MTw Awinda User Manual. Technical report, Xsens Technologies B.V. Pantheon, Enschede, 2018. Available online: `https://www.xsens.com/hubfs/Downloads/Manuals/MTw_Awinda_User_Manual.pdf` (accessed on 2024-09-07).

[158] Alun Owen. Spearman's correlation. Available online: `https://www.statstutor.ac.uk/resources/uploaded/spearmans.pdf` (accessed on 2024-09-07).

[159] Emer P. Doheny, Denise McGrath, Barry R. Greene, Lorcan Walsh, David McKeown, Clodagh Cunningham, Lisa Crosby, Rose Anne Kenny, and Brian Caulfield. Displacement of centre of mass during quiet standing assessed using accelerometry in older fallers and non-fallers. In *2012 Annual International Conference of the IEEE Engineering in Medicine and Biology Society*, pages 3300–3303. IEEE, aug 2012.

[160] Ray-Yau Wang, Fang-Yi Huang, Bing-Wen Soong, Shih-Fong Huang, and Yea-Ru Yang. A randomized controlled pilot trial of game-based training in individuals with spinocerebellar ataxia type 3. *Scientific Reports*, 8(1):7816, may 2018.

[161] Miao He, Hai-nan Zhang, Zhen-chu Tang, and Shu-guang Gao. Balance and coordination training for patients with genetic degenerative ataxia: a systematic review. *Journal of Neurology*, 268(10):3690–3705, oct 2021.

[162] Bart P.C. van de Warrenburg, Janneke A.G. Steijns, Marten Munneke, Berry P.H. Kremer, and Bastiaan R. Bloem. Falls in degenerative cerebellar ataxias. *Movement Disorders*, 20(4):497–500, apr 2005.

[163] A. Andrade. Game engines: a survey. *EAI Endorsed Transactions on Game-Based Learning*, 2(6):150615, nov 2015.

[164] Federica Pilotto and Smita Saxena. Epidemiology of inherited cerebellar ataxias and challenges in clinical research. *Clinical and Translational Neuroscience*, 2(2):2514183X1878525, jul 2018.

[165] W. Ilg, M. Synofzik, D. Brötz, S. Burkard, M. A. Giese, and L. Schöls. Intensive coordinative training improves motor performance in degenerative cerebellar disease. *Neurology*, 73(22):1823–1830, dec 2009.

[166] Roxana Gabriela Burciu, Nicole Fritsche, Oliver Granert, Lutz Schmitz, Nina Spönemann, Jürgen Konczak, Nina Theysohn, Marcus Gerwig, Thilo van Eimeren, and Dagmar Timmann. Brain Changes Associated with Postural Training in Patients with Cerebellar Degeneration: A Voxel-Based Morphometry Study. *The Journal of Neuroscience*, 33(10):4594–4604, mar 2013.

[167] Gregor K Wenning, Carlo Colosimo, Felix Geser, and Werner Poewe. Multiple system atrophy. *The Lancet Neurology*, 3(2):93–103, feb 2004.

[168] Joshua Knight and Ojas De Jesus. *Pilocytic Astrocytoma*. StatPearls [Internet]. StatPearls Publishing, Treasure Island (FL), 2023. [Updated 2023 Aug 23].

[169] National Institute of Neurological Disorders and Stroke (NINDS). Cerebellar degeneration, 2024. Accessed: 2024-07-18.

[170] John D Cleary, Sunil H Subramony, and Laura PW Ranum. *Spinocerebellar Ataxia Type 8*. GeneReviews® [Internet]. University of Washington, Seattle, Seattle (WA), 1993-2024 edition, 2001. [Updated 2021 Apr 22].

[171] Piervito Lopriore, Valentina Ricciarini, Gabriele Siciliano, Michelangelo Mancuso, and Vincenzo Montano. Mitochondrial ataxias: Molecular classification and clinical heterogeneity. *Neurology International*, 14(2):337–356, 2022.

[172] Scott R. Evans. Clinical trial structures. *Journal of Experimental Stroke and Translational Medicine*, 3(1):8–18, jan 2010.

[173] T. Schmitz-Hübsch, S. Tezenas du Montcel, L. Baliko, J. Berciano, S. Boesch, C. Depondt, P. Giunti, C. Globas, J. Infante, J. S. Kang, B. Kremer, C. Mariotti, B. Melegh, M. Pandolfo, M. Rakowicz, P. Ribai, R. Rola, L. Schöls, S. Szymanski, B. P. van de Warrenburg, A. Dürr, and T. Klockgether. Scale for the assessment and rating of ataxia. *Neurology*, 66(11):1717–1720, 2006.

[174] Matthias Grobe-Einsler, Abir T. Amin, Johannes Faber, et al. Scale for the assessment and rating of ataxia (sara): Development of a training tool and certification program. *Cerebellum*, 23:877–880, 2024.

[175] Jennifer L. Moore, Kirsten Potter, Kathleen Blankshain, Sandra L. Kaplan, Linda C. O'Dwyer, and Jane E. Sullivan. A Core Set of Outcome Measures for Adults With Neurologic Conditions Undergoing Rehabilitation. *Journal of Neurologic Physical Therapy*, 42(3):174–220, jul 2018.

[176] Talia Herman, Nir Giladi, and Jeffrey M. Hausdorff. Properties of the 'Timed Up and Go' Test: More than Meets the Eye. *Gerontology*, 57(3):203–210, 2011.

[177] Katherine Berg. Measuring balance in the elderly: preliminary development of an instrument. *Physiotherapy Canada*, 41:304–311, 1989.

[178] Natalia Miranda and Timothy K. Tiu. Berg Balance Testing, 2024. In: StatPearls [Internet]. Treasure Island (FL): StatPearls Publishing; Available from: `https://www.ncbi.nlm.nih.gov/books/NBK574518/` (accessed on 20/11/2024).

[179] Slavka Viteckova, Patrik Kutilek, Zdenek Svoboda, Radim Krupicka, Jan Kauler, and Zoltan Szabo. Gait symmetry measures: A review of current and prospective methods. *Biomedical Signal Processing and Control*, 42:89–100, apr 2018.

[180] Kara K. Patterson, William H. Gage, Dina Brooks, Sandra E. Black, and William E. McIlroy. Evaluation of gait symmetry after stroke: A comparison of current methods and recommendations for standardization. *Gait & Posture*, 31(2):241–246, feb 2010.

[181] Diane Podsiadlo and Sandra Richardson. The Timed "Up & Go": A Test of Basic Functional Mobility for Frail Elderly Persons. *Journal of the American Geriatrics Society*, 39(2):142–148, feb 1991.

[182] Elena Bergamini, Andrea Cereatti, and Gaspare Pavei. Walking symmetry is speed and index dependent. *Scientific Reports*, 14(1):19548, aug 2024.

[183] Arnaud Gouelle and Fabrice Mégrot. Interpreting spatiotemporal parameters, symmetry, and variability in clinical gait analysis. In Bertram Müller, Sebastian I. Wolf, Gert-Peter Brueggemann, Zhigang Deng, Andrew McIntosh, Freeman Miller, and William Scott Selbie, editors, *Handbook of Human Motion*, pages 1–20. Springer International Publishing, Cham, 2017.

[184] Arlene Schmid, Pamela W. Duncan, Stephanie Studenski, Sue Min Lai, Lorie Richards, Subashan Perera, and Samuel S. Wu. Improvements in Speed-Based Gait Classifications Are Meaningful. *Stroke*, 38(7):2096–2100, jul 2007.

[185] Pierre Cabaraux, Sunil K. Agrawal, Huaying Cai, Rocco Salvatore Calabro, Carlo Casali, Loic Damm, Sarah Doss, Christophe Habas, Anja K. E. Horn, Winfried Ilg, Elan D. Louis, Hiroshi Mitoma, Vito Monaco, Maria Petracca, Alberto Ranavolo, Ashwini K. Rao, Serena Ruggieri, Tommaso Schirinzi, Mariano Serrao, Susanna Summa, Michael Strupp, Olivia Surgent, Matthis Synofzik, Shuai Tao, Hiroo Terasi, Diego Torres-Russotto, Brittany Travers, Jaimie A. Roper, and Mario Manto. Consensus Paper: Ataxic Gait. *The Cerebellum*, 22(3):394–430, apr 2022.

[186] Sungsik Son, Kil-Byung Lim, Jiyong Kim, Changhun Lee, Sung I.I. Cho, and Jeehyun Yoo. Comparing the Effects of Exoskeletal-Type Robot-Assisted Gait Training on Patients with Ataxic or Hemiplegic Stroke. *Brain Sciences*, 12(9):1261, sep 2022.

Chapter A

Appendix A

A.1 System Usability Questionnaire

Table 50: Portuguese version of the SUS [119]

Itens	Discordo completamente	Discordo	Neutro	Concordo	Concordo plenamente
	1	2	3	4	5
1. Acho que gostaria de utilizar este produto com frequência.	☐	☐	☐	☐	☐
2. Considerei o produto mais complexo do que o necessário.	☐	☐	☐	☐	☐
3. Achei o produto fácil de utilizar.	☐	☐	☐	☐	☐
4. Acho que necessitaria de ajuda de um técnico para conseguir utilizar este produto.	☐	☐	☐	☐	☐
5. Considerei que as várias funcionalidades deste produto estavam bem integradas.	☐	☐	☐	☐	☐
6. Achei que este produto tinha muitas inconsistências.	☐	☐	☐	☐	☐
7. Suponho que a maioria das pessoas aprenderia a utilizar rapidamente este produto.	☐	☐	☐	☐	☐
8. Considerei o produto muito complicado de utilizar.	☐	☐	☐	☐	☐
9. Senti-me muito confiante a utilizar este produto.	☐	☐	☐	☐	☐
10. Tive que aprender muito antes de conseguir lidar com este produto.	☐	☐	☐	☐	☐

A.2 Scale for the Assessment and Rating of Ataxia

1) Gait

Proband is asked (1) to walk at a safe distance parallel to a wall including a half-turn (turn around to face the opposite direction of gait) and (2) to walk in tandem (heels to toes) without support.

0: Normal, no difficulties in walking, turning and walking tandem (up to one misstep allowed)

1: Slight difficulties, only visible when walking 10 consecutive steps in tandem

2: Clearly abnormal, tandem walking $>$ 10 steps not possible

3: Considerable staggering, difficulties in half-turn, but without support

4: Marked staggering, intermittent support of the wall required

5: Severe staggering, permanent support of one stick or light support by one arm required

6: Walking $>$ 10 m only with strong support (two special sticks or stroller or accompanying person)

7: Walking < 10 m only with strong support (two special sticks or stroller or accompanying person)

8: Unable to walk, even supported

2) Stance

Proband is asked to stand (1) in natural position, (2) with feet together in parallel (big toes touching each other) and (3) in tandem (both feet on one line, no space between heel and toe). Proband does not wear shoes, eyes are open. For each condition, three trials are allowed. Best trial is rated.

0: Normal, able to stand in tandem for > 10 s

1: Able to stand with feet together without sway, but not in tandem for > 10s

2: Able to stand with feet together for > 10 s, but only with sway

3: Able to stand for > 10 s without support in natural position, but not with feet together

4: Able to stand for >10 s in natural position only with intermittent support

5: Able to stand >10 s in natural position only with constant support of one arm

6: Unable to stand for >10 s even with constant support of one arm

3) Sitting

Proband is asked to sit on an examination bed without support of feet, eyes open and arms outstretched to the front.

0: Normal, no difficulties sitting >10 sec

1: Slight difficulties, intermittent sway

2: Constant sway, but able to sit > 10 s without support

3: Able to sit for > 10 s only with intermittent support

4: Unable to sit for >10 s without continuous support

4) Speech disturbance

Speech is assessed during normal conversation.

0: Normal

1: Suggestion of speech disturbance

2: Impaired speech, but easy to understand

3: Occasional words difficult to understand

4: Many words difficult to understand

5: Only single words understandable

6: Speech unintelligible / anarthria

5) Finger chase

Proband sits comfortably. If necessary, support of feet and trunk is allowed. Examiner sits in front of proband and performs 5 consecutive sudden and fast pointing movements in unpredictable directions in a frontal plane, at about 50% of proband´s reach. Movements have an amplitude of 30 cm and a frequency of 1 movement every 2 s. Proband is asked to follow the movements with his index finger, as fast and precisely as possible. Average performance of last 3 movements is rated.

0: No dysmetria

1: Dysmetria, under/ overshooting target <5 cm

2: Dysmetria, under/ overshooting target < 15 cm

3: Dysmetria, under/ overshooting target > 15 cm

4: Unable to perform 5 pointing movements

6) Nose-finger test

Proband sits comfortably. If necessary, support of feet and trunk is allowed. Proband is asked to point repeatedly with his index finger from his nose to examiner's finger which is in front of the proband at about 90% of proband's reach. Movements are performed at moderate speed. Average performance of movements is rated according to the amplitude of the kinetic tremor.

0: No tremor

1: Tremor with an amplitude < 2 cm

2: Tremor with an amplitude < 5 cm

3: Tremor with an amplitude > 5 cm

4: Unable to perform 5 pointing movements

7) Fast alternating hand movements

Proband sits comfortably. If necessary, support of feet and trunk is allowed. Proband is asked to perform 10 cycles of repetitive alternation of pro- and supinations of the hand on his/her thigh as fast and as precise as possible. Movement is demonstrated by examiner at a speed of approx. 10 cycles within 7 s. Exact times for movement execution have to be taken.

0: Normal, no irregularities (performs <10s)

1: Slightly irregular (performs <10s)

2: Clearly irregular, single movements difficult to distinguish or relevant interruptions, but performs <10s

3: Very irregular, single movements difficult to distinguish or relevant interruptions, performs >10s

4: Unable to complete 10 cycles

8) Heel-shin slide

Proband lies on examination bed, without sight of his legs. Proband is asked to lift one leg, point with the heel to the opposite knee, slide down along the shin to the ankle, and lay the leg back on the examination bed. The task is performed 3 times. Slide-down movements should be performed within 1 s. If proband slides down without contact to shin in all three trials, rate 4.

0: Normal

1: Slightly abnormal, contact to shin maintained

2: Clearly abnormal, goes off shin up to 3 times during 3 cycles

3: Severely abnormal, goes off shin 4 or more times during 3 cycles

4: Unable to perform the task

A.3 Berg Balance Scale

1) Sitting to Standing

INSTRUCTIONS: Please stand up. Try not to use your hand for support.

4: able to stand without using hands and stabilize independently

3: able to stand independently using hands

2: able to stand using hands after several tries

1: needs minimal aid to stand or stabilize

0: needs moderate or maximal assist to stand

2) Standing unsupported

INSTRUCTIONS: Please stand for two minutes without holding on.

4: able to stand safely for 2 minutes

3: able to stand 2 minutes with supervision able to stand 30 seconds unsupported

1: needs several tries to stand 30 seconds unsupported

0: unable to stand 30 seconds unsupported

If a subject is able to stand 2 minutes unsupported, score full points for sitting unsupported. Proceed to item 4.

3) Sitting with back unsupported but feet suported on floor or on a stool

INSTRUCTIONS: Please sit with arms folded for 2 minutes.

4: able to sit safely and securely for 2 minutes

3: able to sit 2 minutes under supervision

2: able to able to sit 30 seconds

1: able to sit 10 seconds

0: unable to sit without support 10 seconds

4) Standing to sitting

INSTRUCTIONS: Please sit down.

4: sits safely with minimal use of hands

3: controls descent by using hands

2: uses back of legs against chair to control descent

1: sits independently but has uncontrolled descent

0: needs assist to sit

5) Transfers

INSTRUCTIONS: Arrange chair(s) for pivot transfer. Ask subject to transfer one way toward a seat with armrests and one way toward a seat without armrests. You may use two chairs (one with and one without armrests) or a bed and a chair.

4: able to transfer safely with minor use of hands

3: able to transfer safely definite need of hands

2: able to transfer with verbal cuing and/or supervision

1: needs one person to assist

0: needs two people to assist or supervise to be safe

6) Standing unsupported with eyes closed

INSTRUCTIONS Please close your eyes and stand still for 10 seconds.

4: able to stand 10 seconds safely

3: able to stand 10 seconds with supervision

2: able to stand 3 seconds

1: unable to keep eyes closed 3 seconds but stays safely

0: needs help to keep from falling

7) Standing unsupported with feet together

INSTRUCTIONS: Place your feet together and stand without holding on.

4: able to place feet together independently and stand 1 minute safely

3: able to place feet together independently and stand 1 minute with supervision

2: able to place feet together independently but unable to hold for 30 seconds

1: needs help to attain position but able to stand 15 seconds feet together

0: needs help to attain position and unable to hold for 15 seconds

8) Reaching forward with outstretched arm while standing

INSTRUCTIONS: Lift arm to 90 degrees. Stretch out your fingers and reach forward as far as you can. (Examiner places a ruler at the end of fingertips when arm is at 90 degrees. Fingers should not touch the ruler while reaching forward. The recorded measure is the distance forward that the fingers reach while the subject is in the most forward lean position. When possible, ask subject to use both arms when reaching to avoid rotation of the trunk.

4: can reach forward confidently 25 cm (10 inches)

3: can reach forward 12 cm (5 inches)

2: can reach forward 5 cm (2 inches)

1: reaches forward but needs supervision

0: loses balance while trying/requires external support

9) Pick up object from the floor from a standing position

INSTRUCTIONS: Pick up the shoe/slipper, which is place in front of your feet.

4: able to pick up slipper safely and easily

3: able to pick up slipper but needs supervision

2 unable to pick up but reaches 2-5 cm(1-2 inches) from slipper and keeps balance independently

1: unable to pick up and needs supervision while trying

0: unable to try/needs assist to keep from losing balance or falling

10) Turning to look behind over left and right shoulders while standing

INSTRUCTIONS: Turn to look directly behind you over toward the left shoulder. Repeat to the right. Examiner may pick an object to look at directly behind the subject to encourage a better twist turn.

4: looks behind from both sides and weight shifts well

3: looks behind one side only other side shows less weight shift

2: turns sideways only but maintains balance

1: needs supervision when turning

0: needs assist to keep from losing balance or falling

11) Turn 360 degrees

INSTRUCTIONS: Turn completely around in a full circle. Pause. Then turn a full circle in the other direction.

4: able to turn 360 degrees safely in 4 seconds or less

3: able to turn 360 degrees safely one side only 4 seconds or less

2: able to turn 360 degrees safely but slowly

1: needs close supervision or verbal cuing

0: needs assistance while turning

12) Place alternate foot on step or stool while standing unsupported

INSTRUCTIONS: Place each foot alternately on the step/stool. Continue until each foot has touch the step/stool four times.

4: able to stand independently and safely and complete 8 steps in 20 seconds

3: able to stand independently and complete 8 steps in > 20 seconds

2: able to complete 4 steps without aid with supervision

1: able to complete > 2 steps needs minimal assist

0: needs assistance to keep from falling/unable to try

13) Standing unsupported one foot in front

INSTRUCTIONS: (DEMONSTRATE TO SUBJECT) Place one foot directly in front of the other. If you feel that you cannot place your foot directly in front, try to step far enough ahead that the heel of your forward foot is ahead of the toes of the other foot. (To score 3 points, the length of the step should exceed the

length of the other foot and the width of the stance should approximate the subject's normal stride width.

4: able to place foot tandem independently and hold 30 seconds

3 able to place foot ahead independently and hold 30 seconds

2: able to take small step independently and hold 30 seconds

1: needs help to step but can hold 15 seconds

0: loses balance while stepping or standing

14) Standing on one leg

INSTRUCTIONS: Stand on one leg as long as you can without holding on.

4: able to lift leg independently and hold > 10 seconds

3: able to lift leg independently and hold 5-10 seconds

2: able to lift leg independently and hold ≥ 3 seconds

1: tries to lift leg unable to hold 3 seconds but remains standing independently.

0: unable to try of needs assist to prevent fall

Chapter B

Appendix B

B.1 Multi-class classification approach

Figure 68 and 69 presents the learning curves for VGG16 and ResNet-50, respectively, considering the multi-class single frame classification approach.

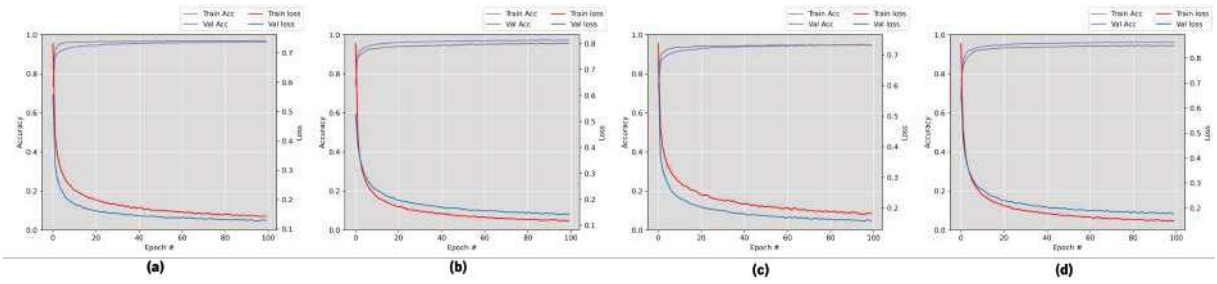


Figure 68: Accuracy and loss training curves for VGG16 model: **(a)** DIF, **(b)** ADD, **(c)** DIF cropped, **(d)** ADD cropped.

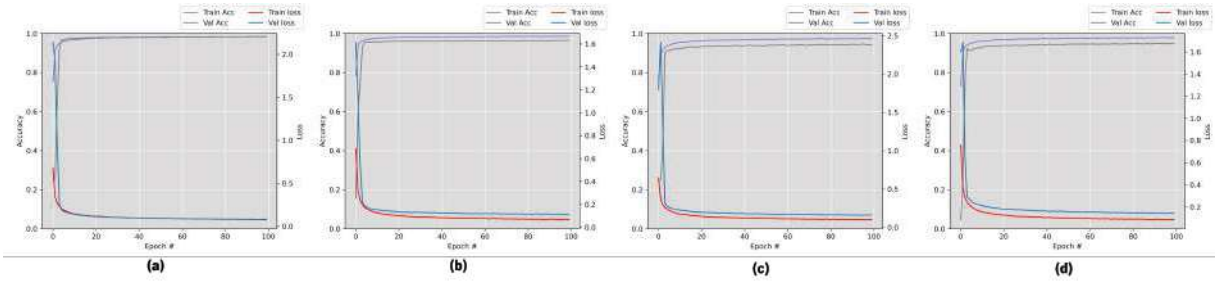


Figure 69: Accuracy and loss training curves for ResNet-50 model: **(a)** DIF, **(b)** ADD, **(c)** DIF cropped, **(d)** ADD cropped.

Figure 70 presents the learning curves for ResNet-50 with the CHATT mechanism.

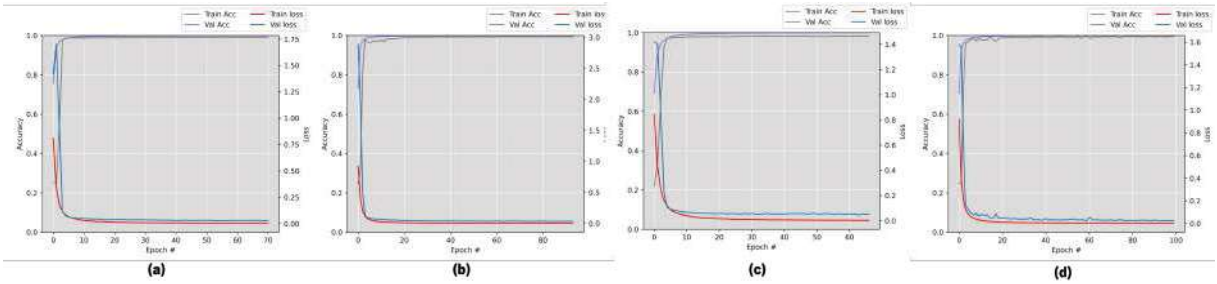


Figure 70: Accuracy and loss training curves for ResNet-50 with an additional CHATT mechanism: **(a)** DIF, **(b)** ADD, **(c)** DIF cropped, **(d)** ADD cropped.

Figure 71 presents the learning curves for the SE layer and the SPATT mechanism.

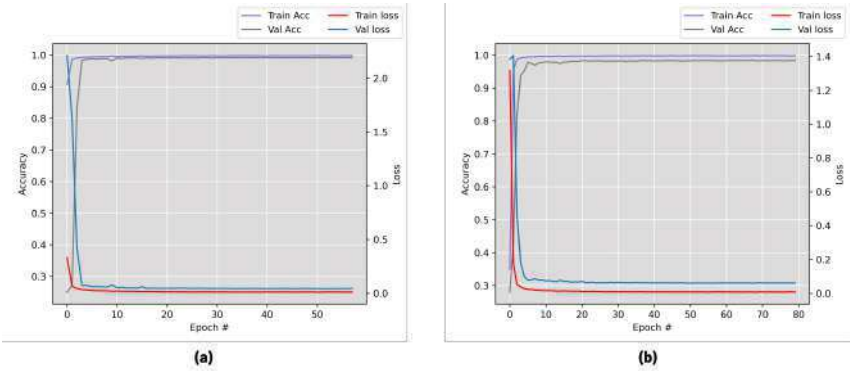


Figure 71: Accuracy and loss training curves for ADD cropped input with ResNet-50 and: **(a)** an additional SE layer and **(b)** a SPATT mechanism.

B.2 Multi-class segmentation-classification approach

Figures 72 and 73 presents the segmentation and classification training curves, respectively, using the U-Net and adapted U-Net model for multi-class classification.

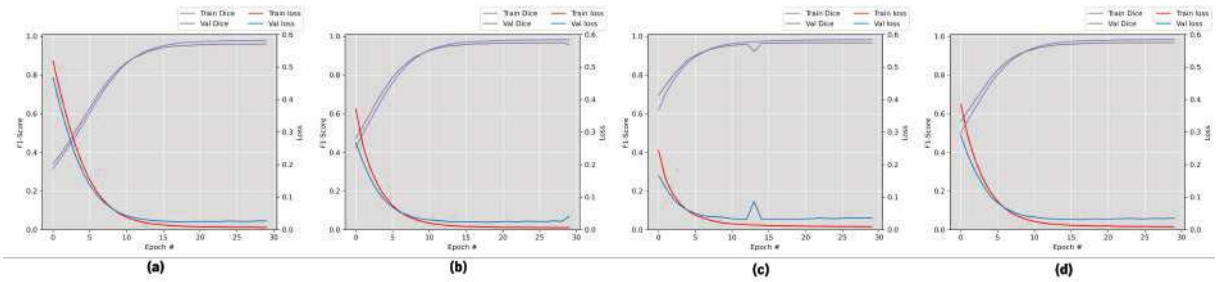


Figure 72: Dice and loss training curves for segmentation: **(a)** DIF, **(b)** ADD, **(c)** DIF cropped, **(d)** ADD cropped.

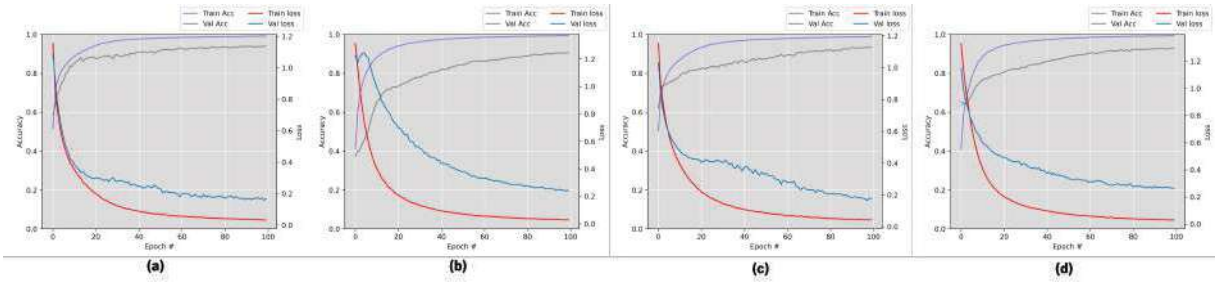


Figure 73: Accuracy and loss training curves for the adapted U-Net model for classification: **(a)** DIF, **(b)** ADD, **(c)** DIF cropped, **(d)** ADD cropped.

To help visualize this model's segmentation ability, Figure 74 show the best and worst cases of segmented images, for each type of input. Notice that, for the cropped ADD, the segmentation of the human body was satisfactory, even in the worst case, although including some noise. Contrarily to this, the other inputs revealed occlusions as the apparent main factor behind a worse segmentation.

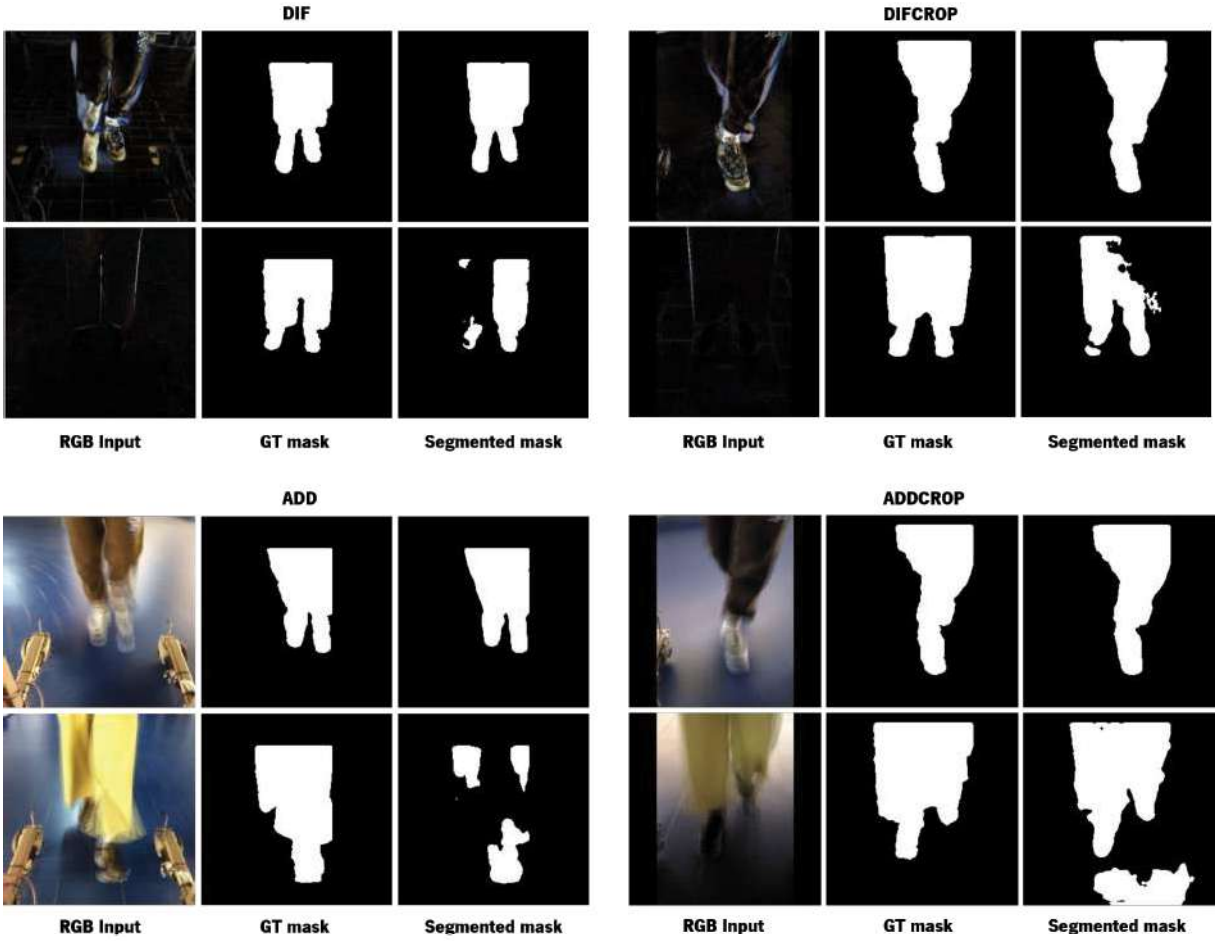


Figure 74: Examples of the best (upper) and worst (lower row) cases of segmented images, along with the respective DIF, ADD, DIF cropped, and ADD cropped inputs.

B.3 Ablation study

Figure 75 presents the learning curves for the ablation studies, namely 75 - **(a)** corresponds to the ablation study where the background is erased, 75 - **(b)** corresponds to the ablation study with different and random hospital backgrounds, and 75 - **(c)** corresponds to the ablation study where background was replaced by random hospital backgrounds and the classes were constrained to STOP and WALK.

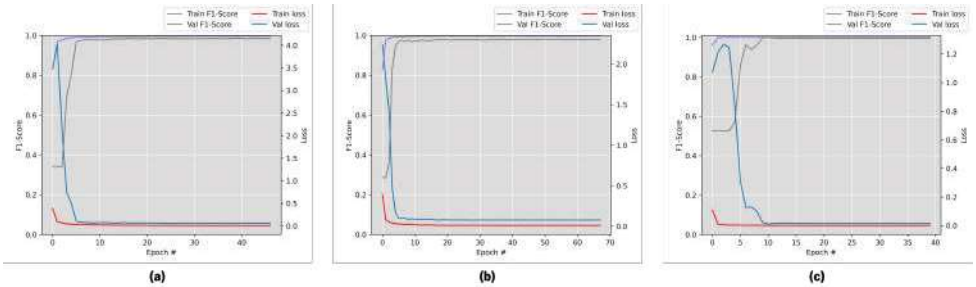


Figure 75: Accuracy and loss training curves for the ablation studies: **(a)** erased background, **(b)** different and random hospital background, and **(c)** frames of **(b)** but classes were constrained to STOP and WALK.

Chapter C

Appendix C

C.1 Training Phase 1

Table 51 presents the times of the 10-MWT and TUG clinical tests considering RAGT and treadmill-assisted training.

Table 51: 10-MWT and TUG times, in s, for both RAGT with WALKit and treadmill-assisted training.

Participant	Smart Walker			Treadmill		
	10-MWT (s)					
	D0	D16	Ratio	D0	D16	Ratio
P1	22.28±1.01	22.25±0.47	**1.00**	21.65±1.23	18.93±0.22	**0.87**
P3	48.29±3.47	45.99±1.73	**0.95**	46.04±1.53	42.81±1.27	**0.93**
P4	84.39±2.02	65.90±4.72	**0.78**	76.38±0.75	76.47±6.61	**1.00**
P5	6.46±0.30	5.66±0.38	**0.88**	5.30±0.26	4.87±0.20	**0.92**
P6	11.98±1.07	10.77±1.25	**0.90**	12.21±0.27	11.81±0.29	**0.97**
P7	11.23±0.81	8.99±0.54	**0.80**	13.37±1.94	9.24±0.04	**0.69**
	TUG (s)					
	D0	D16	Ratio	D0	D16	Ratio
P1	39.09±0.83	35.70±1.83	**0.91**	41.75±3.45	28.77±2.47	**0.69**
P3	53.86±4.22	53.91±6.87	**1.00**	57.77±2.40	55.86±4.28	**0.97**
P4	129.12±10.98	93.26±2.96	**0.72**	118.65±10.62	122.78±3.78	**1.03**
P5	13.24±0.63	10.64±0.36	**0.80**	11.96±0.36	12.04±0.04	**1.01**
P6	31.47±2.00	28.96±3.17	**0.92**	28.80±0.44	33.12±0.88	**1.15**
P7	31.61±2.34	26.75±1.74	**0.85**	36.23±1.31	28.14±0.73	**0.78**

Table 52 presents the spatiotemporal parameters considering RAGT and treadmill-assisted training.

Table 52: Spatiotemporal parameters obtained for each trial of the 10-MWT considering both interventions (WALKit and treadmill)

	Smart Walker				Treadmill			
Participant	**D0 - Rfoot**	**D0 - Lfoot**	**D16 - Rfoot**	**D16 - Lfoot**	**D0 - Rfoot**	**D0 - Lfoot**	**D16 - Rfoot**	**D16 - Lfoot**
Stride excursion (m)								
P3	0.703±0.036	0.741±0.028	0.777±0.011	0.786±0.014	0.803±0.010	0.811±0.015	0.832±0.023	0.839±0.016
P5	1.153±0.024	1.150±0.040	1.250±0.022	1.257±0.029	1.280±0.040	1.280±0.041	1.335±0.024	1.340±0.033
P6	0.898±0.038	0.900±0.044	0.956±0.062	0.959±0.057	0.904±0.055	0.939±0.043	0.925±0.021	0.939±0.028
P7	0.684±0.018	0.685±0.021	0.896±0.052	0.882±0.040	0.650±0.088	0.652±0.077	0.843±0.115	0.836±0.114
Step excursion (m)								
P3	0.530±0.029	0.249±0.012	0.476±0.012	0.339±0.015	0.479±0.025	0.390±0.030	0.530±0.026	0.335±0.023
P5	0.623±0.023	0.580±0.022	0.686±0.019	0.642±0.029	0.685±0.034	0.652±0.044	0.665±0.021	0.736±0.057
P6	0.442±0.038	0.465±0.012	0.459±0.026	0.504±0.031	0.462±0.016	0.498±0.018	0.475±0.015	0.475±0.012
P7	0.464±0.026	0.268±0.022	0.498±0.012	0.445±0.030	0.379±0.049	0.298±0.037	0.533±0.053	0.338±0.058
Stride time (s)								
P3	5.536±0.160	5.524±0.159	5.413±0.049	5.479±0.036	5.524±0.140	5.510±0.128	5.416±0.152	5.431±0.122
P5	1.179±0.017	1.185±0.020	1.143±0.030	1.136±0.028	1.098±0.014	1.100±0.007	1.084±0.025	1.080±0.029
P6	1.976±0.078	1.986±0.077	1.839±0.108	1.843±0.107	1.953±0.026	1.945±0.036	1.933±0.013	1.942±0.014
P7	1.408±0.083	1.410±0.060	1.422±0.038	1.416±0.059	1.552±0.026	1.542±0.019	1.533±0.114	1.535±0.122
Step time (s)								
P3	3.486±0.160	2.038±0.174	3.542±0.113	1.937±0.103	3.508±0.175	2.017±0.028	3.503±0.117	1.928±0.122
P5	0.609±0.026	0.582±0.018	0.565±0.043	0.571±0.033	0.564±0.029	0.533±0.022	0.526±0.049	0.551±0.020
P6	0.998±0.047	0.989±0.096	0.922±0.042	0.926±0.070	0.953±0.006	0.995±0.040	0.988±0.005	0.954±0.012
P7	0.736±0.038	0.674±0.035	0.702±0.054	0.710±0.004	0.757±0.030	0.795±0.018	0.820±0.049	0.709±0.070
Stance time (s)								
P3	4.265±0.212	4.339±0.170	4.134±0.092	4.380±0.024	4.292±0.110	4.316±0.207	4.149±0.121	4.117±0.075
P5	0.707±0.020	0.714±0.014	0.627±0.017	0.592±0.018	0.587±0.015	0.582±0.029	0.595±0.014	0.560±0.038
P6	1.190±0.121	1.184±0.046	1.072±0.141	1.078±0.073	1.179±0.022	1.132±0.016	1.160±0.062	1.176±0.021
P7	0.863±0.059	0.919±0.068	0.842±0.038	0.855±0.049	0.974±0.046	0.946±0.007	0.894±0.117	0.954±0.125
Swing time (s)								
P3	1.271±0.060	1.185±0.049	1.279±0.043	1.099±0.059	1.231±0.031	1.195±0.103	1.268±0.050	1.314±0.141
P5	0.472±0.008	0.471±0.018	0.516±0.025	0.544±0.021	0.511±0.001	0.518±0.023	0.489±0.015	0.520±0.010
P6	0.786±0.057	0.802±0.035	0.767±0.034	0.765±0.048	0.774±0.045	0.813±0.024	0.773±0.048	0.766±0.014
P7	0.545±0.024	0.491±0.041	0.580±0.017	0.561±0.016	0.578±0.064	0.596±0.020	0.639±0.007	0.581±0.034

C.2 Training Phase 2

Table 53 presents the average time to complete the TUG test before and after training with WALKit SRW and an additional biofeedback strategy. In addition, Table 53 also presents the BBS scores of both day 0 and day 16.

Table 53: TUG times and BBS scores of both day 0 and day 16 considering RAGT with WALKit and an additional biofeedback strategy

TUG				BBS			
Participant	**D0**	**D16**	**Ratio**	**Participant**	**D0**	**D16**	**Ratio**
P3	76.77±2.51	74.63±3.67	**0.97**	**P3**	25	25	**1.00**
P5	11.49±1.34	11.88±1.46	**1.03**	**P5**	51	51	**1.00**
P6	27.85±1.27	27.51±0.50	**0.99**	**P6**	34	40	**1.18**

Table 54 presents the average time to complete the TUG test before and after training with WALKit SRW and an additional biofeedback strategy. In addition, Table 54 also presents the BBS scores of both day 0 and day 16.

Table 54: TUG times and BBS scores of both day 0 and day 16 considering RAGT with WALKit and an additional VR-based exergame

TUG				BBS			
Participant	**D0**	**D16**	**Ratio**	**Participant**	**D0**	**D16**	**Ratio**
P3	70.59±4.72	73.29±2.57	**1.04**	**P3**	20	31	**1.55**
P5	13.39±1.45	11.52±0.33	**0.86**	**P5**	48	50	**1.04**
P7	26.62±2.79	24.96±0.53	**0.94**	**P7**	33	35	**1.06**